Blood Flow In Arterial Branches

Graham R. Aird

Thesis Submitted for the Degree of Doctor of Philosophy in the University of Edinburgh, 1985.

Abstract

The principal aim of the research was to identify flow features and effects in the region of arterial branches which may contribute to the localised development of the disease atherosclerosis. To this end, a program of experimental and computational study was followed to develop several areas of research.

The context of the present work is described in chapter 1 in which a general survey of the relevant literature is presented. In this chapter experimental and computational studies covering much of the range of fluid dynamically related topics in this area of research are discussed. The methods of study are described and the results and conclusions discussed with the aim of identifying the specific areas of development to be followed in the subsequent chapters.

The use of a relatively rare method of measurement of local mass transfer coefficients is described in chapter 2 and its adaptation to the study of mass transport in systems of different Schmidt number is discussed. A model of a symmetrical arterial branch was used to provide mass transport data and the results of these experiments are presented and discussed within this chapter.

The finite element method was used to solve the Navier-Stokes equations for flow in a system of similar geometry to that used in the experimental studies. The velocity data generated in this way was then used to solve the mass transport equation and thus to obtain mass transfer coefficients for the system. The effect of varying Schmidt

number upon the magnitude (and accuracy) of the results and the possible implications for the experimental results are discussed.

Chapter 4 contains comparative data for both computational and experimental results and also some data describing the importance of the role of the boundary layer in the resistance to O_2 transfer within the whole blood:arterial wall system. The context of the work within the field as a whole is discussed and areas for further work are identified. A summary and conclusions are contained in chapter 5.

Appendix A contains a procedure by which potential flow in a branched domain can be described and the possible implications for computation of flow distribution in a branched domain. Appendix B contains a discussion of a study of the variation of flow distribution between two limbs of an asymmetric branch with Re. Appendix C contains a procedure by which the constant rate period for mass transport of solute within a swollen polymer may be calculated.

Acknowledgements

I would like to express my thanks to the following:

the MacKenzie Fund (administered by Lothian Health Board) for the funding of this work

the staff and my fellow post-graduate students in the department of Chemical Engineering for much help, advice, sympathy etc when most needed

the technicians of the same department for their fabrication and frequent alteration of various experimental rigs

Drs R Jordinson and A Kitchin for their help and advice within various parts of the project

Dr N MacLeod for his supervision of the overall work

my "office-mates" William Scott and, latterly, Caroline Shirridan for their entertainment and understanding in times of trouble

my parents for their encouragement and non-technical advice

my wife, Judith, for always being there

Contents

List of Figures

List of Tables

Chapter 1 Previous Work Relating to the Study of the Role of Fluid Dynamics in Atherogenesis

1.1 Introduction

The disease atherosclerosis, characterised by hardening of the arteries, manifests itself as plaques or atheroma (Greek meaning gruel!), of which the major component is cholesterol, beneath the arterial endothelium. While the atheroma is apparently harmless in itself, when the disease becomes sufficiently advanced, it can have drastic effects upon the circulation. Blood clotting (thrombosis) is a strong danger, loss of arterial elasticity occurs, the artery becomes weakened increasing the danger of internal bleeding, and restriction of blood supply to the rest of the circulation, causing oxygen deficiency, is a common cause of heart attacks and strokes. The disease mechanism itself is unknown but it is apparently associated with an excess of lipoproteins (closely related to several components of atheroma) in the bloodstream. The disease, which has been described as being of epidemic proportions in some countries, is very common in the Western world, but is relatively rare in the Far East. A cause which has been attributed to this fact is the difference in the diet of the two regions, the Western diet involving heavy intake of animal fats and the Eastern being more vegetable orientated; but the connection is by no means established. However, a high proportion of Western resources are directed towards research into the causes of the disease as well as towards a cure.

There is much evidence to suggest that atherosclerosis is caused, and enhanced, by the nature of the blood flow in the arteries. Several

authors have reported that atherosclerotic lesions tend to form near arterial branches and abrupt bends in the larger arteries, and have concluded that the disease is strongly promoted in regions of highly disturbed flow conditions. For example, Fox and Seed (F5) reported upon early lesions occurring in the major coronary arteries: highly concentrated close to the arterial ostia, their concentration decreased with distance from the ostia. The conclusion that fluid mechanical disturbances are related to lesion formation is supported by the fact that the disease is rarely found in the smaller arteries, in straighter portions of larger arteries, or in the veins.

If development of atheroma is flow-related, the processes which affect it must be one or more of the following:

(i) convective transport of material in the bloodstream into the arterial wall or of transport of material from the wall into the bloodstream

(ii) mechanical effect of fluid shear stress on some propensity of the wall to interact with material on or within it (for example the, removal of the layer of endothelial cells by high shear stress)

(iii) mechanical effect of normal fluid stress (transmural pressure) on wall properties (for example, permeability to lipoproteins)

To identify which, if any, of the above is important, the following features must be understood,

(a) the fluid mechanical characteristics of the flow field in the neighbourhood of the arterial sites of plaque formation and

(b) the nature of the species whose transfer to, or mechanically induced interaction with, the arterial wall initiates atheroma

(c) the mechanism by which (a) and (b) interact to cause formation of plaques.

The remaining sections of chapter 1 contain discussion of these features. Section 1.2 describes some of the studies of location of plaque formation in animals. Sections 1.3 - 1.6 describe respectively methods of study, in vivo studies, in vitro studies and theoretical studies of the fluid mechanical flow characteristics in branched vessels.

Section 1.7 describes some of the studies of macromolecular and oxygen transport and their possible influences upon the disease process. Section 1.8 describes the contents of the remaining chapters.

1.2 Plaque Location

The actual location of the disease in the regions of disturbed flow is the subject of some disagreement, both in human post mortem studies and in studies of experimental animals.

Schwartz & Mitchell (S6) observed plaque formation in the iliac, carotid, vertebral, and aortic arteries of 336 patients and found them primarily in regions expected to sustain high shear stress. Enos et al (E2) also found atherosclerosis predominantly in high shear stress regions. Fox and Seed (F5) on the other hand found left common and anterior descending coronary arteries to be spared of lesions on the flow dividers. Lesions were concentrated on the inner wall of the curve over the heart in the right coronary artery, and on the outer walls of the branch of

the left anterior descending and circumflex arteries. Hugh and Fox (H6) presented pictures of plaques formed in areas expected to be regions of stasis along the outer wall of bifurcations. Grottum et al (G8) found many lesions upon the outer walls of arterial branches but few upon the flow divider.

Using cholesterol fed rabbits, Cornhill & Roach (C4) found lesions formed mostly upon flow dividers, results echoed by Roach & Fletcher (R11), and Cornhill et al (C5). Zarins et al (Z1) however found in general that the divider was free of lesions in similarly tested rabbits, and that lesions occurred where low shear stress might be expected. In addition, Cornhill et al (C4); in the paper previously mentioned, described tests on pigeons which were not fed a cholesterol diet, in which lesions were found to have occurred mostly in regions expected to exhibit low shear stress.

Thus it is apparent within the literature that a wide disparity of views have been expressed as regards the flow characteristics which initiate and propel the disease mechanism. The study of these characteristics is discussed in the following sections.

1.3 Techniques of Flow Study.

With the considerable evidence afforded by such studies as those described in section 1.2 that atherosclerosis is a focal disease dependent at least in part upon the fluid dynamic nature of the flow field, much work has been concentrated upon determining the nature of flow in branched regions. With the increasingly sophisticated techniques becoming available recently, more accurate measurement of point velocities using

non-invasive (Laser- and Ultra-sonic Doppler anemometry) and invasive (hot-wire and -film anemometry) methods have become possible and much work has gone into measuring these quantities both in vitro and in vivo.

Even with such sophisticated instrumentation however, it is still very difficult to obtain indisputably accurate results. Those involved in in vitro work generally construct approximate models of one specific area of the circulation (2 or 3 dimensional), pass fluid through it, and measure point velocities throughout the system. Such work is of limited value because it can only be hoped that the general flow features are consistent with those of the circulation, since substantial differences exist between the model and the physiological situation. Some of these differences are the following,

1. use of non-compliant materials of construction.
2. sharp rather than round cornered branches.
3. 2 rather than 3 dimensional flow regimes.
4. steady rather than pulsatile flow.
5. Newtonian rather than non-Newtonian flow.
6. homogeneous rather than inhomogeneous flow.

Of course, some of these differences are of more significance than others. Cross-sectional area variation due to arterial wall compliance over a heart cycle is not generally more than about 5% in the larger arteries (see Atabek,Ling et al (A5)), so it is possible that the difference between a compliant, natural vessel and a non-compliant model is not important in relation to point velocity and shear stress measurements. It is, however, of great importance in other measurements; for example the study of

pulse propagation in the arterial tree. Again, at shear rates of above 100 sec^{-1} blood behaves as a Newtonian fluid when examined in co-axial cylinder viscometers (thus from the point of view of velocity measurement, as a homogeneous fluid) hence assumptions 5 and 6 are generally assumed valid.

However, in some situations the effects of pulsatile flow rather than steady flow can be considerable. Studying steady flow in a symmetric, 3-dimensional, sharp-cornered branch, Brech and Bellhouse (B4) found no flow reversal due to the effect of secondary flows but did find flow reversal at the outer walls of the branch during the diastolic phase of pulsatile flow, a result which indicates the possibility of regions of stasis occurring. Peak and mean shear stresses measured in pulsatile flow both experimentally and computationally tend to be much higher than in steady flow, and flow conditions in general are more extreme. 2-dimensional model studies of 3-dimensional flows are also of limited value. In 3-dimensional branched flow or flow in bends, flow is skewed towards the flow divider/outer wall and displaces the boundary fluid, setting up helical flow patterns. These secondary flows prevent recirculation in the separation region distal to the branch/bend, as shown by Brech and Bellhouse (B4). These features cannot be simulated by 2-dimensional flow, and thus an important feature of flow in branches/bends is lost.

Exact simulation of the geometrical details of the flow system of interest likewise appears very important. Lutz et al (L7) examined the mesenteric and celiac junctions with the aorta using an in vitro model. One feature of this system is that the flow divider of the aorto-mesenteric junction protudes into the aortic flow stream more than that of the aorto-celiac junction. Lutz et al (L7) found that at identical

flow ratios for the two branches, pulsatile flow separation occurred on the outer wall of the celiac branch and not on the mesenteric during diastole, while there was no separation in either during steady flow runs. Houle and Roach (H8) found no vortex formed in a 90° sharp-cornered branch which was occluded, a result which contrasts with that of Malcolm and Roach (M4), using an identical model with the exception that the branch corners were rounded.

In the same way, the type of flow inlet conditions to an experimental apparatus can be of fundamental importance to the measurement of, for example, shear stress. A feed with blunt velocity profile would be expected to produce far higher shear stresses than a Poiseuille flow feed, but neither type would model adequately flow into, for example, the coronary arteries where velocity profiles are strongly skewed because the branches are oriented at roughly 90° to the aorta.

Such difficulties encountered in in vitro modelling may in principle be avoided in animal experiments. These, however, have limitations of their own. While much work on blood velocity measurement in experimental animals has been done, producing some very plausible results, much doubt still exists about how accurate the measurements are, especially in the region near the arterial wall. Boundary layer flow is much slower than centre-line flow in any flow passage, and thus any invasive device implanted within this region is likely to disturb the flow substantially more and may give misleading results. Hot-wire or -film anemometry is generally carried out with transducer head temperature of 5-10°C above blood temperature. Blood viscosity decreases with temperature, and hence is reduced in the region of the device. If flow

across the anemometer is high, then local fluid will not change temperature significantly and flow will be relatively unaffected by viscosity change. The temperature of the anemometer head must be kept low due to problems of coagulation upon it. With low temperatures, larger errors are caused which in boundary regions may be more severe, and these errors may be compounded substantially when measurement of radial velocity gradient is used to determine shear stress. Use of ultrasonic Doppler anemometry allows measurements to be made without interference to the flow in the artery. Boundary layer velocity measurement is still difficult however, because stray reflections from the wall give misleading echo and frequency shift detected at the transducer head which are not caused by the blood velocity. In addition to these individual problems characteristic of the two measurement techniques is a further complication common to both. The measurements are made in an expanding/contracting vessel where it is difficult to maintain constant the position (with respect to the moving wall) at which the velocity is being measured.

Despite all the problems outlined above much work has been carried out using both in vivo and in vitro methods, and this is discussed below.

1.4 In Vivo Studies of Flow Behaviour.

In vivo study of flow behaviour within the arterial system is, as indicated above, extremely difficult. Access to the flow field is awkward

for obvious reasons and the blood vessels are too small for standard engineering instruments to be of much use. Use of invasive instruments is difficult because of the problems of coagulation and of interference with the flow. In addition there is no such thing as a standard human flow model. Hence extrapolation of experimental results from, for example, animals studies to the corresponding human situation must be done with extreme caution. Thus the fluid dynamicist is faced with an immense problem in trying to define flow in the circulation.

The arterial system is characterised by a large number of flow passages which sub-divide and decrease in diameter with distance from the heart. Because parent vessels normally have larger cross-sectional areas than daughter vessels, boundary velocity gradients in the daughter vessels are characteristically steep with the entrance velocity profiles blunt. If the daughter vessel is oriented at an angle to the parent then skewing of the velocity profile occurs. This is generally the case with flow in a bifurcation. One fluid mechanical question about which there has remained considerable doubt from both in vivo and in vitro experimental work is whether or not reverse flow is a common occurrance at branches. Wells et al (W1) found some evidence of reverse flow in the left common coronary artery during systole, but the magnitude of this reverse velocity was fairly small by comparison with that of forward velocity during the later systolic flow and diastolic phases. Nerem and Seed (N5) found more substantial evidence of reverse flow in the canine descending aorta during their studies of development of disturbance. Given the wide range of flow conditions which occur in the circulation it seems plausible that reversal occurs in some locations, but whether or not it is a stable feature of the flow situation is as yet unknown.

Flow downstream to branches and bends is generally helical (in similar fashion to the situation in a pipe bend). Most reports, however, indicate that such secondary flows are dissipated within 5-6 diameters of the ostia. This finding illustrates how pulsatile flow can aid stability of flow. For example, Nerem, Rumberger et al (N4) reported peak Reynolds' numbers of 3085 in the coronary arteries of a horse. In a straight pipe of circular cross-section, steady flow of this character would probably be turbulent particularly if the feed to the pipe was essentially plug-flow as is the case in coronary flow. Because the flow is pulsatile, secondary flows and disturbed components which develop during the high velocity phase are dissipated during the low velocity phase with the result that these unstable features of flow can only manifest themselves during very high Reynolds' number flow.

Nerem and Seed (N3) defined turbulence as "a velocity waveform with high frequency (ie velocity disturbances) all the way through the deceleration stage of systole". In dogs they found several cases where turbulence occurred but that occurrances of turbulence were less likely as the frequency parameter increased and as Reynolds' number decreased.

Study of the endothelial cell layer has been found to provide qualitative information about flow behaviour. Nerem et al (N5) used electron microscopy to obtain photographs of cell formation in rabbit ostia. They found marked variation in morphology at locations proximal and distal to the flow divider. In the proximal region, cells had short length and small surface area. Near the branch they were aligned at about 45° to the aorta. Aortic and flow divider cells were aligned strongly with expected flow direction, but those on the outer walls of bifurcations

where lower shear stresses were expected were very disorientated. Similar results were obtained by Reidy (R8).

Thus it seems likely that cell morphology studies may yield information about shear stresses occurring in arteries. Because flow is pulsatile, the shapes of cells are more likely to provide information about the nature of the time-averaged flow conditions in any specific location than about eg diastolic flow shear stresses. The technique, though useful for giving an overview of flow conditions, is unlikely to be useful for quantitative measurements of shear stress because an a priori knowledge of cell shapes at birth would be necessary. It is also unlikely that a sufficiently precise definition of cell shape could be obtained in order that accurate computation of shear stress could be done.

1.5 In Vitro Studies of Flow Behaviour

A variety of papers have been published discussing the results of studies of flow in model branches using hot-film or laser Doppler anemometry. Brech and Bellhouse (B4) studied flow in models of branching vessels using hot-film anemometry, and observed the effect of varying the parameters Re (Reynolds' number) and α (frequency parameter). Working with circular cross-section symmetric bifurcations they observed the effects upon flow of both a rounded- and a sharp-cornered bifurcation. They found that helical flow occurred during steady flow, caused by the high inertia centreline flow in the parent vessel displacing the low inertia boundary fluid on the flow divider, preventing formation of a recirculation zone on the outer walls of the branch. They found some reverse flow on

the outer branch walls during the diastolic phase of pulsatile flow. The helical flow patterns observed during steady flow were also found during pulsatile flow, though in the case of the latter the secondary flows were dissipated during the diastolic phase when the instantaneous flow-rate dropped to a minimum. El Masry et al (E3) found similar flow patterns to those found by Brech and Bellhouse in both steady and pulsatile flow. They suggested that when pulse frequency was less than 0.3 Hz, reverse flows were found on one or both outer walls.

Gutstein and Schneck (G3 and S3) used blood as the testing fluid in models of branches of circular cross-section with divider angles of 0°,11°,30°,45° and 60°. Varying flow-rate and frequency, they found separation in all branching channels at or above some critical flow-rate. Below this value they found boundary-layer thickening (using radio-opaque dye to observe boundary flow behaviour). They claimed that separation occurred in the boundary-layer due to a low axial inertial pressure in boundary layer driving against an adverse hydrostatic pressure gradient caused by a cross-sectional area increase. However it would seem reasonable to expect separation to be caused also by inertial forces of the fluid in the sharp cornered branched channels used. Because sharp cornered domains have a very small radius of curvature, at the outer wall high centrifugal forces act upon the fluid flowing round the corner if there is no separation. Generally the induced pressure gradient normal to the wall is insufficient to prevent the inertial forces acting upon the fluid from causing separation.

Rodkiewicz and Roussel (R6) varied distal branch area ratios, and branch angles in a simple mainstream:side branch network and observed

these effects upon

a. the flow ratio of the daughter branches, and

b. flow behaviour in bifurcation regions using hydrogen bubbles.

They found crescent-shaped vortices forming in separation regions of both main- and side- branches, and observed some transport of particulate solids from main to side branch via this vortex motion. Ratios of side/main branch flow were found to increase with (a) decreasing Re, (b) decreasing divider angle, (c) increasing side to main diameter ratio. Rodkiewicz and Howell (R5), using similar apparatus, found flow ratio to be a weak function of frequency parameter.

Rodkiewicz and Roussel's (R6) finding that ratio of branch to main stream flow decreased with increasing Re is not, in itself, surprising, but it is noteworthy that they found this flow ratio to increase to values substantially greater than unity at Re < 1000 (in a branched flow regime where the daughter branches were designed to be identical), and to appear to asymptote towards infinity as Re -> 0. This result was also found by Crowe (C13) studying both flow of water and of a viscous dye solution. Furthermore, Crowe found this result in channels of both square and of circular cross-section, when the liquid was made to discharge into collection beakers. The qualitative behaviour for both fluids was similar but the flow ratio (Fr) vs Re curve for the more viscous solution lay very much closer to the origin. These results appeared anomalous in view of the fact that the flow regimes as described by both sets of authors should be characterised purely by Re. In view of this, an investigation was undertaken in order to establish why such unexpected results occurred. This is reported in Appendix B where it is shown that similar

anomalies were reproduced in circumstances where surface tension effects were found to be responsible and not when care was taken to eliminate these.

Talukder (T2) used fluorescent dyes and cinematography to observe flow behaviour in symmetric models of branches with both steady and pulsatile flows. He observed secondary flows in both steady and pulsatile flows as described by Brech and Bellhouse (B4). In steady flow he found low shear stresses at outer walls of branches but, in the pulsatile situation, vigorous oscillatory motion in separation regions distal to the branching point. He found that this oscillatory motion produced much higher (and alternating direction) shear stresses than steady flow. A flush wall-mounted hot-film probe and anemometer system gave results confirming these beliefs. Both Talukder and Balasubramanian et al (B9) speculated upon the possibility of the alternating shear stress playing some role in the initiation process of atherosclerosis, though neither proposed any specific mechanism.

Ling et al (L2) made measurements in an aortic flow model using hot-film anemometry and found a blunt velocity profile with maximum shear stresses being the in-vivo equivalent of about 130 dyne cm^{-2}, ie about one third of Fry's critical value. They found flow to be transitional between laminar and turbulent, a finding which is compatible with those of in-vivo studies eg Clark and Schultz (C3). Batten and Nerem (B15) extended the in-vitro work of Brech and Bellhouse by comparing flow behaviour in an in-plane (ie flat) 3-dimensional branch with that in a branch which models the curve of the coronary arteries over the heart. The in-plane model reproduced approximately the results of Brech and

Bellhouse. On the curved model, however, overall skewing of the velocity profile was towards the outer wall of the curve rather than towards the flow divider, due, presumably, to centrifugal effects. Helical flow patterns developed shortly downstream from the flow divider. In a study such as this the skewing of the velocity profile depends upon the respective radii of curvature of the surface of the heart and of the outer walls of the branch. Batten and Nerem found some diastolic flow reversal at the inner wall of the model curve over the heart. It should be noted that this area is one in which low shear stresses are expected and is also the region where most lesions were found by Fox and Seed (F5). They did not, however, find velocity skewing towards the outer walls of the branch which was found in horses by Nerem, Rumberger et al. A number of differences between the test media may explain this: for example

1. differences in ratio of the radius of curvature of the outer wall of the branch to the radius of curvature of the surface of the heart,
2. flow inlet conditions,
3. the heart is a pulsating system in which the surface arteries are subject to translational motion and continual expansion and contraction. The in vitro model is not.

Friedman, Hutchins etc. in a series of papers (F3,F6,F14), have modelled branched flow situations experimentally and measured velocities using laser Doppler anemometry. They have found high and low shear stresses occurring in close proximity to one another, time varying points of reattachment and no fully developed turbulence. One of the main

conclusions of their papers is that the accurate determination of the shear stress levels within the arteries from in vivo studies requires very accurate modelling of the flow regime. They found enormous differences in shear stress profiles caused by only minor variations in vessel geometry.

Two other interesting methods used in the measurement of shear stress at vessel boundaries are the following:

1. The electro-chemical technique, in which an electrolyte solution such as potassium ferricyanide is passed through a model of the flow system of interest which has electrodes implanted in the walls. When a current is passed through the solution the ferricyanide ion is converted to ferrocyanide. This reaction is fast by comparison with the rate of diffusion of the ferricyanide towards the electrode, hence the rate of reaction is limited by rate of transport which varies with shear rate at the wall. Thus the shear rate can be found directly by measurement of the current.

This method has been used by Lutz et al (L1 & L3), El Masry et al (E4), and Smith et al (S8). Lutz et al measured shear stress distribution in moulds of the aorto-celiac and -mesenteric junctions, and displayed absolute shear stress variation with location. At the downstream flow ratios and Reynolds' numbers they tested, maximum experimental shear stresses occurred at or just downstream of flow dividers and corresponded to in-vivo shear stresses of between 10 and 100 dynes cm^{-2}, the latter of which is not very much less than the critical stresses that Fry (F1) listed. One interesting discovery of their work was that at

certain flow rates, the shear stress on the aortic side of the aorto-mesenteric flow divider decreased with increasing flow rate. The authors attributed this feature to flow separation at the divider caused by some interplay of flow effects caused by the close proximity of the two bifurcations. Other main features of their results were the observation of high and low shear stresses and of stable and unstable shear stress regions in very close proximity to each other. They found very good correlation of the regions in which they observed strongly fluctuating shear stresses with those at which strong lesion formation in dogs and swine has been found to occur in vivo. El Masry & Feuerstein (E4) studied flow in a model simulating the renal branches of the aorta. Using the electrochemical technique they found that shear stress varies strongly with Re but that it does not vary linearly. Upon the flow divider apex shear stress was found in one case to increase four-fold when Re increased by 25%. An increase in Re of 100% caused a shear rate increase of 23% upon the renal wall of the divider and of 50% upon the aortic wall. Similar studies were performed by and results found by Smith et al (S1).

The electrochemical method has the advantage over velocimetric methods for shear rate measurement that shear rates are measured directly rather than deduced. As is discussed in section 1.3, point velocity measurements by anemometry near a wall can be very inaccurate and the compound errors in computing shear rate more so. With the electrochemical method the only sources of inaccuracy that occur are if

(i) the length of the electrode is too great and

(ii) if the electrode is not mounted flush with the wall thereby causing flow disturbance. Neither of these potential problems need occur

with a reasonable amount of experimental care.

2. The wall-coating erosion technique, in which the walls of the vessel under consideration are coated with a highly viscous liquid and shear stress is measured by the rate of erosion of the coating. Adamson and Roach (A7) used a white dyed viscous coating and a black dyed working fluid (water) and made video-recordings of the change of colour intensity of the wall coating. Using a video-analyser they quantified the rate of change of intensity of the coating which is assumed to vary linearly with shear stress over a known part of the period of the experiment. In this way they predicted the variation of shear stress over the domain of interest. As might be expected, they found considerable azimuthal variation of shear stress in both daughter limbs of a branch for which a side limb makes an angle of 90° both with the upstream limb and with the other daughter limb. They also found that the position of maximum shear stress varied azimuthally with axial position. This latter result lends support to previous in-vitro results (Brech and Bellhouse B4) which indicate occurrance of helical flow in the daughter branches of bifurcations.

This technique has three main advantages over others so far described: (1) shear stresses may be measured with ease over a large number of points (limited only by the resolution of the video system) by re-running the tape, (2) qualitative assessment of wall shear stress variation can be done with ease and (3) the rate of thinning of the coating is, at least in certain circumstances a direct measure of the shear stress at its surface.

The main disadvantages discussed by the authors are: (1) internal geometry is altered over the period of a run, with the accompanying danger that the flow behaviour is changed and (2) shear stress measurement is limited to steady flow.

Another problem upon which the authors did not comment is that if the rate of thinning of the coating is a measure of the shear stress acting on it, the ability to resolve variations of local shear stress over a surface is limited by considerations of continuity affecting flow in the coating itself. Thus the coating will tend to grow in thickness immediately downstream of a region of high shear simply by accumulation of sheared fluid there. Such behaviour would suggest that local shear stress variations may only be measured accurately if the analysis method yields data describing the rate of change of coating thickness. In the present case some correlation between optical density and coating thickness becomes necessary. Tanner et al (T7) describe the theory behind and the experimental practice of operating such a system using an oil film and measuring film thickness using laser interferometric techniques. They have never applied the practice to a complex system such as flow in a branched pipe, however, restricting themselves to the study of turbulent flow in a duct.

1.6 Theoretical Studies of Flow Behaviour

The main purposes of theoretical studies of flow in the arterial system have been

(a) to improve knowledge of rigid vessel flow patterns in the vicinity of such regions as stenoses, bifurcations, etc where atherosclerosis generally initiates.

(b) to provide an estimation of levels of wall shear stress, their spatial variation and their correlation with plaque formation also in rigid vessels.

(c) to provide velocity-pressure data to form the basis of mass transport studies (discussed in section 1.7).

(d) to provide an estimate of the effect of pulsatility upon the flow regime.

(e) to provide an indication of the effects of arterial elasticity upon flow behaviour and axial variation of pressure pulse shape.

Studies of type (e) are prospectively of the greatest direct physiological interest. The difficulties of analysing pulsatile flow behaviour in distensible vessels are, however, very great. Some of them will now be reviewed.

A substantial amount of research has been done in the field of arterial wall elasticity in order to determine the effects of elasticity upon pulsatile flow rates throughout the system (A1,A2,A6,C7,H1,H9,J1,R3,R4,R9).

The main aim of (e) is to identify features of flow which may be associated with physiological disorders. For example, Anliker et al (A1) postulate that shock wave development may be associated with a faulty aortic valve and that the flow characteristics resulting from this disorder may be identified non-invasively using Doppler flow measurement equipment. In vivo studies upon horses and ponies (N6 & W1) revealed the development of low frequency velocity fluctuations in coronary arterial flow. While these pulses were believed initially to be caused by the oscillatory movement especially apparent in the coronary arterial system, subsequent theoretical investigation (R9) has revealed that the fluctuations are induced by the compliant nature of the arterial tissue. Such effects upon blood flow clearly have strong implications for the nature of flow within these arteries and thus can be considered to be of significance in the study of fluid mechanical influences upon the development of arterial disease. Furthermore, one theory of atherogenesis implicates pulse development directly. Lallemand et al (L5) stated that the degree of reflection of a pressure pulse from the aortic bifurcation depends upon the area ratios of daughter:parent limbs and speculated that atherosclerosis is influenced by the degree of reflection of such pulses.

The most common approach to the study of pulse development along the arterial tree has been to assume the domain to be a permeable tapered vessel in which velocity varies only axially. Rumberger (R9) used data from the coronary arteries of a horse to approximate the rate of tapering of the vessel and rate of change of flow rate with distance for his model. He was able to predict that low frequency velocity pulses should be expected in the coronary

arteries of horses, a result supported by two sets of experiments.

Pulse propagation appears most strongly influenced by the elasticity model used to describe motion of the wall. However, the modelling of viscoelastic behaviour of the arterial tissue is awkward. Arteries consist primarily of collagen fibres (which are mainly viscous), elastin fibres (which have purely elastic properties) and smooth muscle cells, but the relative proportions vary from artery to artery. Because collagen fibres are elongation thickening, the viscous effects dominate at high transmural pressure pulses, while at low pressure pulses, elastic effects dominate. Thus the mechanical properties cannot be defined easily.

Nevertheless the incorporation of a viscoelastic term in the tissue's constitutive equation appears to alter significantly the propagation characteristics of the system. For example, Rudinger's (R4) purely elastic wall model predicted that shock waves can occur within centimetres of the aortic valve, a result which cannot be supported physiologically. On the other hand, Holenstein et al's (H1) viscoelastic model predicted no shock wave development at all.

The chief drawback of applying one-dimensional theory to a complex branching system is the amount of approximation which must be made. The arterial system cannot be described accurately as a tapered porous tube as the outflow function used in such methods is in reality a series of step changes in flow rate rather than a continuous outflow. Viscous losses cannot be described by the simple Poiseuille flow model which is commonly used and the viscoelastic

behaviour of the wall is not easily definable. Nevertheless, the most sophisticated models do reproduce some of the salient features of flow found by in vivo study as is discussed in section 1.4. The above difficulties have, however, tended to restrict attention to the analyses of flow in rigid models of the arterial tree.

The most common numerical techniques used for categories (a) - (d) have been the finite difference method (B2,E5,F4,02,03,R12) and the finite element method (D2,D5,G9,K3,T8). These have been used to solve both steady flow and pulsatile flow problems in various flow domains. Most of these studies have been concerned with the behaviour of flow in branches, eg symmetric bifurcations (D2,E5,F4,K3,02), the renal trifurcation (03) and the aorto-renal and -mesenteric bifurcations (G9).

Flow in symmetric bifurcations has been treated using the assumption of a branch whose outer wall forms a sharp corner with the proximal stream. The boundary conditions used for this domain are zero velocity upon the wall and Poiseuille flow at the entrance.

All papers describing studies of this type report high shear stresses occurring upon the flow dividing wall and low shear stresses upon the outer wall. Upon the flow dividing wall shear rate increases very sharply for a short distance downstream from the apex and then decreases monotonically from the maximum. On the outer wall, behaviour is less predictable. Whether or not flow separation is predicted depends very much upon Re, the branch orientation to the upstream section and the ratio of upstream:downstream vessel diameters. For example, Friedman et al (F4) studied both steady and

pulsatile flow for Re = 100. For steady flow they found no reverse flow upon the wall but some during the diastolic phase of pulsatile flow. On the other hand, Kandarpa and Davids (K3) found a substantial separation region formed in this area when Re = 1050. It should be noted that Brech and Bellhouse (B4) cast doubt upon whether reverse flow occurs in this region (at physiological Re at least) during steady flow for a three dimensional domain. Their experimental results showed that secondary flows prevented recirculation even in this region except during pulsatile flow. Thus it could be argued with some reasonable basis that a steady state two-dimensional flow model which predicts reverse flow is in this respect physiologically unrealistic. All studies of flow in a symmetric branch, whether or not they predict reverse flow, report that outer wall vorticity increases in the streamwise direction proximal to the branching point, decreases to a minimum (be it positive or negative) distal to this point and then increases monotonically to the value for Poiseuille flow.

It is very difficult to define accurate boundary conditions for pulsatile flow in models which assume rigid walls. The most convenient way to do so is to enforce laminar flow boundary conditions upon the entrance and exit to the domain under examination and use a pure sinusoidal pulse to describe the velocity profile at both the entrance and exit. This was the procedure followed by O'Brien and Ehrlich (O3) in their study of flow near the aorto-renal arterial branches. O'Brien, et al (O2), however, compared results for both the sinusoidal pulse and a more physiologically realistic pulse. This study indicated that the qualitative behaviour of flow is relatively unaffected by pulse shape, but that quantitatively it is altered substantially. For example the

ratio of in vivo pulse peak velocity to sinusoidal peak velocity was 2.5, and the corresponding ratio of vorticities was greater than this value. Both types of pulse yielded vorticities substantially greater than those found for steady flow.

Neither studies of steady nor pulsatile flow using numerical techniques have indicated shear stress levels to occur which are greater than those specified as critical by Fry (F1) at which the endothelial surface is altered. Kandarpa and Davids (K3) found shear stresses of up to 55 dyne cm^{-2} (ie 5.5 Nm^{-2}) for steady flow at Re = 1050 in a bifurcation modelling the aortic bifurcation. It is possible that a maximum shear stress several times this would occur if pulsatile calculations were performed, ~~but on the other hand, this is a high value of Re~~ for human aortic flow, where generally Re = 4000 approx.

Details of shear stresses predicted by a finite element study of flow in a bifurcation are discussed in chapter 3.

1.7 Mass Transfer Studies

Almost all theories about the factors influencing atherogenesis have been based to some degree upon the principle that the mass transfer behaviour of molecules in the bloodstream plays some significant role and that this mass transfer behaviour is governed by the nature of blood flow. There have been two major areas of study within this field concerning respectively (a) the transport of macromolecules to or from the arterial wall and (b) the transport of

O_2 to the avascular region of the wall. The work relating to (a) is described in section 1.7.1 and that relating to (b) in section 1.7.2.

1.7.1 Fluid Dynamic Features Influencing Plaque Formation

Fry (F1) found that by increasing shear stress in an arterial segment in vitro, he caused an increase in rate of transport of albumin to the endothelium, that structural damage occurred above stresses of 380 dyne cm^{-2} and erosion occurred at 1000 dyne cm^{-2}. He also found that rate of transport increases with transmural pressure, shear rate, and degree of turbulence and flow pulsatility.

Rate of transport of macromolecules to the arterial wall from the bloodstream is controlled by three mechanisms, the degree of effect of each being determined by size of macromolecule and local flow conditions. The three control mechanisms are

(a) diffusion through the fluid boundary layer.
(b) transport through the surface cell layer.
(c) intra-mural transport.

Caro and Nerem (C16) investigated the influence of the diffusion boundary layer upon macromolecular transport using an in vitro apparatus. They passed an albumin solution through an arterial segment in Poiseuille flow conditions so that if the transport process was boundary layer controlled then greater mass transport would occur through the growing concentration boundary layer than further

downstream where the boundary layer was fully developed. However they found no spatial variation in albumin concentration and therefore concluded that transport of macromolecules is controlled at the surface or within the intimal regions.

The effects of transmural pressure upon transport rates of macromolecules into the arterial wall have been studied by Chien et al (C11). They have found that rate of uptake of macromolecules in arterial segments increases with pressure (eg 67% greater uptake in vitro and 83% in situ at 100 mmHg than at 0mmHg, and 303% greater uptake at 200 mmHg. in vitro). They also observed (C14) rates of uptake of particles of known size at different pressures. At a physiological transmural pressure of 100 mmHg particles of size 9-13 nm were found in the interstitial fluid (or vesicles) of the endothelial cell layer and in the subendothelial layer. When this pressure was raised to 200 mmHg. particles of up to 25nm diameter were found in these regions. They point out that lipoproteins have diameters of 19-22 nm and might not be expected to be transported into the wall at pressures of less than 100 mmHg. but that high blood pressure (in cases such as hypertension) may cause enhanced transport into the wall. While peak transmural pressures are not generally as high as 200 mmHg. it should be noted that many authors propose that arterial permeability varies with shear stress. Thus a combination of the two effects could cause a sufficient increase in vesicle size to allow lipoproteins to transfer easily into the wall. A parallel study of the effect of shear stress upon transport of particles of known size into the wall has not been found.

From the results of the above studies it appears that resistance to macromolecular transport from blood to wall is predominantly within the endothelium. From Fry's and others' experiments concerned with variation of permeability with shear stress it seems likely that greatest mass transport occurs in regions of highest shear stress (eg flow dividers etc). Thus if the disease is caused by excessive transport of lipoproteins etc into the wall from the bloodstream it seems likely that the maximum accumulation of cholesterol would occur in areas of high shear stress. This presumption agrees with some, but not all, of the animal studies discussed above. It does not agree with results reported by workers studying arteries of post-mortem humans.

Fry (F1) did, however, suggest that the permeability of the endothelial cell layer to macromolecules is increased by increasing the fluid shear stress to which it is exposed and hence that destruction of this cell layer is not necessary for macromolecular transport between wall and lumen.

As previously stated, some studies indicate a lesion predilection for areas where low shear stresses are expected such as outer walls of an arterial branch or the inner wall of an arterial curve. In these regions low permeability would be expected and thus mass transport across the wall would be reduced. Caro et al (C2) account for this by proposing that high wall shear stress is a controlling rather than a causative influence on the disease. They point out that cholesterol appears to be synthesised by the arterial wall and postulate that the net flux of this component is from the wall into the bloodstream and not vice versa, as is generally assumed. They claim that it is likely

that the high permeability of the wall to macromolecules due to high shear stress allows cholesterol to transfer away from the wall more easily than in low shear stress regions, and that accumulation of cholesterol at the wall initiates the fatty plaques which are associated with the disease. In the case of animal studies previously mentioned, the cholesterol diet may have caused such an increase in cholesterol level in the blood that the natural direction of mass transport for the macromolecule was reversed, with subsequent accumulation of cholesterol at those regions of high shear stress.

Several groups of workers have found that damage to the endothelial cell layer can alter substantially the transport behaviour of macromolecules. Weinbaum et al (W6) found a 10 fold increase in mass transport rate over the experimental period when the endothelial layer was removed. Fry (F9) has found that a break in endothelial integrity due to excessive transmural pressure induces large changes in rate of lipid deposition, while Colton et al (C18) found damage to cells led to increased protein diffusion into the walls. For transport to occur in a process involving fluid mechanical de-endothelialisation, the shear stress would have to be sufficient to remove the cells, or at least to alter them substantially. As stated above, Fry identified the magnitudes of the necessary shear stresses as being 380 dyne cm^{-2} for structural alteration, and 1000 dyne cm^{-2} for cell erosion. Few studies of shear stress variation in the major arteries of animals have, however, made credible the supposition that these critical shear stresses are exceeded, though some work has indicated that they may be closely approached (eg Crowe(C13),Brech & Bellhouse(B4), Benson & Nerem (B10)). Many of those who find results predicting the occurrance of high shear stresses

in vivo, and those who find lesions occurring in regions expected to undergo high levels of shear stress, have postulated physical and chemical changes as described by Fry as being primarily responsible for atherogenesis. However while it seems likely that alteration of the wall structure would provide conditions suitable for initiation of atherosclerosis, there is no conclusive evidence to indicate that such shear stresses are attained in the normal human being. Fox and Hugh (F7) demonstrated the development of regions of stasis on the outer wall of 2-dimensional branched channels, using aluminium powder for flow visualisation purposes. They proposed that atherogenesis occurs either by

1. excessively adhesive platelets forming initial plaques in the vessel wall thus allowing fibrin mesh to grow or
2. excessive stasis regions causing natural blood constituents to adhere to the wall.

These results are shown by Brech and Bellhouse's 3-dimensional study to be of limited value as regions of stasis in 3-d flow are less likely to occur due to secondary flow action. As was described earlier however some reverse flow has been found in animal studies which may cause some regions of partial stasis and provide favourable conditions for either of the mechanisms described by Fox and Hugh.

Thus it seems unlikely that removal of endothelial cells by fluid shear stress within the arteries causes the initiation of the atherosclerotic process as sufficiently high shear stresses do not appear to occur. It is also unlikely that fluid boundary layer resistance to

macromolecular transport is as important as endothelial permeability in the exchange of lipoproteins etc between lumen and wall. The fluid boundary layer may however determine the resistance to the transport of small molecules such as O_2 into the wall and such a resistance plays a role in another possible disease mechanism linking local hypoxia with growth of atheroma. This possibility is discussed in section 1.7.2.

1.7.2 The Possible Role of Oxygen In Atherogenesis.

A further possible causative influence upon the development of atherosclerosis is hypoxia (ie starvation of oxygen supply to the tissue). Several sets of experiments (eg O4, H10) have indicated that animals exposed to an atmosphere with a severe shortage of oxygen, even for comparatively short, regular, periods of time are very much more susceptible to the disease than the control, while those exposed to hyperoxic conditions (high oxygen concentration in atmosphere) are generally much less susceptible. One possible explanation for these observations is that metabolism (or consumption) of lipoproteins etc in the tissue is impaired during hypoxia. Impairment of metabolism would cause an excessive concentration of lipoproteins in the tissue and induce the characteristic plaque development of atherosclerosis in the intimal regions of the arteries. Okamoto et al's (O4) work offers support to this hypothesis, as they found that while tissue concentrations of cholesterol and triglycerides varied markedly with O_2 supply, plasma concentrations of the same compounds did not. The implication is that while there is no consumption of cholesterol etc in the bloodstream and thus no variation with O_2 supply, there is

consumption in the tissue and consequently substantial variation with O_2 supply. Conversely, it has been suggested that both the solubility and the diffusivity of oxygen in the wall are reduced by an excessive lipid concentration in the tissue. In this case, transport of O_2 to hypoxic regions would be restricted, hence causing a snowballing effect of lipid build-up to occur and promoting atheroma.

In vascular arteries, having blood vessels embedded in the walls, oxygen transport is bi-directional (ie O_2 is supplied from both the microcirculation and the large artery) and there exists in the medial region of the wall a point of minimum oxygen concentration. Several of the major arteries are completely avascular (ie they have no vasa vasorum {blood vessel micro-circulation} to supply oxygen to the arterial tissue) and for oxygen supply, rely solely upon unidirectional diffusion of oxygen through the intimal and medial tissue from the lumen. This diffusion of oxygen is hence the only means by which lipids within these vessels can be consumed. In some avascular arteries the diffusion path length of oxygen is very long (for example in the thoracic aorta the distance can be 1mm), thereby causing substantial resistance to transport within these regions with the resulting danger of formation of local hypoxic areas.

Three medical conditions which have been associated with atherogenesis are the following:

(a) high blood pressure, or hypertension.

(b) non-atherosclerotic sub-intimal thickening of the blood vessel.

(c) smoking.

Hypertension has been found to restrict flow of blood in the vasa vasorum, which may reduce oxygen supply to the arterial wall. Non-atherosclerotic sub-intimal thickening causes an increase in the diffusional path length and therefore an increase in oxygen transport resistance. Carbon monoxide (in exhaled tobacco smoke) has haemoglobin binding properties vastly superior to those of oxygen, thus oxygen availability from the blood itself may be severely restricted.

Hence it can be argued that each of these three conditions could induce hypoxic conditions within the arterial wall which initiate the atherosclerotic process.

These observations, however, while interesting in themselves, do not explain why atherosclerosis appears to be a focal disease which develops primarily in regions where disturbed flow is expected. The natural conclusion to be drawn is that the fluid mechanical behaviour of the blood flow in the major arteries must, in some way, influence the rate of oxygen transport into the wall. The most plausible (and obvious) means by which fluid mechanical behaviour could play a role is if the fluid boundary layer resistance to oxygen transport is of the same order of magnitude as or greater than the tissue-side resistance. The diffusivity of O_2 in the tissue varies, depending upon the region of the wall, but is in any case of the order of $10^{-5}cm^2sec^{-1}$ while that of O_2 in plasma is approx $2 \times 10^{-5}cm^2sec^{-1}$ (S18). It is unlikely that oxygen transport is restricted by the endothelial layer in the way that macromolecular transport is (see C14) for the reason that the oxygen molecule is approximately 30 times smaller than the vesicles of the endothelial layer. It therefore seems quite plausible that the fluid

mechanical nature of flow in the artery may influence the rate of transport of oxygen to the wall.

The major goals of research in this field have been

(a) to determine variation of oxygen concentration within the arterial wall

(b) to determine whether or not "normal" O_2 levels within the vessel wall are close to hypoxic conditions,

(c) to determine how easily the reduction of luminal oxygen levels can induce hypoxia,

(d) to determine whether or not the character of the blood flow can induce regions within the arteries wherein the supply of oxygen is impaired significantly.

The methods of study of oxygen transport and distribution have included both experimental and computational work. The computational studies (which are discussed later) have been concerned with all of the work discussed above. The experimental work has been concerned (so far) with categories (a) and (b).

Oxygen distribution within the vessel wall itself has been studied with the use of oxygen pressure micro-electrodes, both with excised arterial segments and with animals in vivo. Such studies are extremely difficult to perform accurately, chiefly due to the effects of tissue stretching upon the electrodes and also due to the fragility of the electrodes in such hostile conditions. Buerk and Goldstick (B18) however studied the variation of P_{O2} (oxygen partial pressure) in rabbit aortic

tissue and in several arteries of dogs in vivo using P_{O2} microelectrodes inserted into the tissue. The results they obtained indicated unequivocally that variation of P_{O2} across the vessel walls studied is not symmetric in the cases where the vessel has a vasa vasorum and that oxygen consumption rate is greater near the endothelial side than the adventitial side (outer edge of the arterial wall). Their oxygen pressure profiles, when used in a computational model of the system, predicted that, in the canine abdominal aorta at least, if the oxygen supply from the vasa vasorum was curtailed then the outer half of the artery would become hypoxic. Crawford et al (C23), on the other hand, also measured variation of oxygen pressure in frozen arterial segments and found that its profile was roughly symmetric across the thickness. They also estimated the ratio of lumen side transport resistance to wall-side resistance to be approx. 2.4 , calculating their values from the product of diffusivity and P_{O2} gradient. It should also be pointed out that their data differed from that of Buerk and Goldstick's (whose data predicted a ratio of oxygen consumption rate to conductivity only one quarter of that of Crawford et al's (C23)). Both studies however indicate that the fluid mechanical nature of the flow can play a significant role in influencing oxygen transport behaviour in the major arteries.

Transport of oxygen within blood is governed by three basic mechanisms: plasma diffusion, plasma convection and convection of oxygen bound reversibly to haemoglobin. The most simplified method of studying oxygen transport to the wall is by assuming the major transport resistance to lie in the boundary layer immediately adjacent to the wall where blood flow is cell-free. This means that blood can

be treated as an homogeneous fluid which has oxygen dissolved in it and that all non-linear terms introduced by the haemoglobin-oxygen reaction can be ignored. The axial and transverse velocities from the convection terms are found by solution of the Navier-Stokes equations. Solution of this equation using numerical techniques for physiological situations of this type is difficult because Pe is very high (of the order of 280000) causing concentration gradients which are low in the bulk flow and which are high in the boundary layer. Numerical solutions are produced for a set of points which correspond to the nodes of either finite element or finite difference meshes (depending upon which method is used). When Pe is high, convective mass transport is much greater than diffusive transport hence concentrations are only steep in the region adjacent to the wall. To define the system well a large number of nodes are needed in the transverse direction close to the wall. The more nodes used in a computation, the processing time is consumed (computing time varies with cube of no of variables). Hence such computations can be extremely costly. Most studies of transport within the blood stream have therefore been restricted to the boundary layer. Ehrlich and Friedman (E5), for instance, solved the Navier-Stokes equations using a finite difference scheme for a symmetric Y-branch and used the solution to evaluate the concentration gradient at the wall analytically. Their results show, as would be expected, qualitative similarity between the curves depicting axial variation of vorticity and surface concentration. This meant that highest rates of transport to the wall were predicted to occur at points of highest vorticity where the concentration boundary layer would be expected to be thinnest (ie upon the flow dividing wall) while the lowest appeared to occur upon the outer wall just distal to the

branching point. The main weakness of their model lies in the assumption of linear variation of axial velocity with distance from the outer wall of the branch distal to the sharp corner. In such a region for two-dimensional flow and Re > 1, the momentum boundary layer would be expected to thicken and flow perhaps to separate from the wall as axial velocity became small. The neglect of axial diffusion in such a region may also be a source of substantial error, particularly near the corner where their results indicated the axial variation of the wall concentration gradient to be very high. The comparative results that they display between the finite difference analysis performed for Pe < 500 and the boundary layer approximation show relatively good qualitative agreement when 50 < Pe < 400. When Pe was greater than this value the difference grid used for the computations became too coarse for accurate results, while when Pe < 50, the model assumption that the diffusion boundary layer lies in a region where velocity varies linearly with distance becomes inaccurate. A point worth noting with respect to this kind of study is that mass transfer is defined by not only by Pe (=Re.Sc) but also Re ie the development of a concentration boundary layer is dependent upon both the diffusion characteristics of the system and the velocity profile throughout the domain. When Sc is high then the solute transport is defined primarily by convection terms and diffusion terms are important only in the region adjacent to the wall where velocities are low. Thus when Sc is high accurate computation of concentration distribution requires meshes which are much more refined in the neighbourhood of the wall than would be required for the computation of the velocity profiles.

Friedman and Ehrlich (F10) compared the effects of various boundary conditions upon the concentration distribution using the same boundary layer formulation. They found that lengthening the upstream section in order to cause the concentration boundary layer to develop further caused a decrease in wall concentration which decreased with respect to the shorter section solution along the test section. This result is as expected because the rate of boundary layer growth along a section decreases with distance (eg Bird et al (B19) show that the thickness of a momentum boundary in an otherwise potential flow regime varies with square root of distance from the leading edge). They also found that the effect upon wall concentration of using a flat rather than parabolic velocity profile at the entrance was minimal. These two studies report only a crude assessment of the concentration boundary layer thickness (assuming linear variation of concentration in this region).

Back et al (B16) also solved the Navier-Stokes equations for flow in stenosed arterial vessels using the finite difference method. Assuming oxygen transport within free plasma to be diffusion and convection controlled and transport of oxygen bound to haemoglobin to be governed by convection only, they added a new concentration variable to the convective terms of the equation governing concentration distribution which is equal to the product of saturated O_2 concentration in haemoglobin, fractional saturation of O_2 in haemoglobin and fractional distribution of red cells in the boundary layer. Assuming their feed concentration of O_2 to be unity and boundary normalised concentrations set at 1/3, they found maximum mass transfer coefficients occurred upon the proximal side of a

stenosis where the shear stress is highest (a similar result to that of Friedman and Ehrlich) and minimum coefficients upon the distal side where a separation region was found. They found very little difference between time averaged and steady state mass transfer coefficients except where the mass transfer coefficients were very low. Even when this was so the maximum difference was only 45%. At points of high mass transfer they found that the convective term characterising the contribution of the haemoglobin reaction played a major role in the transport rate. This is evidenced by the fact that when this term has been included in the computations the resulting transfer coefficients in these regions are very much higher than when it has not. This was found not to be the case in regions of lower mass transfer.

Schneiderman and Goldstick (S11) reached similar conclusions regarding the role of the non-linear convection term. They found that the cell free layer represented a fairly minor resistance to oxygen transfer and that the boundary layer extended well into the bulk luminal flow. Only at the leading edge was resistance predominantly in the cell-free layer but in any case the resistance in this region is very low. The model used by Schneiderman and Goldstick was designed to aid investigation into the conditions necessary for hypoxic regions within the arterial wall to develop. As such, the focus of their work is upon the distribution of oxygen within the wall itself and thus the effects of spatial variation of transport from the lumen are not considered. There is no computational study such as the ones described above which combines an assessment of both luminal and wall transport of oxygen. The same group (S9) did perform a study of transport to a stenosed

vessel using an expression for both axial and radial velocities in terms of axial and radial distances. The results from this study were similar to those of Back et al (B23).

Using the lumen-side concentration gradients predicted by the model of Schneiderman and Goldstick (S12) an approximate mass transfer coefficient of 1.3×10^{-3} cm s^{-1} (ie Sh = 65) is obtained for conditions which were expected to induce local hypoxia in the middle regions of the artery. This value is similar to those found by Back et al (B23) in regions of higher mass transfer. It is very much higher than the coefficients predicted by Back et al in the separation region distal to the stenosis. Again, this can be interpreted as providing indirect evidence that hypoxic conditions can be induced in the arteries by the nature of the conditions of flow.

Thus, like all other areas of engineering study concerned with explaining what role fluid mechanics of blood might play in inducing atherosclerosis, the study of O_2 transport yields several possible ways by which the disease could conceivably be induced. A study of mass transfer in a model of the arterial system was performed by the author, which is outlined in brief in section 1.8.

1.8 Scope of this Thesis

The above summary of the literature suggests that the influence of oxygen transport to and within the arterial wall may well in some

circumstances induce atherosclerosis. It appeared somewhat anomalous that no studies of three-dimensional oxygen transport to the arterial wall have been performed. Bearing in mind that

(a) the lowest transfer coefficients have been predicted to occur in regions of separation

(b) Brech and Bellhouse (B4) predict no flow separation even in three- dimensional branches with sharp corners

(c) atherosclerosis appears to initiate even in arteries where no stenoses exist

it seemed worthwhile to pursue a study of the mass transfer behaviour in an experimental model in which the flow features could be controlled. Chapter 2 contains a report of this experimental study in which mass transfer coefficients were measured in a two dimensional branch.

A parallel study of this domain was performed using the finite element method to solve the Navier-Stokes equations and compute Sherwood numbers (normalised mass transfer coefficients) from the resulting velocity data. The report of the computational procedures and results is contained in chapter 3.

As described above in section 1.5, some seemingly anomalous results were reported by two sets of authors (R6) & (C13). Both found that the ratio of rates of side branch flow to main branch flow in an asymmetric flow domain consisting of two equidimensional downstream branches increased with decreasing Re, asymptoting towards infinity as

Re -> 0. In view of this, an attempt was made to reproduce the experimental apparatus of the workers and to explain these results. This work and somewhat trivial results are described in Appendix β.

Chapter 4 contains a discussion of the results of the experimental and computational work together with an assessment of their significance with respect to the initiation of the disease atherosclerosis. Chapter 5 contains the overall conclusions of the study.

Chapter 2 An Experimental Study of the Variation of Mass Transfer Coefficient in a Symmetric Branched Channel

2.1 Introduction

The transport of O_2 from the lumen into and through the arterial wall is controlled by three factors which are

(a) the concentration boundary layer resistance within the lumen.

(b) diffusive resistance to transport within the intimal and medial layers.

(c) local rate of consumption of O_2 within these layers.

Whilst the relative importance of each of these components in controlling the supply of O_2 to all parts of the avascular arterial tissue varies from region to region, it is of interest to note that both Back et al (B16), studying transport to a stenosed vessel wall using computational techniques and Crawford et al (C23), performing in vivo experiments to determine variation of O_2 pressure within canine femoral tissue, conclude that in the regions of artery which they were studying, the lumen-side transport resistance was the dominant transport- controlling process.

To date, all simulation of O_2 transport to the arterial wall has been by use of computational models or by measurement of O_2 pressure variation across sections of artery in vivo or in vitro. As discussed in chapter 1, section 1.7, the accuracy of the computational models

simulating flow of blood in a two-dimensional domain is limited by the elimination of any three-dimensional secondary flows. Models of transport behaviour between bloodstream and wall are thus necessarily limited by the same problem. Since some in vitro experimental studies (eg Brech and Bellhouse,B4 and Batten and Nerem B15) have shown that strong three-dimensional flows can occur in regions where atherosclerosis is commonly initiated, the validity of any fluid mechanical study which fails to take account of such features appears questionable.

Measurement of luminal transport resistance using arterial segments in vitro is also very difficult. Crawford et al (C23) found major problems of positioning microelectrodes accurately and eliminating all effects of tissue stress upon the measurement of O_2 pressure. Buerk and Goldstick (B18) found similar problems when working in vivo: they also cited the fragility of the electrodes as a major problem when using this method. In addition while such studies supply transport data in physiological regions, a general study within arterial tissue is limited by the lack of consistant geometrical definition.

Because there is little evidence of spatial variation in local tissue properties, the spatial variation of oxygen transport to the wall is less likely to be influenced directly by the transport properties of the wall than by those of the blood-flow. Therefore three-dimensional variation of the transport properties can, in principle at least, be estimated if a suitable technique can be devised for measuring local mass transfer coefficients in such a domain. The advantage of this is that if the spatial variation of mass transfer coefficient, can be found for any

domain of interest, then the oxygen concentration in blood, together with the mass transfer coefficient can be used (perhaps in a simulation package such as that developed by Schneiderman et al S18) in order to assess the effects of boundary layer resistance in the model under study upon medial region O_2 levels in an artery which is geometrically similar. In this way it should be possible to predict approximately what types of flow conditions, if any, may cause oxygen starvation within the tissue.

2.2 Types of Experimental Method for Measurement of Local Mass Transfer Coefficient

As identified by MacLeod (M8), experimental systems for measuring local mass transfer coefficients should ideally be simple to use, easily prepared and altered, produce easily processible results and be usable over a wide range of Schmidt numbers (Sc). Two principal techniques are available for measurement of local mass transfer coefficients, viz (a) profilometric methods and (b) electrochemical techniques.

The method most commonly used to measure these coefficients is the electrochemical technique. As described in chapter 1, Lutz et al (L1) used this method to measure diffusion rates of electrolyte to an isolated electrode implanted in a model wall, from which measurements shear stress could be determined using the Leveque solution. Within the physiological system the boundary layer is well developed, hence when using the method to measure mass transfer coefficients in a model of such a system, the concentration boundary layer must be developed. For studies of transport to a three-dimensional model of

an arterial branch this would be done by making the entire boundary a cathode, whereby the boundary layer growth could start at the flow channel entrance. To measure the local mass transfer coefficient at any location, a small cathode electrode would be implanted upon the surface, isolated from the large cathode. Thus measurement of coefficients over a three-dimensional domain would require a large number of isolated electrodes implanted over the surface of the model. Lutz et al (L1) ,for example, used 75 electrodes in their two-dimensional domain for shear stress measurement. Hence construction of the necessary apparatus is extremely laborious and many individual measurements are required.

The most common profilometric technique used in the past involves the coating of a surface of interest with naphthalene using air as the experimental fluid and the measurement of local thickness before and after an experimental run at various selected sites of interest over the surface by some means such as air-gauging. Again, many such individual measurements are required in order that the variation of transfer coefficient over the surface may be obtained.

A more efficient method for measuring mass transfer coefficients would be a profilometric technique in which rate of transfer could be observed directly - in domains such as three-dimensional arteries, this would be particularly advantageous. Such a method has been developed in Edinburgh and is termed the "Interferometric Swollen Polymer Technique". With this method, a thin silicone rubber coating upon the surface of interest is swollen to saturation by a swelling agent (typically an aromatic ester). The system can be designed fairly easily

so that both the physical and the optical density of the silicone rubber are similar to those of the swelling agent. This means that the rate of surface recession is directly proportional to the rate of evaporation or solution of the swelling agent from the surface into the working fluid during the constant rate period (in which the dominant transport resistance is in the working fluid). The recession occurring in a known time interval can be measured by laser interferometric techniques (either holography or electronic speckle pattern interferometry). Local mass transfer coefficients can thus be computed simply by counting the number of interference fringes passing the point of interest in a given period of time.

Holographic methods have been used with the swollen polymer technique with considerable success in the past by MacLeod and others (K5,K6,K7,K8,M8,H10,M5). A basic introduction to and critical analysis of the technique is given by MacLeod and Todd (M5). They point out that the validity of the method is dependent upon five conditions being fulfilled,

(i) rate of diminution of thickness is proportional to rate of evaporation of the swelling agent.

(ii) effective vapour pressure of the swelling agent over the surface is the same initially and remains constant throughout the period of the run.

(iii) overall resistance to mass transfer is predominantly in the working fluid phase.

(iv) the thickness of the coating at any given point is governed by the local rate of mass transfer - not by lateral diffusion or stress

effects.

(v) the relationship between rates of mass transfer and recession should be uniform despite any inequalities in the original coating thickness.

Conditions (i), (iv) and (v) were found experimentally to be valid for such systems as RTV silicone rubbers swollen to equilibrium with esters or hydrocarbons. Conditions (ii) and (iii) are fulfilled during a certain period of the run in which the polymer coating is not too far from saturation. MacLeod and Todd (M5) describe a procedure by which the length of this constant rate period can be determined a priori from the physical properties of polymer and swelling agent. Thus the swollen polymer technique can be used relatively easily to determine local mass transfer coefficients. This procedure is applied to the current case in Appendix C.

2.3 Use of Optical Techniques to Measure Change in Length

The use of coherent optical techniques to measure variations in length is a technique well used in many applications (eg in plane motion of a surface in shear stress measurement, oscillatory motion of a surface in rotating machinery). In holography the ray of light is split into a reference beam and an object beam. The reference beam is directed through a lens-pinhole arrangement on to a photographic plate (see fig 2.1). The object beam is also directed through a lens-pinhole arrangement and is then reflected from the object under examination on to the photographic plate. Thus a pattern of interferometric fringes corresponding to the wave front generated by the surface

under examination is produced upon the plate. When this pattern is developed photographically the fringe array forms a diffraction grating capable of reforming the original wave front (and hence the surface that gave rise to it) when illuminated by the reference beam alone. If the reconstructed image is viewed through the photographic plate it may be arranged to occupy the same space as the original object. If the original object in its original form is still present the light originating from the object will interfere constructively with the corresponding image on the reconstruction and the object will appear light. If a locus of points upon the original object is then moved such as to alter the optical path length of light by one half wavelength then the light from that locus of points will interfere destructively with the corresponding locus of points on the reconstruction, resulting in a locus of dark points or fringe being superimposed upon the object which otherwise appears light.

When the method is applied to the measurement of rates of surface recession of a swollen polymer, very accurate measurements of mass transfer coefficient can be made and the variation of coefficients over the surface easily assessed, at least in principle. There is, however, one major disadvantage with the method, namely uncertainty of fringe identification - it is often difficult to determine how many fringes have passed over a point in a given period of time because, if viewed in real time, some would be seen to have passed off of the edge of the plate. To follow the progress of a fringe across the interferometric image of the surface a run must be repeated several times over periods of varying length. In this way the rate of fringe traversal of the image can be observed and mass

transfer coefficients determined. This method is, however, somewhat laborious.

A more satisfactory arrangement for observing fringe development is afforded by the more recently developed method of electronic speckle pattern interferometry in which fringes evolving due to the recession of a surface as described above can be viewed upon a video screen and recorded upon video tape or disc. In this system an optical path similar to that for holography is used but the object is viewed through an aperture small enough to generate a speckled image of dark and light dots such as that in fig. 2.2 which depicts a diffusely reflecting flat aluminium alloy plate. These dots are small interference fringes caused by the super-imposition of the reference beam upon the image produced by the object beam reflected from the surface of interest and represent points upon the surface which cause the reflected object beam to interfere either constructively or destructively with the reference beam. If, before an experimental run is performed, such an image is produced upon the face plate of a television camera and stored electronically, then exposure of the camera to the surface under inspection gives a signal that may be subtracted electronically from that of the original image. If, during the run, any specific point upon the surface has been translated out of plane such that the optical path length of the object beam reflecting from that point is altered by one half wavelength then the image of that point upon the camera face after the run will be a dark point caused by destructive interference of the stored image with the real time image. If this point upon the image forms part of a dark fringe, then this fringe represents a locus of points upon the

surface, all of whose translation has caused an alteration in optical path length of one half wavelength. Thus by considering the angle at which the light strikes and reflects from the surface, the distance of translation of all points on such a locus can be determined.

This system has the distinct advantage that a new "original" image or reference state of the surface can be generated at the push of a button rather than by having to arrange a new exposure of the photographic plate. Fringe development can (where the experimental arrangements of the mass transfer system allow) be observed in real time rather than by the frozen fringe images which holography produces. Fringe development can also be recorded upon video-tapes or -discs for subsequent re-examination after the run. The only significant disadvantage of using speckle pattern interferometry rather than holography is that while the grain size upon the photographic plate can be made extremely fine, the pixel size in a video system is relatively coarse. Indeed it is the coarseness of resolution of video systems which prevents their direct application to holography, where the spatial frequency of the micro-fringes constituting a hologram is of the order of the wave number of the light employed. As is described below, this was found to be a significant problem near mass transfer leading edges but it can be overcome by use of a sufficiently flexible optical system.

An electronic speckle pattern interferometer is marketed by Vinten Ltd of Bury St. Edmunds, Suffolk, England, which has facilities for viewing fringe development and video-recording as described above. This instrument, the first available commercially, has been used to study

the variation of mass transfer coefficients over a domain to simulate some features of arterial flow. Those studies are described in the remainder of this chapter.

2.4 Preliminary Work and Considerations

The aim of the experimental study was to examine how the mass transfer coefficient for oxygen varied axially in a branched domain and to demonstrate the value of the swollen polymer technique as a means by which this can be attained. The numerical studies by Ehrlich et al (E5,F10) described computed variation of O_2 concentration in a symmetric bifurcation which was chosen to model a two-dimensional arterial branch. In order that some comparison could be made with the results that they obtained, it was decided that a two-dimensional symmetrically branched channel should be constructed. This is illustrated in fig 2.3.

For any optical system, rigidity of the materials of construction is essential in order that alteration of the optical path length due to undesirable experimental artefacts (eg creep) be avoided. The most suitable materials of construction are hard metals and glass. The machining of glass, however, is extremely difficult, and, in any case, given the necessary frequency of removal and replacement of an optically clear block it was felt that the use of a brittle material such as glass was inappropriate. For this reason several tests of the suitability of both perspex and polycarbonate plastic were performed.

Because the transparent material of construction was to be coated with polymer which was to be swollen with ethyl salicylate, it was necessary to ensure that the solubility of either plastic in the swelling agent was negligible. In addition, the plastic would be removed from the model structure between runs for swelling to resaturate the polymer coating. Such a procedure meant that the structure would be exposed to substantial bending- and shear-stress, both of which may cause creep and affect the optical characteristics of the structure directly or indirectly by causing creep. Therefore the effects of stress upon the structures' optical characteristics were also examined.

2.4.1 Solution of Plastic in Swelling Agent

Both perspex and polycarbonate were found to dissolve in the swelling agent (ethyl salicylate) though to markedly different degrees. The surface of the polycarbonate dissolved completely within hours, making the material completely opaque and unsuitable for use with the swollen polymer technique. Perspex, on the other hand, was found to dissolve very slowly in the swelling agent and retained a relatively (optically) pure surface over the course of several days. It was also found that the polymer tended to peel off the surface of the perspex after several days, probably due to the slight solution of the surface in the swelling agent. Restoration of the surface to presolution clarity was achieved easily by heating the perspex plate in an oven at 60°C overnight (to evaporate the ethyl salicylate) and subsequently by rubbing with perspex polish. It should be noted that periodic restoration of the perspex surface is necessary. If the

perspex has been machined substantially it should also be annealed in order to reduce the level of internal stress set up within the structure. If this is not done then (i) slight creep of the structure may occur, distorting the results and (ii) cracking of the structure along the lines of dislocation within the structure may occur when the structure is exposed to the swelling agent.

2.4.2 Optical Distortion of Plastic Under Stress

A perspex block of dimensions 2 x 1.7 x 40 cm was laid horizontally across two block supports positioned 20 cm apart upon the optical table of the interferometer and the vertical face further away from the light source was coated with matt-white paint to provide a suitable diffusely reflecting surface. A pre-test image of the surface was stored and then a weight was placed upon the centre of the block. When a 24g weight was added, four clear horizontal fringes became visible immediately upon the image. During the experiment there was no subsequent fringe movement, but after approximately three minutes the fringes had faded completely. When an 8g weight was added, again four fringes appeared, but this time took about ten minutes to fade.

These results indicated that the optical characteristics of the block (ie its refractive index) were altered by the initial stress which was caused by the addition of the weights. The fringes upon the image corresponded to lines of distensive and compressive stress in the structure, while their disappearance indicated that creep of the structure had caused stress relaxation and a return to the original refractive index. When the smaller weight was added the rate of creep was lower than during the previous test and therefore the refractive index returned to its original value more slowly.

These conclusions were borne out when a weight was added to the block and left to stand for twenty minutes to reach equilibrium. At the end of this period an image was stored and the weight removed.

Again, horizontal fringes appeared upon the image corresponding to lines of internal stress in the structure. These fringes disappeared after several minutes, again indicating creep of the structure, this time returning to its original state.

These tests indicate that while the optical characteristics of a perspex structure are altered by the application of stress, consequent creep within the structure causes stress relaxation and restoration of the original optical characteristics. For this reason when any experimental channel was constructed for testing, a stress relaxation time of 20 minutes was allowed before a run was started.

4.3 Reflection Techniques

As is shown in figs 2.5a and 2.5b, two basic optical reflection methods can be used to study the variation of mass transfer coefficients across a surface. These are total internal reflection and direct reflection. Both methods were employed in preliminary studies to compare the quality of fringes evolving from the point of impingement of an air-jet.

2.5a

Fig 2.5a illustrates the experimental configuration used to study the total internal reflection. When air is used as the working fluid, the critical angle θ_c of the air-polymer system is given by

$$\theta_c = \sin^{-1}(n_{air}/n_{polymer}) \qquad n = \text{refractive index}$$

$n_{air} = 1.00$ and $n_{polymer} = 1.52 \Rightarrow \theta_c = 41^0$

The prism under study was rotated until the angle of incidence was slightly greater than the critical angle and the diffusely reflecting surface was in view upon the screen by internal reflection from the polymer-air interface. A laminar jet of Re = 1000 (based on jet diameter) was directed at the swollen polymer surface from a distance of 5cm and fringe development observed.

Fig 2.5b illustrates the configuration used to study direct reflection from a rear surface. As with the total internal reflection study, a laminar jet of Re = 1000 was directed at the swollen polymer surface from a distance of 5cm and fringe development observed.

With both configurations, the contrast of the fringes such as those in fig.2.6 produced decreased with time, so that eventually they became indistinguishable from the light background. It was found consistently, however, that while this happened after only about eight fringes using the total internal reflection technique, as many as twenty-five fringes remained clearly distinguishable with the direct reflection method.

The fading of the fringes was believed to be caused partly by the comparatively low resolution of the video monitor and partly by the fact that the fringes were viewed through a glass plate. When the fringe thickness becomes as low as one pixel (unit of spatial resolution upon the video monitor) the fringe becomes indistinguishable from the background. Because roughly similar absolute surface areas were studied using the two methods and because the fringes viewed with total internal reflection were viewed at an acute angle to the

surface, the fringe density upon the monitor observed with this method was considerably greater than with the direct reflection method. In addition, fringes viewed with total internal reflection were viewed through as much as two inches of glass while those viewed with direct reflection were not viewed through any medium more optically dense than air except at the surface itself. Comparisons between fringe quality of surfaces viewed directly and surfaces viewed for example through a glass plate of 1/2 inch thickness showed that the fringe quality is diminished significantly if the surface is viewed through an optically dense medium.

Another possible cause of the fringe disappearance considered was that of surface decorrelation (where the optical configuration of the surface is altered). Examination of the fringe movement, however, indicated that the fringes became more and more thin with time and in any case, many such tests performed with the higher resolution holographic technique have revealed no such decorrelation. For this reason, this possibility was rejected.

2.4.4 Conclusions

These initial tests performed upon clear plastic prompted the following conclusions.

(i) Polycarbonate, while a tougher plastic than perspex, is too soluble in swelling agent to be of use in the swollen polymer technique - at least when ethyl salicylate is the swelling agent.

(ii) Perspex is slightly soluble in ethyl salicylate, but careful monitoring of the condition of the surface and subsequent treatment of it as described above should allow this problem to be overcome.

(iii) While perspex scatters and absorbs more light than glass, satisfactory fringes can be obtained using it as a material of construction.

(iv) Removal from, repositioning upon and bolting to a rigid structure of a perspex plate will probably cause substantial internal stresses to be set up in the plate - allowance for natural stress relaxation of the structure over a period of twenty minutes before the run is performed should overcome this problem.

(v) Periodic stripping of polymer coating from the perspex should be expected. Treatment of the surface as described above with subsequent recoating of the surface should result in a coating suitable for experimental runs being obtained.

(vi) Superior fringe quality was observed when direct reflection of light rather than total internal reflection was used.

For these reasons, the optically clear material used was perspex and all surfaces were viewed using direct reflection from a diffusely reflecting back surface.

2.5 Computation of Local Mass Transfer Coefficients Using the Swollen Polymer Technique

Figs. 2.7 and 2.8 show the two optical paths employed in the present experiments using the direct reflection technique. Fig 2.7

shows a system in which the swollen polymer is coated upon the diffusely reflecting metal surface and in which light passes through both the flow stream and the perspex boundary wall opposite the surface. Fig 2.8 shows the same system with the exception that the polymer is coated upon the perspex wall through which light enters the system.

In deriving the relationship for mass transport coefficient in terms of rate of fringe traversal, the following conditions must be fulfilled in addition to those specified by MacLeod and Todd (M5),

(i) The only surface which is translating is that of the swollen polymer (ie the system is free from the effects of creep);

(ii) Where the transferring surface is viewed through the fluid stream the working fluid is optically homogeneous (ie the refractive index of the working fluid must be constant throughout the system - any alteration of it by eg the presence of evaporated swelling agent within the fluid must be negligible)

Note that if the frozen fringe method is used rather than real time fringe observation, the apparatus can be emptied of fluid before the initial and final observations of the transferring surface and condition (ii) need not apply. If, in addition, the other components of the channel are dismantled before these observations of the transferring wall, condition (i) need not apply either.

Assuming conditions can be fulfilled then for the configurations in figs 2.7 & 2.8 the initial length of the optical path through the

perspex wall, the diffusely reflecting wall and back through the perspex wall is given by

$$S_1 = 2(L_1 + nL_2) \qquad \text{eqn (2-1a)}$$

After the polymer has receded by δ, the path length S_2, is given by

$$S_2 = 2(L_1 + \delta + nL_2 - n\delta) \qquad \text{eqn (2-1b)}$$

Therefore the path length difference caused by a surface recession δ, ΔS, is

$$\Delta S = S_1 - S_2 = 2\delta(n - 1) \qquad \text{eqn (2-2)}$$

The number of (black) fringes thereby generated,

$$N = \Delta S/\lambda = 2\delta(n - 1)/\lambda$$

and the rate of surface recession can be expressed by

$$v = \partial\delta/\partial t = \lambda N'/2(n-1) \qquad \text{eqn (2-3)}$$

where $N' = \partial N/\partial t$ and n = refractive index.

The rate of mass transfer of swelling agent from the surface per unit area, M, is given by

$$M = k_m(c_s - c_o) = k_m c_s$$

when the working fluid can everywhere be taken as pure air,

$$= k_m P_s^* m_s / RT \quad \text{eqn (2-4)}$$

where k_m = mass transfer coefficient

P_s^* = vapour pressure of swelling agent,

c_o = concentration of swelling agent in the working fluid.

c_s = concentration of swelling agent at the surface

m_s = 1/(molecular weight) where all units are consistent.

Also, if ϱ = density of swelling agent then

$$M = \varrho \, \partial\delta/\partial t = \varrho v = \varrho\lambda N'/2(n - 1) \quad \text{eqn (2-5)}$$

and hence,

$$k_m = \varrho\lambda RT m_s N'/2(n-1)P_s^* \quad \text{eqn (2-6)}$$

Eqn (2-6) becomes invalid if the vapour pressure of the swelling agent in the working fluid is not negligible. If this is the case then the true concentration gradients will be greater than those assumed, hence the true mass transfer coefficients will greater than those computed. One means of assessing the axial rate of change in vapour pressure is the following scheme.

The rate of change of transfer rate with axial distance from the leading edge by the above derivation is

$$\partial M/\partial x = k_m(x) W P_s / RT \quad \text{eqn (2-7)}$$

where M = mass transfer rate

x = axial distance from leading edge

W = width of the duct

P_s = swelling agent vapour pressure at mass transfer surface

R = Universal Gas Constant

T = temperature (absolute)

hence

$$M(x) = P_s W/RT.\int k(x)\ dx \qquad \text{eqn (2-8)}$$

The concentration of evaporated swelling agent in the fluid stream is the total rate of evaporation divided by volumetric flow rate, ie

$$c_o = P^*/RT = M/Q = P_s W/RTQ.\int_0^x k(x)\ dx$$

$$\Rightarrow \qquad P^*/P_s = W/Q\int_0^x k(x)\ dx$$

Thus at any point x along the surface, the mass transfer rate is given by

$$\partial M/\partial x = k(x)WP_s = k^*(x)W(P_s - P^*)$$

$$\Rightarrow \qquad k^*(x) = k(x)P_s(P_s - P^*) \qquad \text{eqn (2-9)}$$

Eqn (2-8) was evaluated by integration of k(x) with respect to x graphically. The results plotted in figs 2.15, 2.16 & 2.17 were computed using eqn (2-9).

2.6 Measurement of Local Mass Transfer Coefficients in a Two-Dimensional Model Branch.

2.6.1 Apparatus

A two-dimensional symmetric bifurcation was constructed as illustrated in fig 2.4. The upstream channel was 20 cm in length, 4.8cm in height and 0.8cm in width. Both downstream branches had corresponding dimensions of 10cm x 4.8cm x 0.4cm and the angle between the branches was 90°. The base was constructed from aluminium alloy and the top from perspex. The flow dividing wall, one side of the upstream channel and one downstream outer wall were also constructed from aluminium alloy while, as shown in fig 2.5, the other walls were of perspex. Air was used as the working fluid in all experiments. The flow inlet to the channel was a 1/2cm diameter nozzle which connected to an expanding PVC channel as shown. A Layer of cloth was placed across the channel entrance to promote a uniform velocity profile at the entrance. All walls and the upstream feeder channel were fitted flush with each other and were bolted both to the top and to the base of the model, their removal thus being easily facilitated. The whole model was bolted to the optical table of the interferometer (fig 2.9) during each run. To minimise reflection of the light from the aluminium base, a strip of matt-black paper was cemented to this surface. Air flow rate was measured using a rotameter positioned upstream of the model.

2.6.2 Experimental Preparation

The silicone rubber polymer was prepared by mixing thoroughly a 10:1 weight ratio of RTV 615 monomer and catalyst (GEC Silicone Polymer Div.) which was cast over the surface of interest to form a uniform coating approx. 0.3mm thick. (iii) Curing of the monomer was done overnight at 60°C. The polymer was cast simply by (a) pouring the mixture on to the surface of interest, and (b) bursting all entrained air bubbles on the surface.

2.6.3 Experimental Procedure

Before each run, the polymer coating was immersed in the swelling agent (in this case ethyl salicylate) for at least three hours in order to swell it to equilibrium. The mass transferring surface was subsequently removed and allowed to drain before being dried superficially and bolted to the model channel. The channel itself was then positioned upon and bolted to the optical table of the interferometer and a preliminary image of the surface stored electronically. A standing time of 10-15 minutes was then allowed in order to enable the effects of creep in the perspex components to stabilise (these were considered to have stopped when the fringe movement over the screen had ceased). A new image was then stored, air supply through the model commenced, and fringe development observed and recorded upon video-tape.

Three sections of the model were studied: namely the flow dividing wall, the parent wall near the branching point and the outer wall of the daughter branch. In the former two sections it is physiologically realistic to assume that the boundary layer develops from a leading edge incorporated within the section. For example, a new boundary layer must be formed at the point of flow impingement upon a flow dividing wall. In the latter section, however, this is not the case. The boundary layer development upon a continuous wall at a branching point will initiate at a discontinuity upstream from the bifurcation (such as another bifurcation). For this reason when the outer wall was studied a boundary layer was grown upon the upstream section.

2.7 Data for Computation of Mass Transfer Coefficients

Eqn (2-6) is the equation by which local mass transfer coefficients were found. The data for this equation is as follows

Density of ethyl salicylate (liquid) = 1129 kg m^{-3}

Wavelength of Laser Light = 633 nm

Universal Gas Constant = 8.314 J $mol^{-1}K^{-1}$

Temperature (K) was measured at the time of each run.

Number of gram moles per kilogram of ethyl salicylate = 6.024 mol kg^{-1}

The vapour pressure of ethyl salicylate, P_s^* is given in functional form by Kapur and MacLeod (K6) ie

$$P_s^*(mmHg) = \exp(20.318 - 6790/T) \ , \ 291\ K \leqslant T \leqslant 297\ K.$$

Using an EP411 rubber - ethyl salicylate system, Kapur and MacLeod (K8) found little variation of refractive index with volume fraction of swelling agent. On this basis, it was assumed that the same applies to the RTV 615 polymer used in the present experiments.

2.8 Interpretation of Interferometric Fringe Patterns.

As has been discussed above, the consequence of variation of mass transfer coefficient across the surface of a polymer coating upon the variation of change in thickness of that coating is that in regions of high mass transfer coefficient the rate of decrease in coating thickness is greater than it is in regions of low mass transfer coefficient. Thus in a duct which has one wall coated in polymer and

swollen with (eg) ethyl salicylate such that the coating thickness is initially uniform across the surface the greatest rate of recession occurs at the leading edge. When, at the point of maximum mass transfer coefficient (ie leading edge) the surface has receded by a distance corresponding to one half wavelength in optical path length the image of this point becomes black as described above. As recession continues, the optical path length increases eventually by one more half wavelength and the image of the leading edge becomes white again while points downstream, as they reach a distance of recession corresponding to one half wavelength become black. As the coating at these latter points recedes further, these again become white. Thus the real time image produced by the recession of the coating is one of a black fringe evolving from the point of maximum mass transfer coefficient and moving progressively across points of lower and lower mass transfer coefficient. Fig 2.6 shows the image produced by an air jet impinging upon a flat surface. In this case the point of maximum mass transfer coefficient was the point of impingement. All points around the point of impingement were of lower mass transfer coefficient and the mass transfer coefficient decayed with distance from the point of impingement. This process was modelled on the video screen by; firstly the appearance of a black dot at the image of the point of impingement; secondly the growth of that dot into a black solid circle, and thirdly by the development of a white dot within the black circle thus causing the circle to become a black fringe. This process repeated itself throughout the experimental run, giving rise to the image photographed in fig 2.6. Since the points of maximum mass transfer coefficient act as fringe sources, it follows that points of minimum mass transfer coefficient act as fringe sinks.

Fig 2.10 is a photograph of a fringe pattern observed upon the outer wall of the model bifurcation. Three circular fringes were moving towards the images of points of minimum mass transfer coefficient at which they disappeared (rather than away from points of maximum mass transfer coefficient from which they would have evolved).

The consequence of this surface recession is, naturally, that hollows, troughs, peaks and crests develop upon the surface of the coating. If the surface is initially flat then in the experiment in which air impinges upon the surface, a circular hollow develops which becomes several microns deeper with respect to the rest of the surface. Upon the outer wall of the bifurcation at the three points of minimum mass transfer, three peaks develop which become several microns higher than the rest of the surface. Thus the interferometric fringe pattern becomes effectively a contour map of the surface of interest for which peaks and hollows can be identified by whether fringes are moving towards or away from them.

2.9 Results

2.9.1 General Conclusions

Three sets of runs were performed upon the apparatus at six different values of Re each. The areas studied were the flow divider, the outer wall of the daughter branch and the parent branch. With the exception only of points near the apex of the flow dividing wall, it proved possible to observe fringe development in real time by

shining light through both a perspex wall and an air stream and reflecting it from a diffusely reflecting surface. Prior to the runs being performed, it was felt that substantial difficulties in following fringe movement might be encountered due to the oscillation of the fringes in real time caused by minor variations in the refractive index of air. This turned out not to be the case. Prior to the runs being done, it was planned that all measurements of fringe traversal would be done by simple counting of fringes passing a single point upon the video screen. Because, in some cases, substantial three- dimensional flow effects were encountered, this was not always possible because very large "height-wise" variations of transfer coefficient were found as well as length-wise variations. In these cases, fringes were superimposed upon the video screen by adjustment of an object beam mirror and their rate of movement was observed[VI]

Several problems were encountered with the use of the interferometer itself. While the machine was designed to be operated with the minimum of operator skill, it has become apparent subsequently that, with its being a prototype, several of the optical characteristics were somewhat poorly designed. The net effect of this was that only relatively poor contrast was obtainable and it was, therefore, not possible to identify fringes which were reasonably close together. As is discussed below, this meant that it was impossible to identify, for example, fringes eminating from the apex of the flow dividing wall with the result that a complete profile of the variation of mass transfer coefficient over the whole branched region was not possible. Problems were also encountered with the electronics of the machine. Each time that the machine was switched on, a substantial

warm-up time was required - often as long as 2 hours before pre-superimposed fringes upon the screen stopped traversing the screen. During the course of some runs it became evident that fringes generated by the machine were being superimposed upon the those causing recession of the surface and that results obtained were consequently meaningless. Lastly, when the machine was switched on for an excessive period, electrical interference caused a snow pattern to be superimposed upon the screen. For these reasons several of the results were worthless and the runs had to be repeated. This meant ultimately that not as many runs were done as had been envisaged at the start of the work. The rest of the chapter describes those that were.

2.9.2 Adequacy of the Two-Dimensional Model

The purpose of the experimental program was to examine the variation of mass transfer coefficient in a two-dimensional flow branched environment. The configuration used to achieve this end was as described above a 'Y' shaped channel of rectangular cross-section with an aspect ratio of 10 (see fig 2.4). The inlet axial velocity profile was made uniform across the whole cross-section by the mounting of filter cloth at the channel entrance in order to impose a significant uniform pressure drop upon the system. As can be seen in figs. 2.10, 2.11 and 2.12, however, this did not cause an even variation of mass transfer coefficient across the (vertical) transferring wall. In virtually every run performed there were three maxima and four minima at any axial position. Similar, although not identical, results have been obtained previously in unpublished work from studies of mass transfer

in a rectangular duct using the same swelling agent system as the present with holographic interferometry (Lewin 1978). In this work fringes were found generally to have two peaks (rather than three - see fig 2.14) at positions approximately one sixth of the channel width from either side - these peaks corresponding to points of highest mass transfer. Between the peaks slightly lower mass transfer coefficients were observed and there was relatively little variation of k_m with transverse distance. In general Re for these studies was about an order of magnitude higher than those in the present studies and flow could be described as completely turbulent. The fringe shapes observed in these studies suggested that

(a) the velocity profile in the central portion of the duct was completely flat

(b) elevated values of k_m were induced by the vortical nature of the flow near the corners of the ducts

(c) the sharp reduction of k_m with decreasing transverse distance from the corner was caused by the decreasing velocities expected in this region with decreasing distance from the corner.

While the present set of experiments were conducted in a domain of different geometry and while flow was generally only partially disturbed, conclusions (b) and (c) above hold for them also. The presence of secondary flows near the corners of the channel walls and top suggests that flow in the channel is not developed laminar flow but is disturbed. Such mass transfer characteristics were found in the upstream section as well as in the flow dividing and outer walls of the downstream section hence their presence cannot be related solely to the kind of three-dimensional secondary flows associated with branched flow discussed in chapter 1. No examination was conducted with a

view to determining whether or not such secondary flows were to be found throughout the flow domain as well as the corners, but the upstream flow channel was designed with a view to removing all entry length effects, hence it was assumed that flow was well developed near the branch point except at top and bottom corners. Because a centre-line peak appears in all runs performed, conclusion (a) appears inappropriate. The presence of this peak suggests that the velocity profile in the vertical direction was not flat but, given its symmetry, perhaps parabolic. It was not felt, however, that this velocity variation was, in any of the tests, very significant. Fig 2.13 for example is a photograph of fringes caused by mass transfer of swelling agent in the upstream section of the branched channel with Re = 1500. The three main fringes in this figure are, from right to left, the fifth, sixth and seventh respectively to have passed over the screen from the left hand side. It can be seen that in this figure the maximum transverse variation in fringe number at any point within the central portion is one, which corresponds to a maximum transverse variation of k_m of c. 25%. Upon this basis it was reasoned that the vertical variation of axial velocity was unlikely to be substantially greater than 25% and for the purposes of k_m measurement, therefore, the centre-line peak fringes were taken to be representative of the two-dimensional axial variation of k_m.

A major problem encountered with measuring rates of fringe traversal of the image was that in regions with a strong variation of k_m with distance (in any direction) fringes became very close to one another and upon the video screen, which was of relatively low resolution, their identification became extremely difficult. This problem

could have been overcome by use of a shorter focus imaging lens and with suitable adjustment of aperture and beam intensity, but with the general purpose commercial instrument employed, such adjustment was impossible. For this reason it was not possible to measure accurately mass transfer coefficients upon or near to the apex of the flow dividing wall and would not have been possible to measure such coefficients accurately in the region adjacent to the boundary.

This effect is demonstrated in fig 2.13. This photograph depicts mass transfer fringes in the upstream section of the channel with Re = 1500. In the centre of the photograph where transverse gradients of k_m are low, fringes are well defined while at both the bottom and, and particularly at the top, fringes are decidedly less distinguishable due to the lack of resolution of the video monitor, or more probably, of the whole system.

2.9.3 Variation of Sh with Position

The results plotted in figs 2.15, 2.16 and 2.17 were computed using eqn (2-9). From this equation it is obvious that the gas phase concentration of swelling agent increases with increasing mass transfer coefficient and decreasing volumetric flow rate etc. The highest mass transfer coefficients occurred upon the flow dividing wall, thus the highest concentration of swelling agent was found to occur at Re = 160 (the lowest Re tested). The maximum vapour pressure in the stream was found to be 70% of that at the mass transfer surface at the exit from the channel. When Re = 1900, this figure was 7%. Thus

the effects of increase of swelling agent vapour pressure often cannot be ignored in systems of similar dimensions and flow-rates as the present and the treatment of the coefficients measured directly as is described by eqn (2-9) is necessary to correct the results obtained using eqn (2-6).

Figures 2.15, 2.16 and 2.17 depict variation of mass transfer coefficient with local position for a variety of Re at three different parts of the experimental domain; namely the flow dividing wall, the upstream wall and the outer wall of the channel downstream of the branching point. As can be seen in fig. 2.15, k_m decreases monotonically with axial distance from the apex of the dividing wall. This is caused directly by the monotonic growth of the concentration boundary layer with distance from the leading edge of the mass transferring region which in this case was the apex of the flow dividing wall. Such an effect implies that if all other mass transferring effects are neglected, the flow dividing wall near the apex is not likely to be very as susceptible to hypoxic conditions as other regions because the mass transfer coefficients in that region are comparatively high. This result is supportive of those obtained by Friedman and Ehrlich (F10) in their computational studies and is one which has been used in the past by Caro et al (C2) to support their view that high macromolecular transport transport from the wall in this region causes retardation of atherosclerosis.

A similar result occurs when mass transfer in the upstream section of the system is considered. In this case, as with the flow dividing section, the mass transferring leading edge is well defined and is

coincident with that for momentum transfer. Thus, again, Sh decreases with axial distance from the leading edge.

The rates of growth of momentum boundary layers in each region are affected by different flow features. In the upstream section of the channel the feed velocity profile is approximately flat. This causes a high shear stress at the channel entrance which diminishes with distance as the momentum boundary layer grows. In the flow divider region the entry flow is likely to be reasonably well developed (see chapter 3 - computational work) but the velocity profile is strongly skewed towards the dividing wall. Thus centrifugal forces are liable to restrict boundary layer growth along this wall. In addition, the channel was so designed that the mean velocity in each of the daughter branches was equal to that in the parent branch. Thus since their widths are one half of that of the parent branch, the mean shear stress in the daughter branches would be expected to be greater than in the parent branch even without the skewed velocity profile.

For these reasons it should be expected that both the momentum and the mass transfer boundary layers develop more "slowly" axially upon the flow divider than in the upstream section and correspondingly, that mass transfer coefficients will be higher upon the flow dividing wall. While this is impossible to assess precisely due to the difficulties of measuring Sh in the region of the leading edge, it does appear generally to be the case.

The situation in the third part of the flow domain - the outer wall of the daughter branch - is somewhat different. It is the only

region of the three which has no mass transfer leading edge and for this reason its mass transfer characteristics are substantially more dependent upon flow conditions in other regions of the domain than are those of the upstream and flow dividing walls. Furthermore, because the domain is essentially two-dimensional, there is no reason why the three-dimensional secondary flows observed by Brech and Bellhouse (B4) in this region of their three-dimensional channel should occur. It seems likely that flow separation downstream of the branching point should occur, particularly in view of the fact that the upstream and downstream walls of the model meet at a sharp point.

The results, illustrated in fig. 2.17, indicate that this is the case. As can be seen Sh increases with distance from the sharp corner upon the outer wall at all values of Re tested. Only at the highest Re tested (Re=1330) is the increase of Sh with distance not monotonic. In this case Sh reaches a minimum value close to the corner followed by a subsequent increase with distance away from this point.

From above, these results imply that the concentration boundary layer is thickest near the branch point upon the outer wall and that it decreases in thickness with distance from that point. This is consistent with there being flow separation and reversal in this region as illustrated in fig.2.18. Separation causes low reverse velocities in the region immediately distal to the branch point. Transport in this separation "bubble" is more strongly influenced by diffusion than in others as the convection term is weak. Further downstream, boundary velocities increase as the velocity profile skews less towards the dividing wall, hence the role of convective transport becomes more

important and therefore Sh increases. Beyond the point of reattachment the influence of convection near the boundary decreases axially and, correspondingly, Sh decreases. In the present studies, however, this point of reattachment was not observed and was presumed to be beyond the end of the channel.

This whole effect of skewing of the velocity profile is modified to some extent by the rate of boundary layer growth in the upstream section of the channel. When Re is low the upstream boundary layer grows relatively quickly before the corner and subsequently decreases with distance downstream from this point. If Re is high, however, boundary layer growth over the length of the upstream section is limited, with the net result that the boundary layer continues to grow distal to the corner for a distance dependent upon Re before reducing in thickness with distance downstream up to the point of reattachment of flow. This is why a minimum Sh was found for the highest Re examined.

A preliminary experiment demonstrated the effect of there being no boundary layer growth in the upstream section of the channel. With this configuration it was found that Sh decreased sharply with distance along the whole length of the outer wall for all Re, thus confirming that in this region the boundary layer will only diminish axially if it is sufficiently thick at the corner.

2.8.4 Comparison of Relative Magnitudes of Sh in the Various Regions under Study

By far the most consistent results were obtained for mass transfer measurements upon the flow dividing wall. In this case (fig.2.15) Sh increased monotonically with Re in all axial positions upon the wall. Sh decayed monotonically with distance from the apex in all cases and, particularly when Re was high, there appeared to be a very sharp decay in Sh with distance in the region adjacent to the apex. As will be discussed in chapters 3 and 4, these results are very similar to those predicted by the computational model.

Such consistency was not found for mass transfer coefficients measured upon the perspex outer wall. In the upstream section Sh decayed linearly with distance from the entrance for all Re. The curve for Re = 1500 is closer to that for Re = 1000 than would be expected from the apparent variation of Sh with Re for most other values of Re.

In the downstream section the curves for Re = 1500 and 1900 were separated by a sizeable gap from the curves for smaller Re.

Figs. 2.16 and 2.17 can be used to check for consistency of results between the separate branch regions. Because the concentration boundary layer in the upstream section is still apparently growing with distance at the branch point and because boundary layer thickening would be expected downstream from the branch for reasons discussed above, lower Sh would be expected in the region near to but downstream from the branch than in that upstream. This was found to be the case for all lower values of Re (ie Re < 1500). Each of the curves for the lower Re upon the downstream outer wall, if projected

to the corner (or axis) shows Sh to be very similar to, but less than, that for the upstream wall.

For these reasons it was felt that the results presented were reasonably consistent with each other and - qualitatively at least - with those results which would be expected for a physiological domain of geometric similarity given similar Sc for the systems.

Chapter 3

Analysis of Flow and Mass Transport in a Symmetric Branch Using the Finite Element Method

3.1 Purpose of the Numerical Work

The experiments described in chapter 2 were performed in order to demonstrate a technique by which the basic mass transferring characteristics of the arterial lumen may be predicted. As is discussed in chapters 1 & 2, a major problem with modelling oxygen transport within the arterial system is that while, mechanically speaking, blood behaves like a homogeneous fluid, in terms of oxygen transport, it is non-homogeneous. With this experimental model the system is treated as being homogeneous. The validity of the present experimental model is also limited by the fact that while the Schmidt number (Sc) of the air-ethyl salicylate system is about 2.7, that of the oxygen-blood system is of the order of 2800. Thus the model fails to simulate accurately the relative degrees of importance of convective and diffusive transport in the physiological system. This shortcoming could have been overcome to some extent by the use of water as the working fluid (found to be satisfactory by Kapur and MacLeod K5) as this system has a value of Sc of about 1100, but difficulties with the interferometer resulted in delays and insufficient time for this logical extension to the work to be done.

In order to assess what effect the variation of Sc has upon the mass transport characteristics of the system, it was decided that in

addition to the experimental program, a numerical analysis should also be performed which would model the experimental system. With this study, it should be possible to observe, and perhaps correlate (via some exponential or quadratic function) the variation of Sherwood number (Sh) with Sc for any value of Re of physiological significance. In this way the validity of the mass transport behaviour predicted by the experimental program could be assessed and an appreciation of how the experimental results may be used to predict behaviour in the physiological system obtained.

Because the computational scheme was intended to simulate the experimental flow situation rather than the physiological system directly, the non-linear convection term describing the haemoglobin-oxygen reaction introduced by both Back et al (B16) and by Schneiderman et al (S11, S9), was neglected. Thus the system studied resembled most closely that modelled by Friedman et al (F4) with the major exception that, in this study, the effects of pulsatility were ignored and the axial diffusion term was included.

3.2 Choice of Solution Technique

The flow system under consideration is illustrated in fig 3.1. The solution of the full Navier-Stokes equations and the continuity equation (expressed in dimensionless form in eqns 3-1)

$$\underline{U}.\nabla\underline{U} = -\nabla P + Re\nabla^2\underline{U} \qquad \text{eqn (3-1a)}$$

$$\nabla \underline{U} = 0 \qquad \text{eqn (3-1b)}$$

is impossible in general by analytical techniques and for the system illustrated in fig. 3.1, substantial transverse and axial velocity variation occurs, so that simplification to a system of simultaneous ordinary differential equations is also impossible. The only other feasible method of solution is by use of some numerical method for partial differential equations such as the finite difference or finite element methods. Both of these methods require discretization of the flow domain into a locus of nodes, formation of a system of simultaneous algebraic equations and subsequent solution of this system. The study of arterial flow using both methods is well documented (B2,D2,D5,E5,F4,G9,K3,O2,O3,R12,T8) as is discussed in chapter 1. Both techniques have been applied to studies of flow domains similar to that under present examination (finite difference - F4, finite element - K3). The study of Navier-Stokes flow using the finite difference method, however, entails a mesh of rectangular nodes being set up. This type of mesh is inconvenient for fitting to a domain such as that in fig.3.1 and, in practice, it is often better to transform the coordinates to form a rectangular domain for solution. This problem does not arise in the finite element method which is altogether more suited for modelling flow in domains of awkward shape because the elements formed from the discretized domain can be of virtually any shape and orientation. It is also worth noting that several authors (eg Oden and Wellford 05) have found that the finite element formulation of the Navier-Stokes equations is rather better conditioned than that obtained using the finite difference formulation. For this reason the finite element approach was used to evaluate the equations.

3.3 Choice of the Equation Formulation

The Navier-Stokes equations can be expressed in any of several forms, three of which are (a) stream function formulation, (b) vorticity/stream function formulation, (c) velocity/pressure formulation. Each of the formulations has been tested using the finite element method and each appears to be a powerful method in its own right. In the present work the velocity/pressure formulation was used for the following three reasons.

(i) With some mathematical manipulation the equations can be made only first order in any independent variable. This means that the element interpolation functions (see below) need be made only quadratic. The other formulations both have second order terms which cannot be reduced further.

(ii) The quantities which were under examination in this study were (a) vorticity, (b) stream function (c) concentration and (d) concentration gradient. By solving the equations for the velocities directly, (a), (b) and (c) could be evaluated by solving a system of linear equations which were expressed in terms of velocity, while (d) could then be solved directly from (c). If other variables were evaluated first then the velocities would still need to be found before the concentration profile could be found, thus introducing an extra source of error to the process.

(iii) The velocity/pressure formulation appears to be better for finite element discretization of the flow domain than the

vorticity/stream function formulation (G9).

3.4 Development of the Navier-Stokes Equations for Solution

The domain of fig. 3.1 is discretized into quadrilateral elements (eg see fig.3.2) using the "PAFEC" structural analysis package. Each element contains (see fig. 3.3) eight nodes, each of which has axial and transverse velocity components (both unknown) associated with them and four of which have an unknown pressure associated with them. It is assumed that the variation of velocity and pressure across the element can be defined respectively in terms of the nodal velocities and pressures by the relationships,

$$U = \Sigma\, N_i(\xi,\eta)\, U_i \quad , \; i = 1\text{-}8 \qquad \text{eqn (3-2a)}$$

$$V = \Sigma\, N_i(\xi,\eta)\, V_i \quad , \; i = 1\text{-}8 \qquad \text{eqn (3-2b)}$$

$$P = \Sigma\, M_j(\xi,\eta)\, P_j \quad , \; j = 1\text{-}4 \qquad \text{eqn (3-2c)}$$

where [N] is a quadratic vector interpolation function, [M] is a linear vector interpolation function and U_i, V_i & P_j are respectively the velocities and pressure at nodes i and j respectively. Both functions are expressed explicitly in terms of local coordinates (ξ,η) and are arranged so that at node i, $N_i=1$, $M_i=1$, while $N_j=0$ and $M_j=0$, $(j\neq i)$ (ie at node i $U = U_i$). Choice of interpolation functions reflects the relative rates of variation of the independent variables in the Navier-Stokes equations. Thus velocity, which is 2^{nd} order in X and Y,

is defined by quadratic functions, etc.

Within each element the global coordinates, X and Y, can also be expressed in terms of local coordinates viz

$$X = \Sigma\ N_i(\xi,\eta)\ X_i\ ,\ i = 1\text{-}8$$

or,

$$X = \Sigma\ M_j(\xi,\eta)\ X_j\ ,\ j = 1\text{-}4$$

and likewise for Y. It follows that the local derivatives of U, V, P, X and Y can be expressed in terms of ξ and η ie

eg

$$\partial U/\partial \xi = \Sigma\ [\partial N_i/\partial \xi]\ U_i$$

and hence the global derivatives of [M] and [N] can be found easily within the element in terms of the local coordinates. Substituting eqns 4-2 into eqn (4-1) and integrating across the two-dimensional domain (with respect to dA) gives

$$\int \Sigma\ [(Re.U^*\ N_j - {}^2N_j)\ \{U_j\} + \Sigma\ M_l P_l)]dA \approx 0 \qquad \underline{\text{eqn (3-3a)}}$$

$$\int \Sigma\ N_j U_j\ dA \approx 0 \qquad \underline{\text{eqn (3-3b)}}$$

where U^* is the velocity at (ξ,η) computed using the estimated nodal velocities.

Because eqns (3-2) are not exact definitions of the variation of the independent variables across the element, their substitution into

eqns (3-1) and subsequent integration (eqns 3-3) across the element will yield only approximate solutions.

If, however, the integrands are multiplied by a Galerkin weighting function (see Huebner H11), then these integrals can be made exactly equal to zero. From Taylor and Hughes (T9), these weighting functions are taken to be,

(i) N_i for eqn (3-3a)

(ii) M_i for eqn (3-3b)

Equations 3-3a and 3-3b become

$$\int \Sigma[(Re.N_i U^* N_j + N_i \nabla^2 N_j)\{U_j\} + \Sigma M_l P_l]dA = 0 \quad \underline{\text{eqn (3-4a)}}$$

$$\int \Sigma[M_i N_j]dA \{U_j\} = 0 \quad \underline{\text{eqn (3-4b)}}$$

Using Green's theorem, the viscous term in eqn (3-4a) becomes

$$\int N_i \nabla^2 N_j dA = -\int N_i N_j dA - \int N_i \partial N_j/\partial n \, dS$$

where the latter term is a surface integral which is equal to zero over the whole surface of the domain.

Separating eqn (3-4a) out into the 'X' and 'Y' direction force balance equations, the system can be described by the simple matrix

$$\begin{vmatrix} A_{11j} & A_{12j} & 0 \\ A_{21j} & 0 & A_{23j} \\ 0 & A_{32j} & A_{33j} \end{vmatrix} \begin{vmatrix} U_j \\ P_j \\ V_j \end{vmatrix} = 0 \quad \text{eqn (3-5a)}$$

where

$$A_{11j} = A_{33j} = \int \Sigma \, Re[N_i U^* \partial N_j/\partial X + N_i V^* \partial N_j/\partial Y] \, dA + \int \Sigma \, [(\partial N_i/\partial X)(\partial N_j/\partial X) + (\partial N_i/\partial Y)(\partial N_j/\partial Y)] \, dA \quad \text{eqn (3-5b)}$$

$$A_{12j} = \int \Sigma N_i \partial N_j/\partial X \, dA \quad \text{eqn (3-5c)}$$

$$A_{21j} = \int \Sigma \, M_i \partial N_j/\partial X \, dA \quad \text{eqn (3-5d)}$$

$$A_{23j} = \int \Sigma \, M_i \partial N_j/\partial Y \, dA \quad \text{eqn (3-5e)}$$

$$A_{32j} = \int \Sigma \, N_i \partial M_j/\partial Y \, dA \quad \text{eqn (3-5f)}$$

This is the system of equations which is solved for velocity and pressure.

3.5 Solution Procedure

From eqn (3-5a) it can be seen that each eight noded element has twenty unknowns (four pressure, eight axial and transverse velocities) and that a 20 x 20 square matrix (or element stiffness matrix - so called because the finite element technique was originally devised to deal with structural problems) can be multiplied by the element velocity-pressure vector to give zero. Each local element node is identified by a local node number which corresponds to a specific global node number. Thus each component of the

matrix can be added to the equivalent component of the system stiffness matrix and hence, by integrating over all of the elements, the system stiffness matrix can be constructed. When a convergent solution of velocities is obtained, the global velocity-pressure vector, multiplied by the system stiffness matrix gives zero.

The solution of the equations consisted of the following steps,

(i) estimating global velocity data.

(ii) using the estimated velocity data to construct the system stiffness matrix.

(iii) solving the system of equations for the global velocity-pressure vector.

(iv) checking for convergence.

(v) either stopping if convergence is achieved, or using the new velocity-pressure data to obtain an improved estimate of the solution.

The initial estimates for velocity were zero. Thus the first solution corresponded to the Stokes flow solution (Re = 0). Subsequent computations were for non-linear equations and were solved iteratively. Before solving the system of equations the known velocities and pressures (initial and boundary conditions) were removed from the left hand side to the right and the equations corresponding to these variables discarded. The reduced system was then solved directly using a sparse LU decomposition and Gauss elimination technique (National Algorithms Group routines F01BRF, F01BSF and F04AXF). The solution was assumed to have converged satisfactorily when the maximum percentage difference between new and old data was less than 1%. The

convergence scheme used was Picard iteration (successive substitution), a method which was found satisfactory by Gartling and Becker (G10 & G11).

3.6 Formulation and Solution of the Other Equations

As stated in section 3.3, velocity-pressure data were secondary to the direct requirements of this study but, nevertheless, served as the means by which the desired quantities (concentration, stream function and vorticity) could be obtained. The equations by which these were obtained were the following

$$Pe[U\partial C/\partial X + V\partial C/\partial Y] = \partial^2 C/\partial X^2 + \partial^2 C/\partial Y^2 \qquad \text{eqn (3-6)}$$

$$\partial\psi/\partial Y = U \qquad \text{eqn (3-7)}$$

$$\omega = \partial U/\partial Y - \partial V/\partial X \qquad \text{eqn(3-8)}$$

The rate of mass transfer from the surface per unit area, m, is given by

$$m = k(C_s - C_o) = D(\partial C/\partial n)_{wall}$$

where C_s is wall concentration, C_o is bulk flow concentration = 0.

This implies that

$$k = D/C_s\ [\partial C/\partial n]_{wall} = D/L[\partial C/\partial N]_{wall}$$

where L is the characteristic length of the system, N = n/L.

and therefore that

$$[\partial C/\partial N]_{wall} = kL/D = Sh = \text{Sherwood number}$$

Therefore, by computing the non-dimensionalised concentration gradient at the wall, the local Sherwood number was evaluated. The maximum concentration gradient at any point is oriented in the direction normal to the concentration contour (see fig. 3.4). The gradient of this contour at any point can be found by making C and X the independent variables and then evaluate $\partial Y/\partial X$ using

$$\partial Y/\partial X = (\partial C/\partial X)/(\partial C/\partial Y) \qquad \text{eqn (3-9a)}$$

The normal to this contour has a gradient of $-(\partial X/\partial Y)$ whose angle to the axial direction is $\tan^{-1}(-\partial X/\partial Y)$. The concentration gradient in this direction is given by

$$\partial C/\partial N = (\partial C/\partial X).(\partial X/\partial N) + (\partial C/\partial Y)(\partial Y/\partial N)$$

which gives

$$\partial C/\partial N = \partial C/\partial X \; . \; \cos(\tan^{-1}(-\partial X/\partial Y))$$
$$- \partial C/\partial Y \; . \; \sin(\tan^{-1}(-\partial X/\partial Y)) \qquad \text{eqn (3-9b)}$$

The Sherwood number is found when this equation is evaluated upon the boundary.

As with the variables of the Navier-Stokes equations, the variation of C, ψ and ω over an element was assumed to be described by

equations similar to eqns (3-2). In these cases, all variables were assumed to vary quadratically over an element. All terms in eqns 3-6, 3-7 and 3-8 were then multiplied by the weighting function as described in section 3.4. Green's theorem was applied to eqn (3-6) and all three equations were then integrated over the domain. These processes left the following equations

$$\Sigma \int [Re.Sc.N_i(U^* \partial N_j/\partial X + V^* \partial N_j/\partial Y) + (\partial N_i/\partial X)(\partial N_j/\partial X) + (\partial N_i/\partial Y)(\partial N_j/\partial Y)]dA \{C_j\} = 0 \qquad \text{eqn (3-10)}$$

$$\Sigma \int [N_i \partial N_j/\partial Y]dA \{\psi\} = \Sigma \int N_i N_j]dA \{U_j\} \qquad \text{eqn (3-11)}$$

$$\Sigma \int [N_i N_j]dA \{\omega_j\} = \int N_i \Sigma [U_j.\partial N_j/\partial Y - V_j \partial N_j/\partial X]dA \qquad \text{eqn (3-12)}$$

$$\int N_i N_j \, dA \{C_{xj}\} = \int [N_i \partial N_j/\partial X]dA \{C_j\} \qquad \text{eqn (3-13)}$$

$$\int N_i N_j \, dA \{C_{yj}\} = \int [N_i \partial N_j/\partial Y] \, dA \{C_j\} \qquad \text{eqn (3-14)}$$

where $C_{xj} = \partial C_j/\partial X$ and $C_{yj} = \partial C_j/\partial Y$,

all of which reduced to the basic matrix equation

$$[A]\{\underline{x}\} = \{\underline{b}\}$$

which was solved directly for the respective variables.

3.7 Boundary Conditions

3.7.1 Navier-Stokes Equations

Fig. 3.5 illustrates the flow domain and boundary conditions for the Navier-Stokes equations. The zero velocity boundary condition was applied upon all boundary walls, ie flow dividing wall, upstream and outer downstream walls. In addition, both the flow inlet and the centre-stream (y=0) transverse velocities were set to zero. In the experimental apparatus, a long upstream section of channel fed the bifurcation region. The velocity profile was made to be virtually flat at the entrance to this region by the use of fine-mesh muslin cloth. The rate of boundary layer growth therefore depended upon the value of Re. The profile of axial feed velocity was, for this reason, treated in two different ways.

(i) it was treated as fully developed laminar flow.

(ii) an algebraic equation was used to describe the boundary layer growth.

This is discussed in sect. 3.8.1.

Because the variation in pressure is wholly dependent upon the local viscous and inertial forces, it was not necessary to specify a pressure boundary condition. When no nodal pressures were specified, the magnitudes of local pressure gradients were reasonable, the absolute values of the normalised pressures generated by the

computational process were of the order 10^{13}. For this reason, one nodal pressure was specified to equal zero and the values of all other pressures computed were based upon this value.

3.7.2 Stream Function

Fig. 3.6 illustrates the boundary conditions for the stream function. The streamline upon the centreline (y=0) - flow dividing wall was set to equal zero. The inlet velocity conditions were chosen so that their integral with respect to Y gave unity which was therefore the stream function value upon the upstream - outer wall boundary.

3.7.3 Vorticity

Vorticity, like pressure, is a term whose variation is wholly dependent upon local velocity conditions and does not require boundary conditions. The domain depicted by fig.3.6, however, forms one half of a symmetric bifurcation in which the velocities, pressures etc can be predicted by symmetry. By symmetry, therefore, there can be no rotation of fluid upon the centre-stream (ψ=0), and hence, no vorticity. Thus upon the centre-stream the vorticity was set to equal zero.

3.7.4 Concentration

Fig. 3.6 illustrates the boundary conditions for the concentration profile. Essentially, upon each solid boundary, the concentration was specified as being unity. As with the Navier-Stokes equations, two sets of initial conditions were considered. When the feed velocity was described by Poiseuille flow, the initial conditions were specified to equal zero. When, on the other hand, the momentum boundary layer growth model was used, a parallel concentration boundary layer growth model was applied. This is discussed in section 3.8.2

3.7.5 Concentration Gradient

This quantity is wholly dependent upon the local variation of concentration and therefore needs no specified boundary conditions. Because flow and concentration are defined to be symmetric the concentration gradient could have been defined as zero at Y = 0, however.

3.8 Initial Conditions

3.8.1 Axial Velocity

(a) As stated in section 3.7.1, two sets of initial conditions were applied to the axial velocity. The first condition tested was fully developed Poiseuille flow which is described by the equation

$$U = 1.5(1 - Y^2) \qquad \text{eqn (3-15)}$$

This condition satisfies the stream function boundary condition upon the outer wall ($\psi=1$, $Y=1$).

(b) The latter initial condition was obtained by considering flow in the entrance region of the experimental apparatus. The velocity profile was considered initially to be flat, with a velocity (normalised with respect to mean velocity) of unity (fig. (3.7)). Downstream of the entrance a momentum boundary layer of thickness δ_m developed in which the velocity profile could be expressed as

$$U/U_c = 2[(1-Y)/\delta_m)] - [(1-Y)/\delta_m]^2 \qquad \underline{\text{eqn (3-16)}}$$

where U_c = the magnitude of the flat velocity profile in the centre of the stream.

Thus U_c changed with distance from the leading edge of the momentum boundary layer and could be taken as varying only with X. Eqn (3-15) shows that between the entrance and the point where fully developed flow is assumed, U_c increases in value from 1 to 1.5. Following Sparrow's formulation (in K9 ,p240), U_c can be expressed as a function of X. Using a characteristic length of one half channel width, as in the present study, this relationship becomes,

$$\partial X/\partial U_c = 0.3\ Re\ (9-16/U_c+7/U_c^2)$$

Applying the initial conditions, $U_c = 1$, $X = X_o$, yields

$$X - X_o = 0.3\ Re\ [9(U_c-1) - 16\ \log_e U_c + 7(1-1/U_c)] \qquad \text{eqn (3-17)}$$

The solution of eqn 3-17 was done using a secant search. The volumetric throughput of the channel was found by integrating the velocity with respect to Y. By equating this integral to unity (the normalised volumetric throughput) an expression for δ_m was obtained

$$\delta_m = 3(1 - 1/U_c) \qquad \text{eqn (3-18)}$$

Using this value of δ_m, eqn 3-16 was evaluated to give a velocity profile which was related both to axial distance and to Re.

3.8.2 Concentration

(a) When the Poiseuille flow model was used the initial conditions set for concentration were simply

$$C(X=X_o) = 0$$

and the mass transferring boundary layer was assumed to start at the entrance to the numerical domain.

(b) When the entry-length flow condition was used, it was assumed

that both the momentum and concentration boundary layer leading edges were coincident as is the case with the experimental apparatus. Neglecting axial diffusion (a justifiable assumption in a straight conduit distant from the leading edge such as the experimental apparatus) then if $\delta_c < \delta_m$ where δ_c is the concentration boundary layer thickness, (ie if Sc > 1) eqn (3-6) reduces to

$$\partial/\partial X \int_o^{\delta c} UC \, dY = k$$

where k = mass transfer coefficient. This equation, expressed in dimensionless form, is the following,

$$Pe \; \partial/\partial X \int_o^{\delta c} UC \, dY = Sh \qquad \underline{\text{eqn (3-19)}}$$

where Sh = Sherwood number

Fitting a 3rd order polynomial approximation to C(Y) such that C(Y=0) = 1, $C(\delta_c) = 0$, $\partial^2 C/\partial Y^2(1) = 0$, $\partial C/\partial y(\delta_c) = 0$ yielded

$$C(Y) = 1 - 1.5(Y/\delta_c) + 0.5(Y/\delta_c)^3 \qquad \underline{\text{eqn (3-20)}}$$

Together with eqn (3-16), this expression was substituted into eqn (3-19). Eqn (3-19) contains two unknowns, δ_c and Sh, both of which can be expressed as functions of X. To solve eqn (3-19), another expression in terms of either one of or both of these variables was necessary.

The equation relating convective and diffusive heat transfer in fluid flow is identical in form to eqn (3-6) - the only difference being

that temperature is used instead of concentration and thermal conductivity is used instead of diffusivity. The thermal system is hence completely described by Re and Pr (Prandtl number, analogous to Sc) and the normalised heat transfer coefficient Nu (Nusselt number) is thus directly analogous to Sh. Therefore a study of heat transfer in the entrance region of a straight channel with constant wall temperature is directly analogous to the study presently under consideration. Such a study has been performed by Bhatti and Savery (B20) who developed a semi-analytical solution to the problem. They produced solutions for local Nu as a function of X/Re for $0.01 \leqslant Pr \leqslant 10{,}000$, which covers completely the range of values used in the present study.

When their definition of X was converted to that of the present study then in the range $1 \leqslant Pr \leqslant 10{,}000$, their results could be described by the following relationship

$$Sh = 0.629(X-X_o)^{-0.404}\ Re^{0.404}\ Sc^{0.336} \qquad \text{eqn (3-21)}$$

When this expression was substituted into eqn (3-19) together with eqns (3-20) and (3-16) and the initial condition $\delta_c(X=X_o) = 0$ was applied, upon integration the following non-linear expression was obtained in terms of δ_c

$$U_c[\delta_c^2/5\delta_m - \delta_c^3/24\delta_m^2] = 1.035\ Re^{-0.596}\ Sc^{-0.664}\ (X-X_o)^{0.596} \qquad \text{eqn (3-22)}$$

which was solved using the secant search routine as before. Eqn (3-20) was then evaluated for C(0,Y).

3.9 Stability of the Computational Scheme

The equations were solved for the linear system (Re=0) and the resulting nodal velocity-pressure data were stored computationally. Solutions for non-zero values of Re were obtained by use of successive substitution using the initial values of nodal velocity/pressure data (for Re=0) as initial estimates. When all of the values of the current iteration differed by <1% from those of the previous iteration, the solutions were considered to be converged and the nodal velocity/pressure data were stored. When solutions for any value of Re were required, data from the solution corresponding to the previous highest Re were used for the starting estimate.

This iterative technique was found to be successful when Re $\leqslant$ 300. The required number of iterations for convergence increased with Re and also with coarseness of mesh. Thus if a more refined mesh has been used then converged solutions for velocity would have been possible for higher values of Re. Because this would have required substantially more storage space and computer processing time and also because mean coronary Re is generally less than 300 this procedure was not adopted. Successful convergence was obtained in 2 - 3 iterations when Re $\leqslant$ 100, a number which increased to about 15 when Re = 300. Thus while the scheme was not found to be as successful as was claimed by Gartling and Becker (G10) who found that 5 iterations sufficed even when Re = 10000, it was found adequate for the present problem.

3.10 Results

The data generated by the iterative scheme were used as described in sections 3.6 - 3.8 to compute corresponding vorticity, stream function, concentration and steepest concentration gradient data. Computer graphics facilities were then used to plot streamlines, concentration contours and variation of both boundary vorticities and Sherwood numbers.

3.10.1 Inlet Conditions

Fig. 3.8 illustrates the radial variation of the normalised axial velocity for various values of Re at the entrance to the domain as defined computationally. As can be seen the velocity profile at the inlet to the computational upstream section of the channel is parabolic for each Re used with the exception of Re = 300. In the latter case the flat profile exists only in a very narrow section at the centre of the channel and elsewhere the profile is parabolic. The use of eqns 3.16 and 3.18 therefore had very little effect upon either the flow behaviour or the computed mass transport behaviour within the domain.

The influence of concentration boundary layer upon the domain inlet conditions was substantially greater than that of momentum boundary layer. Figs 3.9a and 3.9b show the variation of concentration with transverse distance from the boundary at X = 0 for Re = 50 & 300 and Sc = 2.7, 50, 300, 1500 & 2800. As can be seen in fig. 3.9a, when Re=50 the inlet concentration becomes non-zero at a point close to the centre of the channel when Sc = 2.7 (ie Pe=135) and that the

transverse distance of this point from the centre increases with Sc. The concentration profile illustrated in fig. 3.9b demonstrates that this distance increases also with Re. Such results suggest that accurate simulation of the inlet conditions to the experimental domain may, in this instance, be of much greater importance in describing transport behaviour than that of the velocity profile at the inlet. If the inlet concentration is assumed to be zero except upon the boundary then the finite element mesh required would have to be exceedingly fine near the boundary in order that the boundary layer growth be described accurately when Re and Sc are high. Because boundary concentration gradients are very high at a leading edge, if the mesh is not sufficiently refined, then it is possible that concentrations at nodes adjacent to the boundary will equal zero. Such an effect means that the interpolation functions used to describe variation of concentration within the boundary elements will be highly inaccurate and that very misleading concentration gradients will be obtained. This effect was observed with some of the coarser meshes examined and to some extent was observed in the most refined mesh used (when Pe was high) when the inlet concentration was set to zero. It was altogether less apparent when eqns 3.16 3.17 and 3.18 were used to describe the inlet conditions.

3.10.2 Nature of Flow in the Domain.

Fig. 3.10 is a computer generated plot of predicted streamlines through one half of the symmetric bifurcation for Re=250. The streamlines are dimensionless, are set to zero upon the flow dividing

wall and centreline and are set to unity upon the outer wall. The streamlines at the entrance to the domain are widely spaced upon the outer wall and closely bunched at the centre (ie consistent with there being developed flow at the inlet). At the exit the streamlines are approximately symmetrically spaced about the centre of the stream, are again bunched in the centre and are widely spaced at the boundaries - corresponding again to developed flow in the stream. The streamlines appear most poorly defined in the region of the branching point where there is, mathematically speaking, a discontinuity (ie a bend of infinite radius of curvature) upon both boundaries. Whilst this infinitely sharp bend configuration could not be accommodated in an analytical study, with the current numerical approach the boundary shape is defined only approximately in any case and could therefore be taken as curved (hence continuous). The rapid change in flow conditions in this region is, however, difficult to simulate accurately with a numerical study. The streamlines plotted appear somewhat sharp pointed in the proximity of the branch because they are plotted as a series of straight lines joining the points at which the stream functions are evaluated, and they change direction sharply in this region. This change in direction of the streamlines in the region proximal to the apex (skews initially away from the dividing wall and then towards it) is caused by the presence of a stagnation point at the apex which is itself caused by the fact that flow is symmetric about the centreline (and therefore centreline flow is irrotational). From this reasoning therefore it would be expected that vorticity at the apex of the flow divider is zero, that it increases sharply with distance along the wall to a maximum and that subsequently it decreases asymptotically to a value corresponding approximately to that expected for Poiseuille flow. Fig.3.11 indicates

that this is the case at Re=250. Although vorticity upon the apex was not specified as a boundary condition it can readily be seen that, as predicted from the streamline diagram, the spatial variation of vorticity is essentially as described above. The dimensionless values of vorticity upon the outer wall and the dividing wall at the channel end were respectively -6.05 and 6.53. Assuming axial velocity along the distal part of the channel (whose outer and flow dividing walls are defined to be located at Y=0.5 and -0.5 respectively) to be given by the equation for parabolic flow,

$$U = 1.5(1-4Y^2)$$

the vorticities predicted from this equation are respectively -6.0 and 6.0. Thus flow both near the outer wall and the dividing wall appears to be well developed and the numerical results strongly supported by prediction using simplified theory. The maximum dimensionless vorticity predicted by the model for Re=250 was 21. This value can be converted to an absolute value for any geometrically similar system by use of the equation 3-23 below

$$\omega = Re.(\partial U/\partial Y).\mu/\varrho L^2 \qquad \text{eqn 3-23}$$

Using average data for the coronary system (L = radius = 0.0015m, μ = 4.10^{-3} kgm^{-1}s^{-1}, ϱ = 1100 kg m^{-3}) gives ω = 8484 s^{-1} which corresponds to a shear stress of 339 dyne/cm^{-1} (33.9 Nm^{-2}). This figure is fairly close to Fry's (F1) much quoted critical shear stress of 400 dyne/cm^{-2} but is different from some predicted by other authors. For example Kandarpa and Davids (K3) predicted shear stresses to be about 5 times

smaller than the present the present for similar Re with similar dimensional and physical data. On the other hand, using the vessel size assumed by Friedman et al (F4) (ie radius = 0.67 cm) the present value becomes approx 17 dyne/cm^{-2} which is a figure substantially lower than the peak vorticity predicted by them of 33 dyne/cm^{-2} for Re = 110 in pulsatile flow studies. Thus it becomes apparent that choice of vessel size plays an important role in the determination of arterial shear stress. It should be pointed out that if the current Re was determined using vessel diameter rather than vessel radius as the base length then in this case Re = 500. This is rather a high value of Re for the coronary circulation for which mean Re is generally about 120. For this reason the above value of shear stress could also be rather high.

Fig 3.10 indicates that very little boundary layer growth occurred upon the outer wall distal to the branching point. No reverse flow was found at any values of Re tested by study of either streamline patterns or vorticity and no negative velocities were recorded. In view of the experimental flow patterns found by Fox & Hugh (F7) and those predicted by Kandarpa and Davids (K3) in which strong recirculation was found in this region this is perhaps surprising. It is quite likely that the mesh used for the flow domain was not sufficiently refined in each of the branch regions for flow to be modelled accurately. In the modelled domain there is a mathematical discontinuity at which if there was no flow separation then there would clearly be infinite acceleration of flow. As this is clearly impossible it follows that the absence of separation in the solution is due to the inaccuracy of the numerical scheme. As lack of storage

space prevented the further refinement of the mesh a focussing technique was employed whereby eqns 3-5 were solved in a strongly refined mesh covering the region adjacent to the outer wall immediately distal to the corner (a similar technique to that described by Gartling & Becker (G10)) using as boundary conditions the computed velocities of the crude mesh. This technique was unsuccessful, however, and boundary vorticities obtained varied widely and somewhat randomly with distance along the boundary. For this reason the focussing technique was abandoned and the above results used.

Slight skewing of the flow towards the outer wall was found in the region proximal to the branch point, development of a relatively large boundary layer was found immediately distal to this point, and relatively little change in boundary flow conditions was found further along this wall. Fig.3.11 shows a sharp increase in vorticity in the region proximal to the branch point, a sharp decrease in that immediately distal to the branch , and a slight smooth increase with distance along the outer wall of the branch, asymptoting to a normalised vorticity of -6.0. The mean vorticities in this region were, as expected, low by comparison with those upon the flow dividing wall. Additionally, if the flow regime under study had had rounded, rather than sharp, corners, the vorticities at the corners would both be very much lower than those actually found. For this reason it is felt that the vorticities obtained in these studies are likely to be very much higher than those which would be found in geometrically similar arterial branches or in the experimental flow channel.

Fig 3.12 shows how vorticity was found to vary with distance along all boundaries for each value of Re evaluated. As can be seen, when Re=0 vorticity upon the outer wall peaks (as described above) at the corner and then very quickly reaches a value of -6.337. Upon the flow dividing wall the vorticity rises quickly from a low value (which should be zero but, due to numerical inaccuracy, is not) to a steady value of 6.337. In this case skewing of the velocity profile is caused only by the presence of the flow dividing wall. Because inertial effects are absent, the velocity profile is affected only in the region of the branch and does not vary with distance in the distal region. Thus vorticity, in this region, is constant. As Re increases the magnitudes of peak vorticity increase and those of minimum vorticity decrease. In each case, however, the Poiseuille flow develops relatively quickly downstream from the branch. The latter effect has been found in most numerical studies (eg Ehrlich (E1), Friedman et al (F4), Kandarpa & Davids (K3)) (presumably partly due to the fact that most laminar flow studies discount any effects of flow instability or turbulence) and is generally found (though to a lesser degree due presumably to effects of instability) in animal experiments (eg Nerem et al (N4), Wells et al (W1), Gutstein et al (G2)).

As inertial effects become more and more important the peaks and troughs in vorticity become increasingly accentuated. It can easily be seen how flow conditions within an arterial branch may vary markedly with distance, particularly if further factors such as pulsatility and three dimensionality are considered. It is felt that the present results, while limited in their accuracy regarding absolute magnitudes of vorticity, serve well to illustrate the complexities of

flow even in such a simplified system.

3.10.3 Mass Transport Characteristics within the Domain.

Similarly, the mass transfer studies provided illustrative, if not quantitatively accurate, information regarding the effects of fluid flow upon transport to and from the wall and evidence generally supportive of the experimental results. Figs. 3.13a and 3.13b are computer generated plots of the variation of concentration within the domain for Re=20,40, and Sc = 2.7 (corresponding to that of the experimental system). The contours which correspond to values of 0.1 - 1.0 (where 1 = boundary concentration) illustrate how even at low values of Pe (=Re.Sc = 50, 100) the rate of boundary layer growth is very small. Pe for the O_2-haemoglobin system in the coronary arteries is of the order 300,000 (Sc = 2800, Re = 110). While in this system the diffusive transport term is minute by comparison with the convective term it can still sometimes prove useful to use systems of low Sc to simulate the transport behaviour of those of high Sc. In several commonly used empirical expressions for estimating local Sherwood numbers (Sh) in systems of known geometry

$$Sh \propto Sc^{0.333}$$

an expression which can be derived from boundary layer theory. Hence even where Sc for two systems differ by a factor of 1000 their mass transfer coefficients may differ by only a factor of 10. Therefore, boundary Sh was computed for a wide variety of Sc and Re in order to assess not only the validity of the experimental results but also how usefully these results may be used to predict the effects of

three-dimensional flow upon arterial mass transport.

Fig 3.14 is a computer generated graph which shows the variation of boundary Sh for Sc = 2.7 and Re = 250. Upon the flow dividing wall the apex forms the mass transfer leading edge and the boundary layer grows monotonically from this point. Thus Sh decays exponentially with distance from the apex (with a peak value of 42) to a minimum value of 4.3. In contrast, upon the outer wall in the region proximal to the branch, Sh increases (virtually) monotonically with distance and peaks at the branch point. Sh decreases sharply with distance immediately from this point before remaining virtually constant at a value of 3.6 along the rest of the outer wall. Thus both sets of curves are very similar to those for vorticity - the only significant difference being that Sh does not reach a minimum upon the outside wall downstream from the branch upon the outer wall (not an unexpected result since if Sc = 1 and $\partial P/\partial X$ is small, the Navier-Stokes equation and eqn (3-6) are identical).

A computer plot of Sh vs distance for all other Sc with Re = 250 is shown in fig. 3.15. The curves for Sc = 50, 300, 1500, 2800 are slightly different in shape to that for Sc = 2.7 and, as would be expected, the higher is Sc, the higher is Sh throughout the domain. The curves for the section upstream from the branch and immediately downstream upon the outer wall lack continuity for Sc > 2.7. In each case, however, Sh increases as the corner is approached in similar manner to that for Sc = 2.7.

Upon the outer wall immediately downstream from the branch, Sh decreases sharply and then increases slightly before becoming relatively constant. These changes in Sh become more pronounced as Sc increases (when Sc=2.7, no increase occurs) and are caused by thickening of the concentration boundary layer in this region. This is similar to the momentum boundary layer growth described above which causes low vorticity in this region. Because velocities are low in this region, convective mass transfer becomes less important and consequently Sh is decreased. As Sc increases, convective transport becomes increasingly influential, thus Sh increases.

Upon the flow dividing wall Sh decreases exponentially with distance for all Sc > 2.7 in a manner similar to that for Sc = 2.7 - the only difference between the two cases is that in the latter, Sh increases initially with distance and then decays exponentially, whilst in the former, only exponential decay occurs. This initial increase in Sh appears to be a numerical oddity generated by the limited accuracy of the scheme. Whilst the concentration boundary layer initiates at a stagnation point in the flow regime (in which diffusive transport dominates), the boundary layer thickness at this point is zero, hence in theory, at least, an infinite mass transfer rate is predicted. In the physical situation other forces (eg electrostatic) which would otherwise be negligible become important, hence this situation cannot be described analytically using purely a convection/diffusion model. With the present numerical scheme the problem does not arise directly, because the domain is only modelled approximately, but as is stated above, local numerical inaccuracies occur.

The curves describing variation of Sh with distance upon the flow dividing wall also have slight discontinuities between elements (though as can be seen, Sh is continuous within each element). This effect is induced by finite element discretisation of the domain and would be less apparent if a more refined mesh was used. It is also possible that use of a linear (rather than a quadratic interpolation function upon the left hand sides of eqns 3.13 and 3.13 would have improved continuity since variation of the concentration gradient is of one order of magnitude less than that of concentration.

Figs 3.16a and 3.16b show the equivalent sets of results for Re = 50 and 0. When Re = 50 and Sc = 1500 or 2800, Sh is more continuous within the upstream section, but is less so beyond the branch point upon the outer wall and the flow-dividing wall. As can be seen peak Sh is much lower in this case than when Re = 250 and the sharp decrease in Sh found immediately distal to the apex of the flow dividing wall is much less pronounced when Re = 50. When Re = 0 (fig 3.16b) transport is completely diffusion controlled and in this case the only reason that there is any variation of Sh is that the inlet concentration boundary condition is zero. When Re = 0, the momentum and concentration boundary layers are fully developed, hence $\delta_c = 1$. Thus from eqn 3.20 it is clear that Sh (=MOD($\partial C/\partial Y$)) = 1.5. This is seen to be the case in the numerical solution.

3.10.4 Effect Upon Sh for Varying Sc

In order that Sh predicted by experiment using a transport system for which Sc = 2.7 (ie ethyl salicylate and air at 20°C) can be extrapolated approximately to that equivalent system for which Sc = 2800 (O_2 and blood at 37°C) a correlation between Sh and Sc is required. As is discussed in chapter 2 introduction, the most commonly used correlation between these parameters is $Sh \alpha Sc^n$. To establish how well this relationship applies in the present case a new variable was defined:

$$Sh_{Sc}(Sc,Re,X) = Sh(Sc,Re,X)/Sh(Sc=2,7,Re,X)$$

ie Sh for any value of Sc,Re X normalised with respect to Sh for Sc = 2.7 for any value of Re and X. Fig 3.17 shows variation of Sh_{Sc} with X for Re = 50. As can be seen, Sh_{Sc} varies slightly with X for Re = 50. For each value of Sc the mean and standard deviations of all boundary points was found and these are tabulated in table 3.2. The standard deviation increased with Sc (thus indicating that the accuracy of any Sh vs Sc correlation decreases with Sc) but was always less than 25% of the mean. A best fit straight line was plotted through a graph (fig 3.18) of ln (mean Sh_{Sc}) vs ln (Sc) which had a gradient of 0.303 (ln Sc was "x" axis). To a best approximation therefore the computations described above give the following correlation

$$Sh \alpha Sc^{0.303}$$

which is close to the theoretical expectation.

The same approach was followed for Sh variation with Re: ie a new variable was defined such that

$$Sh_{Re}(Sc,Re,X) = Sh(Sc,Re,X)/Sh(Sc,Re = 50,X)$$

Sh_{Re} was plotted in fig 3.19 for Sc = 2.7, the mean values tabulated in table 3.3 and a straight line drawn through ln(mean Sh_{Re}) vs ln(Re). In this case, the standard deviation was very small by comparison with mean Sh_{Re}, thus indicating that the correlation between Sh_{Re} and Re was more reliable than that between Sh_{Sc} & Sc. The correlation obtained was

$$Sh_{Re} \alpha Re^{0.409}$$

Thus for the experimental system described in chapter 2, a rough extrapolation of the Sherwood numbers obtained by experiment would be

$$Sh_{extrap} = Sh_{expt}.(Sc/Sc_{expt})^{0.3}(Re/Re_{expt})^{0.41} \qquad \text{eqn (3-24)}$$

(expt = experimental, extrap = extrapolated)

Fig 3.21 shows extrapolation of the solutions for Sh vs distance for Re = 50, Sc = 50 & 2800 from that for Re = 50, Sc = 2.7 using eqn 3-24.

Relatively good correlation was obtained between solutions for Sc = 50 extrapolated for the computed results for Sc = 2.7 and for the computed solutions for Sc = 50 for all parts of the domain. Similar extrapolation to solutions for Sc = 2800 from these for Sc = 2.7 was less successful however. The extrapolated solutions for Sh upon the flow dividing wall were relatively close to the computed results downstream from the apex but those for Sh upon the upstream wall and upon the outer wall in the downstream section, while qualitatively similar in shape, were in magnitude only approximately 60 - 70 % of the computed solutions. This indicates that extrapolation from one solution for low Sc to another with high Sc, while feasible for simple domains, does not appear to give accurate results throughout a branched domain such as the present one. Such poor correlation may, however, be an artefact of the relative inaccuracy of the computational scheme at high Sc, particularly in regions in which Sh is high (as local variation of C is high with respect to mesh fineness). As MacLeod (M8) points out, if Sc > 1 then the ratio of concentration boundary layer/momentum boundary layer thickness (and hence of mass transfer coefficient) is not a strong function of Sc (α $Sc^{0.33}$). While not much detailed study of this type for variation of local mass transfer coefficient with Sc has been done, such studies of overall mass transfer coefficient with Sc have yielded good correlation. Thus reasonable correlation of Sh with Sc should be possible.

From these results it appears that while a rough approximation to the mass transfer behaviour of O_2 in blood may be obtained by using the air-ethyl salicylate system, results by far superior may be obtained by use of a system with Sc more close to that of the O_2 -

haemoglobin system. Such a system could be H_2O - ethyl salicylate for which Sc ≈ 1100.

3.10.5 Comparison with Literature

Because theoretical and experimental studies of transport characteristics of O_2 are relatively rare, it was impossible to correlate directly the present results with others. The only numerical study of O_2 transport of a comparable domain was done by Ehrlich and Friedman (E5). Qualitatively their flow results appear similar to the present (ie vorticity upon the flow dividing wall rises to a peak at the corner and drops sharply beyond it - they also found no flow reversal). Because most of their boundary conditions were for constant wall flux rather than constant wall concentration and because they considered only boundary flow, their results are not directly comparable to the present ones. Their fig 5 contains one plot of flux (approx analogous to Sh) vs axial distance for constant boundary concentration, however, whose shape is very similar to that of the present. Their solutions were for Re = 110, Sc = 2300 and g_o (= approx Sh in the present study) varied between 40 & 10. Fig 3.15 shows that Sh varied between 40 and 70 in the present study within the finite element domain (Sh based upon radius rather than diameter) and was therefore of the same order of magnitude. Additionally, the initial sharp decrease in g_o shown by Ehrlich and Friedman (E5) is found in the upstream section of the flow domain described by the boundary layer growth equations 3-15 - 3-22.

The only data found in the literature with which a suitable comparison between use of the non-linear and the linear models for O_2 transport was that by Back et al (B16). They incorporated a non-linear relationship between O_2 pressure and O_2 concentration in haemoglobin into the basic equation (eqn 3-6) and solved for transport within a stenosed region. The mean Sherwood numbers (computed using radius as characteristic length) varied between 4 and 350 during pulsatile flow throughout the domain for Re = 110 while those for their linear study ranged between 4 and 150 approx. The results indicated that major differences between the conventional linear transport model of eqn 3-6 and the non-linear model describing the O_2-haemoglobin reaction equilibrium only occurred at high Sh - particularly when Sh > 40. Thus it appears from these data that a study such as the present one, in which regions of low Sh are sought using the linear model may yield results reasonably similar to those obtained from a study incorporating a non-linear relationship between O_2 concentration and pressure in terms of magnitude and location of regions of low mass transfer coefficient.

Chapter 4

Discussion of Mass Transfer Results in Chapters 2 & 3

4.1 Comparability of Experimental and Computational Studies

Chapters 2 & 3 presented two separate approaches to the study of variation of mass transfer coefficients within the arterial system with particular reference to the effects of blood flow upon supply of oxygen to avascular tissue in branched regions of the major arteries. In this chapter a comparison of the results is presented in order that the consistancy and value of the two methods can be assessed.

While the experimental and finite element domains in which flow and transport were studied were not exactly similar geometrically, they differed only in the lengths of the downstream branches. In the finite element domain these were 6.2 while those in the experimental domain were 27. These parameters were also identical originally, but it was found during preliminary experiments on the experimental apparatus that the air velocities were sufficiently small that natural convection of the ethyl salicylate caused strong vertical variation of mass transfer coefficients. This problem was alleviated by reducing the channel width to a size which could only be modelled accurately computationally if more elements were added to the domain than was feasible computationally. As it was, the entrance region of the experimental channel was only modelled satisfactorily when a simplified approximation to the entry flow was used to reduce the required number of elements. In addition a possible source of misinterpretation of results

was caused by a lack of suitable equipment to measure velocity variation throughout the domain. This meant that comparisons with computational results of flow were not possible and that basic flow patterns within the domain could only be estimated.

While only 2-dimensional flow could be studied in the computational domain, as is discussed in chapter 2, it proved impossible to remove the 3-dimensional flow effects completely from the experimental domain. These caused some vertical variation of Sh at the top and bottom support plates of the experimental channel.

4.1.1 Sources of Error

The differences between the two sets of results are due probably to shortcomings in both types of model. As stated previously, the computer model describes only the classic viscous- pressure-inertial force balance upon a fluid and neglects flow instabilities turbulence etc. The domain is idealised and the finite element method gives only a numerically approximate solution. While results obtained in simple test flow channels gave expected results, the data obtained for the present domain could not be tested adequately. It was impossible to increase the number of nodes in the domain and observe the effects upon results because of the prohibitive costs involved (the present domain contained 511 nodes and involved the solution of up to 1083 simultaneous equations). The experimental model depends for its accuracy upon reliable vapour pressure data for the swelling agent.

This data has been determined for isobutyl benzoate, methyl salicylate and ethyl salicylate by Kapur and MacLeod (K6) using holographic techniques and has been found to provide good correlation with standard empirical mass transfer models. This source was used to determine the vapour pressure in the present work, but its accuracy has been the subject recent study by WR Paterson (personal communication) who has found the vapour pressure of ethyl salicylate to be rather higher than that determined by Kapur and MacLeod (K5). A further possible source of error was the speckle pattern interferometer itself which required some "warm-up" time before it stabilised and did occasionally generate fringes when the system was completely immobile.

Thus several sources of discrepancy do exist between the two methods and as will be seen below, the results differ by varying degrees with Re and locality. Nevertheless, in all cases Sh for both methods of measurement is of similar magnitude and it is probable that better agreement would be obtained if some of the above sources of error could be alleviated.

4.2 Results

The measured and computed variations of Sh within the upstream section are plotted in fig 4.1 for Re = 150 and Sc = 2.7. As can be seen, when $X < -4$ the curves are qualitatively similar in shape (ie Sh decreases with distance from flow entrance) and the (computationally derived) absolute values of Sh are about 60% of those obtained by

experiment; these being reproduced from the work of Bhatti & Savery (B20). When $x \geqslant -1$ the computational results are generated by finite element analysis and from this point Sh increases sharply with X. This increase appears to be caused by sharp skewing of the velocity profile towards the outer wall (and consequent increase in vorticity) in this region immediately upstream from the branch (see fig 3.11). Such a effect was not found,however, with the mass transfer experiments carried out. In these, for all Re, a monotonic decrease in Sh with distance from entrance was found (see fig 2.15) with no increase even very close to the branch point (such an effect would have been made apparent by pronounced branching of fringes at this point).Similarly, a lack of behavioural consistency was found for Sh variation upon the outer wall of the downstream section (fig 4.2). In the "computational" case Sh was very high at the branch point (ie Sh = 7.3) but dropped sharply to S = 3.3 for $0.3 \leqslant X \leqslant 6.11$. The corresponding experimental results showed simply a monotonic increase of Sh with distance from the branch (ie no sharp decrease from the branch point).

It is probable that these discrepancies in behaviour upon the outer wall can be explained (at least in part) by there being no flow separation predicted by the computer model (due, probably, to the lack of mesh refinement - see chapter 3). Because flow is predicted not to separate in this region, stronger skewing towards this wall is predicted computationally than occurs experimentally. Boundary layer growth in this region is therefore more restricted and a higher initial vorticity and Sh is predicted. In the experimental domain, as the reattachment point is approached, the concentration boundary layer decreases in thickness and Sh increases. The point of reattachment

was not located within the flow region in any of the experiments performed in the present study, however, so it was not possible to observe the point of maximum mass transfer or to determine the variation of its location with Re.

Better qualitative agreement with results was obtained for the more simple flow in the region of the flow dividing wall as is shown in fig 4.3, the computer model predicted Sh to be very high at the apex, initially to decrease sharply with distance and then to asymptote to a value of about 3. The experimental apparatus was not able (as discussed in chapter 2) to describe mass transfer behaviour in te immediate vicinity of the apex because the rate of change of Sh observed caused excessive fringe bunching. This in itself suggests at least strong qualitative agreement with the computational results, but as is discussed in chapter 2 a more flexible interferometric system would be required in order to verify the quantitative accuracy. In the region of common axial distances from the apex between the two models, experimentally determined Sh was generally about 70% of that of the computational model and the former appeared to asymptote to a value of about 2.

4.3 Assessment of O_2 Transport Using the Experimental Results

The values of Sh found for the air/ethyl salicylate system can be used to predict the variation of O_2 levels within the medial and intimal regions of the arterial wall. Rate of O_2 consumption per unit volume of artery is

$$Q_{O_2} = Dk\left(\partial P_{O_2}/\partial Y\right) \qquad \text{eqn } (4-1)$$

where D = O_2 diffusivity within the tissue, k = O_2 solubility within tissue.

Within the medial (innermost) region it may be assumed that a minimum P_{02} is reached (this is reasonable if the region is not hypoxic) hence the boundary conditions are the following

$$P = P_2 \text{ @ } Y = Y_2,\ \partial P/\partial Y = 0 \text{ @ } Y = Y_3$$

Thus within this region

$$P_{02} = Q_{02}/Dk(0.5Y^2 - 0.5Y_2^2 - YY_3 + Y_2Y_3) + P_2 \qquad \text{eqn (4-2)}$$

where Y_3 is the point of minimum P_{02} and Y_2 is the location of intimal/medial tissue interface.

Within the intimal region it may be assumed that at $Y = Y_2$ (ie the intimal/medial interface), $\partial/\partial Y$ is the same for both regions. The boundary conditions are the following

$$P = P_1 \text{ @ } Y = Y_1 \text{ and } \partial P/\partial Y|_{Y=Y2} = Q_{02}/Dk(Y_3 - Y_2) \text{ @ } Y = Y_2$$

and these give

$$P_{02} = Q_{02}/Dk(0.5Y^2 - YY_3 - 0.5Y_1^2 + Y_1Y_3) + P_1 \qquad \text{eqn (4-3)}$$

The mass flux m_{02} of O_2 from the lumen into the wall is expressed in terms of mass transfer coefficient k_m by

$$m_{02} = kk_m(P_o - P_1) \qquad \text{eqn (4-4)}$$

where P_o = luminal P_{02}

But at the intimal/luminal interface,

$$m_{02} = Dk\partial P/\partial Y|_{Y=Y1} = Q_{02}(Y_3 - Y_1)$$

hence

$$P_1 = Q_{02}/kk_m(Y_1 - Y_3) + P_o \qquad \text{eqn (4-5)}$$

Using the data (table 4.1) for Q_{02}, k, Y and D from Schneiderman and Goldstick (S11) and the minimum value of Sh found upon the outer wall of the branch for Re = 160 during the experimental program, eqns 2-8 - 2-11 can be evaluated. From eqn (3-24)

$$Sh_{extrap} = 2.05(2800/2.7)^{0.303} = 16.8$$

Assuming a vessel radius of 1.5mm, $k_m = 2.24 \times 10^{-3}$ cm/s

hence eqn (4-5) becomes

$$P/11 = P_o - 11.7$$

eqn (4-3) becomes

$$P_2 = P_1 - 52.1$$

eqn (4-2) becomes

$$P_3 = P_2 - 19.4$$

These figures indicate that for the above dimensions and mass transfer coefficients, the highest O_2 pressure drop occurs across the intimal region and that the pressure drop of O_2 across the wall is 83.2 Torr. Schneiderman and Goldstick (S11) assumed that $P_{02} = 85$ Torr within the bloodstream and their results suggest that P_{02} becomes very close to zero at the point of minimum mass transfer with the pressure drop across the blood/wall interface being relatively small.

If the mass transfer coefficient was halved then in the system described above

$$P_1 - P_0 - 23.4$$

and hypoxic conditions would occur. Thus luminal O_2 transport properties may influence the occurrance of hypoxic conditions within the wall. These results are very dependent upon the exact dimensions, O_2 transport properties and O_2 consumption rates of the tissue, however, and can give only an approximation of the O_2 profile across the wall. Their value is strongly dependent upon the accuracy of the simplifications made from the physiological situation. These are discussed below.

4.4 Accuracy of the Modelling Techniques and Development to the Physiological Situation

The experimental model described above used substantial simplifications in its description of flow and transport in arterial branches. The major differences between model and reality are following:

(i) steady flow rather than pulsatile

(ii) rigid walls rather than compliant

(iii) constant rather than axially varying concentration boundary condition

(iv) linear rather than non-linear relationship between solute vapour pressure and concentration

(v) very simplified branch system

(vi) two- rather than three-dimensional flow regime.

Because of this the results described and discussed in chapters 2 and 4 cannot be taken to be quantitatively accurate but should be considered merely as a step towards describing flow and transport in arterial branches. Because the computational model was intended to simulate the experimental model rather than directly the physiological situation (in order to assess the relationship between Sh and Re, Sc for a range of Sc) the validity of the results with respect to the true situation is also highly limited. The major differences between this and the finite element domain are the same as above together with the fact that the mesh used was probably rather cruder than required in places of high shear or mass transport.

Both Back et al (B16) and Schneiderman et al (S10) have published results which indicate that pulsatility of blood flow has little effect upon O_2 transport, both the Navier-Stokes equations and the O_2 transport equation being solved using the finite difference technique. However, their results may contain significant inaccuracies in transport rates in the vicinity of the wall. Schneiderman et al's model took account of wall motion (as function of pressure) but its flow domain was very simplified with respect to the geometries of regions prone to atheromatous growth.

Experimental simulation of the effects of pulsatility upon O_2 transport using the swollen polymer technique was not attempted during the present study. From the above results it was felt unlikely that substantial effects upon transport due to pulsatility would be observed and additionally, it would be very difficult to obtain accurate results. The accuracy of the swollen polymer technique is strongly dependent upon the rigidity of the materials of construction of the model, particularly if fringe development is observed in real time. A pulsating medium would be unlikely to satisfy this criterion. In this respect, use of the electrochemical technique would be more appropriate and useful measurements of time varying Sherwood numbers could be obtained. Such a study could well be extended to pulsatile studies in compliant media (should a suitably conducting wall coating be available) using elastin or its synthetic equivalent (described by Dorrington (D8)).

The transport model which both the experimental and the computational programs simulated had constant boundary concentrations. This may limit substantially the accuracy of the simulation, particularly

because it is assumed that luminal mass transfer is the rate limiting O_2 transport step.

This means that oxygen reaching the arterial wall is transported rapidly within the wall and that O_2 concentration at the wall is strongly a function of luminal mass transport. This problem has been tackled by Ehrlich and Friedman (E5) by assuming constant O_2 flux into the wall with varying wall O_2 concentration and by Back t al (B16) who assigned a function of axial distance and time to wall concentration and solved for O_2 concentration within the lumen. Ehrlich and Friedman (E5), as described in chapter 1, found qualitative similarity between wall P_{02} variation for constant wall flux and wall flux for constant wall P_{02}. They made no comments about the variation of P_{02} throughout the domain, however, hence a useful assessment of the effects of each of the boundary conditions was not possible. Further investigation of this problem would be useful in determining the validity of the work described in previous chapters.

In the present experimental study, however, it is impossible to vary wall concentration in a reliable fashion. In principle it would be possible to swell only partly any selected region of the polymer-coated boundary thereby causing P_{es} (es = ethyl salicylate) locally to be small. If this was done, then detailed knowledge of the rate of variation of P_{es} with coating thickness would be necessary and, in any case, the system boundary conditions would then be time varying. A far greater knowledge and understanding of the diffusive behaviour of swelling agent in polymer coating would be required before this was possible.

Both the results of Back's et al (B16) and of Schneiderman's et al (S9,S11) works indicated that the oxygen-haemoglobin reaction has a significant effect upon the rate of O_2 transport to the arterial wall. Prior to these investigations it was believed that the major resistance to O_2 transport lay in the red cell-free region adjacent to the wall. These investigations indicated that this was not the case and that the boundary layer may be up to 10 times as thick as this cell-free layer. One author (Back et al (B16)) indicated that mass transfer rates may be twice as high when the non-linear O_2-Haemoglobin equilibrium relationship is coupled with the simple diffusion-convection model as when only the simple model is used. Back's et al (b16) study did indicate, however, that in regions of low mass transfer, the transport characteristics for both cases were fairly similar and, therefore, that experimental and computational models which do not (or cannot) take account of this non-linear relationship may still predict realistic mass transfer coefficients assuming that there are no other artefacts in the model. Further computational verification of this would be necessary in order to assess better the applicability of the results produced by the present experimental model.

The latter two differences between the models used in this work and the physiological situation (viz simple flow system and 2-d flow) could be substantially removed by use, experimentally, of a more realistic flow domain which incorporated several branches and whose limbs were approximately circular in cross-section. The only major difficulty in working with a circular cross-section would be the choice of optical path through the model. Use of total internal reflection, even if it produced usable fringes, would (as seen in fig 4.4) require an

extremely exact knowledge of the angles of reflection from the polymer surface at all points upon the surface of interest. These angles would vary spatially across the surface thus complicating immensely the computation of mass transfer coefficients. A better method of viewing surface recession in such a system is illustrated in fig 4.5. Refraction through a focussing lens means that the beam can be made to pass through the glass surface at 90^0 to all surfaces. Diffuse reflection from the opposite wall would cause major problems with scattered light from many parts of the surface being detected at one point by the camera and consequently, some loss of fringe contrast would occur (fig 4.5). Direct reflection from a remote diffusely reflecting surface should, however, minimise the amount of stray light entering the camera. Thus the swollen polymer technique should allow measurement of the variation of mass transfer coefficients in 3-dimensional flow domains as well as 2-dimensional ones.

Three dimensional flow cannot be studied easily computationally using numerical approximations because of the astronomical computer processing times and storage space involved. For similar reasons, extension of the current 2 dimensional domain to, for example, a multibranching one would prove equally difficult. While work is proceeding at present into new ways of solving partial differential equations more efficiently using both new numerical techniques (eg the Integral Representation Techniques for Navier-Stokes equations, Wu (W12)) and new types of computer (eg ICL's Distributed Array Processor (DAP) which performs multiple matrix operations simultaneously) there remains much development to be done before solution of the Navier-Stokes equations for such complex systems can be done easily.

A major drawback of the air-ethyl salicylate system used in the present work was the low Sc (= 2.7) of the system. For O_2-haemoglobin systems Sc = 2800 and,as was indicated by the computational results, transport behaviour for such systems differs substantially from that for Sc = 2.7. Use of a water-ethyl salicylate system has been tried by Kapur and MacLeod (K5) who measured fringe development holographically for flow impinging upon a flat plate. For this system, Sc = 1100, therefore results which relate better to the physiological situation may be expected if satisfactory fringe development can be obtained. Because the refractive index of water (1.35) is rather closer to that of ethyl salicylate (1.52) than that of air, fringes of good quality would be harder to obtain and fewer fringes per unit mass transfer coefficient would be observed in a given time. Direct viewing of a surface through moving liquid may well prove difficult due to slight fluctuations in optical density of the liquid.

A discussion of several current theories for how fluid mechanical flow features may influence atherogenesis was presented in chapter 1. In each case an artery was subjected to relatively severe conditions (eg high shear stress, low shear, endothelial cell layer removal etc) designed to test the proposed mechanism for atherogenesis and results presented which supported or rejected accordingly the respective theses. Within the study of O_2 transfer the results presented in chapters 2 and 3 together with various others (B16,S9,S10,S11,C23,B18,H10,O4) show that not only can hypoxic conditions appear to cause development of plaques but that strong variation of O_2 conditions within the lumen is possible. The major problems within this area of research still to be addressed thoroughly are

(i) the effect of localised O_2 starvation upon the wall.

(ii) the effect of 3-dimensional flow conditions upon O_2 transport.

The first problem is very much one requiring the attention of the biologist. Further work related to how O_2 starvation affects the nature of both the tissue and of the endothelial cells with regard to the transport of macromolecules is needed. It has been postulated that (04) O_2 starvation restricts metabolism and allows lipid growth. An assessment of how strongly this may influence plaque formation and comparison of the relative importances of this and of the effects upon cells and tissue of hypoxia will compliment the engineering studies (see below) and should provide an improved understanding of the role of O_2 transport in the disease process.

The second is one which requires an engineering approach. Detailed programmes combining studies of both the fluid dynamic nature of blood flow within a branched luminal domain and the variation of the mass transfer coefficient with axial and azimuthal position would provide some understanding of this. None of the experimental work done to date (see sects 1.4,1.5,1.8) has attempted this. Because of the experimental difficulty of measuring O_2 transfer coefficients the focus experimentally has been in developing and testing P_{02} measurement techniques. Until suitable instrumentation is developed such techniques will be of limited value. An in vitro model, however, using for example the swollen polymer method with a water-ethyl salicylate system of mass transfer coefficient measurement coupled with a laser-Doppler anemometry study of flow would yield considerable information about the correlation of mass transport with flow conditions in well defined

conditions.

Such experimental methods as the above could also be of value in other physiological applications. For example, Caro et al (C2) used mass transfer principles in their assessment of the role of concentration boundary layer in transport of macromolecules from the arterial wall into the bloodstream. Galanga and LLoyd (G12) used the electrochemical method to examine the variation of local mass transfer coefficients near prosthetic heart valves. Dumas and Barozzi (D9) analysed heat transfer to blood flowing in a duct using Finite Difference methods. In each of these cases use of the swollen polymer technique could have be made in order to predict rates of transport of mass or heat in a biomedical application.

Chapter 5

Summary of the Thesis

The work presented in the preceding chapters has been motivated by the apparent correlation of location of atherosclerotic lesion formation with regions of strong asymmetry in blood flow profile. Two lines of investigation have been developed; namely

(i) study of the cause of an apparent lack of correlation between distribution of flow in downstream limbs of an asymmetric branch with Re, and

(ii) the use of experimental and computational technique to describe the mass transfer of O_2 from the lumen into the arterial wall.

It has been found (appendix B) that the tendency for flow to enter the side branch of an asymmetric branched domain preferentially, found independently by two sets of workers, was caused by an artefact of the experimental apparatus used by the workers. By minor alteration of the geometry of the side channel exit it was found that substantial alteration of the relationship between flow distribution between the branches & Re occurred. Similarly, alteration of this relationship occurred when the solid surface was greased slightly and when one of two inter-connected end reservoirs was contaminated with detergent. In each case the only feature of the system which was altered substantially was the energy of formation of air-water interface at the channel exit. When the system was immersed in water (in order to remove all surface effects from the channel exits) and flow distribution observed by measurement of the rate of advance

of a dye front, no such tendency was observed. Indeed, flow in the straight limb was generally higher than that in the side limb and increased with Re relative to that in the side limb. The suggestion by Crowe that the uneven distribution of flow in the branches was caused by the Coanda effect was examined experimentally and found invalid. The Coanda effect is a bistable condition whereby in a branched domain all flow proceeds exclusively down either of two branches or, in an expanding channel, attaches itself to either side wall. No such signs of bistability were observed in the current work and only at very low flow rates did flow proceed along one branch only. For these reasons it was concluded that

(i) the results obtained by Crowe (C13) and by Rodkiewicz and Roussel (R5) were misleading by their neglect of surface tension effects.

(ii) any further studies of this type should be done in environments where no surface effects will be encountered and

(iii) there is no evidence to suggest that similar in vivo branch configurations would give similar results to those found by these authors.

The swollen polymer technique has been used to measure the variation of Sherwood number in a two dimensional domain simulating an arterial bifurcation. It has been possible to predict with relative ease rates of mass transfer along all walls of the branched domain with the exception of regions where high mass transfer coefficient gradients occurred. These could also be measured if a more flexible interferometric system was used. The Sherwood numbers obtained were of similar magnitude to those found computationally and those inferred

from published computational data. Qualitatively the variation of Sh within the domain and with Re was very much as would be expected; high Sh decreasing with distance along both the flow dividing walland the wall upstream from the branch with low Sh increasing with distance along the outer wall.

The results indicated that flow separation and reversal occurred upon the outer wall of the branch and that the recirculation zone extended beyond the channel exit for all Re (ie a distance of 25 channel widths). This effect may well not occur in the physiological situation because the three dimensional domain will undoubtedly generate compensatory secondary flows (as found by Brech and Bellhouse (B4)). In addition separation was undoubtedly enhanced by the presence of a sharp corner in the domain. Arterial branch points are characterised by smooth curvatures rather than sharp bends.

Incorporation of the mass transfer coefficients obtained experimentally into a model of O_2 diffusion and consumption in the wall indicated that while the O_2 pressure difference across the boundary layer was small by comparison with that across the intimal and medial regions of the wall, because the O_2 pressures in the middle of the wall may be very low, the magnitude of the O_2 mass transfer coefficient may well play an important role in determining whether or not O_2 starvation occurs.

The finite element method has been used to determine local velocities, pressures, vorticities, concentrations and Sherwood numbers within the domain used experimentally for comparative purposes and for

assessment of the variation of Sh with Schmidt number (Sc). The model predicted the vorticities at the inlet and outlet of the domain to be similar to these for Poiseuille flow. For this reason velocity and vorticity measurements were believed to be reasonably accurate at least in these regions. Flow separation upon the outer wall was not predicted, however, due probably to the use of too coarse a mesh in the region of the branch. The peak vorticities predicted upon the flow dividing wall were slightly below the corresponding critical shear stress of 40 Nm^{-2} as defined by Fry (F1). Appropriate use of slightly different dimensions, however, could imply the predicted shear stress either to be well in excess of this figure or well below it, hence on this basis it is quite plausible that some endothelial damage caused by fluid shear stresses could occur in some arteries. This is a reasonably sweeping statement, however, as it has been made without consideration of the Re likely to occur in arteries of dimensions wherein this critical shear stress is predicted to be succeeded.

The Sherwood numbers predicted by the model were quantitatively similar to both those found experimentally and those found in the literature. The qualitative differences found in the relationship between Sh and distance for computational and experimental work were believed also to have been caused by use of too coarse a mesh. These results have, however, been use to correlate Sh with both Re and with Sc in order that mass transfer data generated by experiment using an air-ethyl salicylate system may be used to predict the behaviour in an O_2-haemoglobin system. The resulting correlation (eqn 3-24) was in close agreement with the well known empirical relationship between Sh and Sc and was very similar to that derived from the results of Bhatti

and Savery's (B20) computational work (eqn 3-21).

From computational results obtained by Back et al (B16) it appears that O_2 transfer coefficients can be predicted with reasonable accuracy in regions of low O_2 transfer using a linear relationship between O_2 concentration and pressure within haemoglobin. If this is the case, then the swollen polymer method appears to offer a convenient means of measuring and observing rates of mass transfer in models of arterial branches and could be used conveniently both to predict O_2 transfer behaviour in three dimensional models and to generate other heat and mass transfer data in physiological systems.

With regard to the problem of identifying mechanisms related to fluid dynamics likely to be responsible for causing atherogenesis, the above results and conclusions present some further evidence for a possible role of high shear stress in the initiation of the disease and a possible role for low transport of O_2 into the wall in the initiation of the disease. In the case particularly of O_2 transport the closeness in magnitude of Sh to those found in other studies offers some support to the belief that such a study can give useful information.

Appendix A

For a domain such as that described in Appendix B, by making the three flow streams of infinite length, an analytical solution of the flow field can be obtained for potential flow. The boundary conditions for potential flow differ from those for the viscous flow studies described in chapter 3 in that plug flow is assumed at the entrance to the channel and the zero velocity boundary condition at the boundary is inappropriate. The dividing streamline is assumed to meet the boundary at the tip of the flow divider and consequently the tip is a point of stagnation. The velocity at the sharp corner on the outer wall is defined as infinity. The velocity of the side branch is taken as $U.\exp(-L_2)$ and that of the main branch as $U.\exp(-L_1)$ where U is the upstream feed velocity. The domain is represented in fig.A1.

Variation of absolute velocity q along the boundaries is as follows.

$A_\infty B_\infty$ $\quad \theta = 0,$ $\quad U \geqslant q \geqslant U.\exp(-L_1)$

$\Rightarrow \quad \ln U \geqslant \ln q \geqslant \ln U - L_1$

(Eqn A1) $\Rightarrow \quad 0 \leqslant \ln U/q \leqslant L_1$

$A_\infty E$ $\quad \theta = 0$ $\quad U \leqslant q \leqslant \infty$

$\Rightarrow \quad 1 \leqslant q/U \leqslant \infty$

(Eqn A2) $\Rightarrow \quad 0 \geqslant \ln U/q \geqslant -\infty$

ED_∞ $\quad \theta = \alpha,$ $\quad \infty \geqslant q \geqslant U.\exp(-L_2)$

(Eqn A3) $\Rightarrow \quad -\infty \leqslant \ln U/q \leqslant L_2$

CB_∞ $\quad \theta = 0, \quad 0 \leqslant q \leqslant U.\exp(-L_1)$

$\Rightarrow \quad -\infty \leqslant \ln q \leqslant \ln U - L_1$

(Eqn A4) $\Rightarrow \quad \infty \geqslant \ln U/q \geqslant L_1$

CD_∞ $\quad \theta = \alpha, \quad 0 \leqslant q \leqslant U.\exp(-L_2)$

(Eqn A5) $\Rightarrow \quad \infty \geqslant \ln U/q \geqslant L_2$

The domain of fig.A1 is transformed to the ξ plane of fig.A2 using the transformation,

(Eqn A6) $\qquad \xi = \ln U/v = \ln U/q + i\theta$

where v is complex velocity defined by $v = q.\exp(-i\theta)$

In this plane the points C and E become infinite while those of A, B and D become finite, A representing a source while B and D represent sinks.

The ξ plane is transformed to the t plane of fig.A3 upon which only the boundaries remain real using the general relation

(Eqn A8)

$$\Rightarrow \xi = k.\ln t + L$$

At F, $t = 1$ and $\xi = i\alpha$, $\Rightarrow i\alpha = k.0 + L$, $\Rightarrow L = i\alpha$

At A, $\xi = 0$ and $t = -1$, $\Rightarrow 0 = k.\ln(-1) + i\alpha = ki\pi + i\alpha$

$$\Rightarrow k = -\alpha/\pi$$

Thus

(Eqn A9) $\qquad \xi = -\alpha/\pi \ln t + i\alpha$

and

(Eqn A10) $$t = -\exp(-\xi\pi/\alpha)$$

At B (fig A2), $\xi = L_1 \Rightarrow t = -t_1 = -\exp(-L_1\pi/\alpha)$,

therefore,

(Eqn A11) $$t_1 = \exp(-\pi L_1/\alpha)$$

At D (fig A2) $\xi = L_2 + i\alpha \Rightarrow t = t_2 = -\exp(-\pi/\alpha(L_2 + i\alpha))$

therefore,

(Eqn A12) $$t_2 = \exp(-\pi L_2/\alpha)$$

From Milne-Thompson (M12), p201, the velocity at complex distance z from a source of strength m situated at position z_0 is,

(Eqn A13) $$v = d\omega/dz = m/(z-z_o)$$

where ω = complex potential

z = complex distance

v = complex velocity

The strength of the source at A_∞ is the volumetric flow-rate which is m = U.H/π, while the strengths of sinks B and D are respectively

$$m_1 = U.H.\pi^{-1}.\exp(-L_1) \;\&\; m_2 = U.H.\pi^{-1}.\exp(-L_2).$$

The velocity for a domain consisting of one source and two sinks will be simply the difference between $m/(z-z_o)$ for the source and the sum of $m/(z-z_o)$ for the sinks. Expressed in terms of t, this becomes

(Eqn A14) $$\partial\omega/\partial t = m/(t+1) - m_1/(t+t_1) - m_2/(t-t_2)$$

Therefore by integration,

(Eqn A15) $$\omega = m.\ln(t+1) - m_1.\ln(t+t_1) - m_2.\ln(t-t_2)$$

In the domain of fig.(A1), $H = H_1 = H_2$ and by continuity $m = m_1 + m_2$, therefore

(Eqn A16) $$U.H = U.H_1.\exp(-L_1) + U.H_2.\exp(-L_2)$$

(Eqn A17) $$\Rightarrow 1 = \exp(-L_1) + \exp(-L_2)$$

Since

$$\partial\omega/\partial z = v = U.t^{\alpha/\pi}.\exp(-i\alpha)$$

$\partial t/\partial z$ can be found by division. At point C, $v = 0$ and $t = 0$, therefore both $\partial\omega/\partial z$ and $\partial t/\partial z = 0$, thus $\partial\omega/\partial t = 0$.

Equation (A14) reduces to

(Eqn A18) $$\exp(\pi/\alpha - 1)L_1 - \exp(\pi/\alpha - 1)L_2 = 1$$

In the domain under consideration, $\alpha = \pi/4$, thus solution of simultaneous equations (A17) & (A18) gives the values of L_1 and L_2 of 0.7142 and 0.6725 respectively which correspond to a flow ratio, Fr = 1.043.

If the flow dividing streamline lies at another point than C in fig A1, then this value of Fr will not necessarily occur. In this instance the stagnation point would lie distal to C in either of the branches and C would be infinity.

Appendix B

A STUDY OF THE RELATIONSHIP BETWEEN REYNOLDS' NUMBER & FLOW DISTRIBUTION IN A BRANCHED CHANNEL

Introduction

Crowe (C13) tested the influence of upstream Reynolds' number (Re) on the ratio of fluid flow in the downstream limbs of a bifurcated channel 3mm in diameter as shown in fig.B1. The flow model, whose limbs were of the same cross-sectional shape and area as the portion upstream of the bifurcation, consisted of a straight channel 20cm in length with a side branch 10cm in length commencing 10cm from the entrance at an angle of 30° to the axial direction. The channel ends were open to the atmosphere in order to ensure that the end pressures were equal. Defining the flow ratio (Fr) as the ratio flow in branch/flow in mainstream, he obtained curves for Re vs Fr similar to those in fig.2 for a) water and for b) a 14% mass dye solution (using Milling yellow dye) in water. The dye solution viscosity was in the range 10-15cP, while viscosity of water was 1cP.

Crowe's results indicated that when viscosity is altered, the Fr-Re relationship, while retaining the same form, changes quantitatively. The curve describing the relationship invariably exhibits a maximum Fr; but for the more viscous fluid this is much closer to the origin (ie is reached at much lower Re). This indicates that Fr is not a function of Re alone.

Rodkiewicz & Roussel (R5) performed similar tests upon a branched flow system using downstream limb diameters of 1.25 inches and varying the side branch-mainstream angles. In this case the channel ends were submerged under constant head overflow tanks which were carefully levelled to provide identical end conditions. The behaviour they observed was similar to that observed by Crowe (C13) but they found Fr became greater than unity at much larger values of Re.

As Re -> 0, momentum forces become small and the flow rates in the two branches are determined by viscous resistance alone. Because the branches in the experiments described above were of virtually equal dimensions, as Re -> 0 viscous resistance in each branch should become equal, and the flow ratio should approach unity. This has been found not to be the case. An additional anomaly is that if Fr becomes equal to ∞, as reported, there is a pressure difference but no flow between the entrance and the exit of the mainstream. Crowe (C13) explains this as being an example of the Coanda effect, in which flow may be conveyed down one branch only under the influence of a low pressure region occurring immediately beyond the sharp bend. The Coanda effect is generally found in symmetric flow regimes (eg Y-branches, expanding ducts etc); in particular those in which there is flow into an expanding cross-section. In an expanding duct, flow along the axis is neutrally stable because hydrostatic pressure is high in the centre and low at the boundaries. If an asymmetric radial pressure is applied instantaneously to the flow the velocity profile immediately skews and the flow becomes attached to one wall. This condition remains when the asymmetric pressure is removed. The direction in

which the asymmetric pressure acts is irrelevant and consequently the condition is bistable. There is no evidence in Crowe's thesis to suggest that bistability exists (perhaps not surprisingly in an asymmetric model) thus it seems unlikely that the flow inequality observed can be explained satisfactorily by an effect of which this is a prominent feature.

The Navier-Stokes equations show that for given boundary conditions, the flow, if governed solely by viscous, inertial and pressure forces, is defined uniquely by Re no matter what fluid is used. As has been described Fr is here found not to be determined purely by Re.

These results thus pose two immediate problems.

(i) Why does Fr -> ∞ as Re -> 0 ?

(ii) Why is Fr apparently not a unique function of Re?

These anomalies merit further examination in view of the physiological importance of low Re branched flows. Accordingly, tests on branched channels have been conducted in order to study these phenomena and these are described below.

Experimental

Several tests upon a diverging duct seem to remove any doubt about whether or not Crowe's assertion that the Coanda effect causes Fr to tend to infinity at low Re is correct. These revealed that, for $1700 < Re < 6000$ the flow was always bistable, and attached itself to either duct wall. When a flow divider was inserted to the model, making it a 2-dimensional Y-branched channel, the flow became monostable. This indicates that at the values of Re at which Crowe's work was done the Coanda effect does not occur, and that some other consideration is needed in order to explain why $Fr \rightarrow \infty$.

It was decided to test a model similar to that used by Crowe (C13) in order to see if his results were reproducible. Fig.B1 illustrates the basic apparatus used. The square cross-section channels were milled in a PVC block and the dimensions of the upstream and each of the downstream branches were 3mm x 3mm x 100mm. The channels were cut of square cross-section primarily because of the greater ease with which the walls could be made continuous at the bifurcation. Crowe (C13) found little difference between results whether the channels were of square or circular cross-section. To enable the flow to be observed, the channel-block was covered with a perspex lid which was bolted on. The angle between the downstream channels was 45°. A constant head was maintained by an overflow in the head tank, which discharged into a lower reservoir. The head tank was fed from the lower reservoir by a pump. In the first experiments flow from the channels was discharged into the atmosphere, as with Crowe's apparatus. Flow-rates were measured by

weighing the fluid collected in beakers placed below the exits in a known period of time.

The variation of flow ratio with Reynolds' number was studied using two fluids: water, and a glycerol/water solution of viscosities 1cP and 10cP respectively. The viscosities were measured using a Haake co-axial cylinder viscometer. The results are plotted in fig.B3, with those of Crowe (C13) superimposed. There is very little agreement between the two sets of results. Where Crowe's curves for both liquids show increasing flow ratio with decreasing Re, present results for water show Fr decreasing monotonically with Re whereas those for the glycerol solution show that Fr first increases with decreasing Re and then suddenly decreases sharply to zero. At no point does the flow ratio of either fluid exceed unity. The present results were similar to those of Crowe only in that poor correlation between the Fr-Re curve for water and that for the more viscous solution was found both in the present work and in that done by Crowe (C13).

The present results do offer support to Crowe's finding that when the fluid is changed, the relationship between Fr & Re is altered. This implies that some fluid mechanical property of the testing fluids other than those considered in the conventional formulation of the Navier-Stokes equations must also be taken into account in order that the flow system be defined fully.

Because new surface is created at the channel exits as the fluid discharges into the atmosphere surface energy is expended. It seems likely that surface tension could be one such property. If surface

tension is significant in the system, then in order to define the flow fully a new dimensionless parameter incorporating it must be defined. One such parameter could be

$$Rw = Re^2/We = \rho\sigma d/\mu^2$$

where σ = surface tension,

and We = Weber number = $\rho u^2 d/\sigma$

Rw is dependent only on the static properties of the fluid and the characteristic length d. If no other forces are significant, then Rw and Re will define the system fully. The values of Rw for water and for the water-glycerol solution were found to be 216000 and 1940 respectively. The surface tensions of the liquids were determined using a torsion balance. Because these values differ by a factor of 100, any effect of surface tension upon the flow system might be expected to be made apparent. In order to observe the effect of

(a) testing a fluid of Rw similar to water, and

(b) using a fluid of density and viscosity similar to water but of different surface tension,

the first experiments were repeated with heptane and a detergent solution in water, for which the values of Rw were respectively 247000 and 131000. The values of Rw for heptane and water are similar and the soap solution is fluid mechanically similar to water, differing only in its surface tension. It should be noted that the values of Rw for all the fluids are substantially different from that of the glycerol solution.

Plots of Fr vs Re for heptane and the detergent solution are contained in fig.B4 and those for water are super-imposed. The curves for the three are qualitatively very similar, as would be expected if Fr = fn(Re,Rw), and each can be divided approximately into 3 parts, viz. the regions $0 \leq Re \leq 200$, and $1000 \leq Re \leq 4000$ when the gradient is positive (ie when Fr increases with increasing Re) and the region $200 \leq Re \leq 1000$ when the gradient is negative (ie when Fr decreases with increasing Re).

The section of the curve where $200 \leq Re \leq 1000$ shows Fr increasing (as expected) to unity with decreasing Re as the influence of inertial forces upon the flow diminishes.

Fr begins to increase with Re when $Re > 2000$ and becomes relatively constant when $Re \approx 6000$. The relationship between Fr and Re for $Re > 6000$ has not been investigated here, but it is interesting at this point to speculate upon the results for flows in which viscosity is small. Appendix A contains a formulation of the equations describing potential flow in this domain. Equation (A1) in Appendix A is the following

$$(Fr+1)^3 - ((Fr+1)/Fr)^3 = 1$$

which gives a value for Fr of 1.043 for a branch angle of 45°. This implies that as $Re \to \infty$ in the systems discussed above Fr approaches a value just greater than unity; ie more flow enters the branch than the mainstream. This result is obtained using theory which incorporates different boundary conditions from those which occur in reality in

viscous flow even at very high, non-physiological Re; namely non-zero velocity conditions at solid boundaries and infinite velocity at the sharp cornered entrance to the side branch upon the outer wall and using a 2-dimensional infinite domain rather than the 3-dimensional domain under examination. For water-flows of high Re Fr increases with increasing Re. Whether or not Fr -> 1.043 as Re -> ∞ cannot be ascertained easily using water for the simple reason that the apparatus would not stand up to the high pressures involved.

If the angle is π/4 then Fr = 1.000 ie if viscous forces were negligible throughout the domain then Fr would be greater than unity. It is possible that as Re -> ∞, Fr -> 1.000 . When Re becomes less than 200 however, Fr starts to decrease with decreasing Re and side branch flow stops when Re > 0.

In addition, a number of tests were devised in order to observe the effects upon flow of altering the method of discharge and measurement and of eliminating all effects of surface tension.

(i) each channel was made to discharge over a weir which was contained within a reservoir attached to the model as illustrated in fig.B5. The weir heights were measured carefully using a depth micrometer and adjusted until the difference was less than 0.1mm. The discharged liquid was caught in a beaker as described before, and flow rates determined by timing the run. With this configuration Fr decreased with decreasing Re but reproducibility of results was poor. Because it is impossible to make the heights of the weirs absolutely equal it is likely that slight differences in level distorted the values of

Fr obtained at low flow rates. However this does not explain satisfactorily the lack of reproducibility in the results. During the runs a meniscus formed at the tops of the weirs due to the effects of surface tension. The heights of these menisci varied proportionally with flow-rate (ie the higher the flow-rate the higher the meniscus-height), hence it was felt that height differences in the menisci should, if anything, have an equalising effect upon the flow-ratios.

(ii) the reservoirs described above were joined by 1/2 inch pipe and the weirs removed. The channels now discharged into the reservoirs below the liquid surface in each, which was held at a common level by the connecting pipe. A water-dye interface was introduced by a sudden switch of feed to the model from a reservoir containing clear water to one containing a solution of bromo-thymol blue dye. Flow through the branched channel was timed using a stop-watch placed upon the apparatus and recorded using a video camera and recorder. The flow-rate was determined by following the rate of advance of the velocity front. Variation of flow-rate due to the progressive change in hydrostatic head in the exit-reservoirs over the course of a run was prevented by use of a constant rate infusion pump.

Variation of Fr with Re was extremely erratic at low flow rates and it was impossible to tell what effect varying Re had upon Fr. Close inspection of the reservoirs during different runs revealed that the angle of contact between the water and the wall in each of the reservoirs varied greatly, causing the surface sometimes to be concave

upwards, and at other times to be concave downwards. Such a finding means that the surface tension characteristics of the reservoirs were generally different from each other and varied from run to run (caused presumably by varying degrees of contamination). Contamination of the weir system may also be a reason for the inconsistency of the results in that configuration.

(iii) the channel was placed in a large reservoir of water and water flow-rates in the branches recorded using video equipment as described above. With this configuration there should be no effects caused by surface tension as the flows discharge into a large body of the same liquid which has no solid surface near the exit local to either channel. The results from this set of runs are plotted in fig.B6. There does not appear to be any tendency in this case for more flow to enter the side branch than the main one at any value of Re tested. When Re is high, Fr is low and when Re decreases Fr tends towards unity as was predicted in the introduction to the chapter. Furthermore, the results were much more reproducible in this case than in previous configurations.

Because the behaviour observed in the latter experiments described above (where all end effects were believed to have been eliminated) was as expected and that observed by Crowe (C13) (using a system where end effects had not been removed) was anomalous, it seems likely that the effects of surface tension at the channel end (of which he took no account) could explain his curious results. The remaining difficulty to be considered is that Crowe (C13) and Rodkiewicz & Roussel (R5) reported no problems with reproducibility of

results, whereas the results of the former tests described here (using a system similar to the one he describes) were highly erratic. It is possible that their experimental systems were less susceptible to variable contamination of the exposed surfaces than the ones used in this case. As is described below, however, much more consistent results (which are similar to those of Crowe (C13) and of Rodkiewicz and Roussel (R5)) can be obtained if the geometry of the branch is altered.

At low flow rates, viscous forces alone should determine flow distribution in this geometric configuration. There are, however, two ways in which surface tension could cause an inequality between the surface effects at the channel ends,

(a) slight contamination of one or other of the channel exits.

(b) minor differences in detailed geometry of the channel exits.

The effects of these factors upon the system were tested as described below.

Effects of Deliberate Contamination of the Discharge Reservoirs

Two cylindrical reservoirs were constructed from the weirs described above by attaching a 1/2 inch connecting pipe to the weir exits and were filled with water to a level-marker. A pre-selected amount of detergent was added to one reservoir to make the surface tension of the liquid in it 0.048 Nm^{-1}. The value of σ for water at

298K was 0.073 Nm^{-1}. The curves in fig.B7 show that the relationship between Fr & Re depended highly on the relative surface tensions of the reservoirs at low Re but less so at high Re; at low Re, if σ in the side branch reservoir is low, Fr becomes high, while if σ in the other reservoir is low, then Fr becomes low. These results can be explained in terms of reservoir contamination. Early experiments by Ablett (reported in C22) indicate that when a horizontal cylinder which rests in a reservoir of liquid in such a way that a small meniscus of liquid is formed at the interface with the wall, the angle of contact between the liquid and the vessel surface varies with rate of cylinder rotation. This implies that in any system where a liquid surface is moving relative to a solid boundary (such as is the case in the reservoir experiments described above), the angle of contact between the two will vary with rate of relative motion. This means that even in a configuration where no new surface is being formed a driving pressure is necessary to overcome the axial component at the air-water-wall interface. Referring to fig.B8, if P_a = atmospheric pressure (an infinitesimal distance above the liquid surface) then

$$\delta P_2 = \delta P_3 = P_a$$

If δP_2 & δP_3 represent the pressure drop due to surface tension across the liquid surface in the reservoir, and δP_4 & δP_5 represent the pressure drop between the channel entrance and a point an infinitesimal distance below the liquid surface, then

$$P_1 - P_a = \delta P_4 + \delta P_2 = \delta P_5 + \delta P_3 \quad \text{(Eqn B1)}$$

When the surface characteristics in the two reservoirs are identical and the surfaces rise at the same rate, the angles of contact and hence the pressure drop due to surface tension are identical.

$$\text{ie} \qquad \delta P_2 = \delta P_3$$

In this case, $\delta P_5 = \delta P_4$, and the flow situation is determined purely by Re.

From observations of the system, while the rate of change of the surface height is the same in each reservoir, the angles of contact are different, implying that $\delta P_2 \neq \delta P_3$. Consider the case when $\delta P_3 < \delta P_2$. Eqn (B1) implies that $\delta P_5 > \delta P_4$, hence the flow rate in the mainstream is driven under a higher pressure gradient, and is greater than the side branch flow. In this case Fr -> zero, and represents the situation where detergent was added to the mainstream reservoir. When the surface tension in the side branch reservoir was reduced by addition of detergent $\delta P_2 > \delta P_3$ and Fr -> ∞.

Effect of Geometry Alteration

A semi-circular groove 3mm in diameter was cut in the end of the side branch only as shown in fig.B9 in order to create different end configurations between the channels. The runs were repeated for all four working fluids: water, heptane, glycerol solution and detergent solution and in addition several tests were conducted using pulsatile flow for various values of the frequency parameter $\alpha = d\sqrt{(f/\upsilon)}$ (f =

frequency parameter, υ = kinematic viscosity). The steady flow results (plotted in fig.B9) showed much greater uniformity and reproducibility in this configuration than when the channel ends were similar. All the curves depict Fr increasing with decreasing Re at lower Re and Fr increasing with Re at higher Re. As Rw decreases, the curves become closer to the origin.

It appears that the alteration of the side branch geometry has caused a decrease in the work done by the fluid in forming new surface. Because the pressure difference between the fluid inlet pipe and the ends of both of the branches is the same, the pressure drop in the side branch due to viscous losses must be greater than in the main stream and hence its flow rate greater. The alteration of the geometry must also have decreased the characteristic diameter, d, of the side branch at exit and therefore the role of surface tension in the side branch flow is reduced. These results also illustrate the validity of the parameter Rw in defining the flow. While specific fluid mechanical properties of heptane and water are substantially different, the value of Rw for each is relatively similar and the curves obtained for both in fig.B10 are very close together.

When pulsatile flow was applied to the apparatus (using a sinusoidal pulse and minimum velocity of zero) the plot of Fr vs Re (based on mean flow rate) was virtually identical to that of steady flow for the same working fluid. Frequency parameter was not found to be of any significance at all; when it was set at 2.12 for both water and for the glycerol solution the curves were identical to those for the corresponding fluids in steady flow.

At low Re during the pulsatile flow tests, when there was no flow in the main branch, a surface tension bubble was formed at the channel exit which inflated and deflated continuously during the cycle. This gave visual evidence that surface tension was preventing flow in the main branch and implied that it was altering the flow distribution characteristics of the channel.

4. Conclusions

The experiments described above indicate that the flow systems examined by Crowe and by Rodkiewicz & Roussel (R5) cannot be characterised by Re and relevant geometric factors alone: another dimensionless parameter containing surface tension is also required. From the results obtained using the channel immersed in a reservoir, it seems reasonable to conclude that as Re -> zero, Fr -> unity, rather than either zero or ∞. This is consistent with the introductory discussion in which doubt was expressed over the experimental results found by Crowe (C13) whereby Fr -> ∞ as Re -> zero and suggests that both his apparatus and that of Rodkiewicz and Roussel (R5) contained some flaw which allowed surface tension effects to cause an uneven distribution between the downstream limbs. For a system wherein the influence of surface tension can be neglected, the flow ratio will be purely a function of Reynolds' number. This is likely to be the situation in natural arterial systems, for which, accordingly, the apparatus used by Crowe (C13) and by Rodkiewicz and Roussel (R5) do not provide a valid model.

Why Fr -> ∞ rather than zero in the systems tested by Crowe (C13) and by Rodkiewicz and Roussel (R5) as Re decreases is, as yet, unknown. It may have been due simply to differences in channel end conditions associated with differing surface conditions becoming apparent only at low flow rates when the ratio of surface tension forces to all kinds of flow forces becomes large.

The value of this type of study, in terms of physiological implication, may well be limited. About 90% of the pressure drop across the circulation occurs in the peripheral arteries. Because of this, if a lesion is formed at a large bifurcation causing for example a doubling of local pressure drop, the effect upon distribution of flow throughout the network may well be negligible. This is why a stenosis in a major bifurcation is not generally considered clinically significant until about 50% of the arterial cross-section is blocked; fluid mechanically the stenosis may well not be significant in influencing flow distribution until it is even more severe. Similarly a study of the variation of Fr with Re in such models as described above may be of limited value because of the relative insignificance of the pressure drop across the branch compared with that across the whole circulation. Thus Rodkiewicz and Howell's conclusion that flow to various parts of the body can be controlled by simple adjustment of pulse shape or frequency is somewhat short-sighted. A more valid representation of the flow situation would be a model bifurcation in which the branches discharge into long thin tubing such that the ratio of pressure drop in the branch to that over the total system is physiologically realistic. A study of the effect upon flow distribution of Re or of stenoses would probably reveal much smaller dependency of

Fr upon either independent variable in such a system than in those discussed above. Flow in the microcirculation is controlled substantially by signals from the brain to the smooth muscle cells in the arterial wall which cause the vessel cross-section either to contract or to dilate as is necessary. This process is known as auto-regulation and it is more likely that control of flow in the major arteries is done in this way than by varying flow parameters as is suggested by Rodkiewicz and Howell.

Appendix C

Estimation of the Constant Rate Period of Mass Transfer

The second condition specified by MacLeod and Todd (M5) which must be fulfilled if the swollen polymer method is to be valid is that the effective vapour pressure of the swelling agent must not vary significantly either over the surface under study or during the course of the experiment. They (MacLeod and Todd M5) present a method by which the period of time over which this approximation is valid can be approximated. Their method invokes the assumption that if the effective vapour pressure during a run does not drop to a level less than 95% of the initial vapour pressure, then it can, for experimental purposes, be considered constant over the whole course of the run. This method is now used to estimate the duration of this constant rate period using data from the present set of results.

Initial polymer coating thickness = 0.03 cm = δ_1

approximate diffusivity of ethyl salicylate in the silicone rubber

$$D = 10^{-6} \text{ cm } s^{-1}$$

Equilibrium volume fraction of ethyl salicylate $\varphi_1 = 0.575$.

MacLeod and Todd's eqn (1) gives $\chi = 0.72$, χ is a constant characteristic of the system.

Using their fig 3 the change in volume fraction of swelling agent for which a 5% drop in vapour pressure is sustained [$f_1 = \varphi_1 - \varphi_2 = 0.16$.

The rate of mass transfer of swelling agent per unit surface area was found by MacLeod and Todd (M5) by weighing samples before and after each run. This value can now be found more easily by using interferometry. Using eqn 2.5

$$M = \rho v = \rho\lambda(\partial N/\partial t)/2(n-1)$$

The maximum rate of fringe traversal recorded during the experiments was

$$\partial N/\partial t = 0.0128\ s^{-1}$$

hence $M = 8.74 \times 10^{-6}$ kg $m^{-2}s^{-1}$

Substituting this value, together with those above into MacLeod and Todd's eqn (18) for δ'/δ (maximum allowable change in polymer thickness/initial thickness) yields

$$\delta' = 0.0000795\ m$$

and use of this value in their eqn (9) gives

$$t' = 171 \text{ minutes}$$

This is the maximum allowable duration of a run before the rate of mass transfer of the swelling agent becomes dependent upon rates of diffusion within the polymer.

Nomenclature

A	area
A_{ij}	components of stiffness matrix according to eqns 3-5
c	concentration
c_o	concentration of swelling agent in working fluid
c_s	concentration of swelling agent at surface
c_X	$\partial c/\partial X$
c_Y	$\partial c/\partial Y$
d	diameter (hydraulic mean = 4 x Area/Perimeter)
D	diffusivity
f	frequency
Fr	flow ratio (side branch flow/main branch flow)
H	channel width (appendix A)
i	$(-1)^{0.5}$
k	solubility of O_2 in tissue (chapter 4)
k_m	mass transfer coefficient
k_m^*	adjusted mass transfer coefficient
L_1, L_2	geometric path lengths of light
L	characteristic length (taken as 1/2 width of stream in chapters 2 & 3)
L_1, L_2	variables defining ratio of flow distribution in a potential flow branched domain (only in appendix B)
m	rate of mass transfer/unit surface area
m	strength of source (only in appendix A)
M	mass transfer rate per unit width
M_i,[M]	linear interpolation function
m_{02}	mass flux of O_2 through tissue

m_s molecular weight

N number of fringes generated (chapter 2)

N = n/L

N' rate of fringe generation = $\partial N/\partial t$

N_i, [N] quadratic interpolation function

n normal distance (chapter 3)

n refractive index (chapter 2)

P hydrostatic pressure

Pe Peclet number = uL/D

P_{02} O_2 pressure

P_{es} ethyl salicylate (swelling agent) pressure

P_s^* surface vapour pressure of swelling agent (chapter 2)

q volumetric flow rate as defined in appendix A

Q volumetric flow rate per unit width

Q_{02} O_2 consumption per unit tissue volume

R Universal Gas Constant

Re Reynolds' number = $\rho u L/\mu$

Rw Re^2/We

s tangential distance (chapter 3)

S optical path length of light

ΔS change in optical path length

Sc Schmidt number = $\mu/\rho D$

Sh Sherwood number = $k_m^* L/D$

Sh^* Sherwood number adapted to account for reduced swelling agent driving force

Sh_{extrap} Sh extrapolated from that for Sc = 2.7 ; Re = 50 using eqn (3-24)

Sh_{Re} Sh normalised with respect to that for Re = 50

Sh_{Sc}	Sh normalised with respect to that for Sc = 2.7
t	function generated by eqn A10
t	time
T	absolute temperature
$\underline{U}$	velocity vector
u	axial velocity
u^*	axial velocity based on use of estimated nodal velocities and eqns 3-2
{u}	vector of nodal velocities
U_c	velocity in centre-stream
U_o	mean velocity of stream
U	$=u/U_o$
v	transverse velocity
{v}	vector of nodal velocities
v^*	transverse velocity based on use of estimated nodal velocities and eqns 3-2
V	$=v/U_o$
w	complex velocity $= u + iv$
We	Weber number $= \rho u^2 L/\sigma$
x	axial distance
X	x/l
X_o	axial coordinate of leading edge of momentum boundary layer
y	transverse coordinate
Y	y/L
z	complex distance $= X + iy$

Greek Letters

α acute angle of branch at flow divider in potential flow domain (appendix A)

α frequency parameter ($=d(f/\upsilon)^{0.5}$)

δ distance of recession

δ_c thickness of concentration boundary layer

δ_m thickness of momentum boundary layer

η local nodal coordinate

θ_c critical angle of total internal reflection

λ wavelength of light

μ viscosity

ξ local nodal coordinate

ξ function generated by eqn (A6) only in appendix A

ϱ density

σ surface tension

Σ sum of

υ kinematic viscosity

ψ stream function

ω vorticity

A1) Anliker M,Rockwell RL, & Ogden E, "Non-Linear Analysis of Flow Pulses and Shock Waves In Arteries",Zeitschrift fur Angewandte Mathematik und Physik,V22,p217 (1971)

A2) Anliker M,Rockwell RL, & Ogden E,""Non-Linear Analysis of Flow Pulses & Shock Waves In Arteries",Zeitschrift fur Angewandte Mathematik und Physik,V22,p563 (1971)

A3) Agrawal, Talbot & Gong "Laser Anemometer Study of Flow Development In Curved Pipes." J.Fluid Mechanics, v85, p497.

A4) Aggarwal JK,"Development of a Hot Film Gauge Suitable for Measurement of a 3-D Velocity Meter",J.Physics,ser E, p733,V7, 1974 (sci instrs)

A5) Atabek HB, Ling SC & Patel DJ, "Analysis of Coronary Flow Fields In Thoracotomised Dogs", Circulation Research, V37, p752, 1975.

A6) Anliker M,Histand MB, & Ogden E,"Dispersion & Attenuation of Small Artificial Pressure Waves in The Canine Aorta", Circulation Research, V23,p539,(1968).

A7) Adamson SL & Roach MR "Measurement of Wall Shear Stress in a Glass Model Renal Bifurcation by a Technique that Monitors Rate of Erosion of an Opaque Coating Dye", Biorheology, V18, p9-21, 1981

A8) Ahmed SA, Giddens DP "Velocity Measurements in Steady Flow Through Axisymmetric Stenoses at Moderate Reynolds' Numbers", J.Biomechanics, V16, p505, 1983.

B1) Bergel DH, Nerem RM & Schwartz D "Fluid Dynamic Aspects of

Arterial Disease", Atherosclerosis, V23, p253, 1976.

B2) Back LH, Radbill & Crawford DW "Analysis of Pulsatile Flow Through Diseased Coronary Arteries of Man", J.Biomechanics, V10, p339, 1977.

B3) Bergel DH "Cardiovascular Fluid Mechanics", Academic Press, London & New York, 1972.

B4) Brech R & Bellhouse BJ "Flow in Branching Arteries", Cardiovascular Research, V7, p593, 1973.

B5) Bergel DH "Elastic Properties of Arterial Wall (Static)", J.Physiology, V156, p445, 1961.

B6) Bergel DH "Elastic Properties of Arterial Walls (Dynamic)", J.Physiology, V156, p458, 1961.

B7) Blackshear PL "Deposition of Platelets on Filtering Walls", Proc.Specialist's Meeting, Ohio St.Univ., Sept 1974, p63.

B8) Blackshear PL, Vargas CF, Vargas CB, Pribyl JG, & Blackshear GL "Hydraulic Conductivity of Intact Endothelium, Permeability of Media & Consolidation Properties in the Intact Rabbit", Proc. Specialist's Meeting, Ohio St Univ, Aug 1978, chp 17.

B9) Balasubramanian K, Mabon RF & Giddens DP "Flow in Carotid Bifurcation", Proc Specialist's Meeting, Univ Houston, Nov 1980, p78.

B10) t2 Benson TJ, Nerem RM & Pedley TJ "Assessment of Wall Shear Stress in Arteries Applied to the Coronary Circulation", Cardiovascular Research, V14, p568, 1980.

B11) Boughner DR & Roach MR "Effect of Low Frequency on the Arterial Wall", Circulation Research, V29, p136, 1971.

B12) Booth FVMcL,"Arterial Wave Propagation In Vivo", AGARD Conference Proceedings, no.65,(1970)

B13) Bergel DH & Schultz DL "Arterial Elasticity & Fluid Dynamics", Progress in Biophysics & Molecular Biology, V22, p1, 1971.

B14) Boughner DR & Roach MR "Effect of Low Frequency Vibration on Arterial Wall Elastin", AGARD Conference Proceedings, No.65, Naples, 1970.

B15) Batten JR & Nerem RM "Model Study of Flow in Curved & Planar Arterial Bifurcations", Cardiovascular Research, V16, p178-86, 1982.

B16) Back LH, Radbill & Crawford DW "Analysis of O_2 Transport of Pulsatile Flow to Diseased Coronary Arteries of Man", J.Biomechanics, V10, p763-774, 1977.

B17) Bharadvaj BK & Giddens DP "Steady Flow in Model of Human Carotid Bifurcation (I) Flow Visualisation, (II) Laser Doppler Anemometry", J.Biomechanics, V16, p349, 1982.

B18) Buerk DG & Goldstick TK,"Arterial Wall Oxygen Consumption Rate Varies Spatially", Am. J. Physiology,V243,p948-58,(1982)

B19) Bird RB,Stewart R,& Lightfoot G,"Transport Phenomena", Wiley,NY,(1960)

B20) Bhatti MS & Savery CW.,"Heat Transfer in the Entrance Region of a Straight Channel:Laminar Flow with Uniform Wall Temperature",J.Heat Transfer,V100,p539,(1978),ASME

C1) Caro CG, Schroter R, Seed WA & Pedley TJ "Mechanics of the Circulation", 1978.

C2) Caro CG, Fitzgerald JM & Schroter RC "Atheroma & Arterial Wall Shear; Observation, Correlation & Proposal of a Shear Dependent Mass Transfer Mechanism for Atherogenesis", Proc Royal Soc London(B), V177, p109, 1971.

C3) Clark C & Schultz DL "Velocity Distribution in Aortic Flow", Cardiovascular Research, V7, p601, 1973.

C4) Cornhill JF & Roach MR "A Quantitative Study of Localisation of Atherosclerotic Lesions in the Rabbit Aorta", Atherosclerosis, V23, p489, 1976.

C5) Cornhill JF, Levesque & Nerem RM "Quantitative Techniques for the Study of the Arterial Wall", Proc Specialist's Meeting, Ohio St Univ, Aug 1978, chpt 7.

C6) Cornhill JF & Roach MR "Quantitative Method for the Evaluation of Atherosclerotic Lesions", Atherosclerosis, V20, p131, 1974.

C7) Chandran KB, Hosey RR, Ghista DN & Vayo VW "Analysis of Fully Developed, Unsteady, Viscous Flow in a Curved Elastic Tube Model to Provide Fluid Mechanical Data for Circulatory Pathological, and Physiological Situations and Assisting Devices", J. Biomechanical Engineering, ASME, V101, p114, 1979.

C8) Colton CK, Brateler RL, Smith KA, Chisholm GM, Lees RS & Zilversmit DB "Transport of Albumin & Low Density Lipoproteins in the Arterial Wall", Proc Specialist's Meeting, Ohio St Univ, Sept 1974, p51.

C9) Caro CG "Metabolic & Mechanical Studies on the Transport of Macromolecules Across the Arterial Endothelium", Proc Specialist's Meeting, Ohio St Univ, Sept 1974, p58

C10) Caro CG, Schroter RC and Fitzgerald JM "Arterial Wall Shear & Distribution of Early Atheroma in Man", Nature, V223, p1159, 1969.

C11) Chien SUsami S, Fon-Chung Fan, Skalak R, Weinbaum S & Caro CG "Effects of Mechanical Disturbances on Uptake of Macromolecules by the Arterial Wall", Proc Sp Meeting, Ohio St Univ, Aug 1978, chpt 16.

C12) Caro CG, Laver-Rudich Z, Meyer F, Liron N & Ebel W "Albumin Transport in the Rabbit Common Carotid Artery", Proc Sp

Meeting, Ohio St Univ, Aug 1978, chpt 18

C13) Crowe WJ "Studies of Arterial Branching in Models Using Birefringence", Ph.D., Univ of Florida, 1969.

C14) Chien S, Fan FC, Laufer L, Arminski L, Weinbaum S & Handley DA "Effects of Pressure Variations on Macromolecular Transport by the Arterial Endothelium", Proc Sp Meeting, Univ Houston, Nov 1980, p38

C15) Colton CK, Schneiderman G, Ramirez CA, Smith KA & Lees RS "Labelled Albumin Transport into Normal & De- Endothelialised Rabbit Thoracic Aorta In Vivo", Proc Sp Meeting, Univ of Houston, Nov 1980, p42

C16) Caro CG & Nerem RM "Transport of ^{14}C-4 Cholesterol Between Serum & Wall in the Perfused Dog Common Carotid Artery", Circulation Research, V32, p187, 1973.

C17) Caro CG "Mechanical Factors in Atherogenesis", in Cardiovascular Flow Dynamics & Measurements, eds Hwang & Normann, Univ Park Press, Baltimore, 1977.

C18) Caro CG, Fitzgerald JM, & Schroter RC "Wall Shear Rate in Arteries & Distribution of Early Atheroma", AGARD Conference Proceedings, 1970.

C19) Chandran KB & Yearwood TL "Experimental Study of Physiological Pulsatile Flow in a Curved Tube", J.Fluid Mechanics, V111, p59, 1981

C20) Cho YI, Back LH & Crawford DW "Pressure Difference - Flow Rate Variation in Femoral Artery Branch Casting of Man for Steady Flow", J.Biomechanical Engineering, V105, o258, 1983.

C21) Chisholm GM, and Bohner M "Transmural ^{125}I Albumin Concentration in the Rabbit Aorta During Acute Hypoxia", Atherosclerosis, V14,

p195, 1983.

C22) Champion FC & Davy N "Properties of Matter", Student Phys Vol 3, London,1947.

C23) Crawford DW, Back LH,& Cole MA,"In Vivo Measurements of the Boundary Layer Oxygen Gradient in the Normal Dog Femoral Artery", Proc Sp Meeting, Houston, Nov 1980,p67

D1) Duncan, Buck & Lunch "Effect of Pressure & Stretching on Passage of Labelled Albumin into the Canine Wall", J. Atherosclerotic Research, V5, p69, 1965.

D2) Davids N & Kandarpa K "Contributions to the Analysis of the Fluid Dynamic Field at Branching Sites", Proc Sp Meeting, Ohio St Univ, Sept 1974, p16.

D3) Dewey CF, Kenon DE, Wijesinghe A, Bussolari SD & Zwerling HK "Studies of the Forces Acting upon Arterial Endothelium", Proc Sp Meeting, Ohio St Univ, Aug 1978.

D4) Dewey CF, Gumbrone MA, Bussolari SR & Cruise SA "The Dynamic Response of Vascular Endothelial Cells to Fluid Shear Stress", Proc Sp Meeting, Univ Houston, Nov 1980, p24.

D5) Davids N, Cheng RC,"Transient Laminar Flow in Ducts of Arbitrary Cross-Section by Finite Element Methods",J.Biomechanics,V5,p485-99,(1972)

D7) Diller TE & Mikic BB,"Oxygen Diffusion in Blood:a Translation Model of Shear-Induced Augmentation", J.Biomechanical Eng, ASME,V105,p346, (1983)

D8) Dorrington K,"Rubber-Like Elasticity in the Body;Study of Elastin and its Synthetic Analogue,Poly 2- Hydroxyethyl Methacrylate (PHEMA),D.Phil Thesis, Oxford, (1977)

D9) Duma A & Barozzi GS, "Laminar Heat Transfer to Blood Flowing in

a Circular Duct",Int J.Heat & Mass Transfer,

E1) Ehrlich LW,"Digital Simulation of Periodic Fluid Flow in a Bifurcation",Computers and Fluids,V2,p237,(1973)

E2) Enos WF,Beyer JC, & Holmes RH,"Pathogenesis of Coronary Disease in American Soldiers Killed in Korea", J.Am.Medic.Assoc.,V158,p912,(1955)

E3) El Masry OA, Feuerstein IA & Round GF, "Experimental Evaluation of Streamline Patterns And Separated Flows in a Series of Branching Vessels, with Implications for Atherogenesis and Thrombosis", Circulation Research,V608,1978

E4) El Masry OA and Feuerstein IA, "Electrochemical Surface Shear Rate Evaluation in Models of the Renal Artery",J.Biomech.Eng., ASME,V104, p290,(1982)

E5) Ehrlich LW & Friedman MH,"Steady Convective Diffusion in a Bifurcation",IEEE Trans on Biomedical Engin.,V24,p12,1977)

F1) Fry DL,"Acute Vascular Endothelial Changes Associated with Increased Blood Velocity Gradients",Circulation Research,V22,p165,(1968)

F2) Fry DL,"Certain Histological & Chemical Responses of the Vascular Interface to Acutely Induced Mechanical Stress in the Aorta of a Dog",Circulation Research,V24,p93,(1969)

F3) Friedman MH, Bargeron CB, Hutchins, Mark FF & Deters OJ,"Hemodynamic Measurements in Human Arterial Casts,Correlation with Histology and Luminal Area",J.Biomech.Engin.,Trans ASME,V102,p247,(1980)

F4) Friedman MH, O'Brien V, & Ehrlich LW,"Calculations of Pulsatile Flow Through a Branch",Circulation Research,V36,p277,(1975

F5) Fox B,and Seed WA,"Location of Early Atheroma in Human Coronary

Arteries",J.Biomech.Engin,ASME,V103,p208,(1981)

F6) Friedman, Hutchin, Bargeron CB, Deters OJ, Mark FF,"Correlation of Human Arterial Morphology with Hemodynamic Measurements in Arterial Casts",J.Biomech.Engin,ASME,V103,p204,(1981)

F7) Fox JA,& Hugh AE,"Localisation of Atheroma:A Theory Based on Boundary Layer Separation",British Heart Journal,V28,p388,(1966)

F8) Friedman MH,"Shear Profiles & Diffusion in Idealised Flows Through a Y-Branch",Proc.Spec.Meeting,Ohio St Univ,Sept 1974

F9) Fry DL, "Some Arterial Changes Associated with Hemodynamic Events",Proc.Spec.Meeting,Ohio St Univ,Sept 1974

F10) Friedman MH & Ehrlich LW,"Effect of Spatial Variations in Shear on Diffusion at the Wall of an Arterial Branch", Circulation Research,V37,p446,(1975)

F11) Feuerstein IA, El Masry OA & Round G "Arterial Bifurcation Flows - Effects of Flow Rate and Area Ratio", Can.J. of Physiol & Pharmacology,V54,p795,(1976)

F12) Fernandez RC & DeWitt & Botwin "Pulsatile Flow Through a Bifurcation with Applications to Arterial Disease",J.Biomechs,V9,(1976),p575

F13) Friedman MH "Transport Through a Growing Boundary Layer to a Permeable Wall", AIChE,V22,p407,(1976)

F14) Friedman MH, Deters OJ "Arterial Geometry Affects Hemodynamics", Atherosclerosis,V46,p225-31,(1983)

G1) Goldsmith & Karino,"Blood Cells in a Region of Flow Separation", Proc.Spec.Meeting,Ohio St Univ,Aug 1978

G2) Gutstein, Farrell & Schneck,"In Vivo Demonstration of Junctional Blood Flow Disturbance by Hot Wire Anemometery"Atherosclerosis,V11,p485,(1970)

G3) Gutstein WH & Schneck DJ "In Vitro Boundary Layer Studies of Blood Flow in Branched Tubes",J.Atherosclerotic Research,V7,p295,(1967)

G4) Gessner FB "Hemodynamic Theories of Atherogenesis",Circulation Research,V33,p259,(1973)

G5) Greene ER & Histand MB "Ultrasonic Assessment of Simulated Atherosclerosis: In Vivo and In Vitro Comparisons", J.Biomechan.Engin,ASME, V101,p73,(1979)

G6) Gutstein WH, Schneck DJ & Marks JO "In Vitro Studies of Local Blood Flow Disturbance in a Region of Separation",J.Atherosclerotic Research,V8,p378,(1968)

G7) Gutstein WH,"Neurocirculatory Relationships and Atherogenesis", Proc.Spec.Meeting,Ohio St Univ,Aug 1978

G8) Grottum P, Svindland A & Walloe L "Localisation of Atherosclerotic Lesions in Bifurcations of Main Left Coronary Artery",Atherosclerosis,V47,p55,(1983)

G9) Gokhal W, Tanner RI & Bischoff KB "Finite Element Solution of Navier-Stokes Equations for 2-D Steady Flow Through Section of Canine Aorta Model", J.Biomechs,V11,p241,(1978)

G10) Gartling D & Becker E "Finite Element Analysis of Viscous Incompressible Fluid Flow",Computer Methods in Applied Mechanics & Engineering,V8,p51-60,(1976)

G11) Gartling D & Becker E "Finite Element Analysis of Viscous Incompressible Fluid Flow - Applications",Computer Methods in Applied Mechanics and Engineering,V8,p127-138,(1976)

G12) Galanga FL & JR Lloyd "An Experimental Study of the Flow-Induced Mass Transfer Distribution in the Vicinity of Prosthetic Heart Valves",J.Biomech.Engin,ASME,V103,p1,(1981)

H1) Holenstein R, Niederer P & Aniker M, "A Viscoelastic Model for Use in Predicting Arterial Pulse Waves",J.Biomech.Engin,ASME,V102,p318,(1980)

H2) Histand ,Miller & McLeod,"Transcutaneous Measurement of Blood Velocity Profiles & Flow",Cardiovascular Research,V7,p703,(1973)

H3 Hall PH,"Unsteady Viscous Flow in a Pipe of Slowly Varying Cross-Section",J.Fluid Mechanics,V64,p209,(1974)

H4) Histand MB,& Miller CW,"Non-Invasive Ultrasonic Detection of Atherosclerosis",Proc.Spec.Meeting,Sept 1974,Ohio St Univ.

H5) Hollis TM & Markle RA,"Shear Stress Induced Histamine Synthesis and its Relation to Albumin Permeability in the Arterial Wall",Proc. Spec.Meeting,Ohio St Univ,Aug 1978.

H6) Hugh AE & Fox JA,"The Precise Localisation of Atheroma and its Association with Stasis in Carotid Artery",Brit.J.Radiography,V43,p377,(1970)

H7) Histand MB,"The Influence of Hemodynamics on the Development of Atherosclerosis",Proc.24th Ann.Conf.Engin. in Medic. & Biol,(1971).

H8) Houle S & Roach MR,"A Case for High Shear as a Cause of the Localisation of Sudanophilic Lesions in Rabbits",Atherosclerosis,V40,p231,(1981)

H9) Hunt WA,"Calculations of Pulsatile Flow Across Bifurcations in Distensible Tubes",Biophysical Journal,V9,p993,(1969)

H10) Harper AJ & MacLeod N,"Hot Spots in Heat Transfer",Physics Bulletin,1978,p13

H11) Huebner KH,"Finite Element Method for Engineers",Wiley,NY,(1975)

H12) Helin P & Lorenzen IB,"Arteriosclerosis in Rabbit Aorta Induced by Systemic Hypoxia",Angiology,V20,p1,(1969)

J1) Jones E,Anliker M,& Chang I,"Effects of Viscosity & Constraints on

Dispersion & Dissipation of Waves in Large Blood Vessels", Biophysical Journal,V11,p1085,(1971)

K1) Khalifa AMA & Giddens DP,"Analysis of Disorder in Pulsatile Flows with Application to Post-Stenotic Blood Velocity Measurements in Dogs",J.Biomechanics,V11,p129,(1978)

K2(Keller KH,"The Influence of Shear Dependent Diffusion in Blood in Athero- and Thrombo-genesis",Proc.Sp.Meeting,Ohio St Univ,Sept 1974.

K3) Kandarpa K & Davids N,"Analysis of the Fluid Dynamic Effects on Atherogenesis at Branching Sites",J.Biomechanics,V9,p735,(1976)

K4) Kimmel E & Dinnar U, "Pulsatile Flow in Tapered Tubes - A Model of Blood Flow with Large Disturbances", J.Biomech.Engin,ASME,V105,p112,(1983)

K5) Kapur DN & MacLeod N,"Holographic Determination of Local Mass Transfer Coefficients at a Solid-Liquid Boundary",AIChE J.,V21,p184,(1975).

K6) Kapur DN & MacLeod N,"Vapour Pressure Determination for Certain High-Boiling Liquids by Holography",I & EC Prod Res. & Dev.,V15,p50,(1976).

K7) Kapur DN & MacLeod N "The Estimation of Local Heat Transfer Coefficients for Two Dimensional Surface Roughness Elements by Holographic Interferometry", in Engineering Uses of Coherent Optics, by E. Robertson (ed),C.U.P.,(1976)

K8) Kapur DN & MacLeod N "The Determination of Local Mass Transfer Coefficients by Holographic Interferometry - 1",Int.J.Heat & Mass Transfer,V17,p1151,(1974).

K9) Knudsen JG & Katz DL, "Fluid Mechanics and Heat Transfer",McGraw Hill, New York,1958

L1) Lutz R, Cannon J, Bischoff K, Dedrick R, Stiles R & Fry DL "Wall Shear Stress Distribution in a Model Canine Artery During Steady Flow",Circulation Research,V41,p391,(1977).

L2) Ling SC, Atabek HB, Fry DL, Patel DJ, & Janicki JS "Application of Heated-Film Probes to Hemodynamic Studies",Circulation Research,V23,p789,(1968).

L3) Lutz RJ, Cannon JN, & Munroe RE "Shear Stress Measurements in Model Arteries During Steady & Pulsatile Flow",Proc.Spec.Meeting,Ohio St Univ,Sept 1974.

L4) LoGorfo FW, Soncrant T, Teel T & Dewey CF "Boundary Layer Separation in Models of Side-to-End Arterial Anastomoses",Archives of Surgery,V114,p1369,(1979)

L5) Lallemand RC, Brown KGE & Boulter PS "Vessel Dimensions in Premature Atheromatous Disease of Aortic Bifurcation",Brit Med J,p255,(1972).

L6) Levensen ,"Pulsed Doppler: Determination of Diameter, Blood Flow Velocity & Volumetric Flow in Brachial Artery",Cardiovascular Research, V15,p164,(1981).

L7) Lutz RJ, Hsu L, Monawat A, Zrubek J & Edwards K "Comparison of Steady & Pulsatile Flow in a Double Branching Arterial Vessel,"J.Biomechanics,V16,p753,(1983).

L8) Lewin DR "Analysis of Turbulent Mass Transfer in Entrance Region of a Rectangular Duct using Holographic Interferometry", Undergrad. Research Report, Dept. Chem. Engin., Univ of Edinburgh, May 1978.

M1) Mark FF,Bargeron CB,Deters OJ & Friedman MH "Experimental Investigations of Steady and Pulsatile Laminar Flow in a 90°

Branch",J.Applied Mechanics,ASME,V44,p372,(1977).

M2) Manikko A, Mottonen M & Tenhu M "Location of Atherosclerotic Plaques in the Coronary Arteries",Proc.Spec.Meeting,Ohio sT Univ, Aug 1978

m3) Muller-Mohnsson H, Kratzer M & Baldauf W "Microthrombus Formation in Models of Coronary Arteries caused by Stagnation Point Flow Arising at the Sites of Atherosclerosis and Thrombosis",Proc.Spec.Meeting,Ohio St Univ,Aug 1978

M4) Malcolm AD & Roach MR "Flow Disturbances at the Apex & Lateral Angles of a Variety of Bifurcation Models and their Roles in the Development and Manifestations of Arterial Disease",Stroke,V10,p335,(1979)

M5) MacLeod N & Todd RB "Experimental Determination of Wall Fluid Mass Transfer Coefficients using Plasticized Polymer Surface Coatings",Int.J.Heat & Mass Transfer,V16,p485,(1973)

M6) Milne-Thompson L, "Theoretical Hydrodynamics",McMillan & Co Ltd, London,(1960).

M7) Mizushina T," The Electrochemical Method in Transport Phenomena", Advances in Heat Transfer,V7<p87,(1971).

M8) MacLeod N "Convective Mass Transfer and its Measurement", lectures given at the Von Karmen Institute , Brussels,May 1982.

N1) Nerem RM & Cornhill JF "The Role of Fluid Mechanics in Atherogenesis",J.Biomech Eng,ASME,V102,p181,(198)

N2) Nerem RM, Seed WA, & Wood NB "Experimental Study of Velocity Distribution and Transition into Turbulence in the Aorta",J.Fluid Mechanics,V52,p137,(1972).

N3) Nerem RM & Seed W," An in vivo Study of Aortic Flow Disturbances",Cardiovascular Research,V6,p1,(1972)

N4) Nerem RM Rumberger JA, Gross DR, Muir WW & Geiger GL, "Hot-Film Coronary Artery Measurements in Horses",Cardiovascular Research, V10,p301,(1976)

N5) Nerem RM, Levesque MJ & Cornhill JF "Vascular Endothelial Morphology as an Indicator of the Pattern of Blood Flow",J.Biomech.Engin,ASME,V103,p172,(1981)

N6) Nerem RM, Mosberg AT & Schwerin WD "Transendothelial Transport of I-Albumin",Biorheology,V13,p71,(1976)

N7) Nerem RM, Rumberger JA, Gross DR, Hamdin RL & Geiger GL "Hot-Film Measurements of Coronary Blood Flow in Horses", Proc Spec Meeting, Ohio St Univ, Sept 1974

N8) Nerem RM, Levesque MJ & Cornhill JF "Arterial Fluid Mechanics and the Endothelium",Proc.Spec.Meeting,Univ of Houston,November,1980

N9) Nerem RM "Coronary Hemodynamics:-Measurements and Theoretical Studies",Cardiovascular System Dynamics-Models & Measurements,(eds) Kenner T & Busse R, Plenim Press, New York,(1982)

O1) O`Brien V "Wall Shear in Unsteady Branching Flow",Proc.Spec.Meeting, Ohio St Univ,Sept 1974

O2) O`Brien V, Ehrlich LW & Friedman MH "Unsteady Flow in a Branch",J.Fluid Mechanics,V75,p315,(1976)

O3) O`Brien V & Ehrlich LW "Simulation of Unsteady Flow at Renal Branches",J.Biomechanics,V10,p623,(177)

O4) Okamoto R, Hatani M "The Effect of Oxygen on Development of Atherosclerosis in WHHL Rabbits",Atherosclerosis,V47,p47(1983).

O5) Oden JT & Wellford LC "Analysis of Flow Of Viscous Fluids by the Finite Element Method",AIAA Journal,V10,p1590,(1972)

P1) Pedley TJ "The Fluid Mechanics of Large Blood Vessels",C.U.P.(1980)

P2) Perroneau P, Gisbertz K-H, Steckmeier B & Xheard M "In Vitro &

In Vivo Experimental Studies of Pulsatile Flow Patterns in Curved & Stenotic Vessels",Proc.Spec.Meeting,Ohio St Univ,Sept 1974.

R1) Roach MRR "Possible Role of Geometry of Flow Divider in the Genesis of Atherosclerosis", Proc.Spec.Meeting, Ohio ST Univ,Sept 1974.

R2) Rodkiewicz CM "Brief Discussion: Possible Separation and Stagnation Regions of the Arterial Tree",Proc Spec Meeting,Ohio St Univ Aug 1978.

R3) Rumberger JA, & Nerem RM "A Method of Characteristics Calculation of Coronary Blood Flow",J.Fluid Mechanics,V82,p429,(1977).

R4) Rudinger G "Shock Waves in Mathematical Models of the Aorta",J.Applied Mechanics,ASME,p34,(1970).

R5) Rodkiewicz CM & Roussel CL "Fluid Mechanics in a Large Arterial Bifurcation",J.Fluid Engin.,ASME,V95,p108,(1973)

R6) Rodkiewicz CM & Howell R "Fluid Dynamics in Arterial Bifurcations", AIAA Journal,V9,p2284,(1971).

R7) Roach MRR "Effects of Blood Flow on the Arterial Wall",Proc.Spec.Meeting, Ohio St Univ Sept 1974

R8) Reidy MA "Relationship of Blood Flow and Endothelial Cell Morphology",Proc.Spec.Meeting,Ohio St Univ,Aug 1978.

R9) Rumberger JA "A Non-Linear Mathematical Model of Coronary Blood Flow",Ph.D.thesis,Ohio St Univ 1976

R10) Roach MR & Fletcher J "Alterations in the Distribution of Sudanophilic Lesions in Rabbits after Cessation of Cholesterol Diet",Atherosclerosis,V32,p1,(1979)

Roach Mr & Fletcher J "Effect of Unilateral Nephrectomy on Location of Aortic Sudanophilic Lesion in Cholesterol Fed

Rabbits",Atherosclerosis,V24,p327,(1976)

R12) Robertson JM, Clark ME & Cheng LC "A Study of the Effects of a Transversely Moving Boundary Upon Plain Poiseuille Flow",J.Biomech,Engin,ASME,p318,(1982)

S1) Smith KA, Colton CK, & Freedman RW "Shear Stress Measurements at Bifurcations ",Proc Spec Meeting,Ohio St Univ,Sept 1974

S2) Schwartz CJ, Bell FP, Somer JB & Gerrity R "Focal & Regional Differences in Aortic Permeability to Macromolecules",Proc.Spec.Meeting,Ohio St Univ,Sept 1974

S3) Schneck DJ & Gutstein WH "Boundary Layer Studies in Blood Flow",ASME Paper No.66-WA HF-4
B

S4) Stein PD, Walburn FJ & Sabbah HN "Disturbances of Flow in the Descending Aorta, Particularly in the Presence of Atherosclerosis",Proc.Spec.Meeting,Univ of Houston,Nov 1980.

S5) Skalak R, Keller SR & Secomb TW "Mechanics of Blood Flow",J.Biomechan.Engin.ASME,V103,p102,(1981)

S6) Schwartz CD & Mitchell JRA "Observations of Localisation of Arterial Plaques",Circulation Research,V11,p63,(1962)

S7) Sabbah HN & Stein PD "Effect of Aortic Stenoses on Coronary Flow Dynamics",J.Biomech Eng,ASME,V104,p221(1982)

S8) Stettler JC, Niederer P & Anliker M "Theoretical Analysis of Arterial Hemodynamics Including Influence of Bifurcations",Annals of Biomedical Engineering,V9,p145,(1981).

S9) Schneiderman G, Ellis CG, & Goldstick TK "Mass Transport to Walls of Stenosed Arteries, Variation with Re & Flow Separation",J.Biomechanics,V12,p869,(1979).

S10) Schneiderman G, Mockros LF & Goldstick TK "Effect of Pulsatility on Oxygen Transport to the Human Arterial

Wall",J.Biomechanics,V15,p849,(1982).

S11) Schneiderman G & Goldstick TK "Significance of Luminal Plasma Layer Resistance in Arterial Wall Oxygen Supply",Atherosclerosis,V31,p11,(1978)

S12) Schneiderman G & Goldstick TK "Carbon Monoxide-Induced Arterial Wall Hypoxia & Atherosclerosis",Atherosclerosis,V30,p1,(1978)

S13) Stetson K "New Design for Laser Image-Speckle Interferometer", Optics and Laser Technology,V2,p179,(1970)

T1) Talukder N, Karayannacos PE, Nerem RM & Vasko JS "An Experimental Study of the Fluid Dynamics of Multiple Non-Critical Stenoses",J.Biomech.Engin,ASME,V99,p74,(1977)

T2) Talukder N "An Investigation on the Flow Characteristics in Arterial Branchings",ASME paper no 75-APMB-4.

T3) Thibault LE & Fry DL "Hydrodynamically Induced Shear Stress Effects on Evans Blue Dye Uptake",Hemodynamics and the Arterial Wall - Proc.Spec.Meeting, Univ Houston,Nov 1980.

T4 Turitto VT, Weiss HJ & Baumgartner HR "Platelets,Flow and the Vessel Wall", Proc.Spec.Meeting, Univ Houston,Nov 1980.

T5) Texon M "The Hemodynamic Concept of Atherosclerosis",Bulletin of NY Acad. of Medicine,V36,p263,(1960).

T6) Tracy RE, Strong JP & Toca V "Relationship of Raised Atherosclerotic Lesions to Fatty Streaks in Coronary Heart Disease & Hypertension",Atherosclerosis,V33,p125,(1979).

T7) Tanner R & Blows LG "A Study of the Motion of Oil Films on Surfaces in Air Flow with Application to Measurement of Skin Friction", J.Physics ser E, Sci. Instr. 9, p194, (1976)

T8) Tong P & Fung YC "Slow Particulate Viscous Flow in Channels & Tubes - Application to Biomechanics",J.Applied

Mechanics,ASME,p721,(1971).

T9) Taylor C & Hughes TG "Finite Element Programming of the Navier-Stokes Equations,Pineridge Press,Swansea,UK,(1980).

V1) Vest CM (ed) "Holographic Interferometry", John Wiley & Son, NY, (1979), p269

W1) Wells MK, Winter DC, Nelson AN, & McArthy TC "Blood Velocity Patterns in Coronary Arteries",J.Biomech.Engin,ASME,V99,p26,(1977)

W2) Womersley JR "An Elastic Tube Theory of Pulse Transmission & Oscillatory Flow in Mammalian Arteries",Wright Air Development Center Techn. Report,(1957).

W3) Womersley JR "Mathematical Theory of Oscillatory Flow in a Pulsating Tube",J.Physiology,V127,p38,(1955)

W4) Womersley JR "Flow in the Larger Arteries and Relation to Oscillating Pressure",J.Physiology,V124,p31,(1955)

W5) Wells MK, Wintr DC, Nelson AW & McArthy TC "Hemodynamic Patterns in Coronary Arteries",Proc. Spec.Meeting,Ohio St Univ,Sept 1974

W6) Weinbaum S, Lewis C & Caro CG "Theoretical Models and Electronmicroscope Studies of the Transport of Macromolecules across Arterial Endothelium and their Uptake by the Arterial Wall,Proc.Spec.Meeting,Ohio St Univ,Sept 1974

W7) Wolinsky H "Hemodynamics, Lipoprotein,Metabolism & Atherosclerosis",Proc.Spec.Meeting,Ohio St Univ,Aug 1978.

W8) Weinbaum S, Pfeffer R, Skalak R & Chien S "Theoretical Studies & Laboratory Model Experiments in Arterial Wall Transport",Proc.Spec.Meeting,Aug 1978.

W9) Weinbaum S & Caro CG "Macromolecule Transport Model for the Arterial Wall",J.Fluid Mechanics,V74,p611,(1976).

W10) Walburn FJ, Sabbah HN & Stein PD "Flow Visualisation in a Mold of an Atherosclerotic Human Abdominal Aorta",J.Biomech.Eng,ASME,V103,p168,(1981).

W11) Walburn FJ & Stein PD "Flow Characteristics in Symmetrically Branched Tubes Simulating the Human Aortic Bifurcation",J.Biomech.Eng,ASME,V102,p340,(1980)

W12) Wu JC & Wabbah MM "Numerical Solution of Viscous Flow Equations Using Integral Representations",in Lecture Notes on Physics,V59,Springer-Verlag, NY,p448,(1976)

XY1) Young DF "Effect of a Time Dependent Stenosis on Flow Through a Tube",J.Engin. in Industry,ASME,V90,p248

XY2) Young DF & Tsai "Flow Characteristics in Models of Arterial Stenoses,"J.Biomechanics,V6,p395,(1973)

XY3) Young DF "Fluid Mechanics of Arterial Stenoses",J.Biomech.Eng,ASME,V101,p157,(1979)

Z1) Zarins CK, Taylor KE, Lundell MI & Glagov S "Aortic Ostial Morphology & the Localisation of Atherosclerotic Lesions:Preliminary Observations",Proc.Spec.Meeting,Ohio st Univ,Aug 1978

Z2) Zeller H, Talukder n, & Lorenz J "Model Studies of Pulsating Flow in Arterial Branches and Wave Propagation in Blood Vessels",AGARD conference Procs,no.65,(1970)

FIG 2.2

Speckle pattern of a Diffusely Reflecting Surface

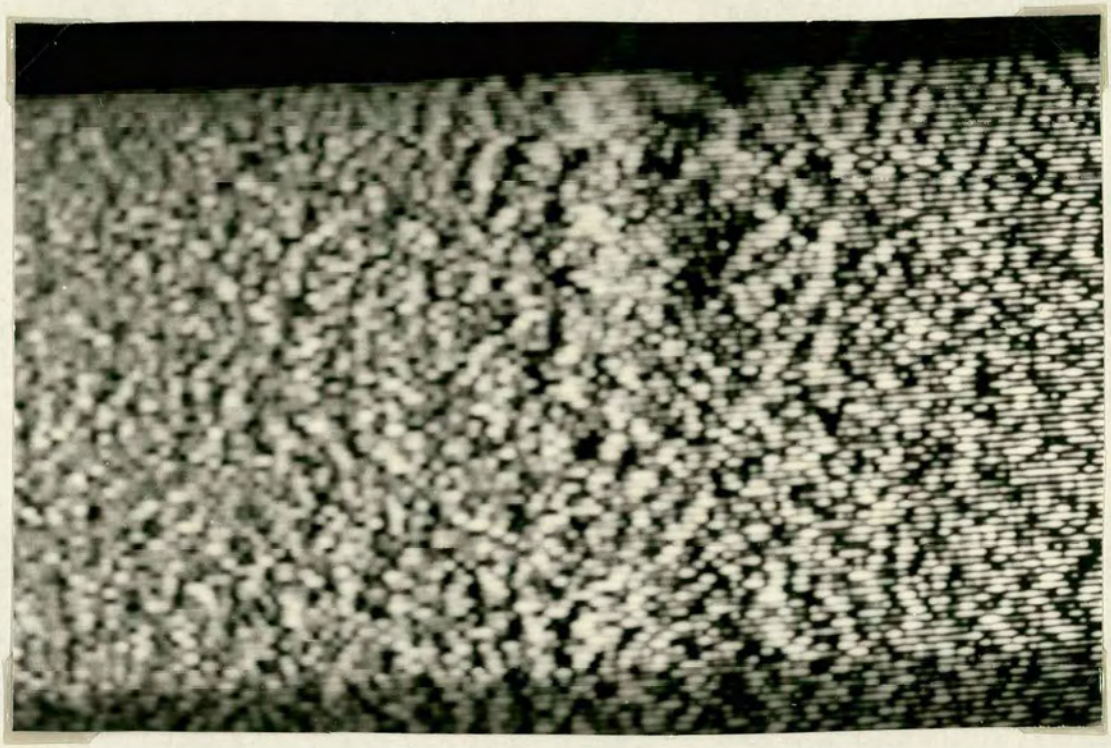

FIG 2.3 Optical Path of Vinten Electronic Speckle Pattern Interferometer

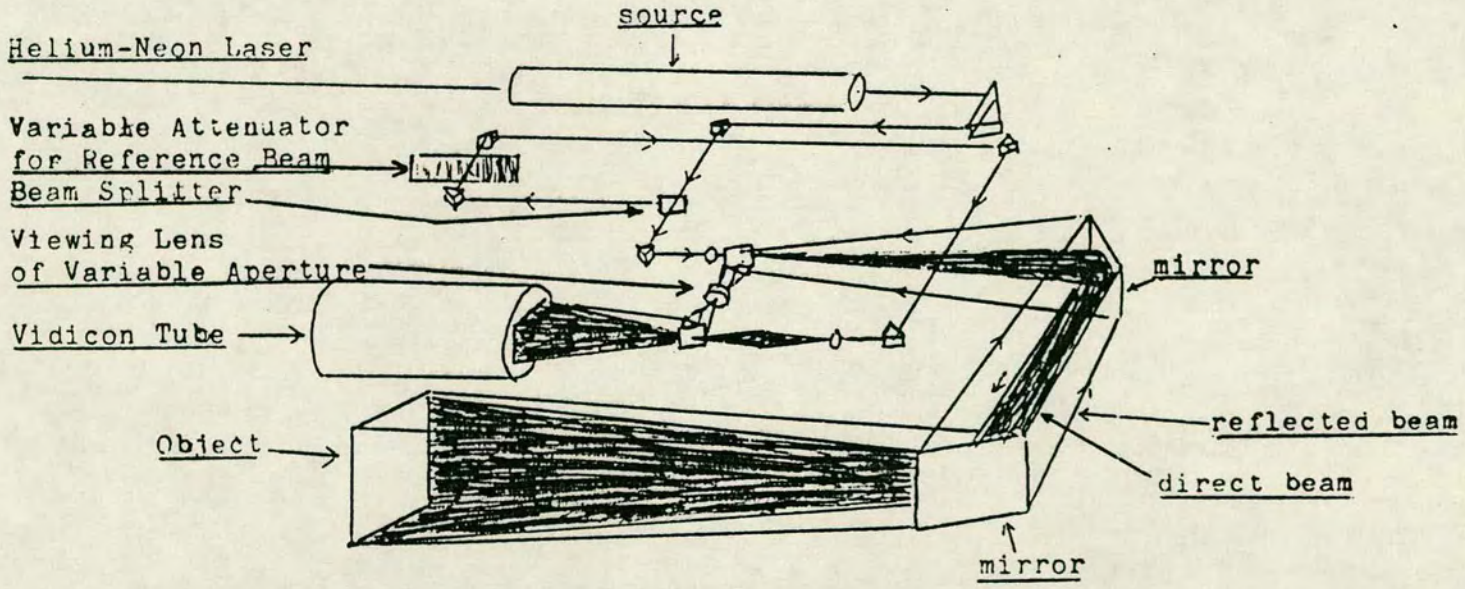

FIG 2.4 Experimental Flow Domain

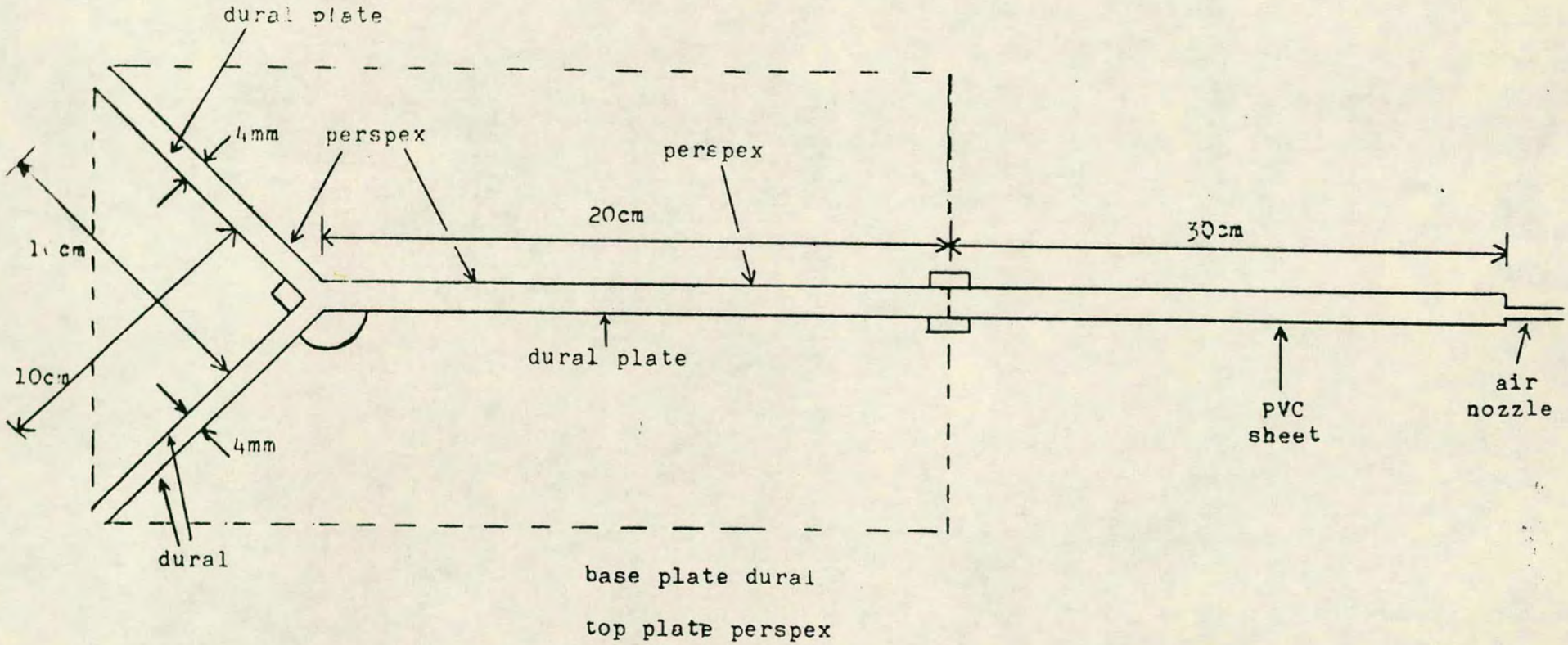

FIG 2.5a

Use of Total Internal Reflection Upon A Prism

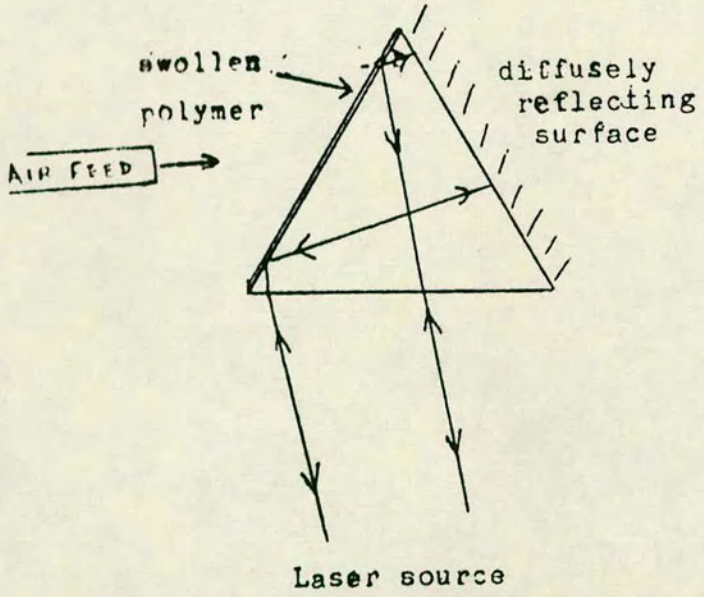

FIG 2.5b

Use of Direct Reflection From A Prism

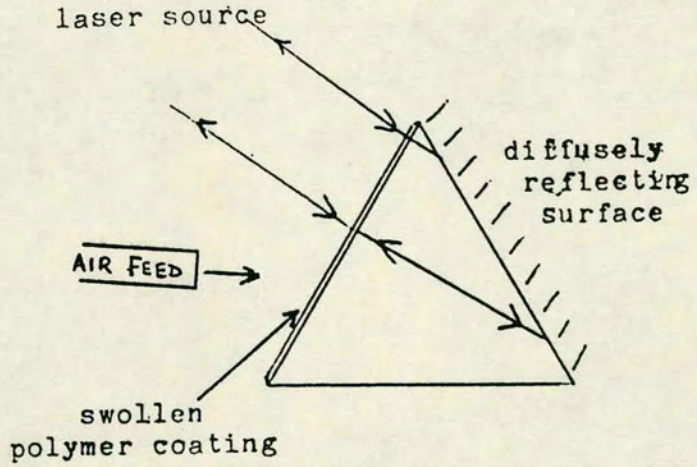

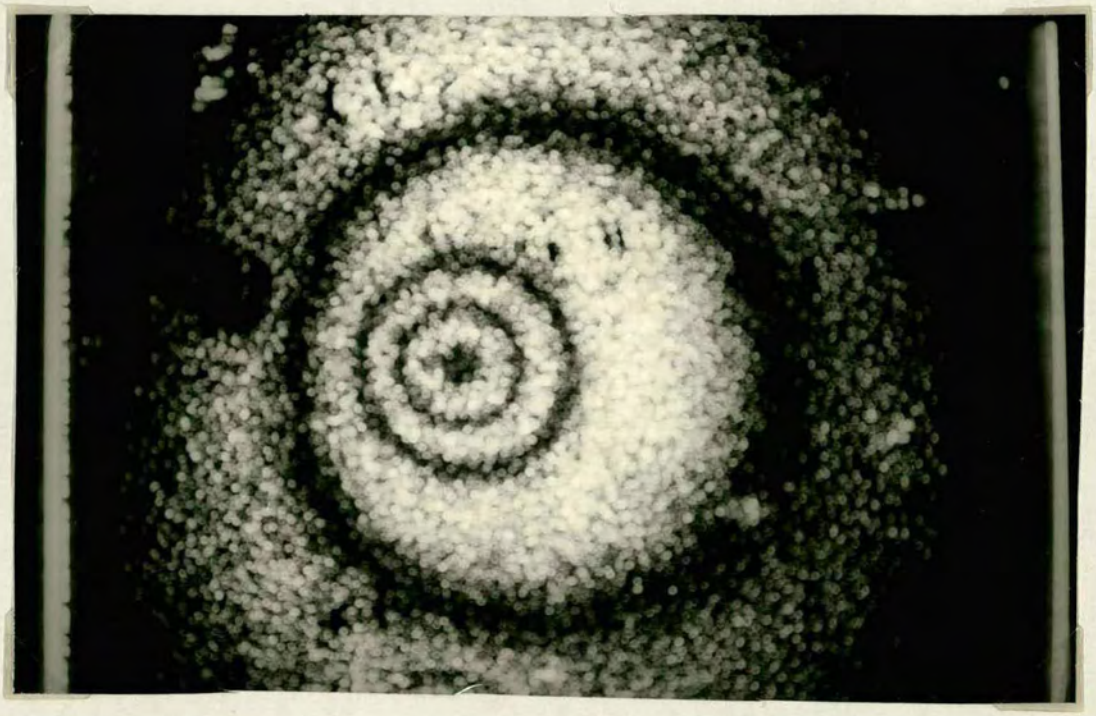

FIG 2.6

Contours of Equal Mass Transfer Coefficient Emanating from the Point of Impingement of an Air-Jet upon a Flat Surface.

FIG 2.7

Optical Path of Light In Mass Transport System (polymer coating upon reflecting surface)

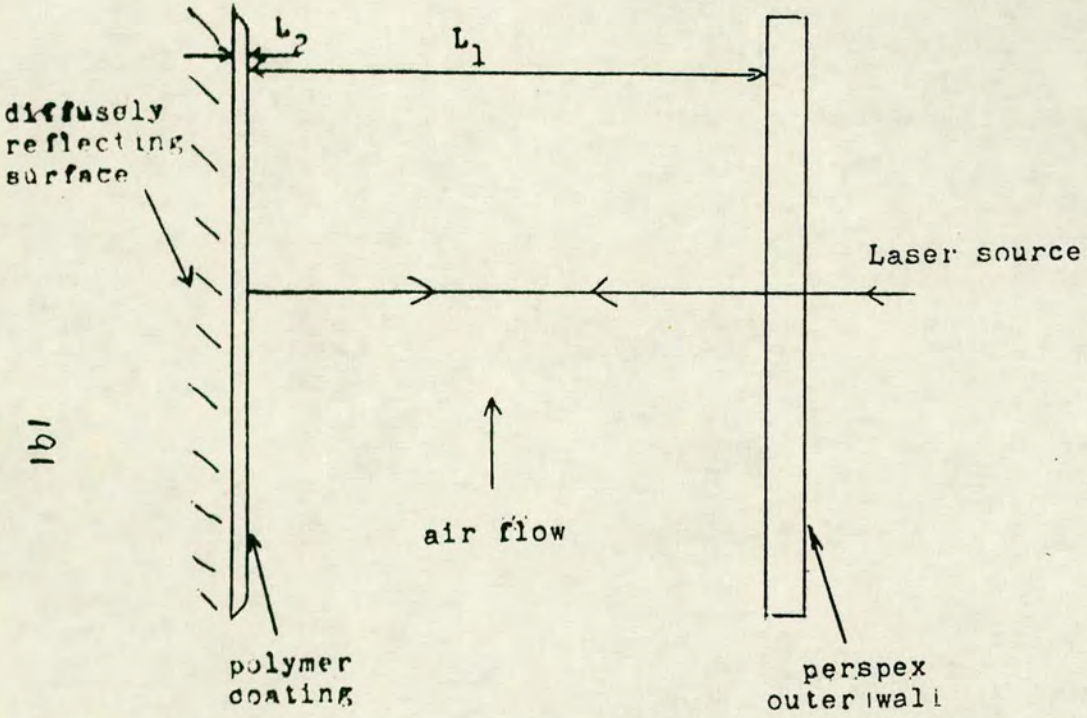

FIG 2.8

Optical Path & Distances For System with Polymer Coating upon Perspex Wall.

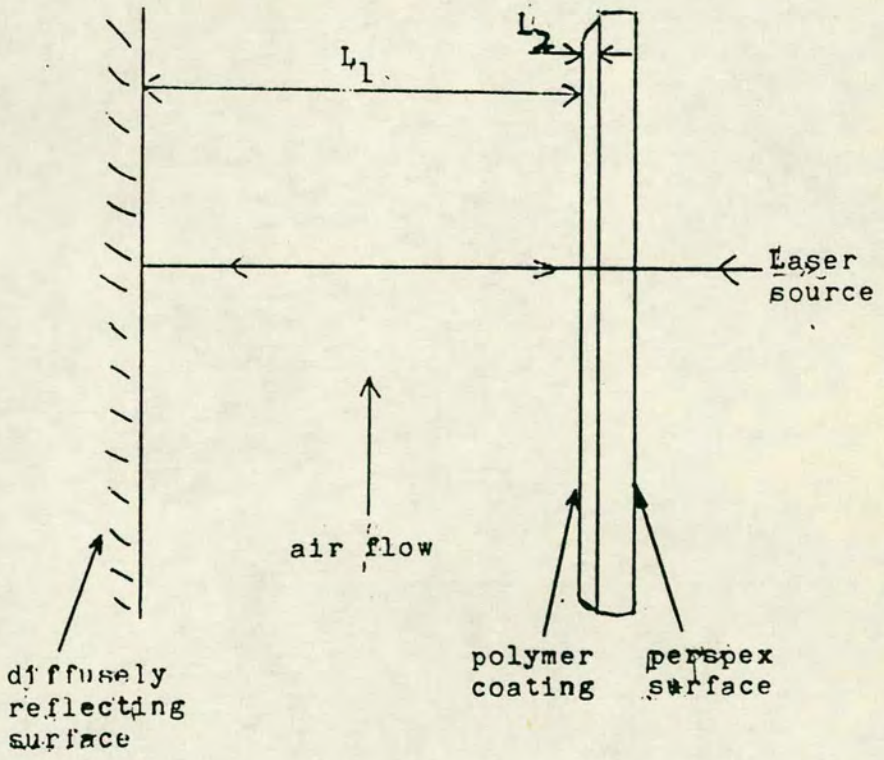

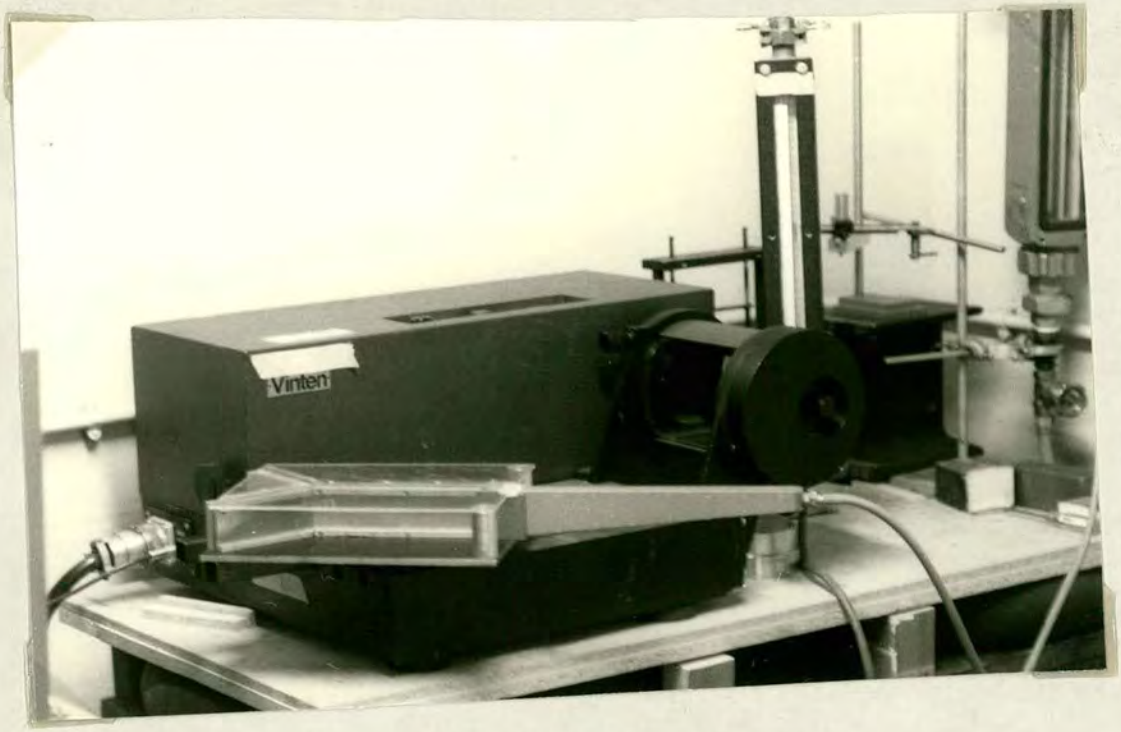

FIG 2.9

Model Branch Located upon Optical Table of Interferometer

FIG 2.10

Fringes upon Outer Downstream Wall of Channel; Re = 1900

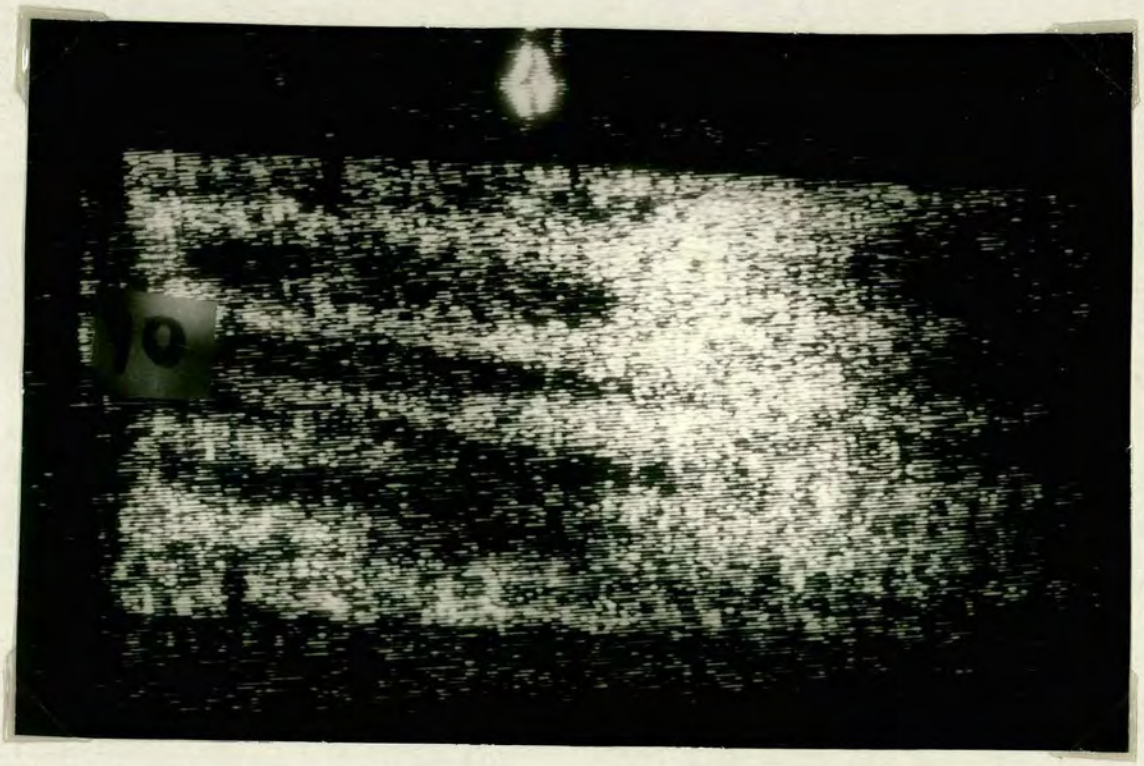

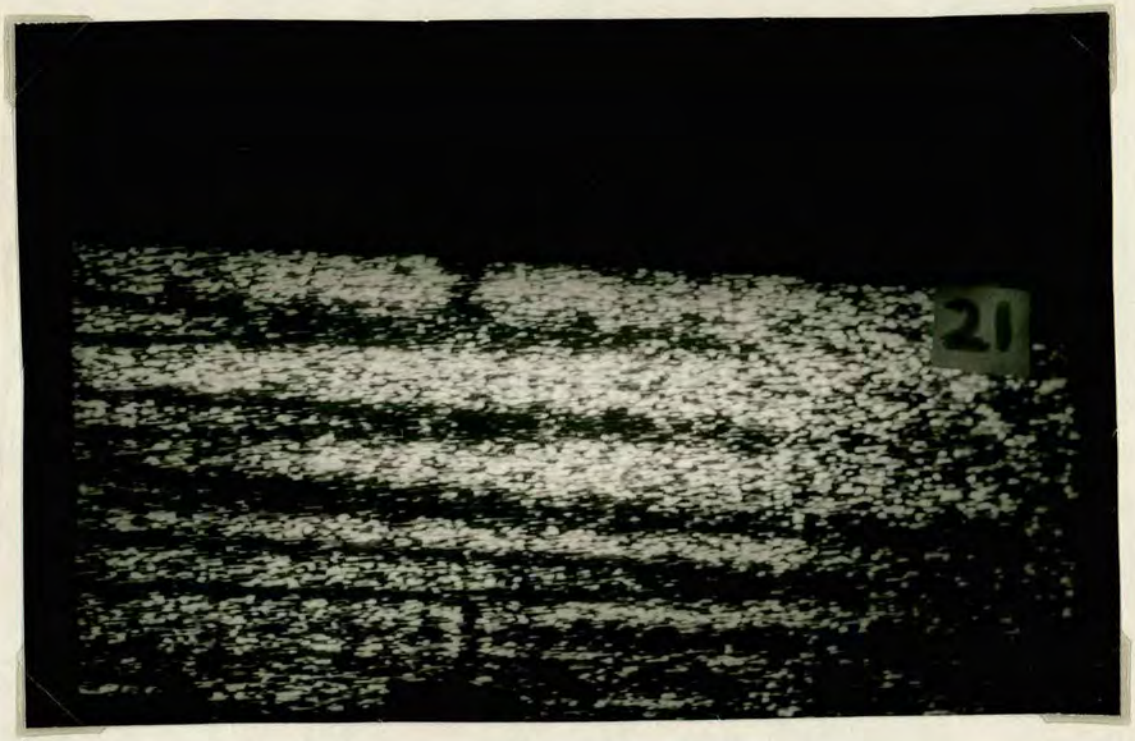

FIG 2.11

Fringes upon Upstream Wall; Re = 330

Fig 2.12

Fringes upon Upstream Wall ; Re = 1900

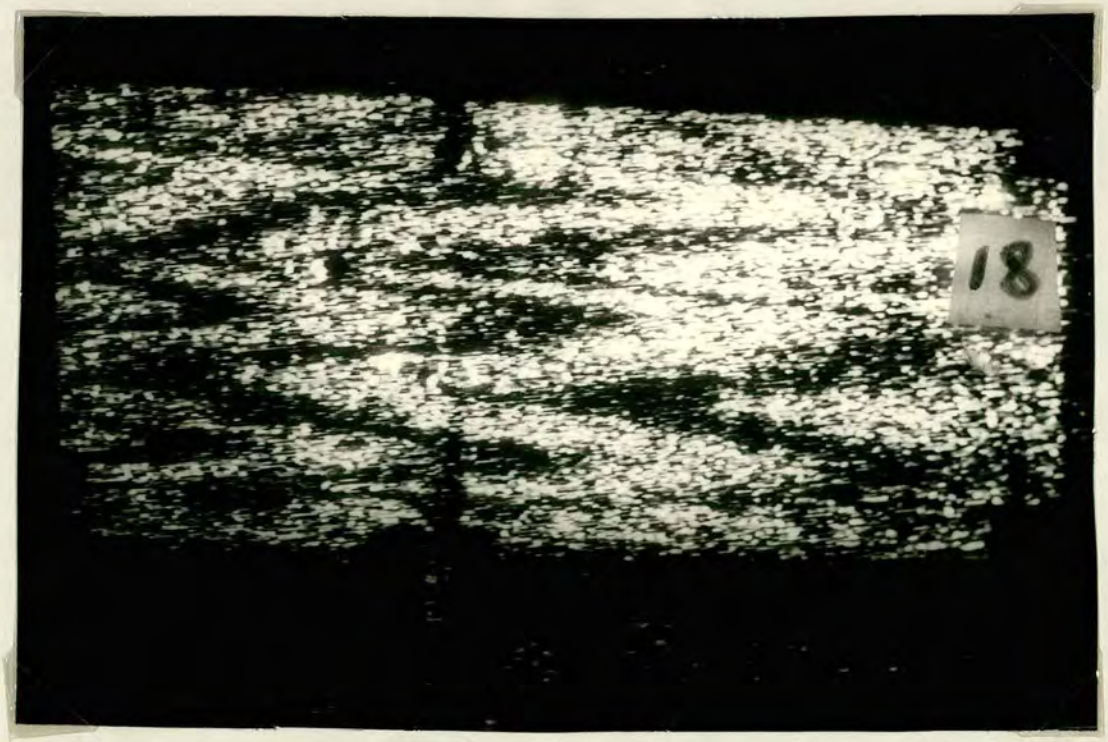

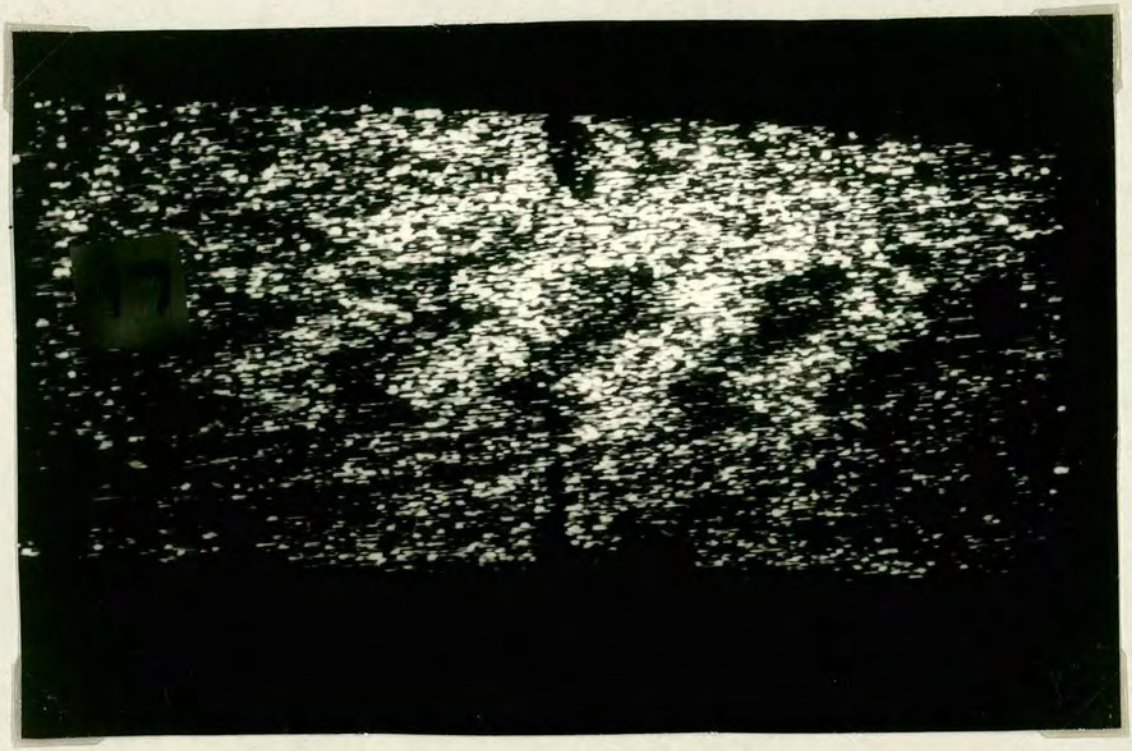

FIG 2.13

Fringes upon Upstream Wall; Re = 1500

FIG 2.14

Holographic Fringes (by Lewin) Depicting Mass Transfer Contours in a Rectangular Cross-Sectioned Duct

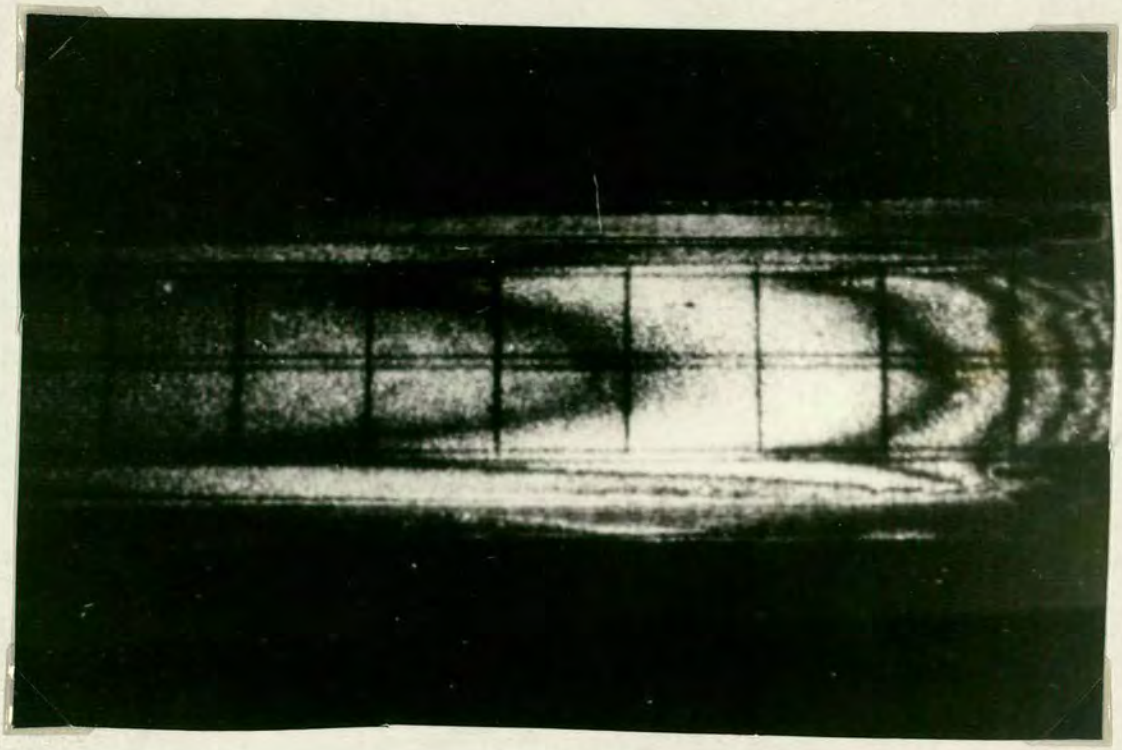

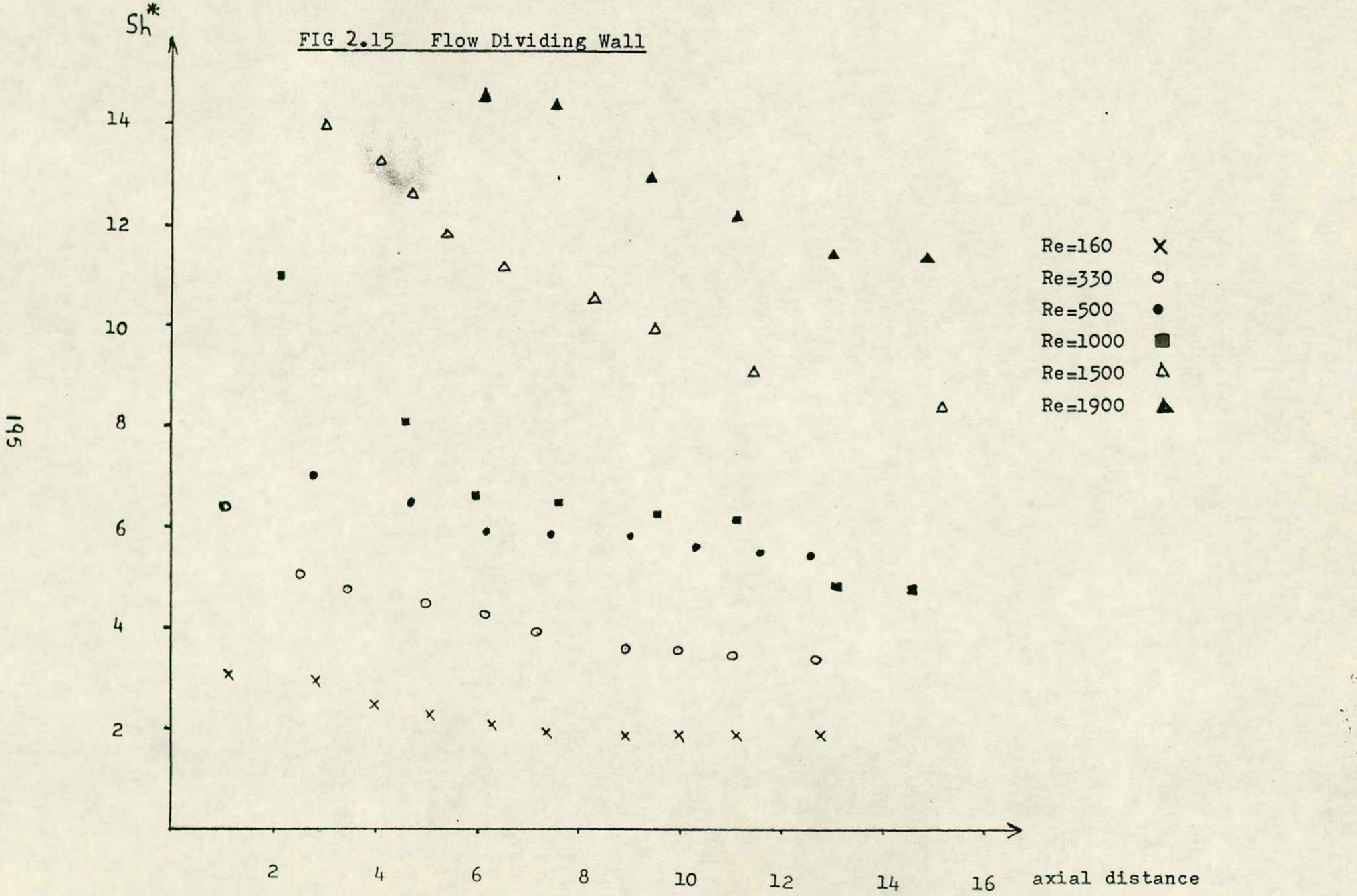

FIG 2.15 Flow Dividing Wall

FIG 2.16 Upstream Wall

Sh^* vs axial distance

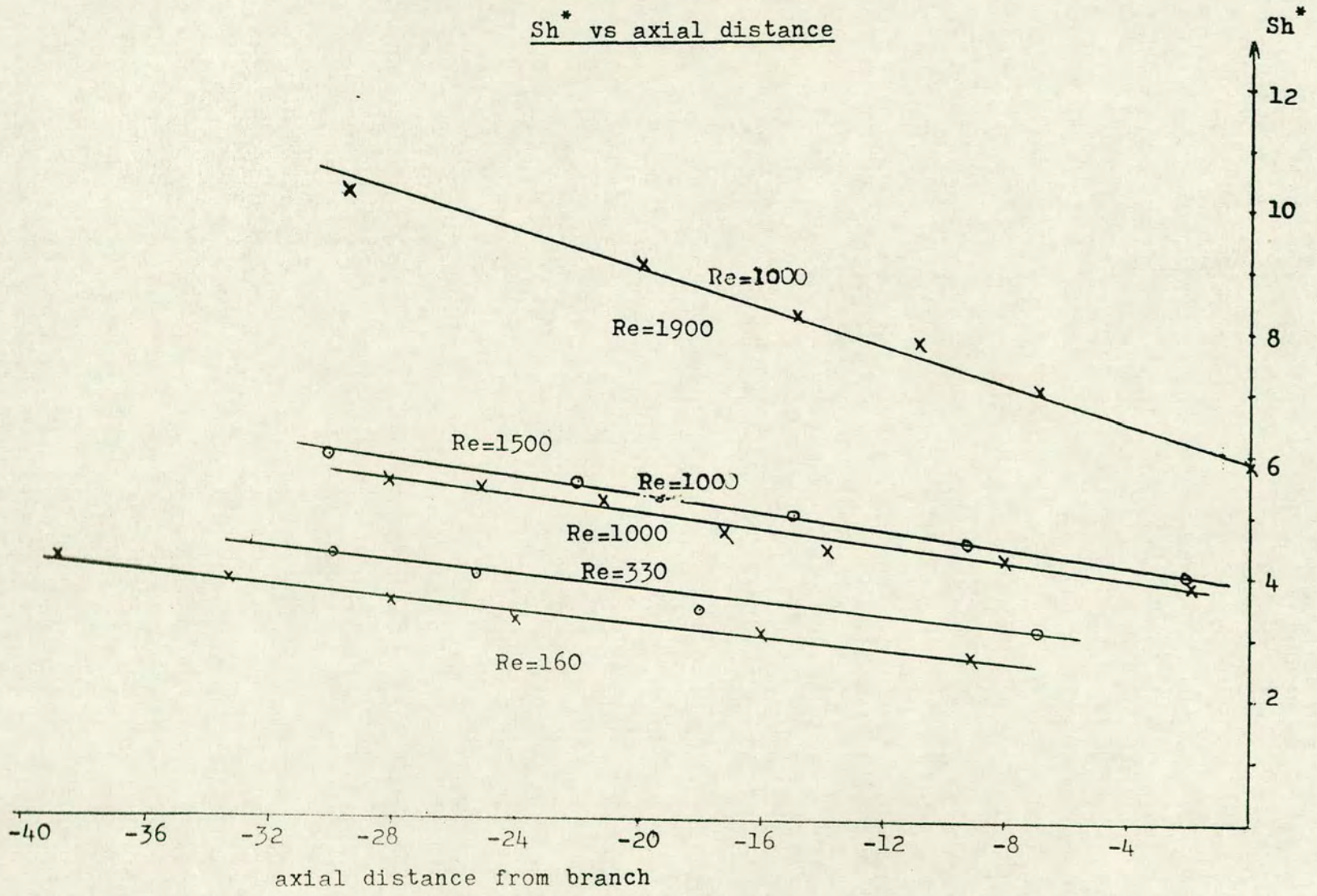

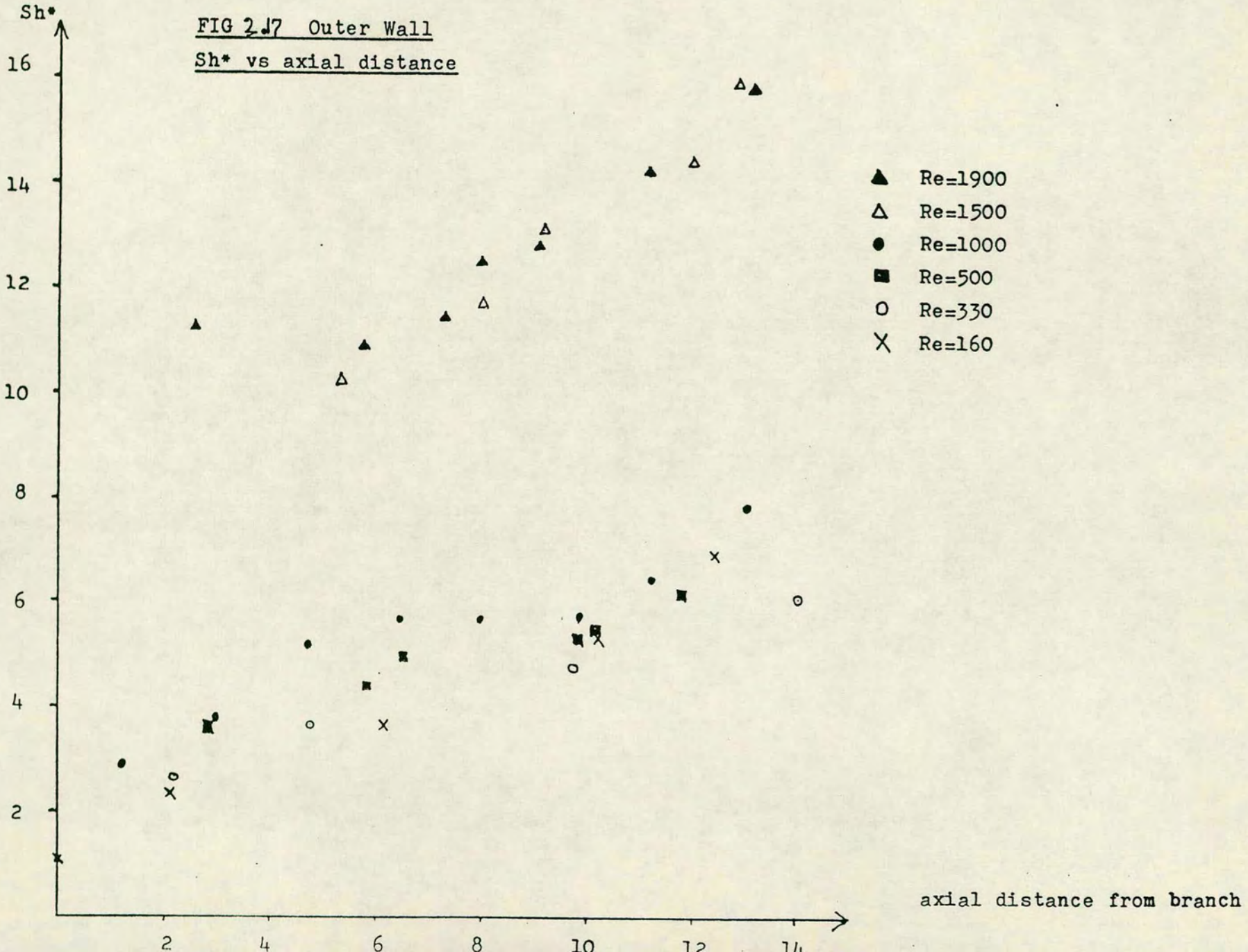

FIG 2.17 Outer Wall

Sh* vs axial distance

FIG 2.18

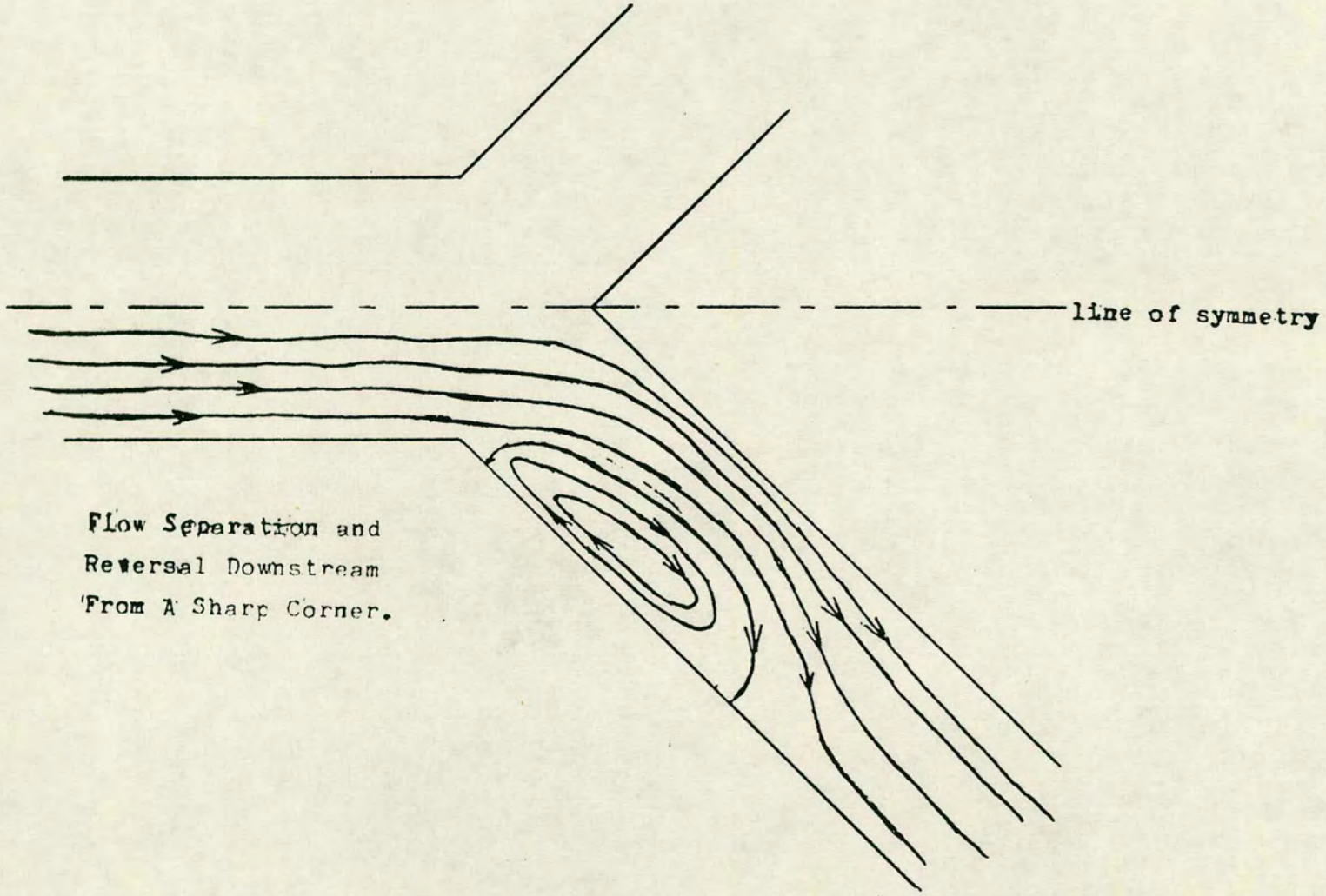

Flow Separation and
Reversal Downstream
From A Sharp Corner.

FIG 3.1 Mathematical Flow Domain

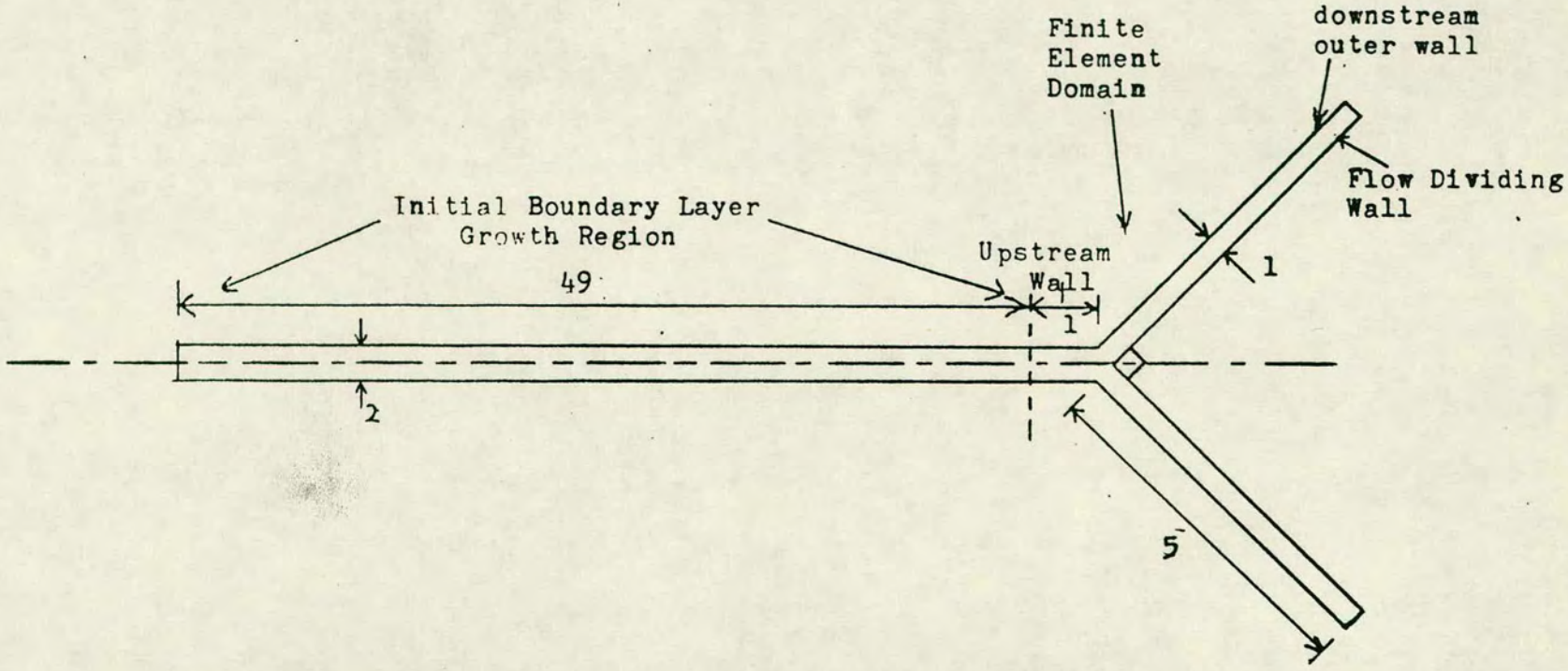

FIG 3.2
Finite Element Domain for Flow in a Symmetric Branch
(511 nodes; 152 elements)

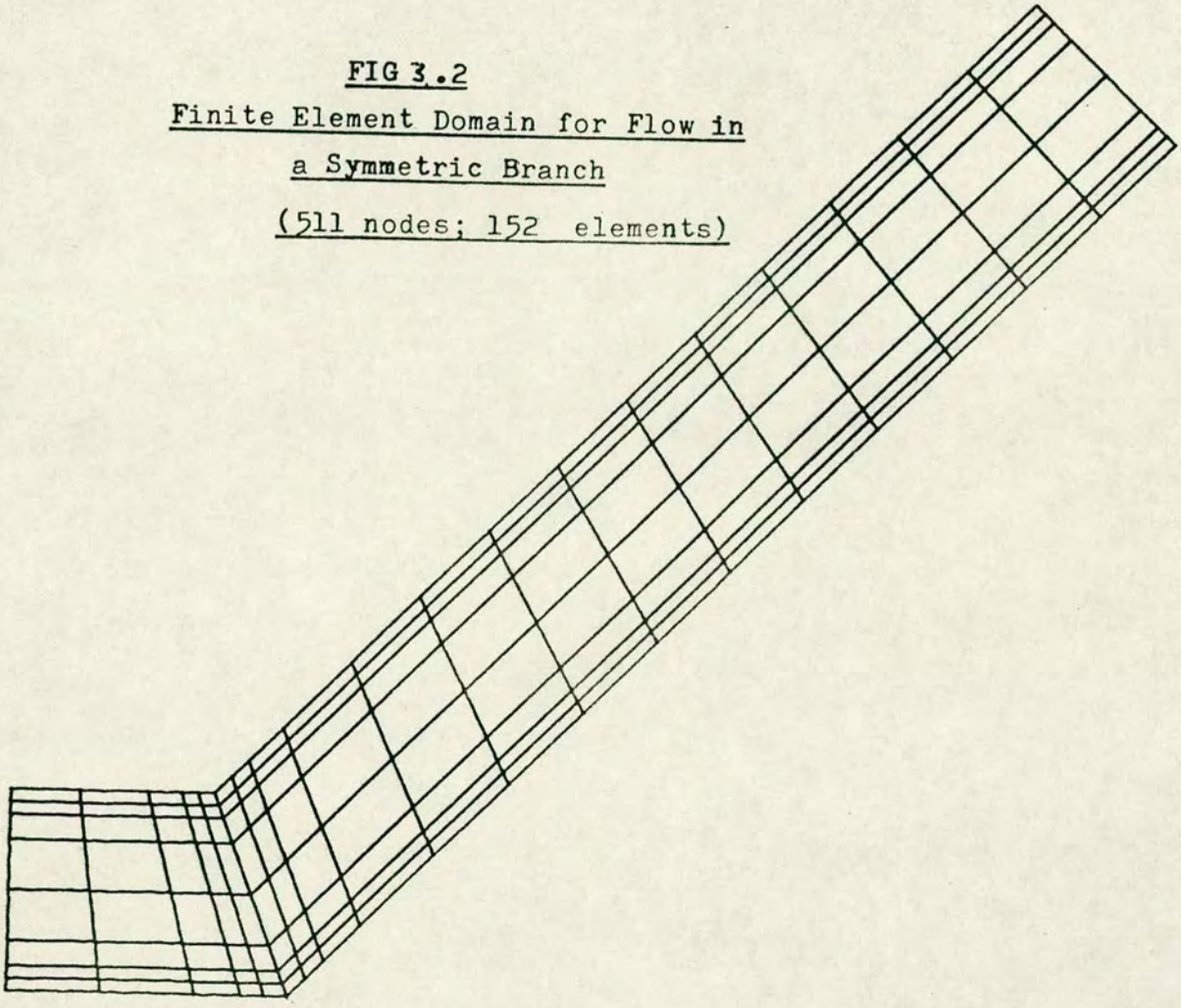

FIG 3.3

Local Coordinates for An
8 Noded Quadrilateral Element.

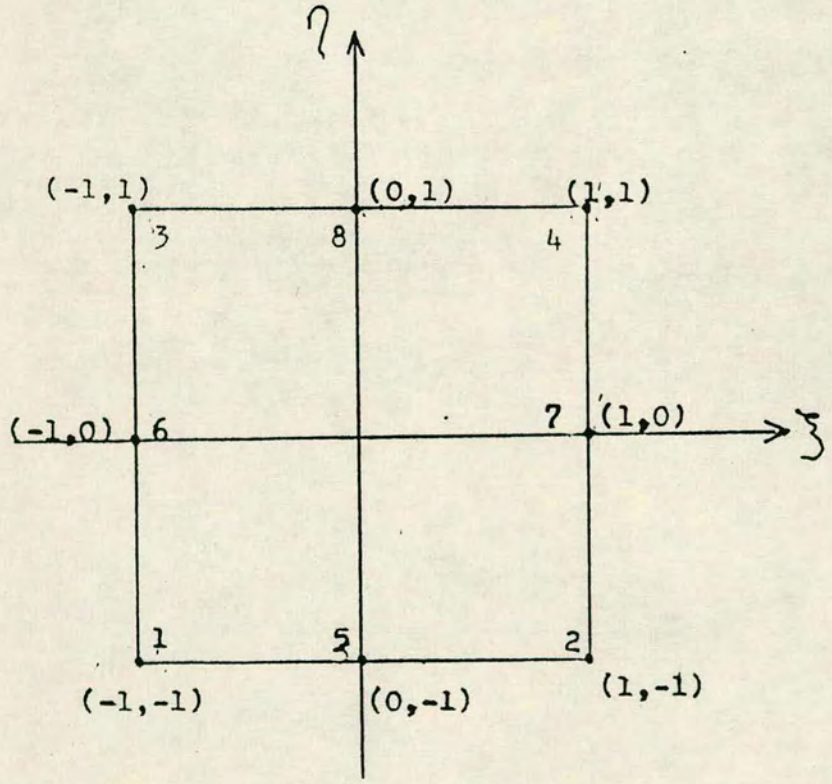

FIG 3.4

Evaluation of Concentration Gradient

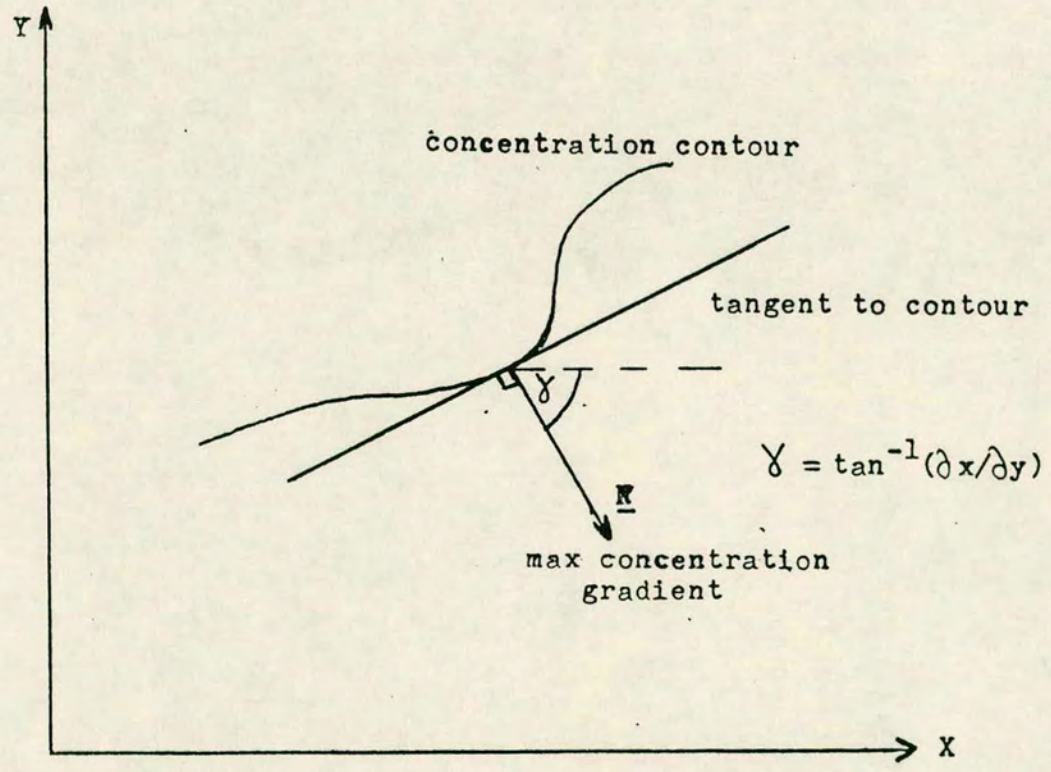

N = direction normal to concentration contour

FIG 3.5

Boundary Conditions for Navier-Stokes Equations

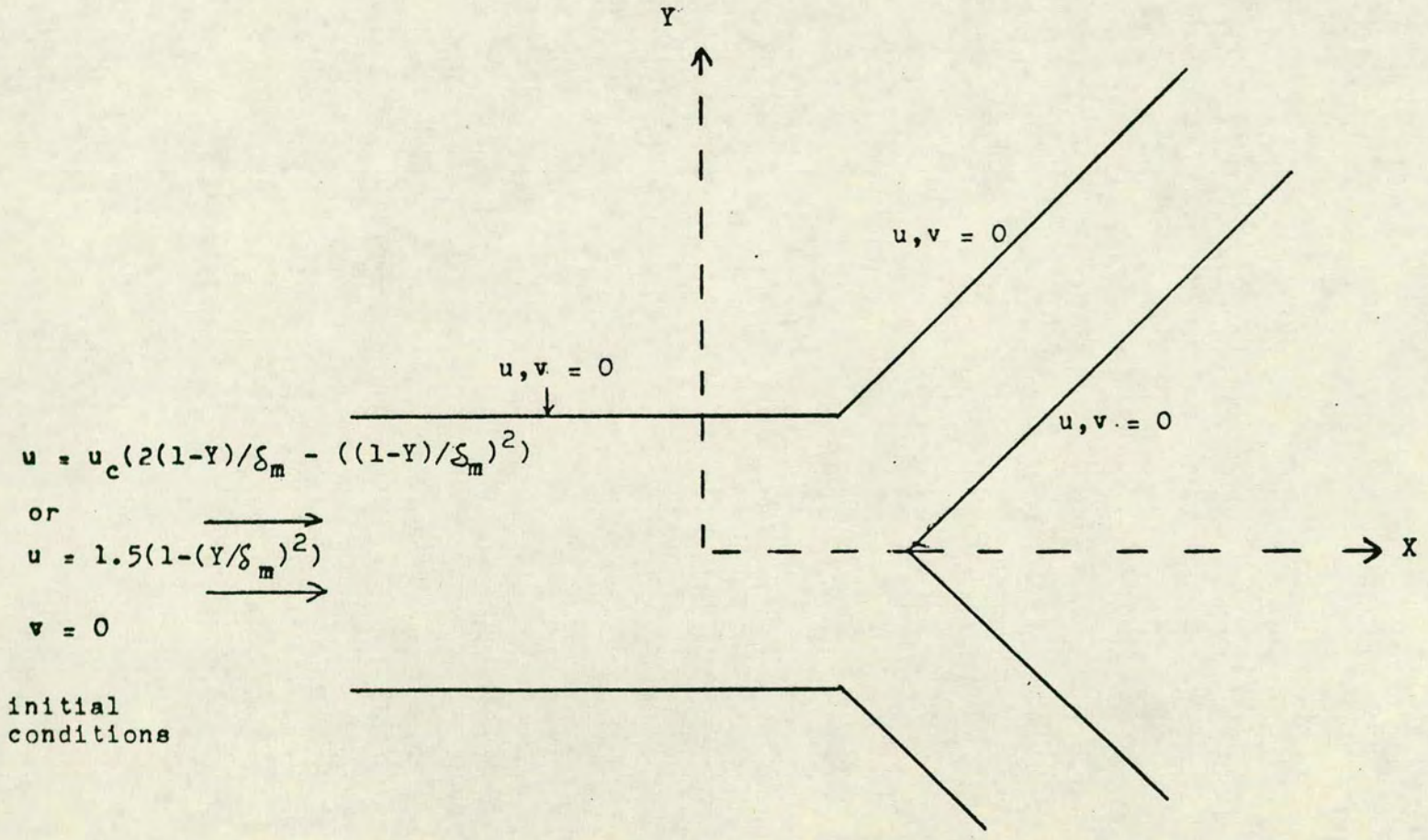

FIG 3.6

Boundary Conditions for Stream Function, Vorticity and Concentration.

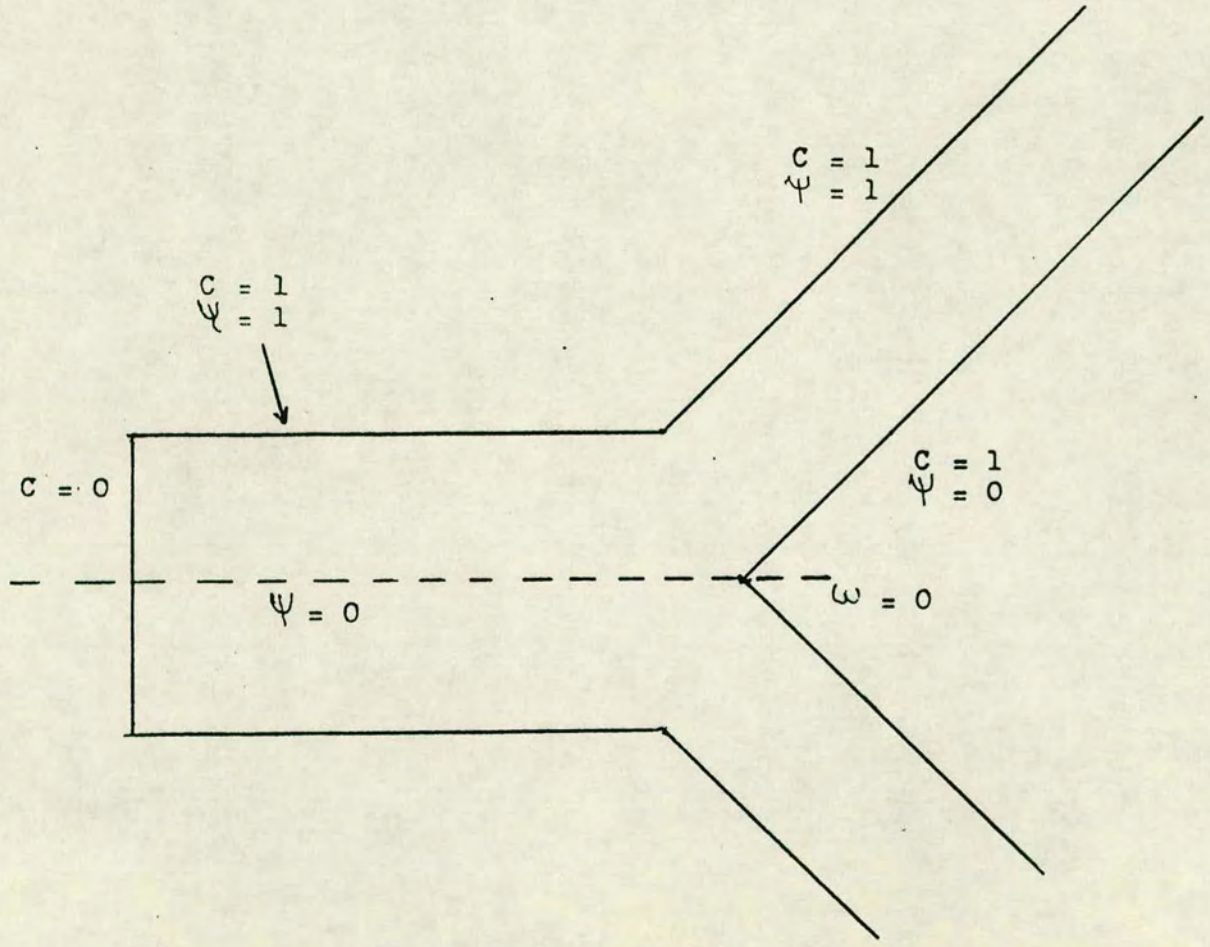

FIG 3.7

Boundary Layer Growth Model and Equations

$$\frac{u}{u_c} = \frac{2(1-Y)}{\delta_m} - \left[\frac{1-Y}{\delta_m}\right]^2 \qquad \delta_m(X) = 3(1 - 1/u_c)$$

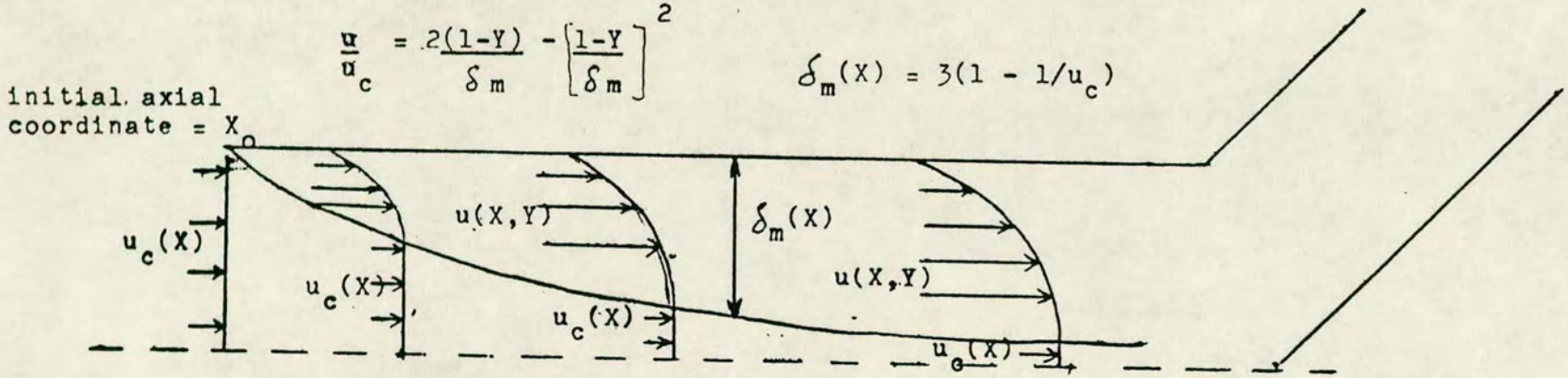

$$X - X_o = 0.3\ Re(9(u_c-1) - 16 \log_e u_c + 7(1 - 1/u_c)$$

Initial Concentration Equations

$$C(X,Y) = 1 - 1.5\frac{Y}{\delta_c} + 0.5\left[\frac{Y}{\delta_c}\right]^3$$

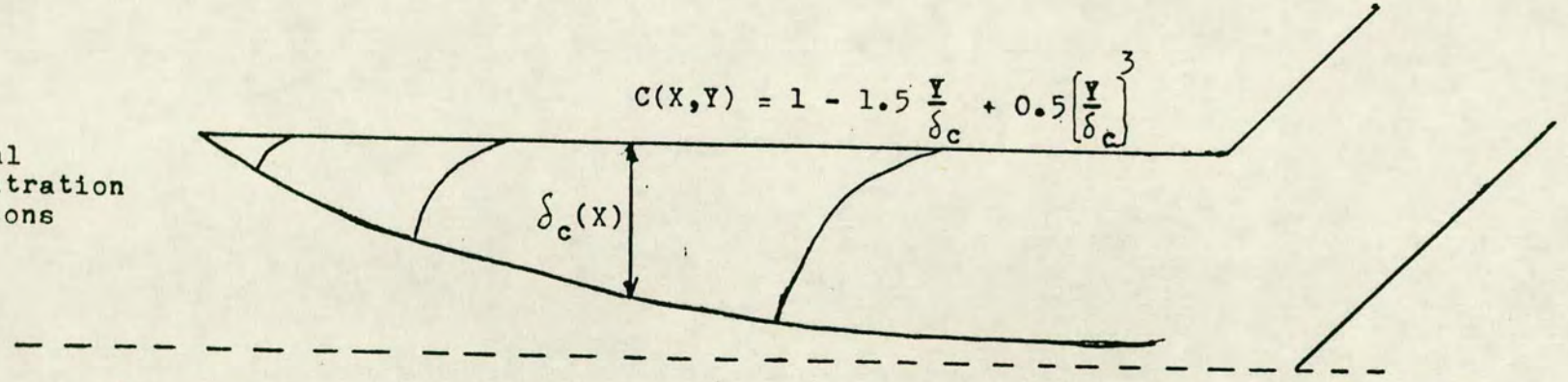

$$u_c\left[\frac{\delta_c^2}{\delta_m} - \frac{\delta_c^3}{\delta_m^2}\right] = 1.035\ Re^{-0.596} Sc^{-0.664} (X - X_o)^{0.596}$$

FIG 3.8

Axial Velocity Profile at Entrance to Finite Element Domain for a Variety of Reynolds' Numbers.

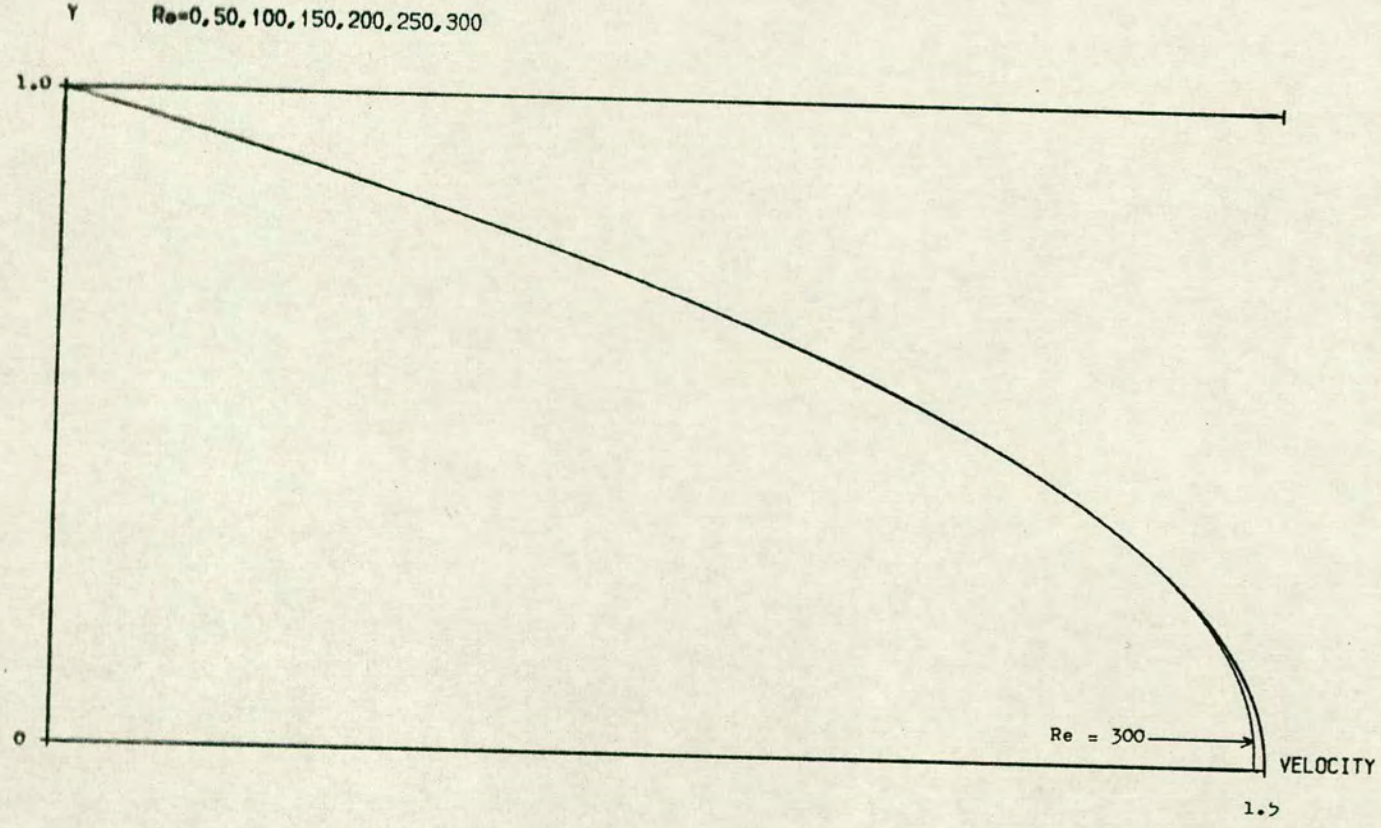

FIG 3.9a

Concentration Profiles at Inlet to the Finite Element Domain

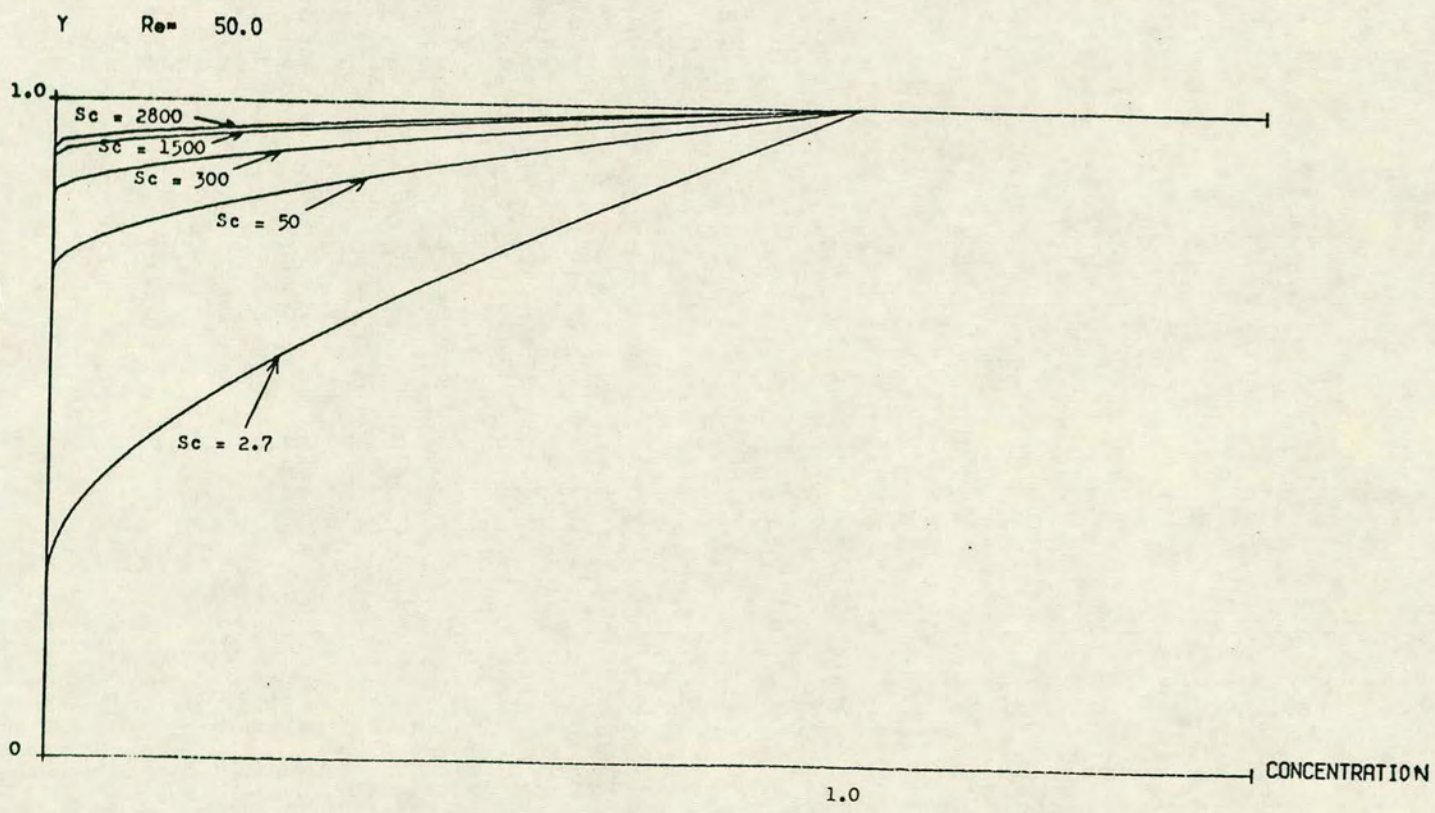

FIG 3.9b

Concentration Profile at the Inlet to the Finite Element Domain

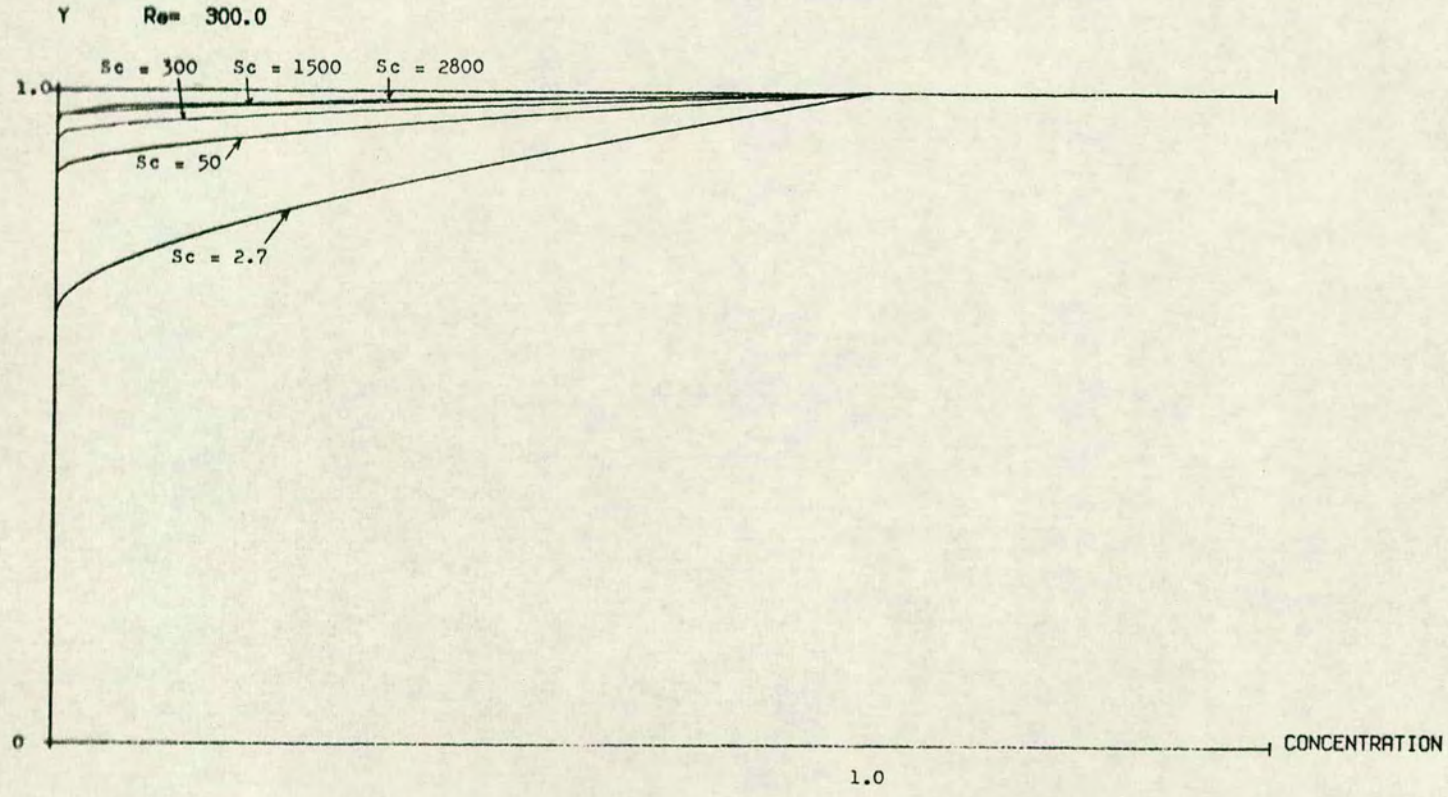

FIG 3.10

Streamlines from flow in a symmetric branch (at 45 deg to axis).
Proximal branch width = 2 x distal branch width.
Plotted stream function values = 100 x dimensionless values.
Reynolds' Number = 250.0

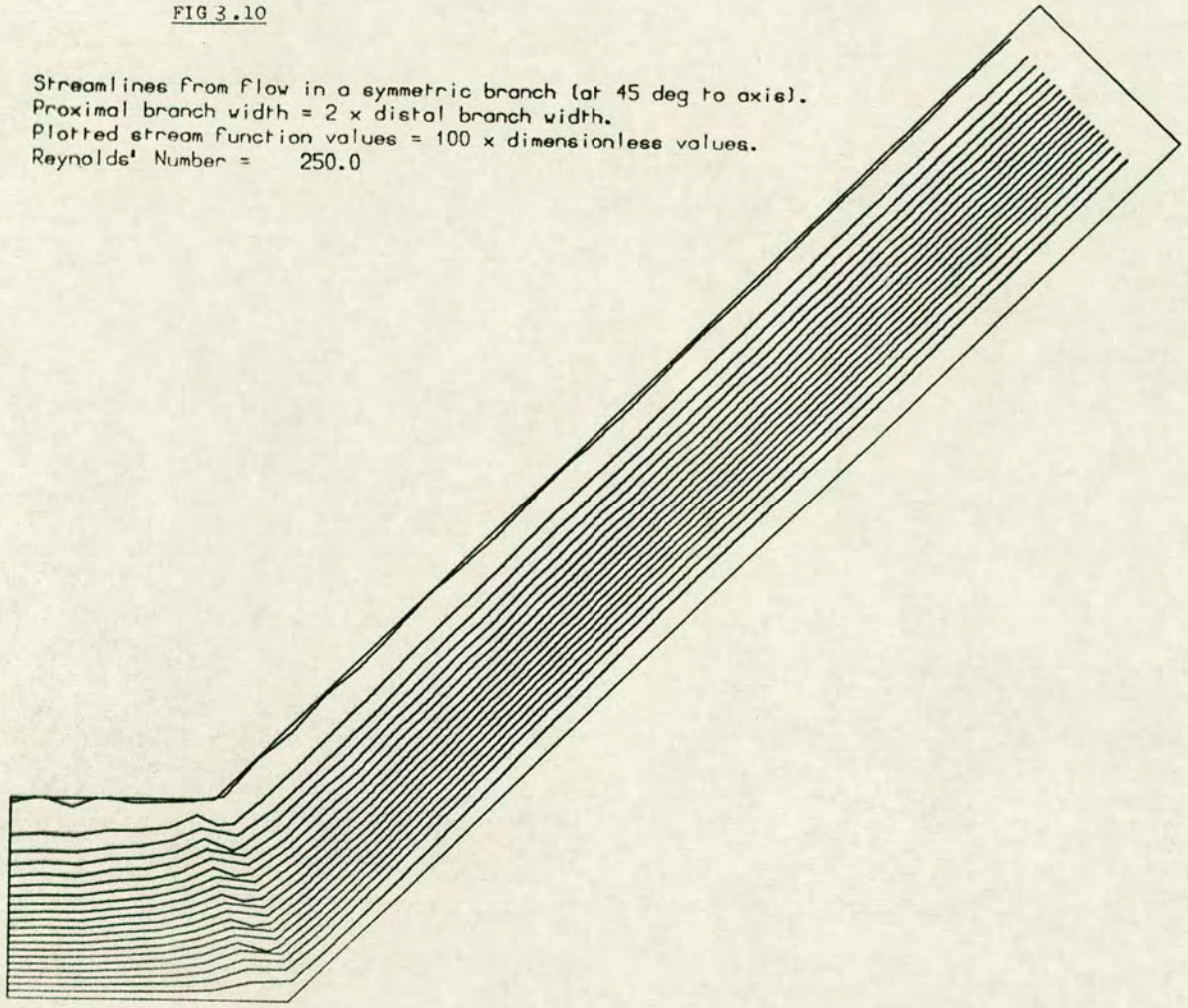

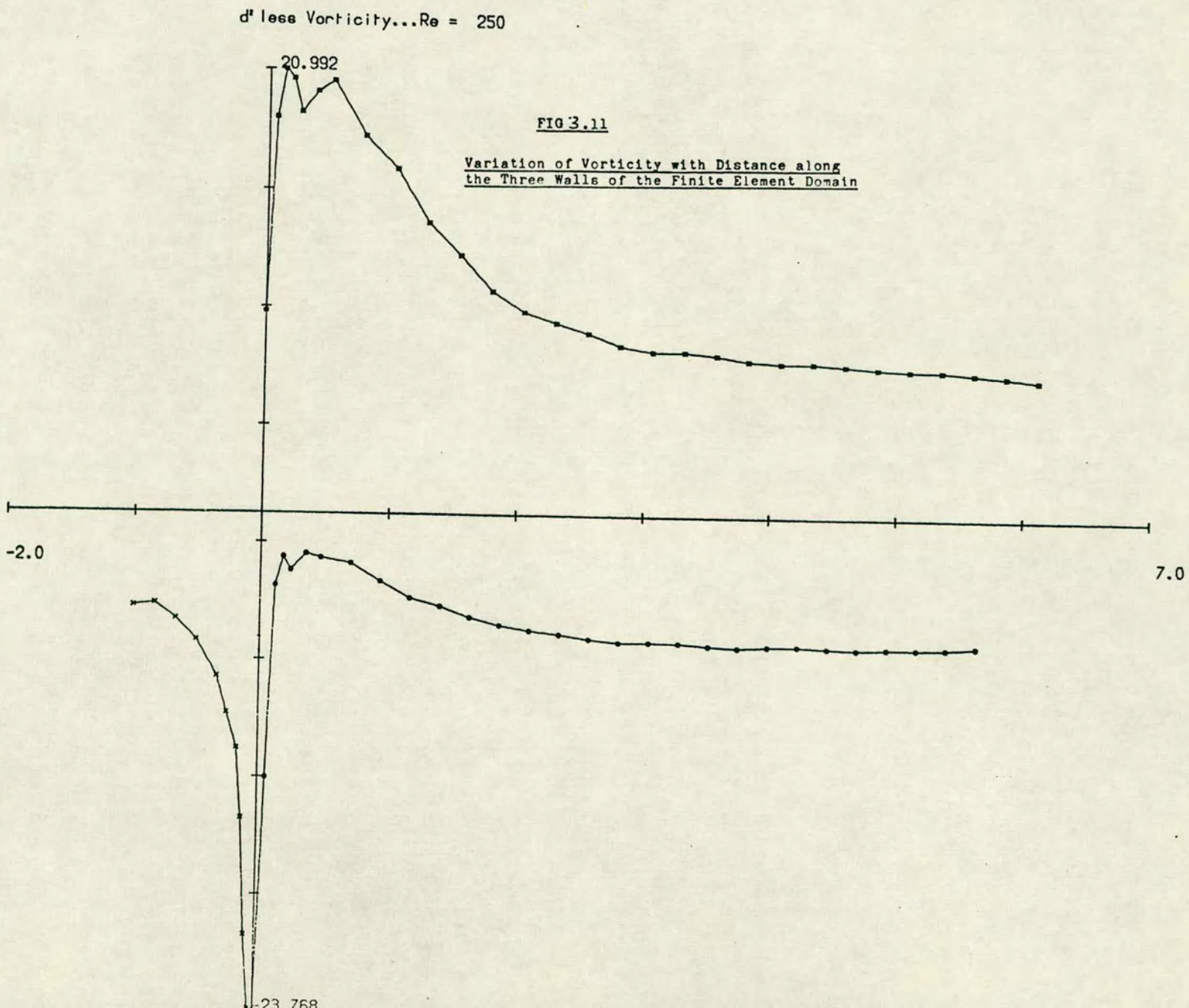

FIG 3.11

Variation of Vorticity with Distance along the Three Walls of the Finite Element Domain

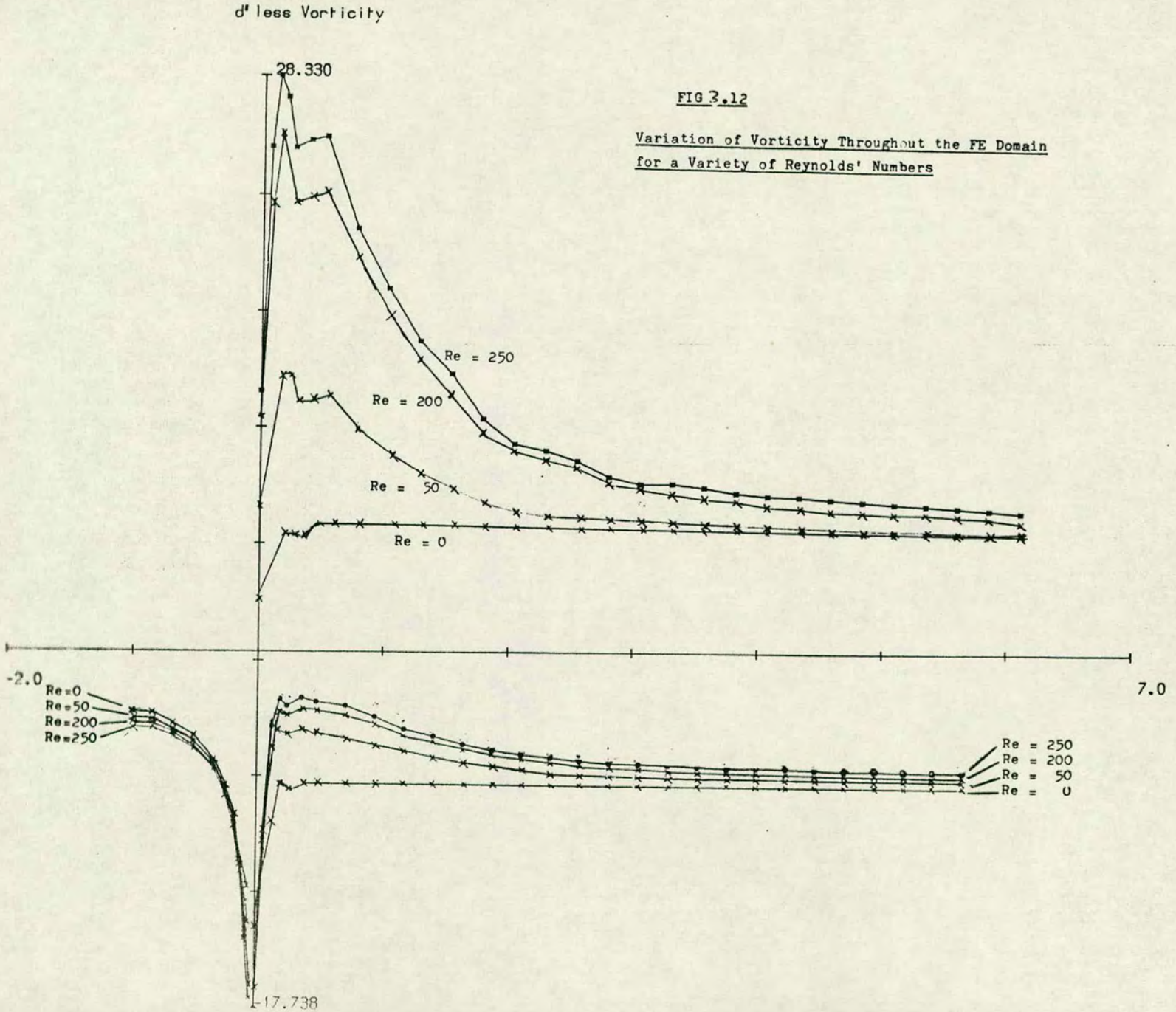

FIG 3.12

Variation of Vorticity Throughout the FE Domain for a Variety of Reynolds' Numbers

FIG 3.13a

Concentration contours in symmetric branched channel.
Wall conc. = 1. (contours=100 x d' less concentration.)
Feed conc. = 0
Re = 20.0. Sc = 2.5.

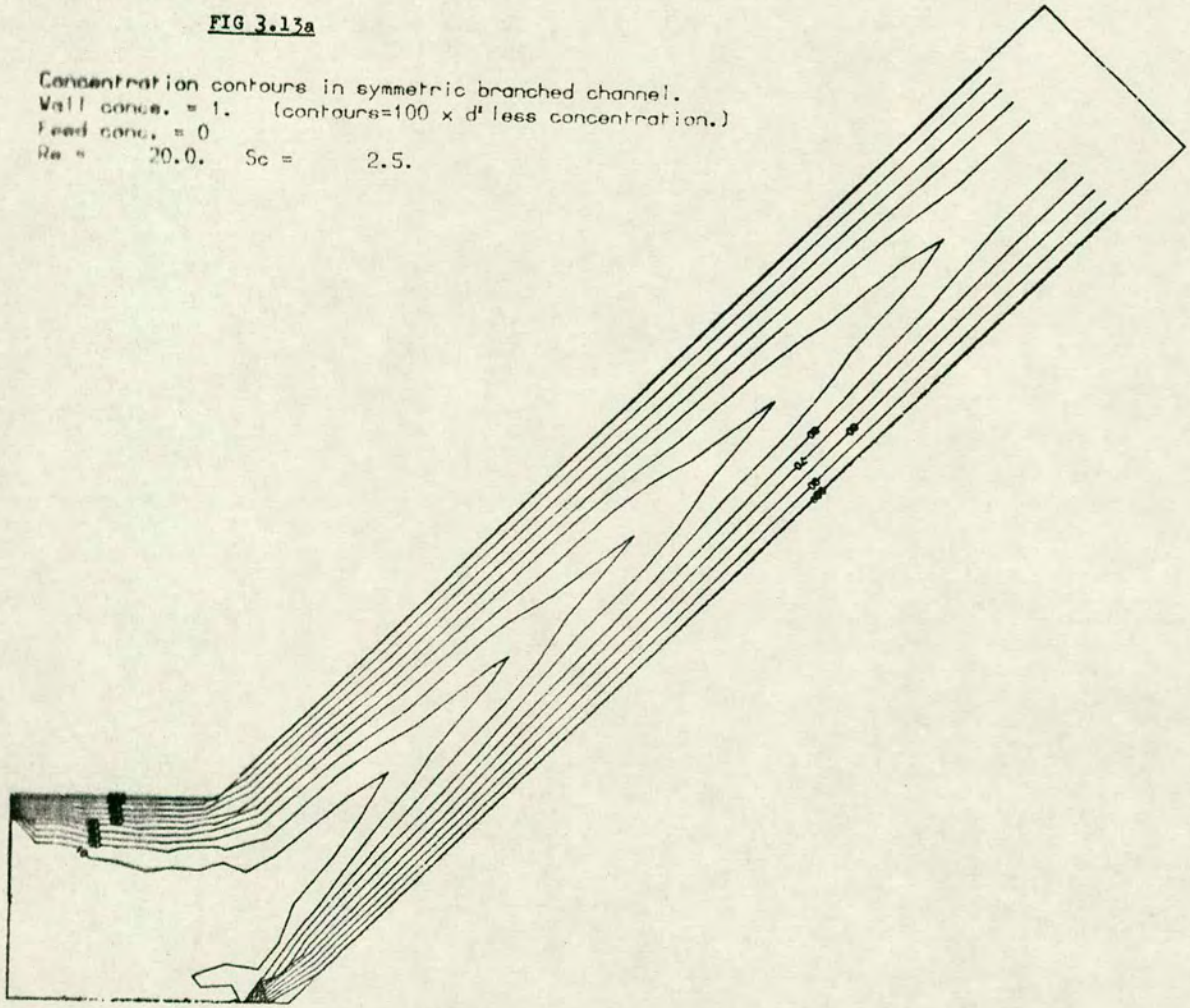

FIG 3.13b

Concentration contours in symmetric branched channel.
Wall concs. = 1. (contours=100 x d'less concentration.)
Feed conc. = 0
Re = 40.0. Sc = 2.5.

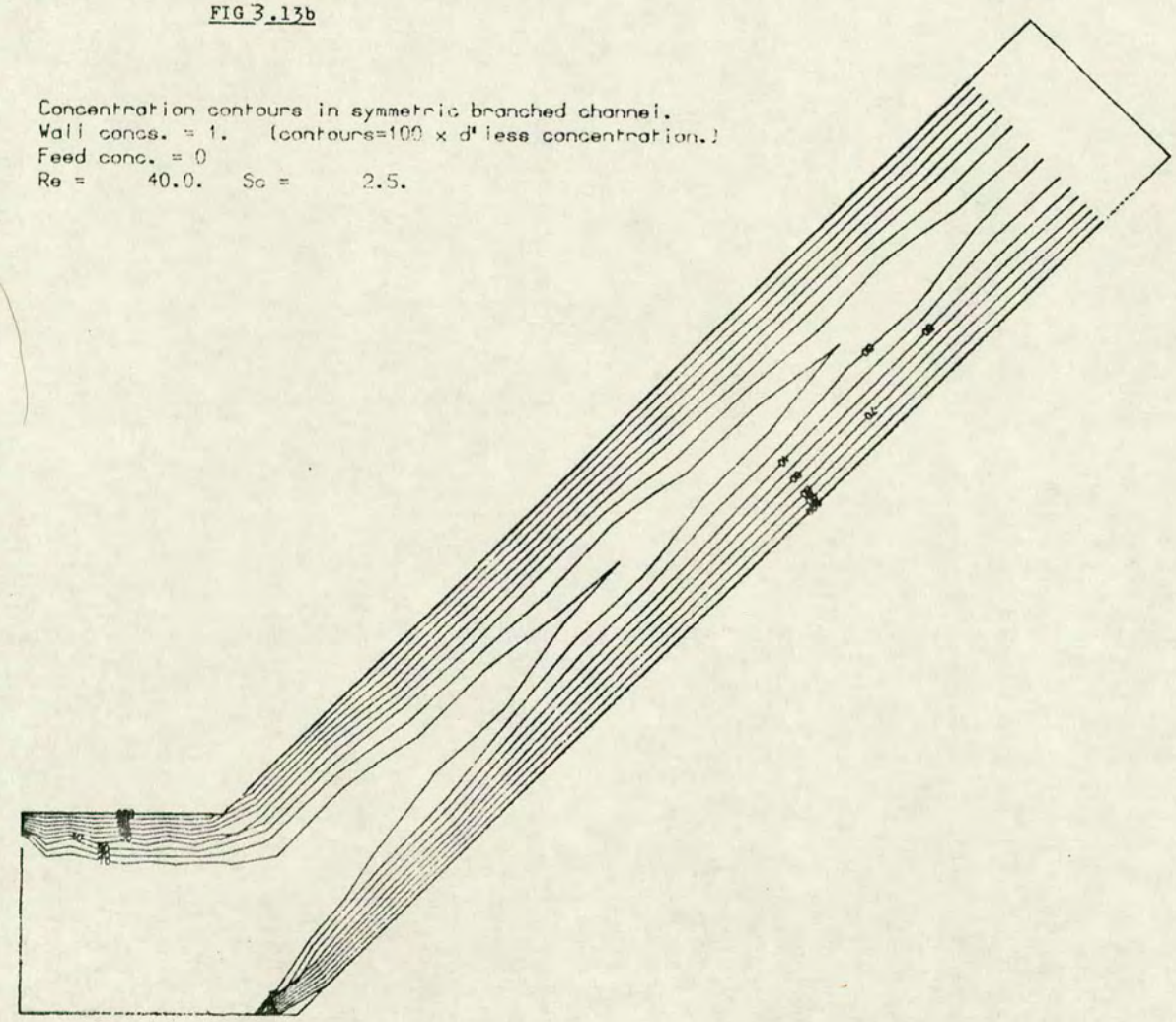

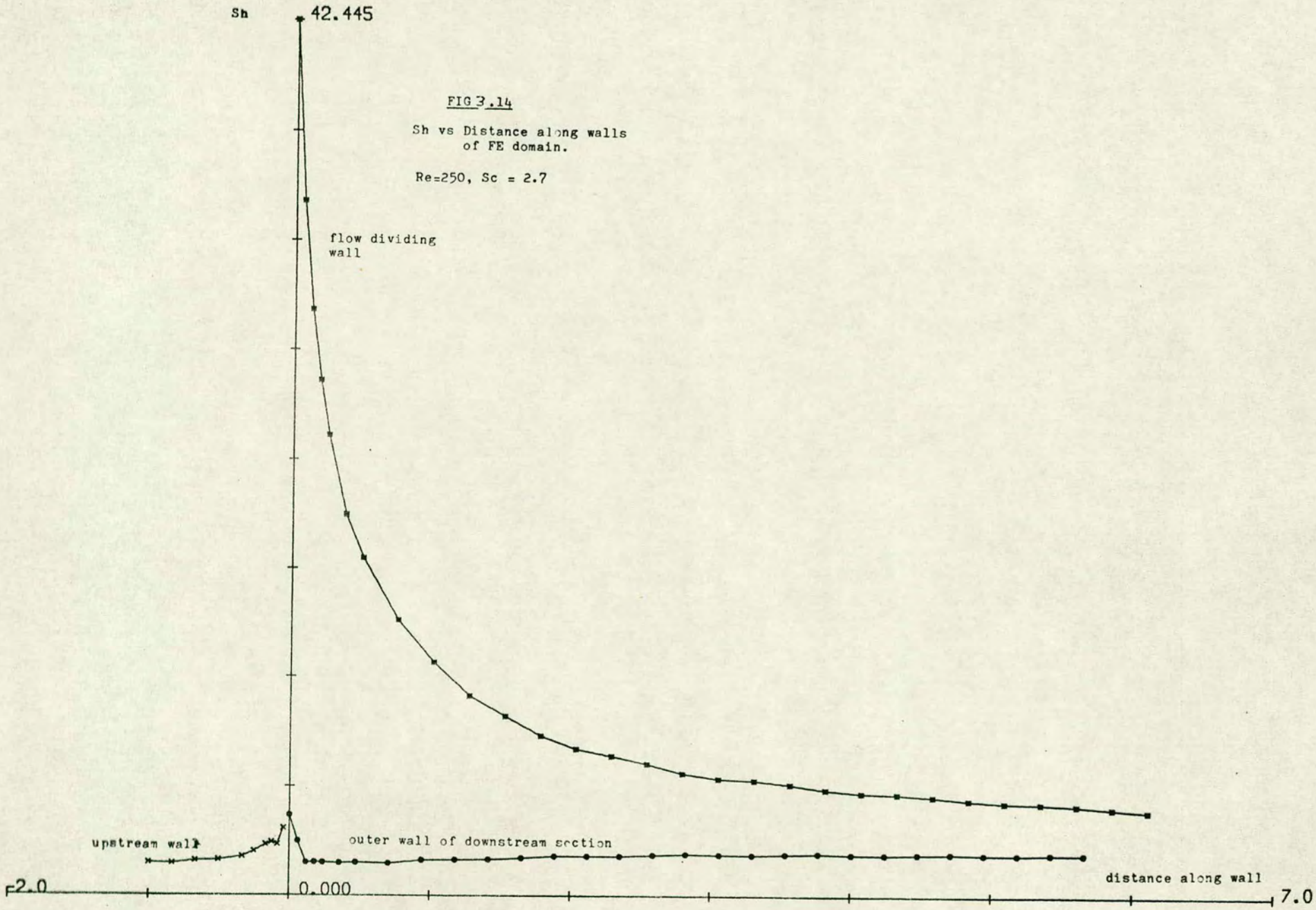

FIG 3.14

Sh vs Distance along walls of FE domain.

Re=250, Sc = 2.7

FIG 3.15

Symbols { x = upstream section wall
o = downstream section outer wall
* = flow dividing wall

Sh vs distance along wall.

Re = 250; Sc = 2.7, 50, 300, 1500, 2800

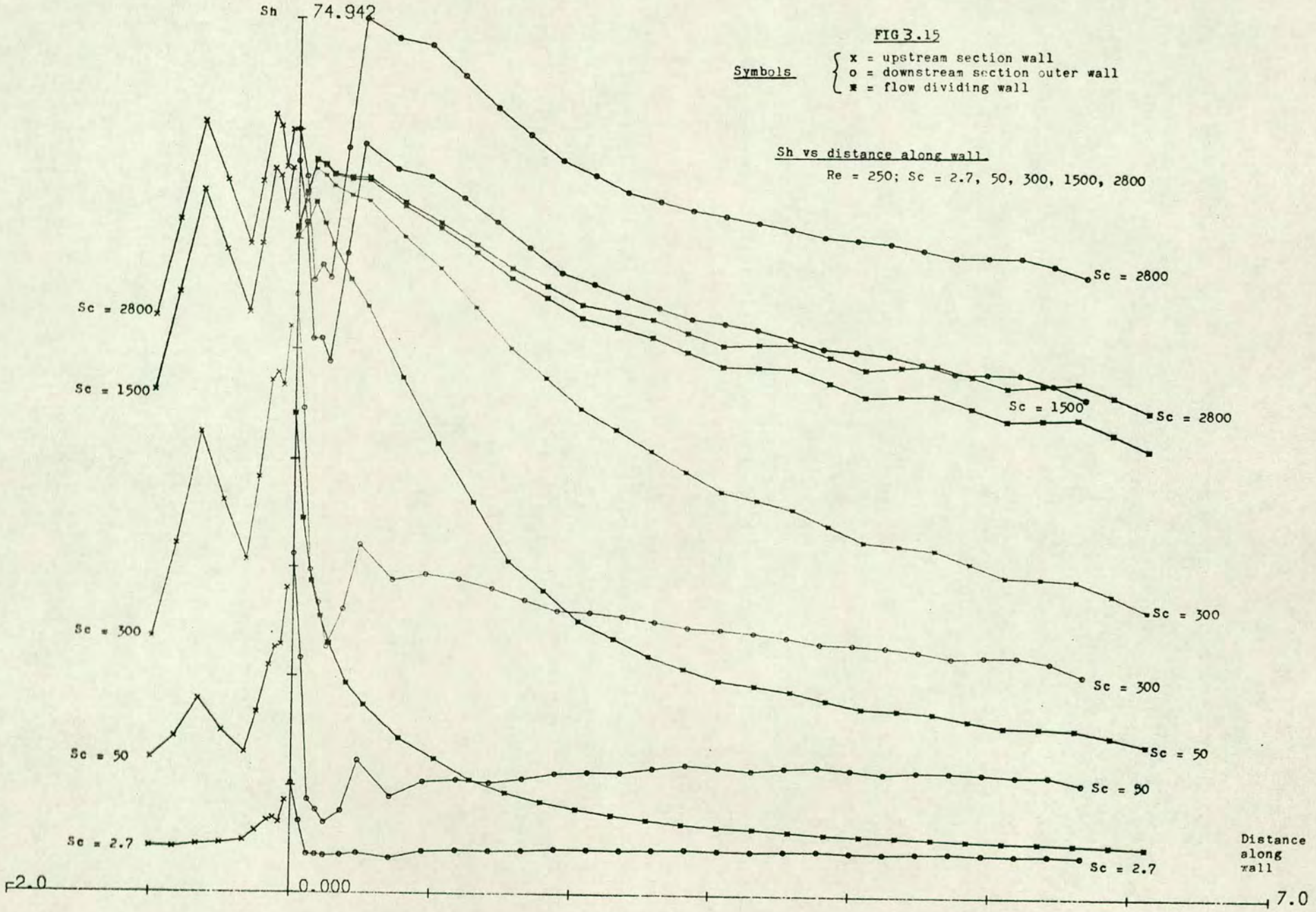

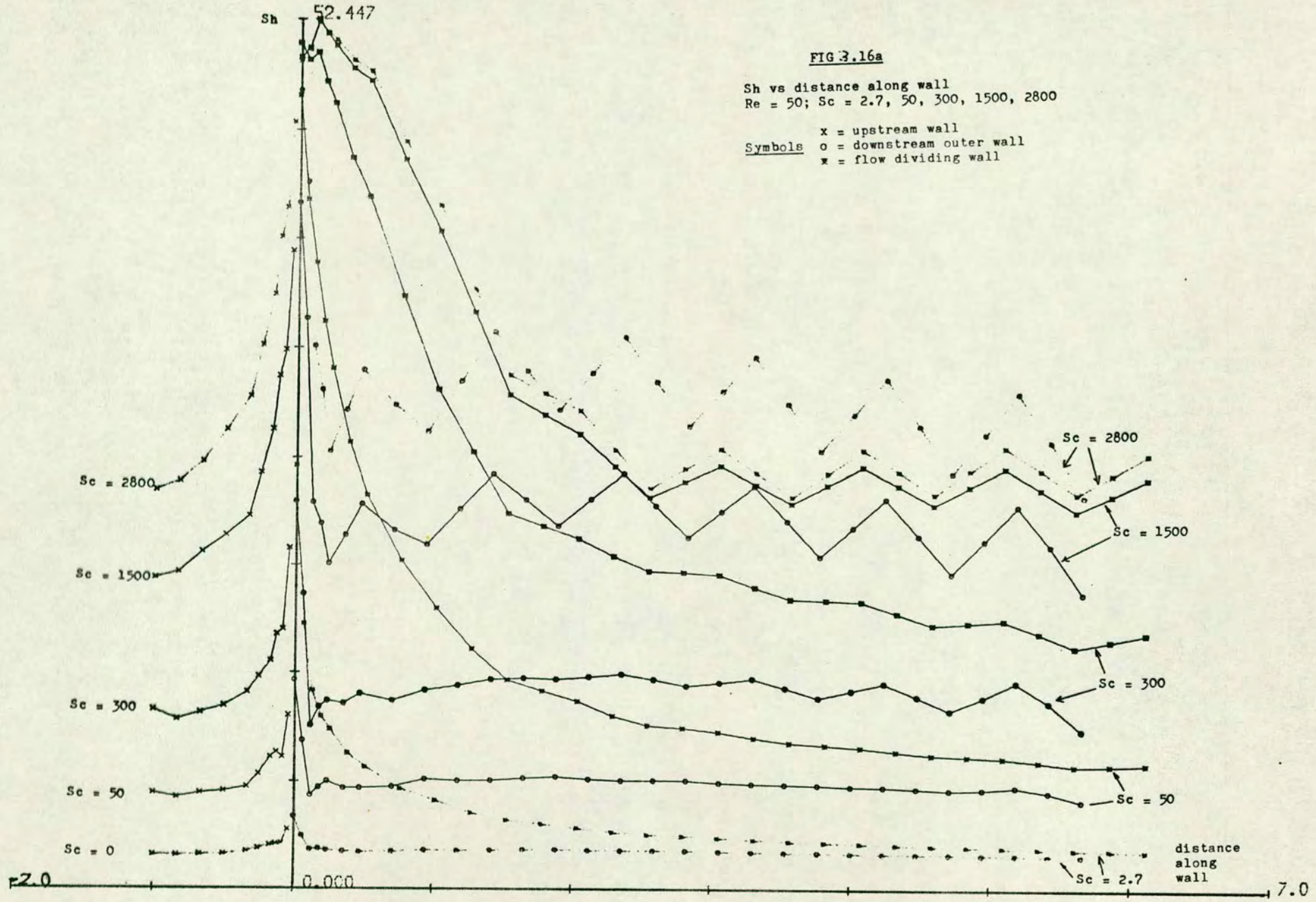

FIG 3.16a

Sh vs distance along wall
Re = 50; Sc = 2.7, 50, 300, 1500, 2800

Symbols
x = upstream wall
o = downstream outer wall
* = flow dividing wall

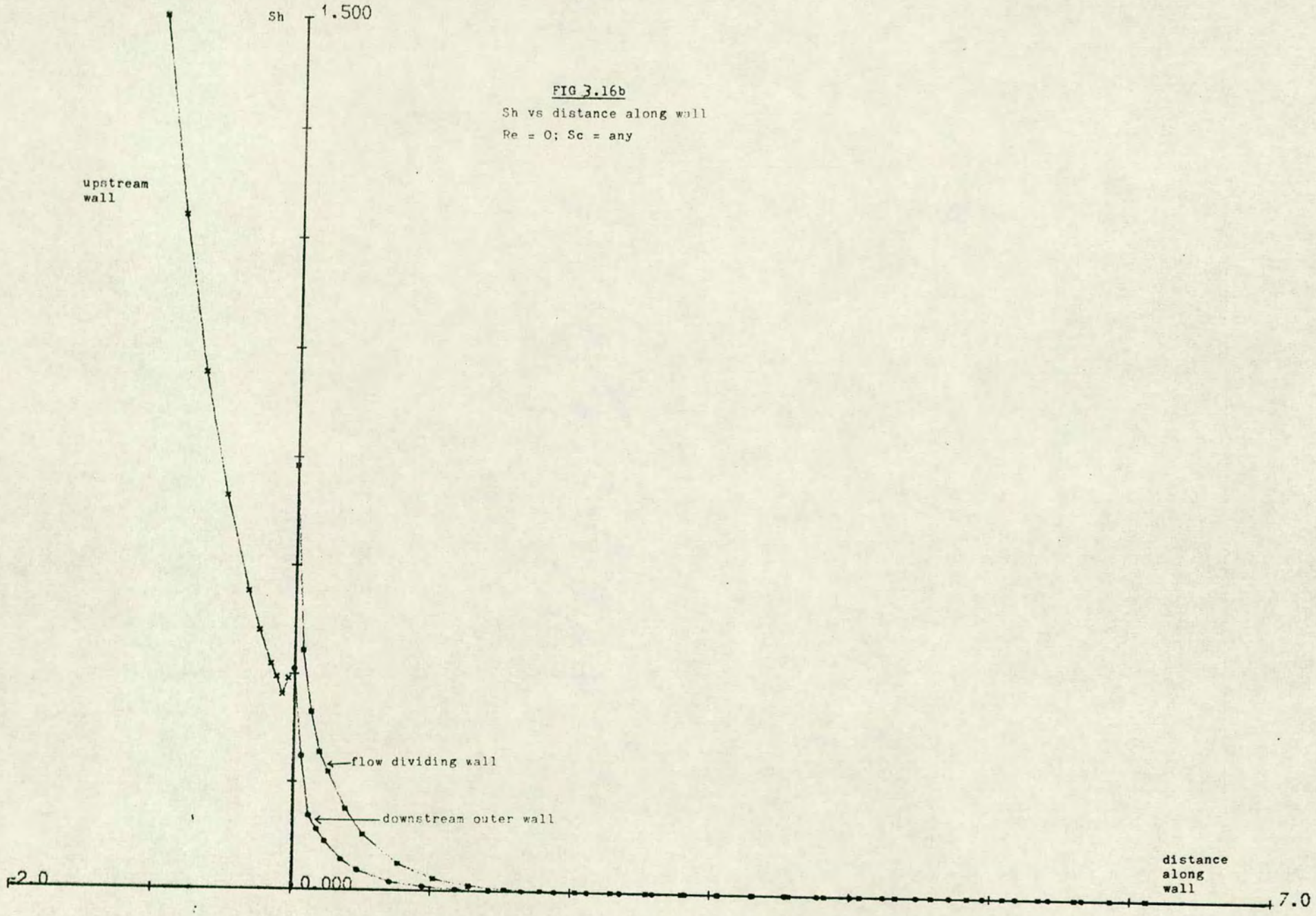

FIG 3.16b

Sh vs distance along wall

Re = 0; Sc = any

FIG 3.17

Variation of Sh_{sc} with X (distance along wall)

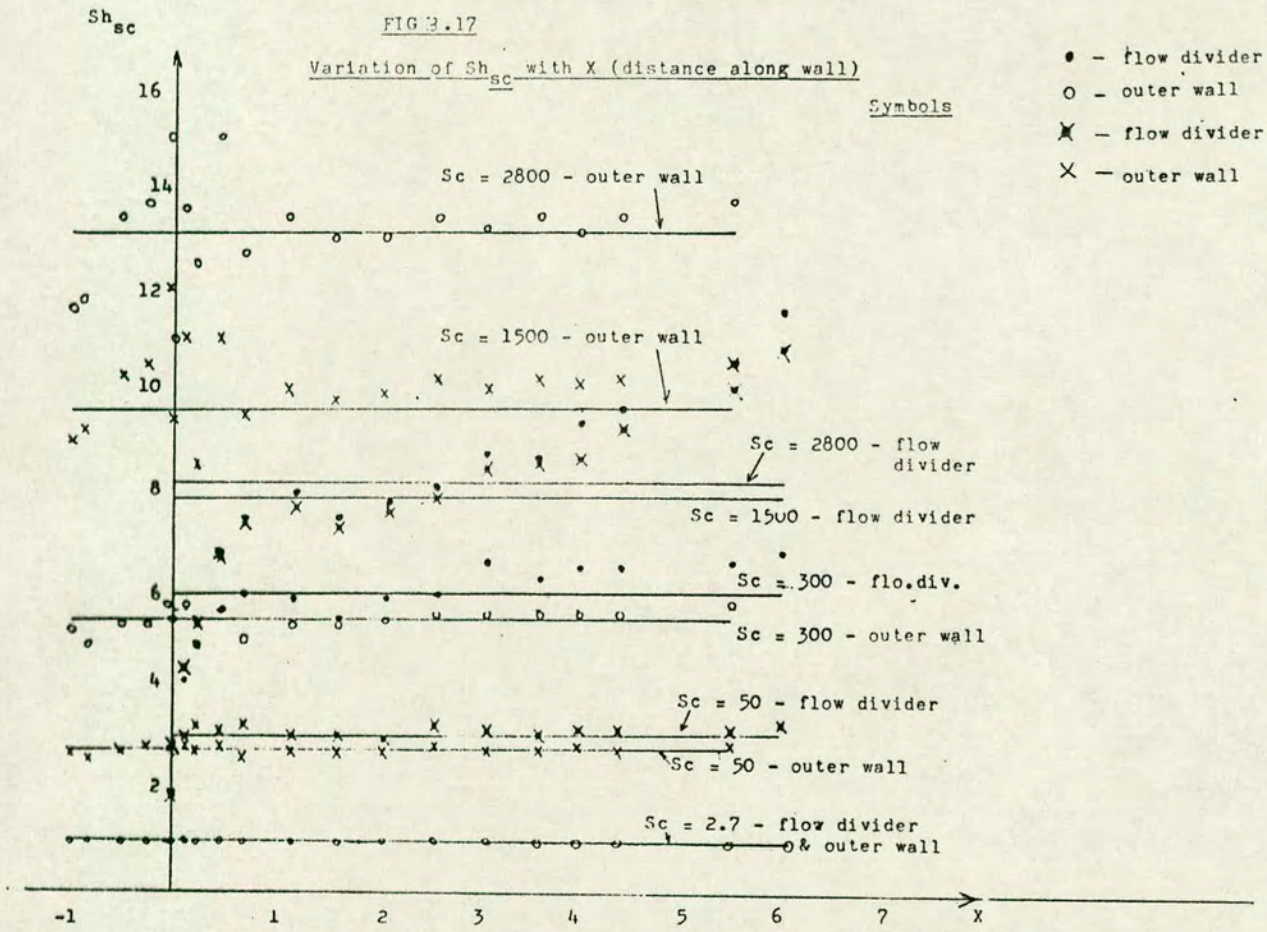

FIG 3.18

Log_e(mean Sh_{sc}) vs Log_e Sc

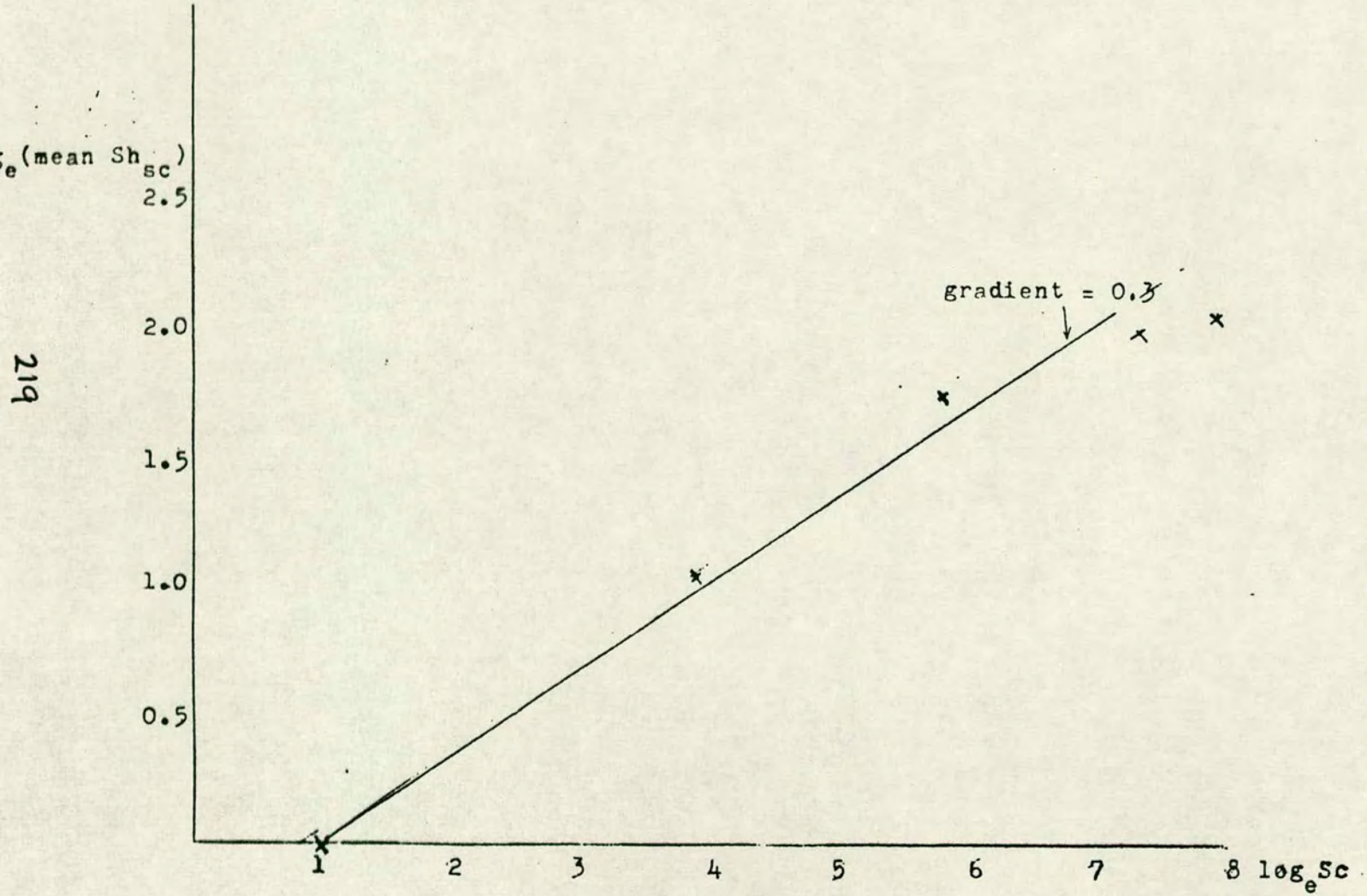

FIG 3.19

Sh_{re} vs X (distance along wall)

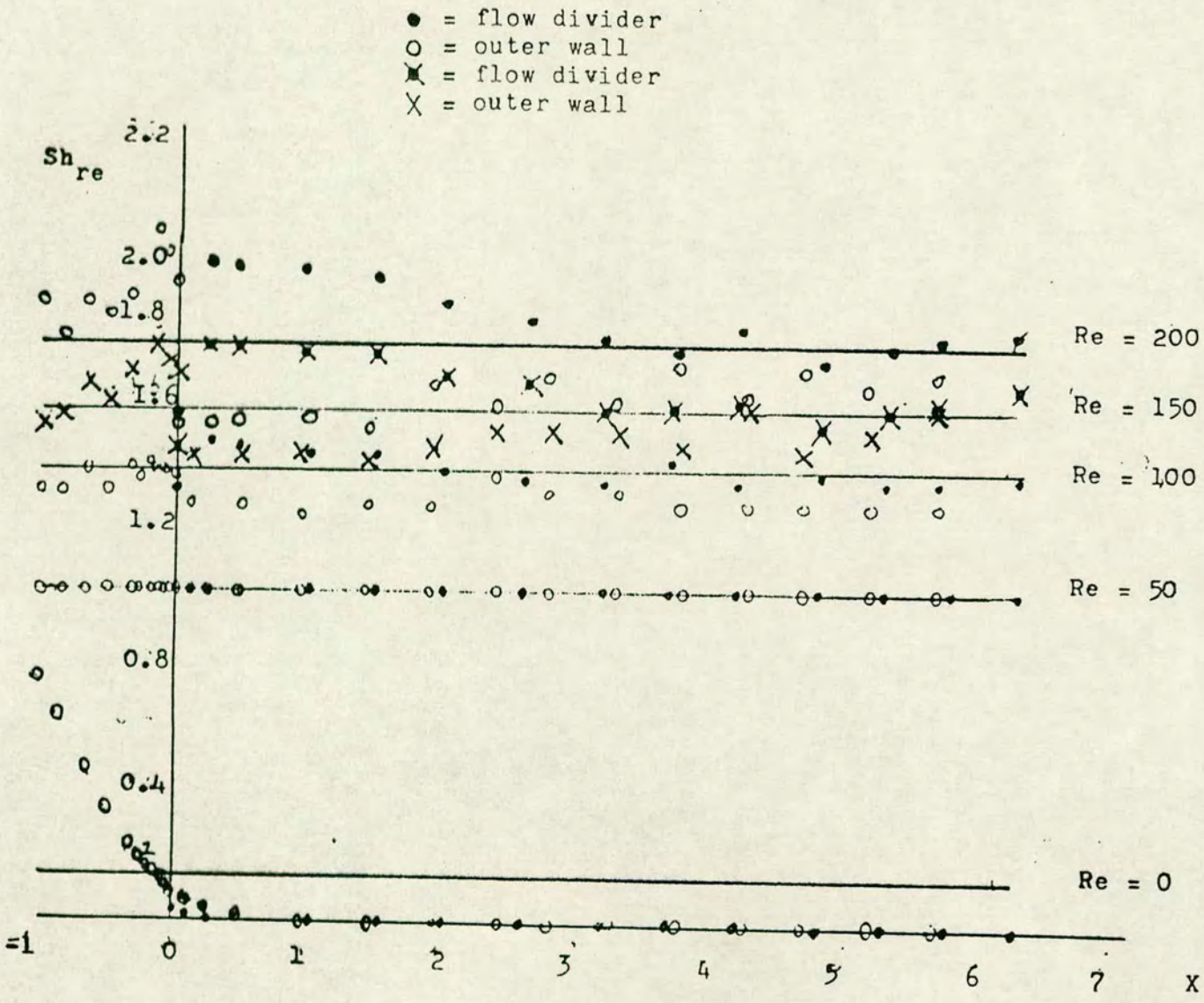

FIG 3.20

$\log_e$ (mean Sh_{re}) vs $\log_e$ Re

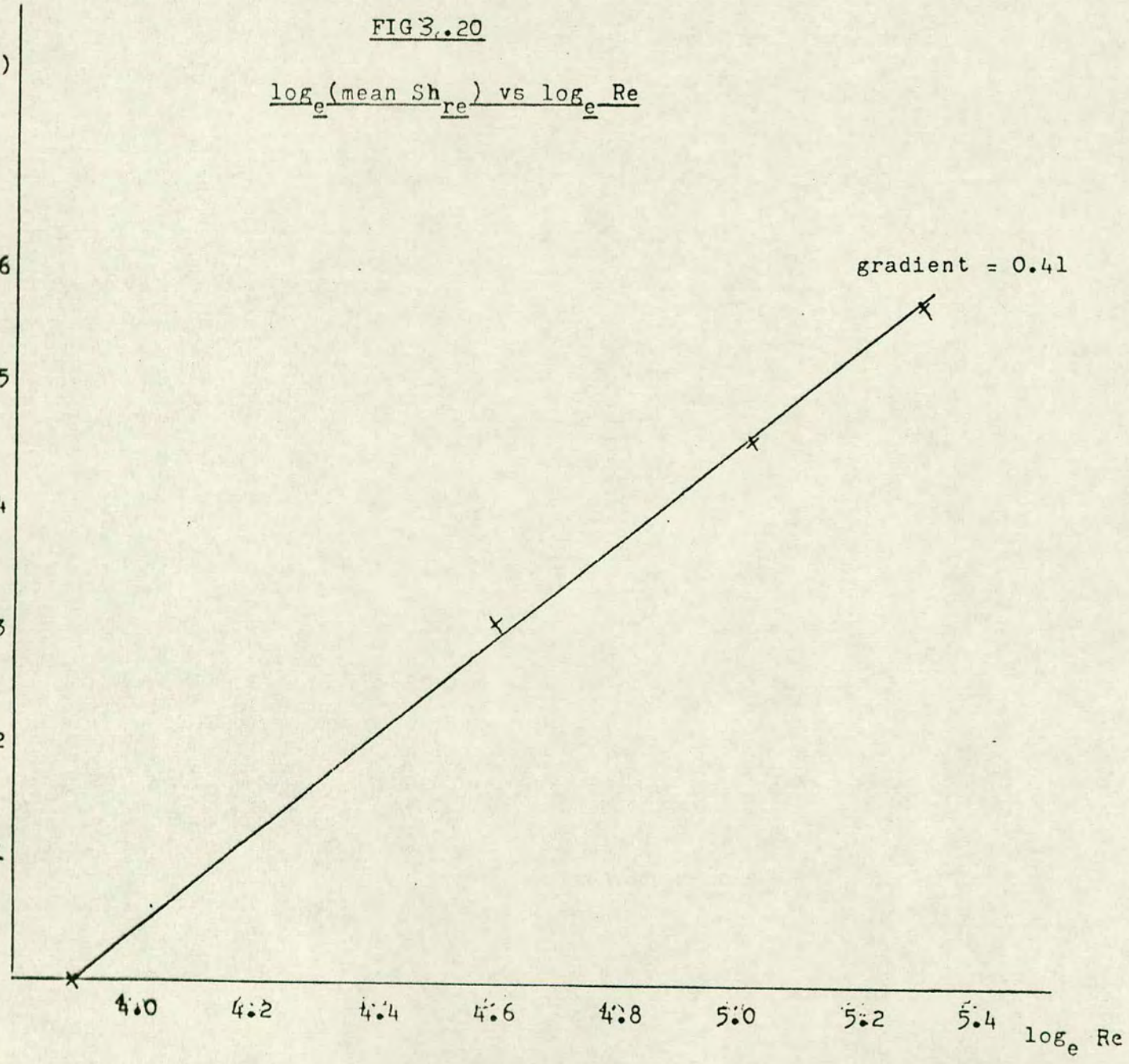

FIG 3.21

Comparison of Extrapolated Sherwood nos with Computed ones.

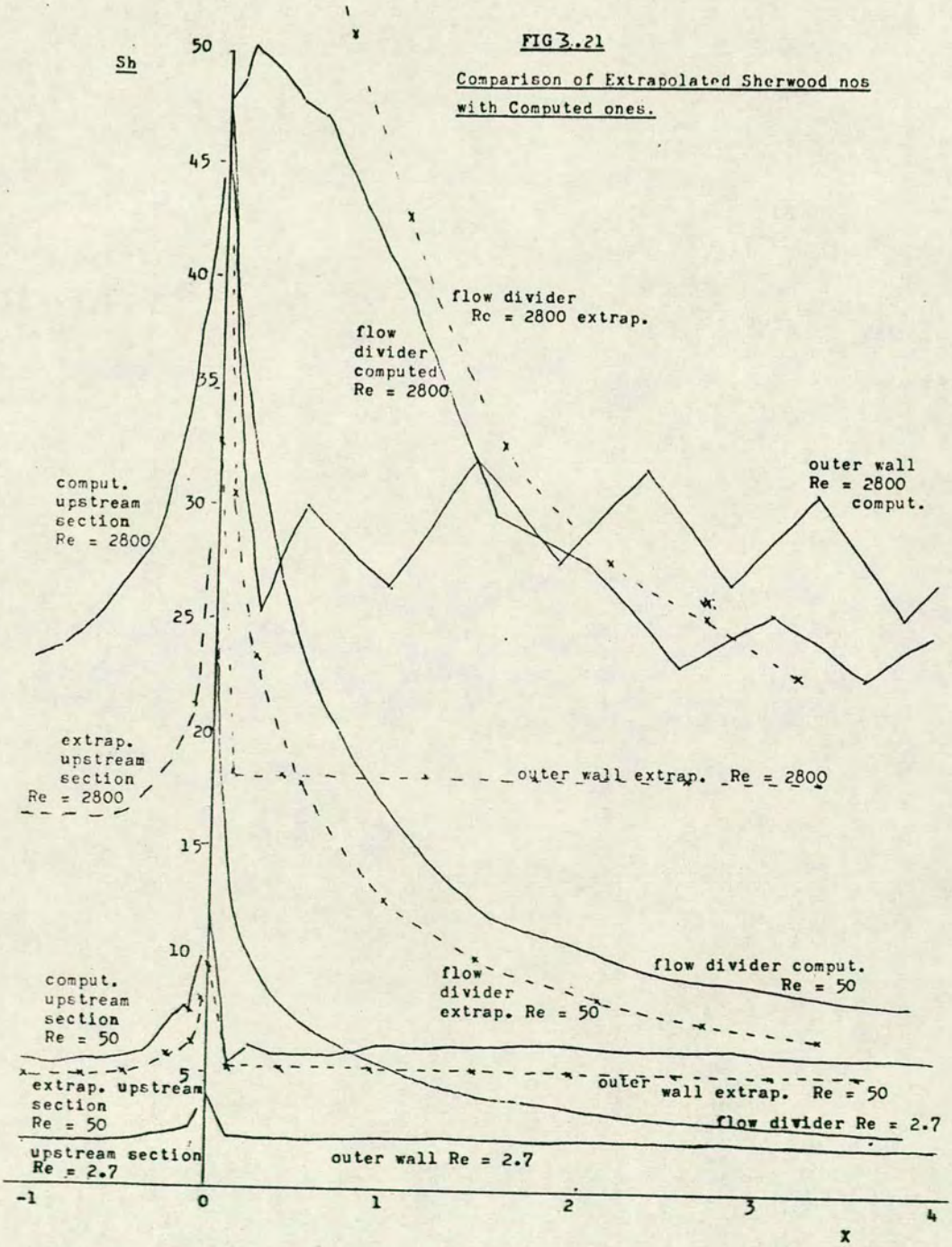

FIG 4.1

Upstream Section; Re = 150, Sc = 2.7

Sh vs distance; computational vs experimental

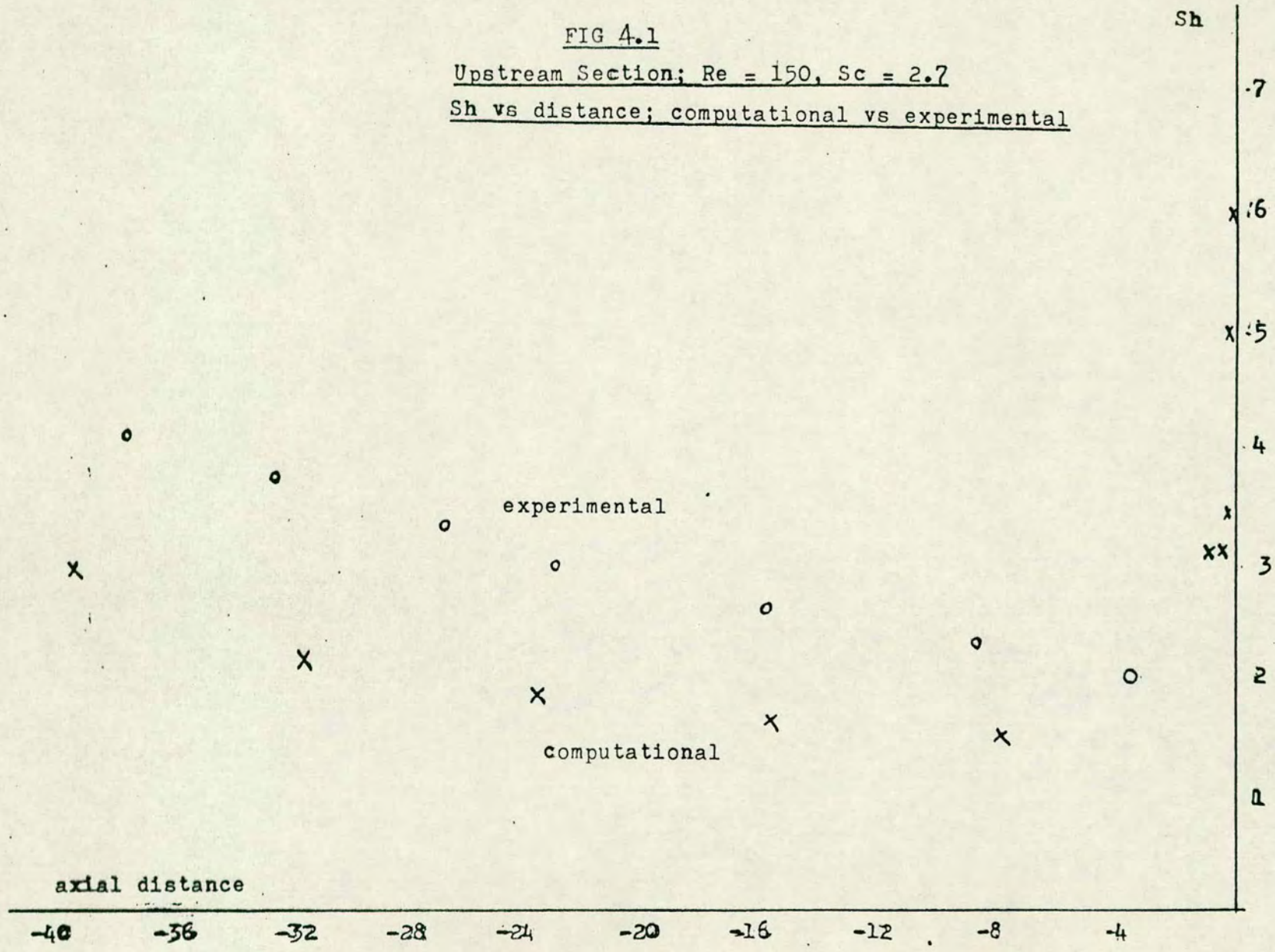

FIG 4.2

Outer Wall; Re = 150, Sc = 2.7

Sh vs distance; computational vs experimental

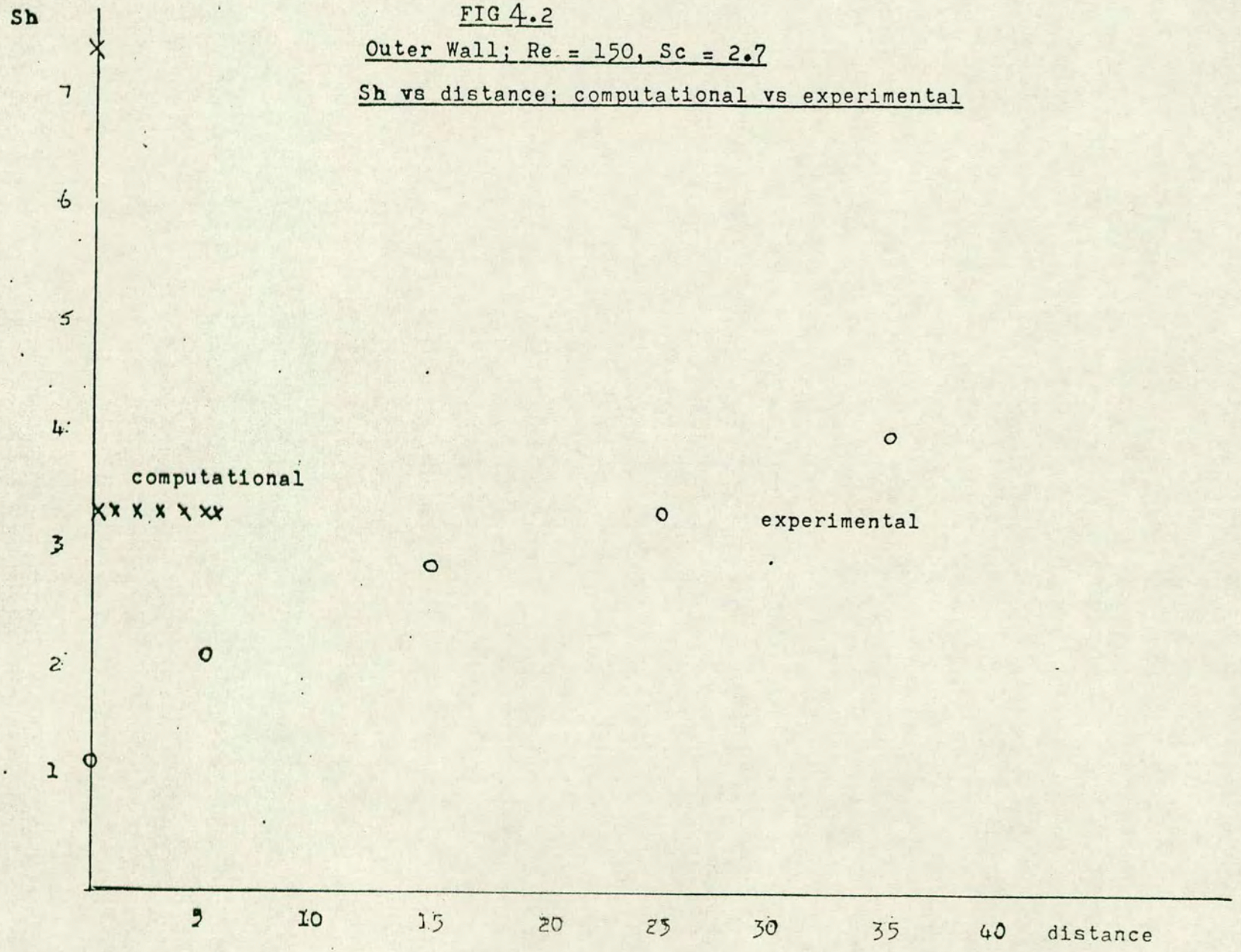

FIG. 4.3

Flow Divider; Re = 150, Sc = 2.7

Sh vs distance; computational vs experimental

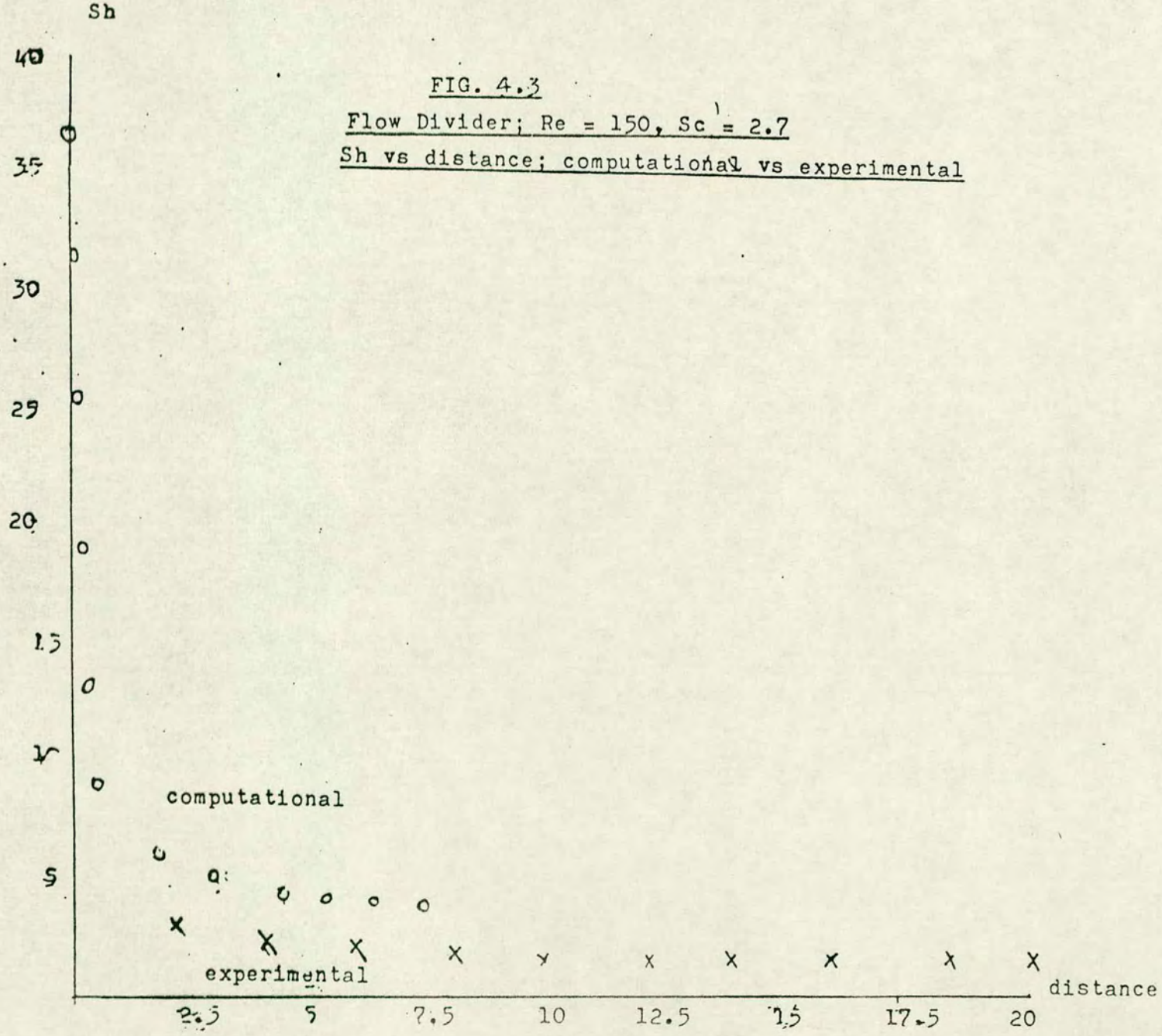

FIG 4.4

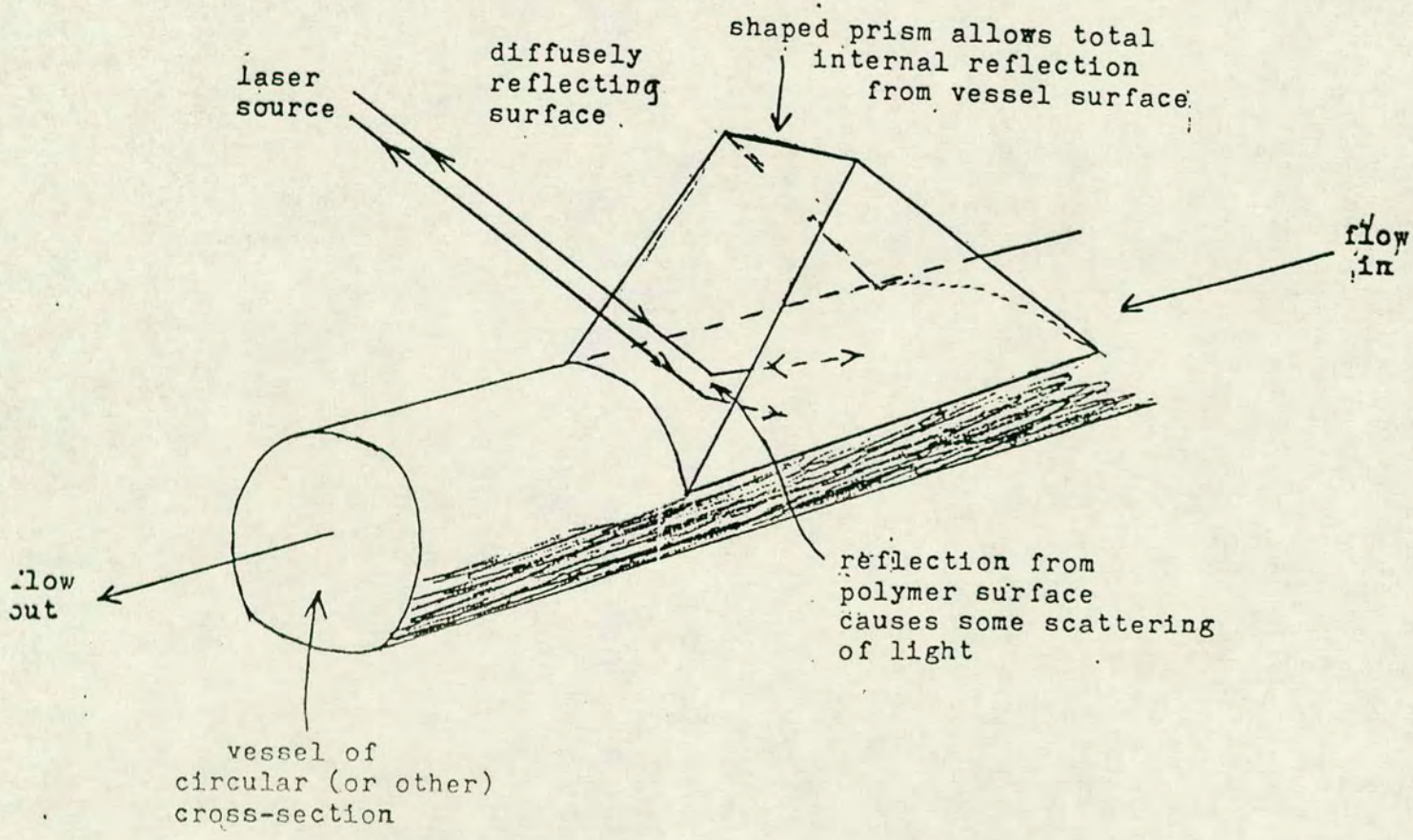
laser source
diffusely reflecting surface
shaped prism allows total internal reflection from vessel surface
flow in
flow out
reflection from polymer surface causes some scattering of light
vessel of circular (or other) cross-section

FIG 4.5a

Direct Reflection from Wall

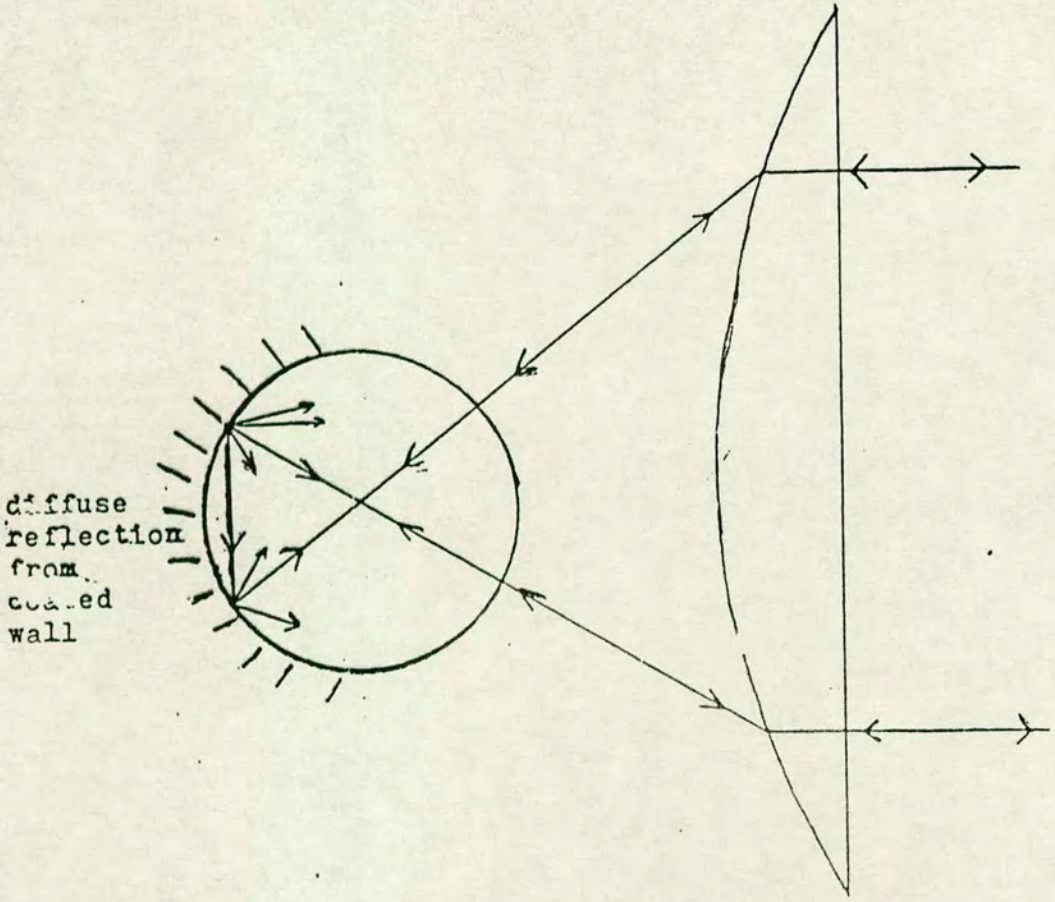

FIG 4.5b

Direct Reflection from a Remote Surface

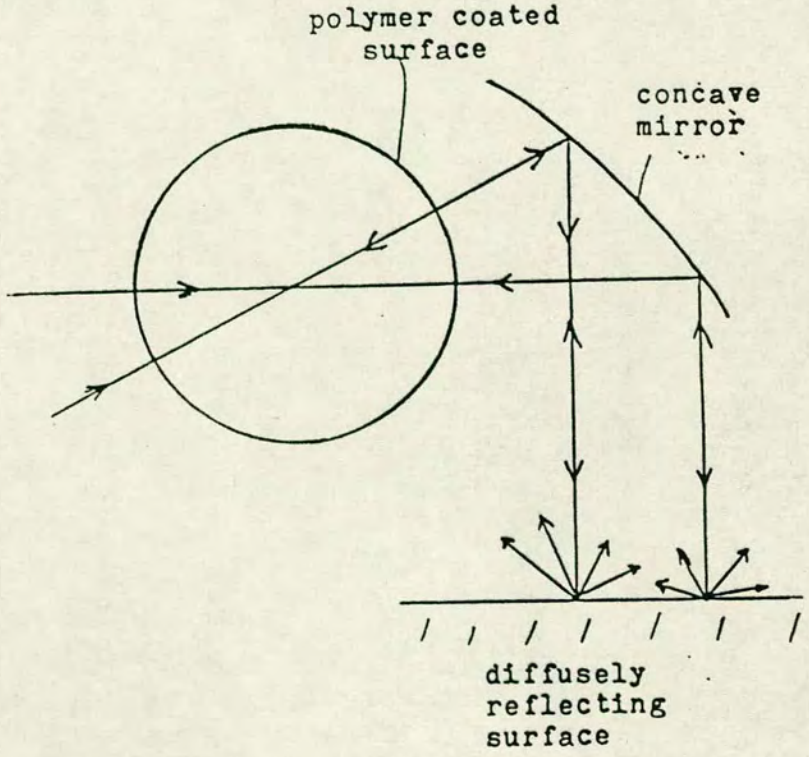

FIG A1

Z plane

Potential Flow Domain - Asymmetric Branch

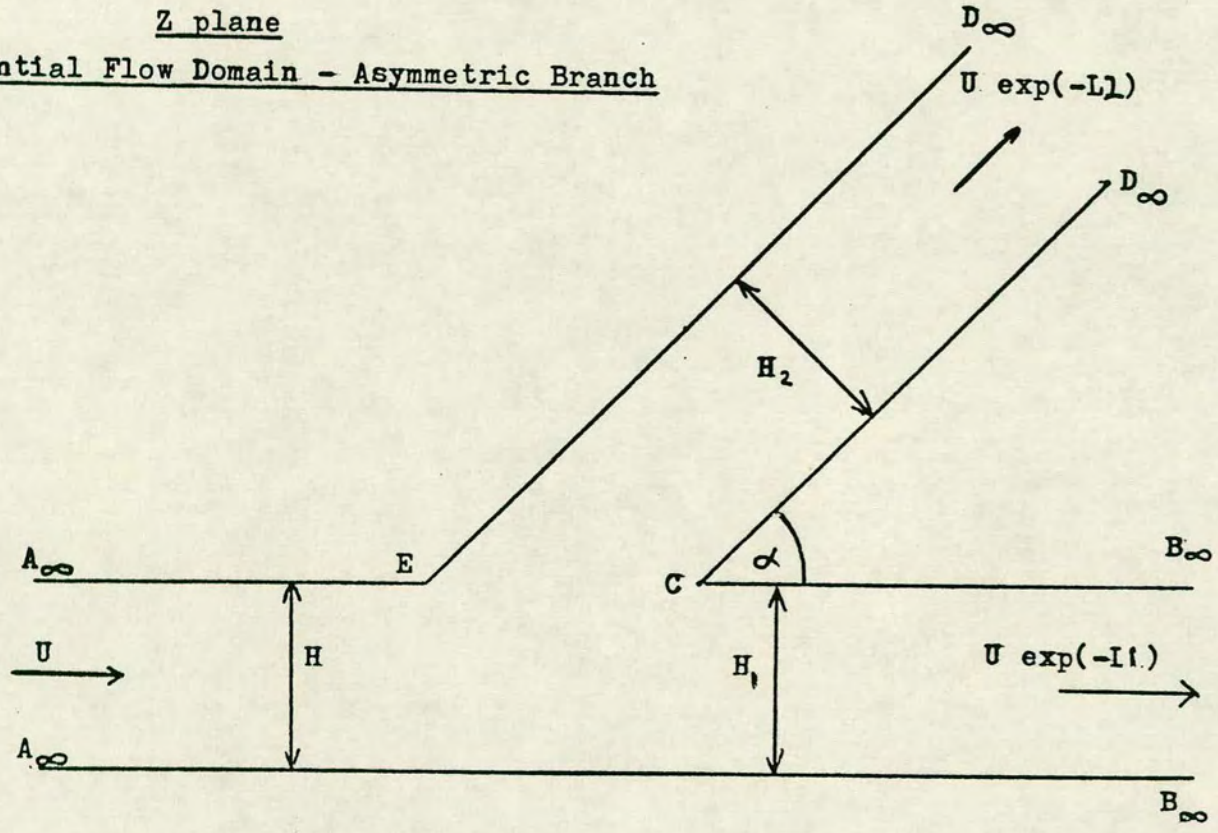

FIG A2

ζ plane

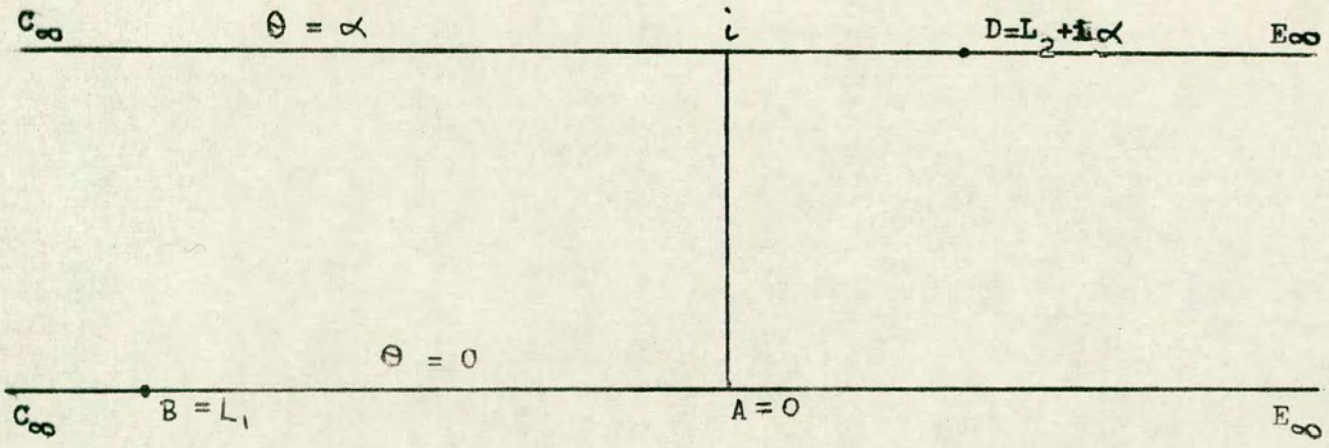

FIG A3

t plane

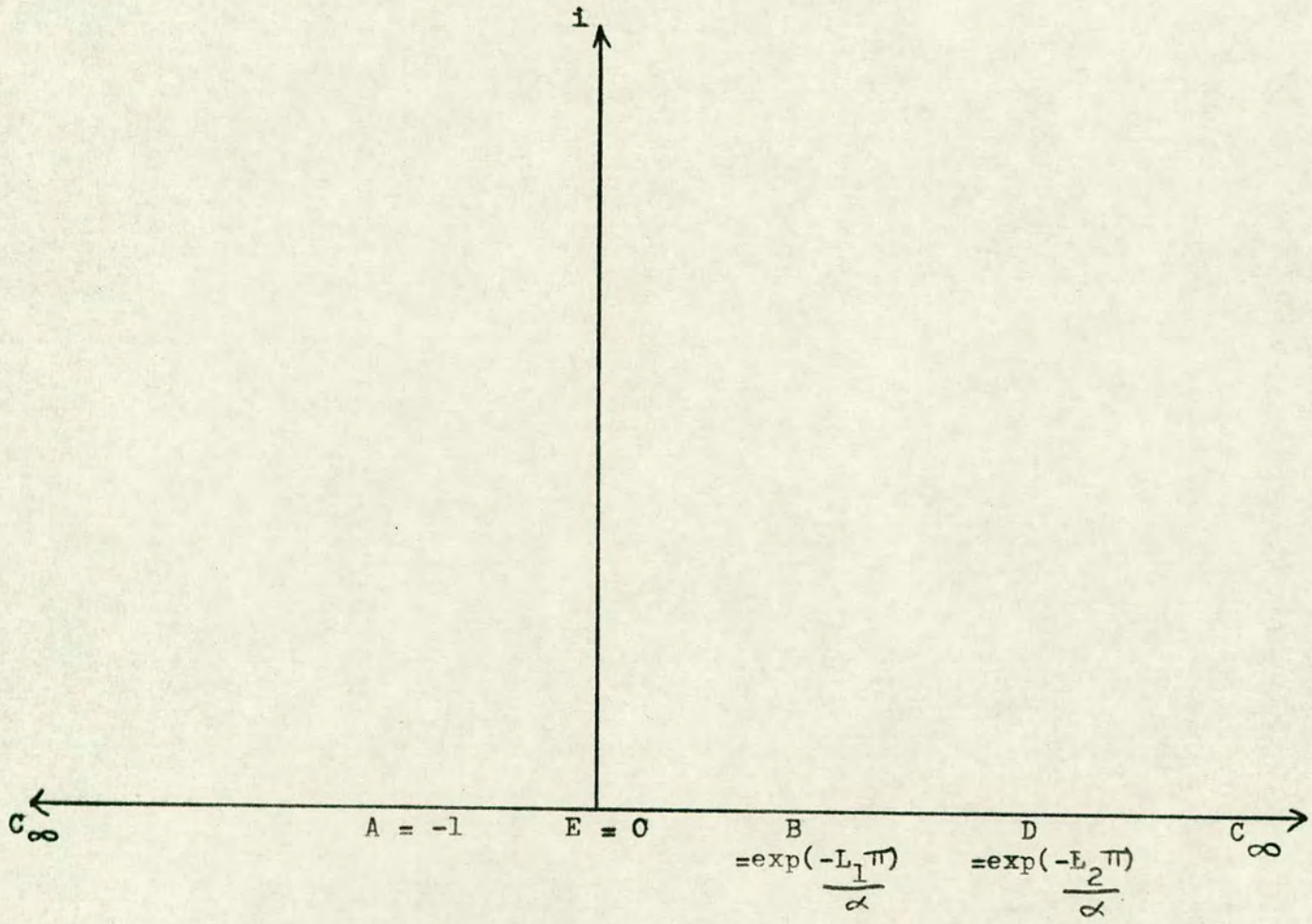

Asymmetric Bifurcation and Apparatus **Fig.8.1**

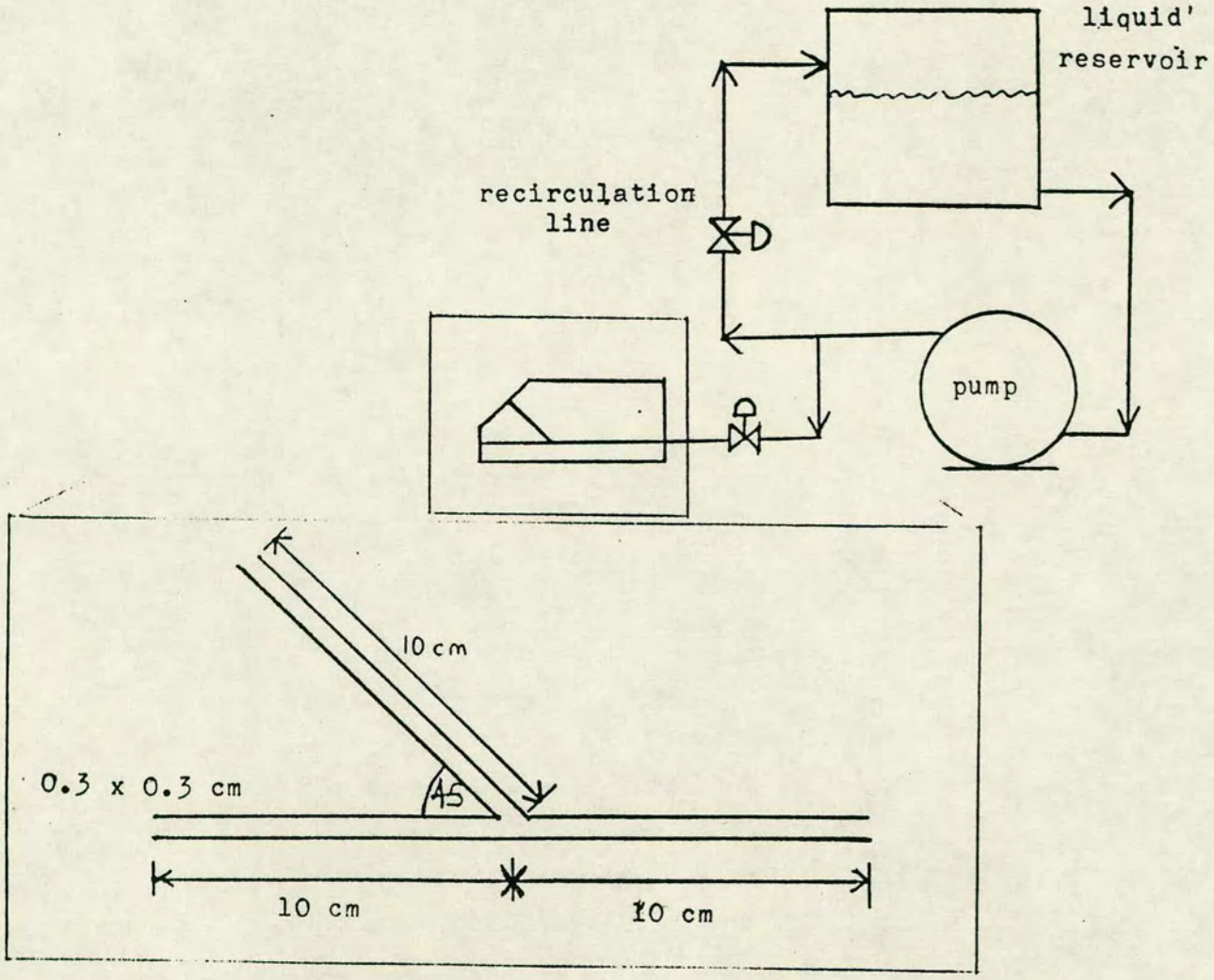

FIG B.2

Fr vs Re: Crowe's results for water and viscous dye solution.

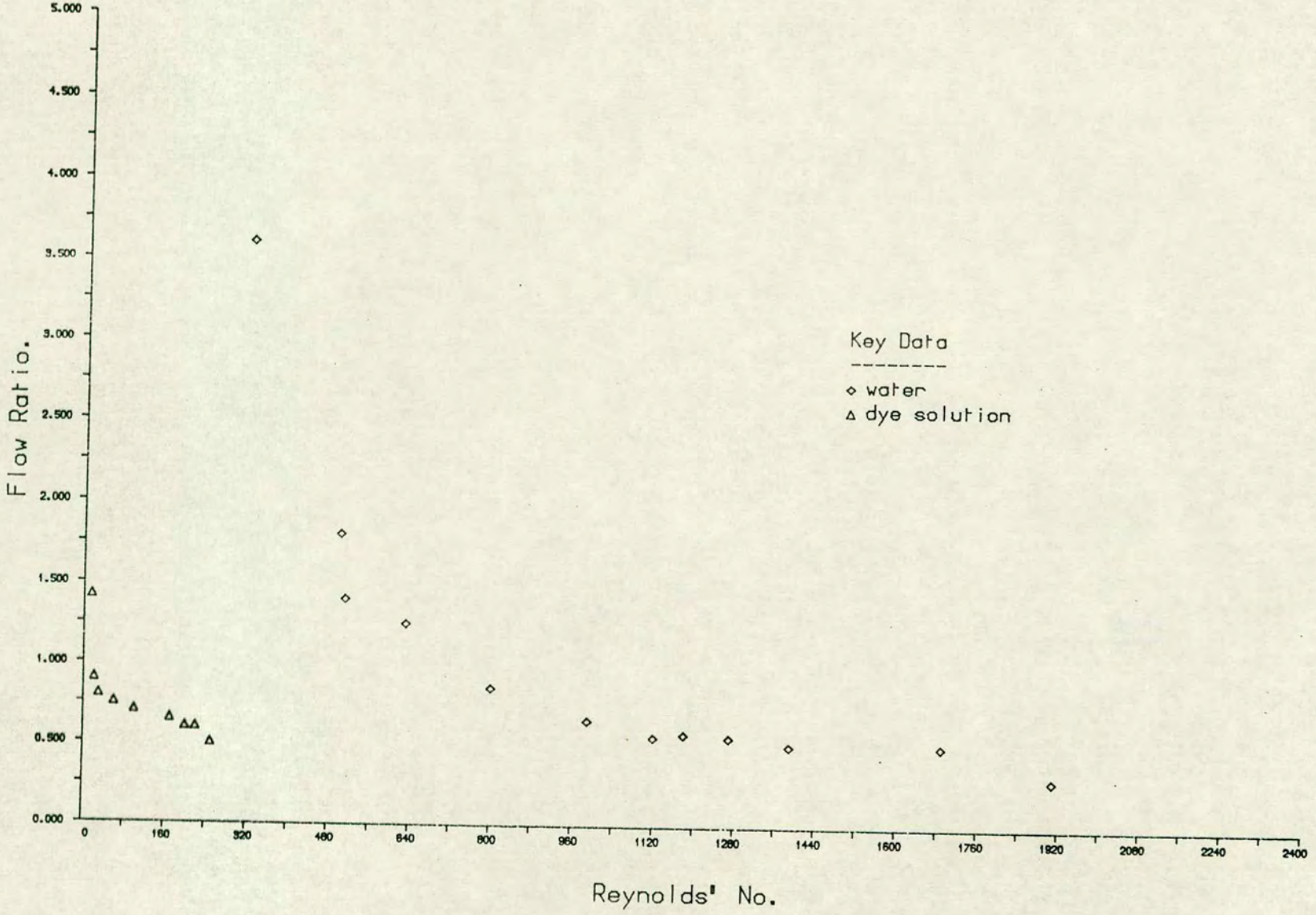

FIG 8.3

Fr vs Re: For water and glycerol solution.

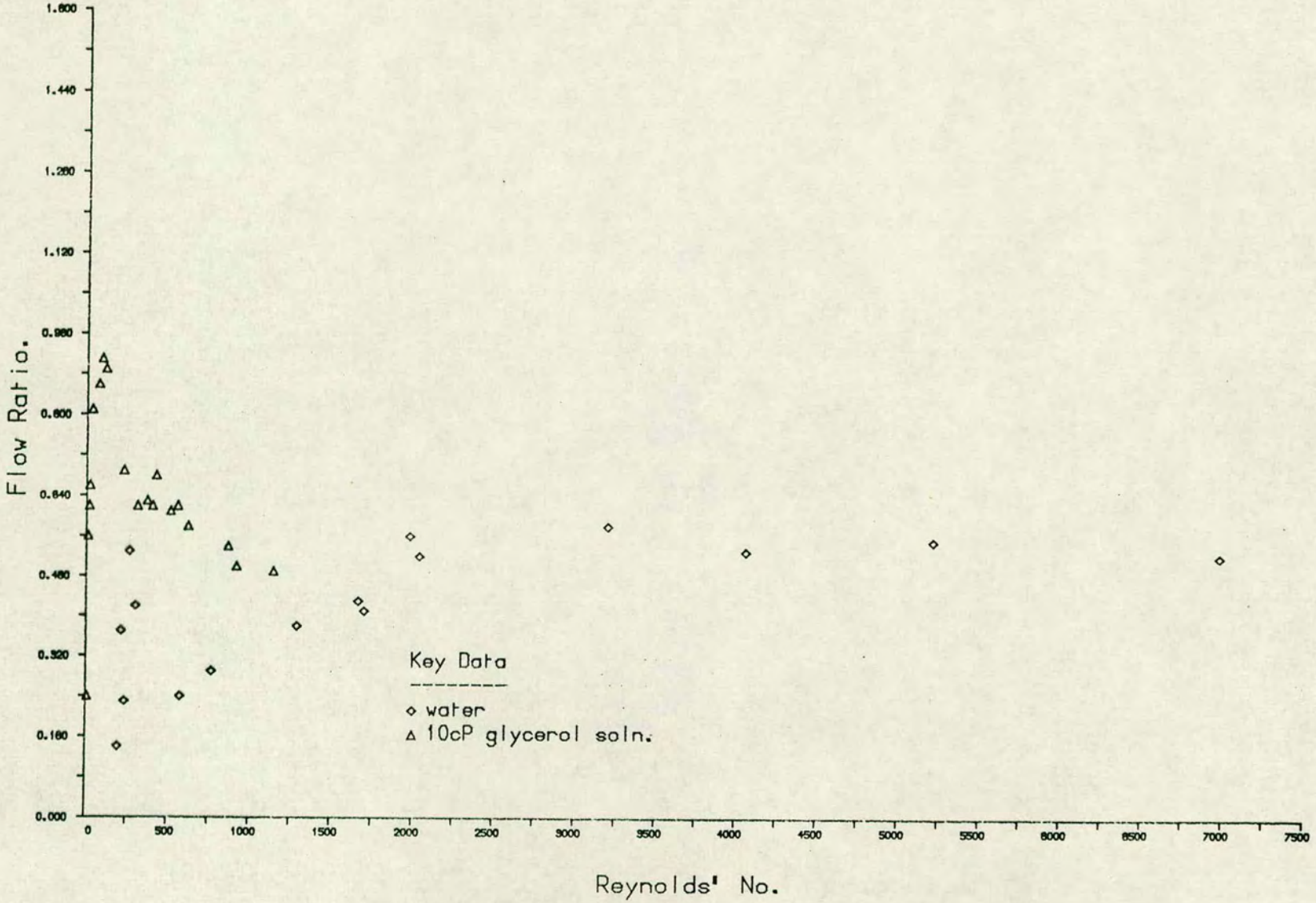

FIG B.4

Fr vs Re: heptane, detergent solution and water.

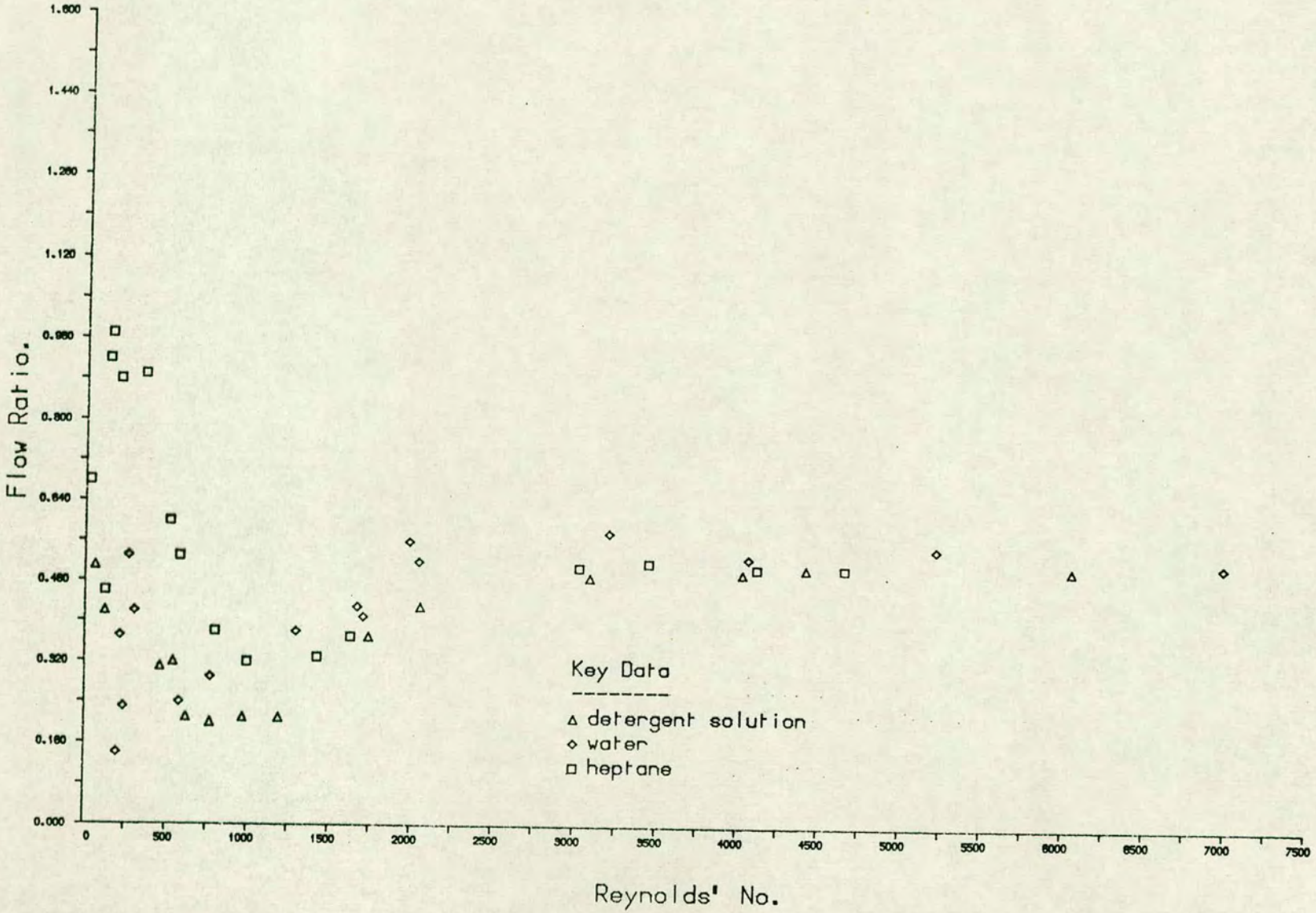

FIG 8.5 Bifurcation, Reservoirs & Weirs

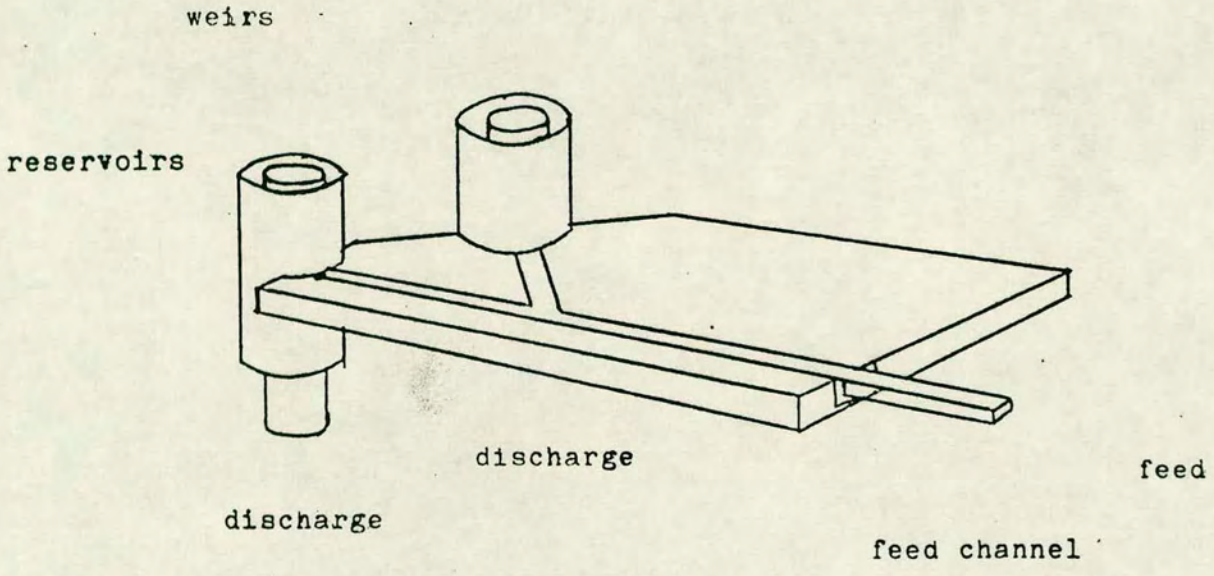

FIG B.6

Fr vs Re: channel immersed in reservoir.

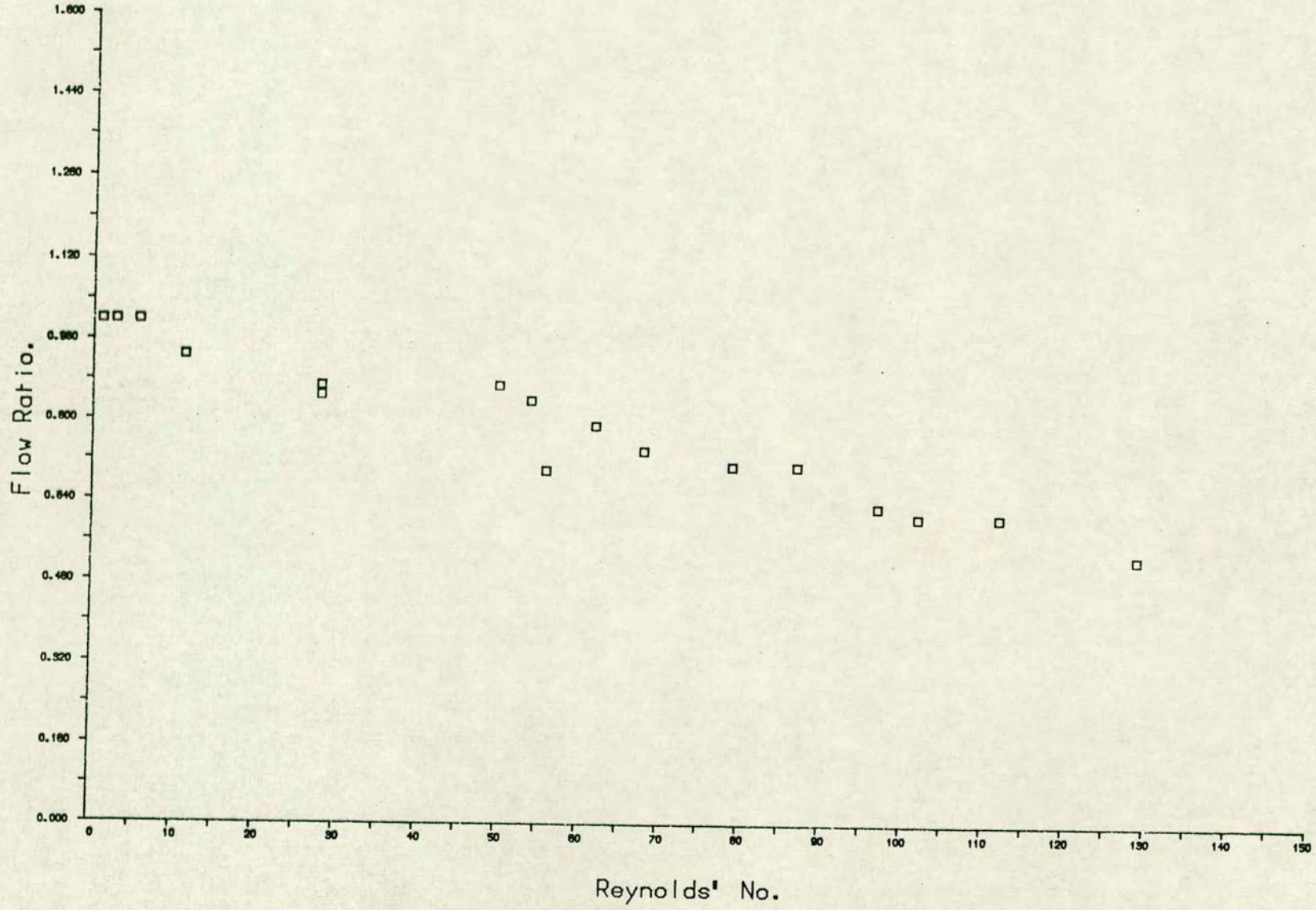

FIG 8.7 Pressure Nomenclature for Eqn B.1

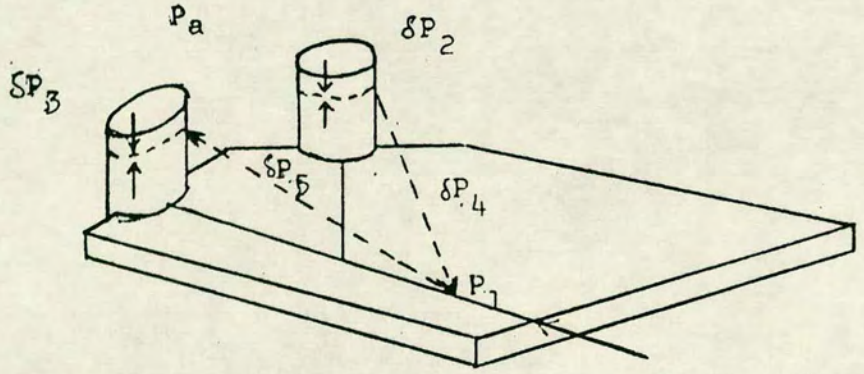

FIG 8.8 Altered Side Branch Geometry

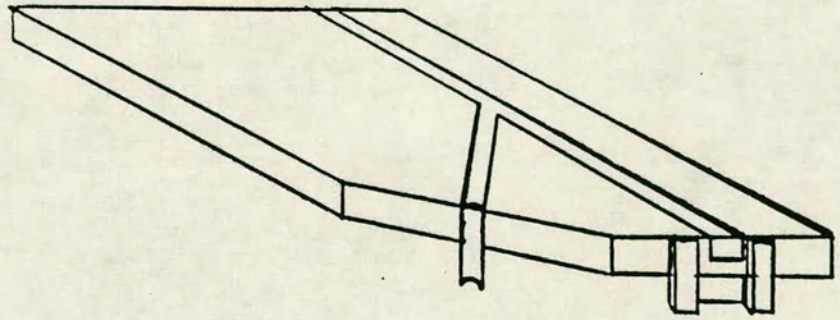

FIG B.9

Fr vs Re: for altered geometry.

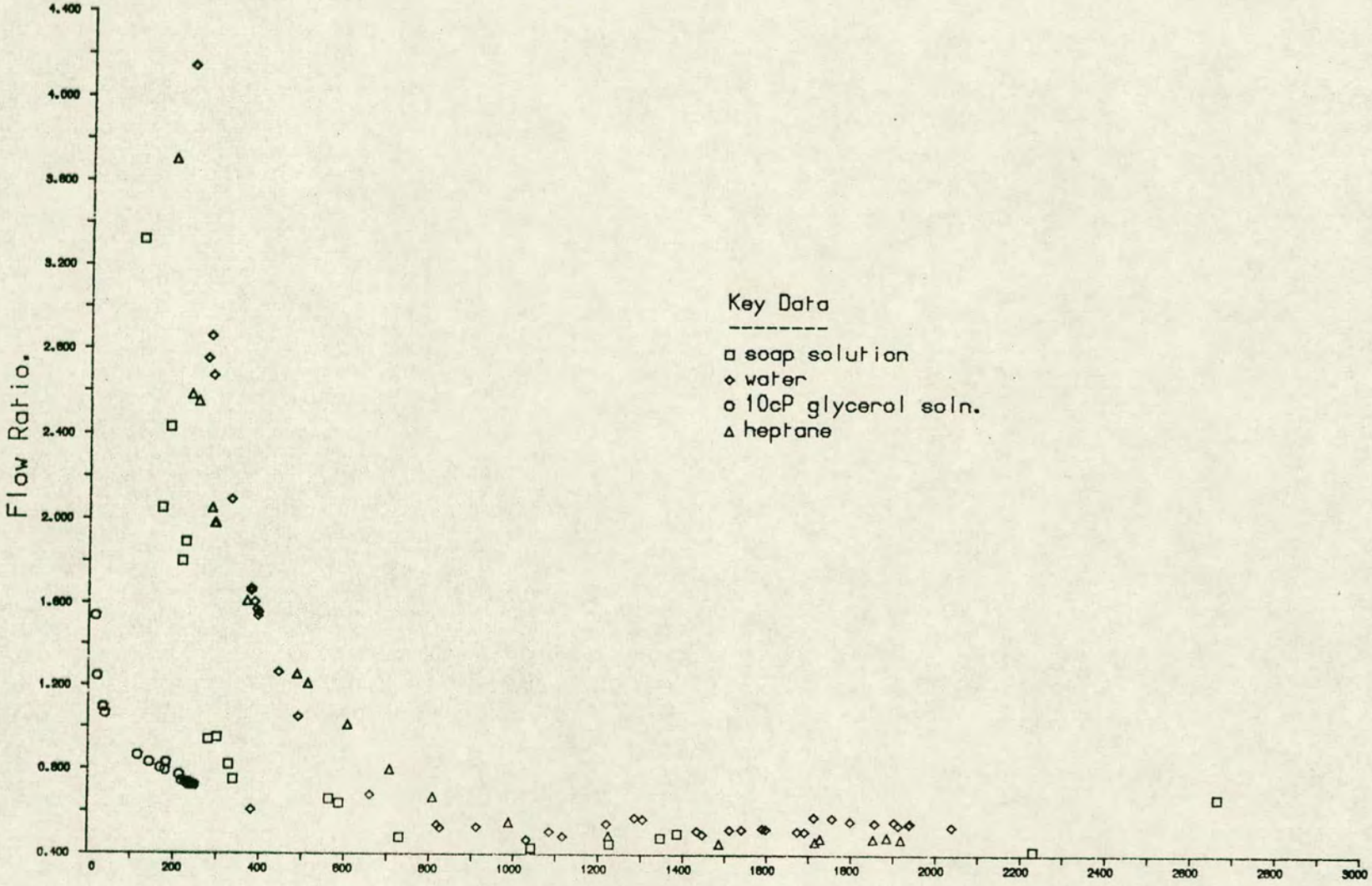

Table 3.1

Variation of Mean and Standard Deviation of Sh with Sc

Sc	Mean	Standard Dev
2.7	1	0
50	2.93	0.09
300	5.48	0.69
1500	8.78	1.7
2800	11.08	1.9

Table 3.2

Variation of Mean and Standard Deviation of Sh with Re

Re	Mean	Standard Dev
0	0.08	0.16
100	1.33	0.047
150	1.5	0.11
200	1.76	0.17

TABLE 4.1

$Q_i = 3.5 \times 10^{-5}$ ml O_2/Torr ml (tissue)
$Q_m = 2.1 \times 10^{-5}$ ml O_2/Torr ml (tissue)
$D_i = 0.7 \times 10^{-5}$ cm^2/s
$D_m = 0.9 \times 10^{-5}$ cm^2/s
$D_p = 2.0 \times 10^{-5}$ cm^2/s
$k_i = 2.4 \times 10^{-5}$ ml O_2/Torr ml (blood)
$k_m = 2.4 \times 10^{-5}$ ml O_2/Torr ml (blood)
$y_1 = 0.0$mm
$y_2 = 0.1$mm
$y_3 = 0.5$mm
Sh = 2.05
r = 1.5mm